



University of
Sheffield

School of
Medicine &
Population Health

Defining the perivascular tumour microenvironment
after neoadjuvant chemotherapy within triple
negative breast cancer and correlation to metastasis

Richard Allen

Registration number:150210522

A thesis submitted in partial fulfilment of the requirements for the degree of
Doctor of Philosophy

The University of Sheffield
Faculty of Health
Division of Clinical Medicine

April 2024

Acknowledgements

I would like to acknowledge the role and support of my primary supervisor, Professor Claire Lewis. From first giving me the chance to undertake my project, her continued patience and support throughout, helping me get over each hurdle and the opportunities she has opened for me.

Additionally, from my supervisory team, Dr Russell Hughes, who was a great mentor in and out of the lab and instilled in me best practice. And Professor Munitta Muthana, who stepped in after Russell and has been a great supporter in encouraging me to plough on and complete my work.

A thank you to the following individuals, charities and companies that have all been instrumental in building my knowledge or enabling work to be carried out:

Team Verrico, who have provided the funds for me to carry out my research.

Professor Angie Cox and the Breast Cancer Now Tissue Bank, in collecting and making available the TNBC samples and/or accompanying anonymised patient data.

Maggie Glover, who has taught me everything to do with histology and allowed me to “borrow” numerous reagents from her laboratory.

Dr Patricia Vergani of Sheffield teaching hospitals, who generously took time to guide me through breast tumour pathology.

Dr Anna Junker Jenson, and the supporting team at Neogenomics Laboratories, USA. Without this collaboration, I would be forever counting immune cells.

Professor Roger Kamm, who generously gave me the opportunity to visit his Mechanobiology lab at MIT to learn about microfluidics and Dr Michelle Chen, who took the time to show me around.

Thank you to Lydia as well, who was brought along on this journey with me. I couldn't have done it without you and your continued, support, sacrifices and love.

And importantly, a final acknowledgement to the patients whose samples were used within my project. They generously donated their tissues and shared their data for research purposes, it's all too easy to forget that each sample has a person behind it.

Declaration

The candidate confirms that the work submitted is their own, except where work that has formed part of a jointly authored publication has been included in Chapter 5: Changes in the Immune Landscape of TNBC After Neoadjuvant Chemotherapy: Correlation with Relapse [104]. The contribution of the candidate and the other authors to this work has been explicitly indicated in section **4.2.5**. The candidate confirms that appropriate credit has been given within the thesis where reference has been made to the work of others.

Publications

Kwan, A., et al., *An Overview of the Bench to Bedside Models of Breast Cancer in the Era of Cancer Immunotherapy*. Medical Research Archives, 2024. **12**(6)

Moamin, M.R., et al., Changes in the immune landscape of TNBC after neoadjuvant chemotherapy: correlation with relapse. *Frontiers in Immunology*, 2023. 14: p. 13.

Williams, S.T., et al., Precision oncology using *ex vivo* technology: a step towards individualised cancer care? *Expert Reviews in Molecular Medicine*, 2022: p. 1-48.

Published abstracts

Gagg H, Williams S, Allen R, Conroy S, Rominiyi O, Wells G, Rantala J, Danson S, Helleday T, Collis S. *Ex vivo*-led drug discovery in glioblastoma. *Brain Tumor Res Treat*. 2022 Mar;10(Suppl):S240.

Juncker-Jensen, A., et al., 828 Quantifying perivascular immune cells in the stroma of human triple negative breast tumors using deep learning spatial analytics. *Journal for Immunotherapy of Cancer*, 2021. 9(Suppl 2): p. A867-A867.

Moamin, M.R., et al., Perivascular accumulation of immunosuppressive cells in the stroma of human triple negative breast carcinomas: implications for immunotherapy. *Cancer Research*, 2021. 81(13): p. 1.

Table of contents

| | |
|---|-----------|
| Acknowledgements | 1 |
| Declaration..... | 2 |
| Publications..... | 3 |
| Published abstracts..... | 3 |
| Table of contents | 4 |
| List of figures..... | 7 |
| List of supplementary figures | 9 |
| List of tables..... | 9 |
| Abbreviations..... | 10 |
| Abstract..... | 13 |
| Chapter 1 General introduction | 14 |
| 1.1. Triple negative breast cancer | 14 |
| 1.1.1. Current treatments for TNBC..... | 15 |
| 1.1.2. Chemotherapeutic agents used in TNBC..... | 16 |
| 1.1.3. Treatments beyond chemotherapy..... | 17 |
| 1.1.4. Response rates and survival in TNBC | 18 |
| 1.1.5. Risk assessment in early breast cancer | 19 |
| 1.1.6. Biomarkers in breast cancer..... | 20 |
| 1.2. The tumour microenvironment..... | 22 |
| 1.3. Origins of macrophages | 24 |
| 1.4. Macrophage activation | 26 |
| 1.5. Tumour-associated macrophages..... | 28 |
| 1.5.1. Tumour angiogenesis | 30 |
| 1.5.2. Immunosuppression in tumours | 32 |
| 1.5.3. Metastases | 33 |
| 1.6. Macrophage function by location | 34 |
| 1.6.1. Tumour nest..... | 35 |
| 1.6.2. Tumour stroma..... | 35 |
| 1.6.3. Perivascular niche | 36 |
| 1.6.4. Invasive edge..... | 37 |
| 1.6.5. Hypoxic/Necrotic areas | 38 |
| 1.7. Multi-omic analysis of TAMs | 38 |
| 1.8. TAM responses to chemotherapy..... | 42 |

| | | |
|--|--|-----------|
| 1.8.1. | Chemoresponsiveness of tumours..... | 42 |
| 1.8.2. | Prevention of recurrence | 44 |
| 1.9. | Therapeutic targeting of TAMs. | 45 |
| 1.10. | Introduction to Methods..... | 49 |
| 1.10.1. | Multiplex immunofluorescence artificial intelligence segmentation..... | 49 |
| 1.10.2. | Immune microenvironment models of breast cancer | 50 |
| 1.10.2.1. | In vivo models of breast cancer | 50 |
| 1.10.2.2. | Ex vivo assays that attempt to preserve the TME integrity | 50 |
| 1.10.2.2.1. | Patient derived organoids | 52 |
| 1.10.2.2.2. | Dispersed methods | 52 |
| 1.10.2.2.3. | Microfluidic models..... | 52 |
| 1.11. | Summary | 53 |
| 1.12. | Project hypothesis and aims | 55 |
| Chapter 2 Materials and methods | | 56 |
| 2.1 | Materials and methods | 56 |
| 2.1. | Materials | 56 |
| 2.1.1. | List of reagents | 56 |
| 2.1.2. | List of commercial kits..... | 57 |
| 2.1.3. | List of materials | 57 |
| 2.1.4. | List of antibodies | 58 |
| 2.1.5. | List of Neogenomics antibodies | 59 |
| 2.1.6. | List of cell lines | 59 |
| 2.1.7. | List of equipment | 60 |
| 2.1.8. | List of software..... | 60 |
| 2.1.9. | List of breast cancer now TNBC samples..... | 61 |
| 2.2. | Methods | 63 |
| 2.2.1. | Ethics | 63 |
| 2.2.2. | Optimisation of staining for perivascular macrophages | 63 |
| 2.2.2.1. | Optimisation of CD68, MRC1 and CD31 stains in TNBC | 63 |
| 2.2.2.2. | Haematoxylin and eosin (H&E) staining of TNBC sections | 63 |
| 2.2.2.3. | Immunohistochemistry (IHC) | 64 |
| 2.2.2.4. | Immunofluorescence (IF) staining of TNBC sections..... | 64 |
| 2.2.2.5. | Biotin signal amplification | 65 |
| 2.2.2.6. | Image acquisition of perivascular staining | 65 |
| 2.2.2.7. | Assessment of dual labelling | 66 |
| 2.2.2.8. | Assessment of PV TAMs | 66 |
| 2.2.2.9. | Quality assurance of IHC | 66 |

| | | |
|----------|--|----|
| 2.2.3. | Multiplex analysis of TNBC sections | 67 |
| 2.2.3.1. | Human TNBCs | 67 |
| 2.2.3.2. | Selection of ROIs | 67 |
| 2.2.3.3. | Multiplex staining of TNBC sections by NeoGenomics Labs (NGs)..... | 68 |
| 2.2.3.4. | Quantitative image analysis using AI..... | 70 |
| 2.2.3.5. | Quality assurance of MultiOmyx staining | 72 |
| 2.2.4. | Generation of a microfluidic model | 72 |
| 2.2.4.1. | Subculture of human cell lines | 72 |
| 2.2.4.2. | Cell counting..... | 73 |
| 2.2.4.3. | Generation of fibroblast-conditioned medium | 73 |
| 2.2.4.4. | Immunofluorescent labelling of live cells..... | 74 |
| 2.2.4.5. | Generation of tumour spheroids..... | 74 |
| 2.2.4.6. | Generation of a microvascular network..... | 74 |
| 2.2.4.7. | Perfusion with tumour cells | 77 |
| 2.2.4.8. | Immunofluorescent staining of DAX-1 chips..... | 78 |
| 2.3. | Statistical analysis..... | 78 |

Chapter 3 Establishment and validation of immunostaining protocols for quantifying perivascular, tumour-promoting macrophages in human TNBCs on of PV Macrophages by Histological Analysis 80

| | | |
|--------|---|-----|
| 3.1 | Introduction | 81 |
| 3.1. | Results | 81 |
| 3.1.1. | Topography of triple negative breast cancers..... | 81 |
| 3.1.2. | Optimisation of IHC protocol for MRC1 ⁺ perivascular TAMs in TNBC | 82 |
| 3.1.3. | Optimisation of dual and triple IHC stains | 86 |
| 3.1.4. | Dual labelling with CD68 and MRC1 using IHC in sequential stained TNBC sections..... | 90 |
| 3.1.5. | Triple immunofluorescence | 91 |
| 3.1.6. | Validation of CD68 as a macrophage marker in TNBC sections using immunofluorescence staining. | 93 |
| 3.1.7. | Validation of MRC1 as a marker for PV TAMs in TNBCs..... | 94 |
| 3.1.8. | MRC1 ⁺ TAMs are mainly located in the stroma compared to the TCIs. | 96 |
| 3.2. | Discussion..... | 98 |
| 3.3. | Concluding remarks..... | 101 |

Chapter 4 Quantitative analysis of leukocytes and CXCR4 expression in human TNBC: Changes after neoadjuvant chemotherapy and correlation with metastasis 102

| | | |
|------|--------------------|-----|
| 4.1 | Introduction | 103 |
| 4.1. | Hypothesis..... | 107 |
| 4.2. | Results | 108 |

| | | |
|--|--|------------|
| 4.2.1. | Defining the spatial characteristics of TNBCs using AI-based image analysis | 108 |
| 4.2.2. | The stroma is more vascularised than TCIs in TNBCs. | 110 |
| 4.2.3. | Macrophage staining characteristics in TNBC sections. | 111 |
| 4.2.4. | Effect of neoadjuvant chemotherapy on the distribution and activation status of TAMs, CD4+ and CD8+ T cells, and Tregs..... | 114 |
| 4.2.5. | Declaration of contribution | 114 |
| | Supplementary figures and tables | 128 |
| 4.2.6. | NK cell infiltration is not altered by NAC and does not correlate with metastasis. | 134 |
| 4.2.7. | CXCR4 expression by cancer cells does not correlate with metastasis in untreated or NAC- treated TNBC | 135 |
| 4.2.8. | CXCR4 expression does not increase after NAC. | 136 |
| 4.2.9. | TAM expression of CXCR4 | 138 |
| 4.3. | Discussion..... | 139 |
| 4.4. | Concluding remarks..... | 147 |
| Chapter 5 Use of a microfluidics assay to model the stromal perivascular niche in TNBC..... | | 149 |
| 5.1 | Introduction | 150 |
| 5.2. | Aims..... | 151 |
| 5.2.1. | Impacted Aims..... | 152 |
| 5.3. | Results | 153 |
| 5.3.1. | Generating a microvascular network in the MFAs..... | 153 |
| 5.3.2. | Assessment of microfluidic flow | 156 |
| 5.3.3. | Perfusion of tumour cells | 158 |
| 5.3.4. | Co-culture with tumour spheroids | 159 |
| 5.4. | Discussion..... | 160 |
| Chapter 6 General discussion | | 163 |
| 6.1 | Wider considerations of the perivascular niche in tumours | 163 |
| 6.2. | Clinical implications..... | 165 |
| 6.3. | Further work and directions..... | 165 |
| | References | 168 |

List of figures

| | | |
|------------|--|----|
| Figure 1-1 | The origins of macrophages. | 25 |
| Figure 1-2 | Simplified view of the different states of macrophage activation. | 28 |

| | |
|--|-----|
| Figure 1-3 Precursors of Tumour-associated macrophages. | 29 |
| Figure 1-4 TAMs and the different compartment of the tumour microenvironment (TME). | 34 |
| Figure 2-1 TNBC tumour H&E with 20 ROIs selected | 68 |
| Figure 2-2 MultiOmyx™ tissue retention table..... | 70 |
| Figure 2-3 Defining the TCI, stroma and perivascular areas..... | 71 |
| Figure 2-4 Mixing of cells and solutions prior to injection in the DAX-1 chip..... | 75 |
| Figure 2-5 Schematic of the DAX-1 3D cell culture chip. | 77 |
| Figure 2-6 Perfusion of tumour cells through the vascular network..... | 78 |
| Figure 3-1 Identification of TCIs vs stromal areas in TNBC tumours. | 82 |
| Figure 3-2 Optimised single stains using TNBC tumours. | 85 |
| Figure 3-3 IHC staining of dual and triple stains on human TNBC tumours. | 87 |
| Figure 3-4 Detection of marker co-localisation in sequential sections. | 91 |
| Figure 3-5 Use of IF methods for staining and quantification. | 92 |
| Figure 3-6 Co-localisation of CD68 with CD45. | 94 |
| Figure 3-7 Co-localisation of MRC1 with CD68. | 96 |
| Figure 3-8 Expression of CD68 and MRC1 within TNBC tumours. | 96 |
| Figure 3-9 The characteristics of PV macrophages in treatment naïve vs. neoadjuvant chemotherapy treated TNBC tumours. | 97 |
| Figure 4-1 MultiOmyx™ Assay Workflow | 104 |
| Figure 4-3 Area and cell density of the TCI, stroma and perivascular regions..... | 110 |
| Figure 4-4 Vessel characteristics in untreated vs NAC treated TNBCs | 111 |
| Figure 4-2 Macrophage marker co-localisation and detection using CD68 and CD163. | 113 |
| Figure 4-5 NK cells density within the TME | 134 |
| Figure 4-6 Overall CXCR4 density within TNBC..... | 136 |
| Figure 4-7 Differences in CXCR4 in Untreated vs NAC treated tumour..... | 137 |
| Figure 4-8 Stromal/TAM expression of CXCR4 | 138 |
| Figure 4-10 Location of immune cell subsets within the TME in TNBC. | 140 |
| Figure 5-1 Different approaches to using primary tumours in an ex vivo setting..... | 151 |
| Figure 5-2 Microfluidic model setup of the TME | 152 |
| Figure 5-3 Generation of a microvascular network..... | 154 |
| Figure 5-4 Effects of fibroblasts on microvessel formation in MFAs | 155 |
| Figure 5-5 Microfluidic assay characteristics. | 157 |
| Figure 5-6 Perfusion of CSFS-labelled, MDA-231 tumour cells through the microvascular network..... | 158 |
| Figure 5-7 Generation of tumour spheroids..... | 160 |
| Figure 6-1 Microenvironment crosstalk | 163 |

List of supplementary figures

| | |
|--|-----|
| Suppl. Figure 1 Reduced density of stromal CD163+ TAMs correlate inversely with metastasis..... | 128 |
| Suppl. Figure 2 Representative appearance of PD-L1 expression by CD163+ TAMs and PanCK+ cancer cells in high/moderate PD-L1-expressing TNBCs. | 128 |
| Suppl. Figure 3 Frequency and distribution of TIM-3-CD163+TAMs. (A) TIM-3-CD163+ TAMs were present throughout the stroma in untreated and NAC-treated tumors. | 129 |
| Suppl. Figure 4 Receiver Operating Characteristic (ROC) curve analysis of the ability of three stromal TAM subsets to predict the development of metastasis in NAC-treated patients within 3 years of surgical removal of primary tumors (ROC analysis of data at the level of whole tumor sections). | 129 |
| Suppl. Figure 5 Expression of TIM-3 in human TNBC: correlation with RFS after NAC..... | 130 |
| Suppl. Figure 6 No effect of NAC on various CD163+ TAM subsets..... | 130 |
| Suppl. Figure 7 Correlation graphs for significantly different comparisons seen in Suppl. Table 2. | 131 |

List of tables

| | |
|---|-----|
| Table 1 Breast cancer subtypes. | 14 |
| Table 2 Drugs used for the treatment of TNBC. | 17 |
| Table 3 Summary of TMN tumour classification [29]. | 20 |
| Table 4 Definitions of biomarker types | 20 |
| Table 5 Summary of key biomarkers used within breast cancer | 22 |
| Table 7 Summary of immune cell markers | 23 |
| Table 8 Subsets of TAMs based off single cell omics. | 41 |
| Table 9 Clinical trials targeting TAMs. | 46 |
| Table 10 Single staining optimisation..... | 84 |
| Table 11 Dual staining optimisation. | 88 |
| Table 12 MultiOmyx™ multiplex antibody panel..... | 105 |

Abbreviations

| | |
|----------|---|
| AI | Artificial intelligence |
| ANG2 | Angiopoietin-2 |
| BLBC | Basal-like breast cancer |
| BLBC | Basal-like breast cancer |
| BRCA1 | Breast cancer gene 1 |
| BRCA2 | Breast cancer gene 2 |
| CA4P | Combretastatin-A4P |
| CAFs | Cancer-associated fibroblasts |
| CAR | Chimeric antigen receptor |
| CCR2 | C-C chemokine receptor type 2 |
| CSF-1 | Colony stimulating factor 1 |
| CSFE | Carboxyfluorescein succinimidyl ester |
| CTLA4 | Cytotoxic T lymphocyte-associated protein 4 |
| CXCL12 | C-X-C motif chemokine 12 |
| CXCR4 | C-X-C motif chemokine receptor type 4 |
| DPBS | Dulbecco's phosphate buffered saline |
| DTIC | 5-(3,3-dimethyl-1-triazenyl)-1H-imidazole-4-carboxamide |
| ECGM MV2 | Endothelial cell growth medium MV2 |
| ECGM2 | Endothelial cell growth medium 2 |
| ECM | Extra cellular matrix |
| EDTA | Ethylenediaminetetraacetic acid |
| EGFR | epidermal growth factor receptor |
| EMP | Erythron-myeloid progenitor |
| ER | Oestrogen receptor |
| FBS | Foetal bovine serum |
| FEC-T | Fluorouracil, epirubicin, cyclophosphamide and docetaxel (Taxotere) |
| FFPE | Formalin fixed paraffin embedded |
| FISH | Fluorescence in situ hybridisation |
| FN1 | Fibronectin 1 |
| FOLR2 | Folate receptor beta |
| GFP | Green fluorescent protein |
| H&E | Haematoxylin and eosin |
| hEGF | Human epidermal growth factor |

| | |
|---------------|--|
| HER2 | Human epidermal growth factor receptor 2 |
| hFGF | Human fibroblast growth factor |
| HIF-1 | Hypoxia inducible factor 1 |
| HIF-2 | Hypoxia inducible factor 2 |
| HLF | Human lung fibroblast |
| HSC | Haematopoietic stem cell |
| HUVECs | Human Umbilical Vein Endothelial cells |
| ICIs | Immune checkpoint inhibitors |
| IF | Immunofluorescence |
| IFN- γ | Interferon- γ |
| IGF | Insulin like growth factor |
| IHC | Immunohistochemistry |
| ISG15 | Interferon-stimulated gene 15 |
| LAG-3 | Lymphocyte-activation gene 3 |
| LYVE1 | Lymphatic vessel endothelial hyaluronan receptor 1 |
| MARCO | Macrophage receptor with collagenous structure |
| MDSCs | Myeloid derived suppressor cells |
| MFA | Microfluidic assay |
| MHC class II | Major histocompatibility complex class II |
| M-MDSCs | Monocyte-related myeloid-derived suppressor cells |
| MMTV-PyMT | Mouse mammary tumour virus-polyoma middle tumour-antigen |
| NAC | Neoadjuvant chemotherapy |
| NCRs | Negative checkpoint regulators |
| NLRP3 | NOD-like receptor protein 3 |
| OHRI | Ottawa Hospital Research Institute |
| PanCK | Pan cytokeratin |
| PARP | Poly-ADP ribose polymerase |
| PBMCs | Peripheral blood mononuclear cells |
| PDX | Patient derived xenograft |
| pCR | Pathological complete response |
| PD-1 | Programmed death 1 |
| PD-L1 | Programmed death ligand 1 |
| PDMS | Polydimethylsiloxane |
| PDX | Patient derived xenograft |
| PFS | Progression free survival |

| | |
|---------------|--|
| PgR | Progesterone receptor |
| PV | Perivascular |
| PVN | Perivascular Niche |
| qPCR | Quantitative polymerase chain reaction |
| qPCR | Quantitative polymerase chain reaction |
| RD | Residual disease |
| RFS | Relapse free survival |
| RNA-seq | RNA Sequencing |
| ROI | Region of interest |
| scRNA-seq | Single cell RNA sequencing |
| SDF-1 | Stromal derived factor |
| SEM | Standard error of the mean |
| SIRP α | Signal regulatory protein alpha |
| SPP1 | Secreted phosphoprotein 1 |
| TAM | Tumour associated macrophage |
| TBS | Tris buffered saline |
| TCI | Tumour cell island |
| TEMs | TIE2 expressing monocytes |
| TGF β | Transforming growth factor beta |
| TIM-3 | T-cell immunoglobulin and mucin domain 3 |
| TIM-4 | T-cell immunoglobulin and mucin domain 4 |
| TIMs | Tumour infiltrating monocytes |
| TMA | Tissue microarray |
| TME | Tumour microenvironment |
| TMEM | Tumour microenvironments of metastasis |
| TNBC | Triple negative' breast cancer |
| Tregs | Regulatory T cells |
| TRMs | Tissue resident macrophages |
| TROP-2 | Trophoblast cell-surface antigen 2 |
| VEGFA | Vascular endothelial growth factor A |
| WLE | Wide local excision |

Abstract

Background: Triple negative breast cancer (TNBC) remains a formidable challenge due to its high metastatic potential, limited treatment options and poor survival rates. In mouse models of cancer, tumour associated macrophages (TAMs) have been shown to accumulate around tumour blood vessels, where they promote tumour angiogenesis, immunosuppression and metastasis, reduce the efficacy of frontline anti-cancer treatments, and drive relapse.

Methods: Multiplex immunofluorescence staining and AI-based image analysis were used to quantify TAMs (and other immune cells) in perivascular (PV) and non-PV areas of human TNBCs in both untreated and neoadjuvant chemotherapy (NAC)-treated TNBCs. This was assessed in both tumour cell islands and the tumour stroma. Follow-up data for a 3-year period after surgery enabled these immune features to be correlated with metastasis. An *ex vivo* microfluidics assay was also established to model the PV features observed in TNBC sections. This used human endothelial cells to create perfusable microvessels in a fibrin gel, fibroblasts, cancer cells and macrophages.

Results: In tumours from patients who developed metastases after NAC, there were significantly lower levels of stromal CD163⁺ TAMs (especially those expressing the negative checkpoint regulator, T-cell immunoglobulin and mucin domain 3, 'TIM-3') than in those from disease-free patients. Although these cells were predominantly PV in tumours, significant differences in their density between the above 2 patient groups were only seen in non-PV areas of the stroma. CD4⁺ T cells (but not CD8⁺ T cells) preferentially located to PV areas in all TNBCs, whereas Tregs only did so only after NAC. Distinct subsets of CD4⁺ and CD8⁺ T cells formed PV clusters with CD163⁺ TAMs and Tregs which were retained after NAC.

Conclusions: The density of stromal TIM-3⁺ CD163⁺ TAMs may represent a new biomarker in NAC-treated TNBC to identify patients at a higher risk of relapse.

Chapter 1 General introduction

1.1. Triple negative breast cancer

The most recently published figures in England (2017) show there were 305,683 newly diagnosed cases of cancer in England. Of those cases 46,109 (15.1%) were women with breast cancer making it the most common cancer in England. The number of deaths in 2017 from breast cancer totalled 9,502, making breast cancer to rank as 4th highest cause of all cancer related deaths in England [1].

Breast cancer is a heterogeneous disease resulting in differing pathologies, therapeutic responses, and overall outcomes. Despite advances that have highlighted its molecular complexity indicating that there are up to 10 different subtypes [2], treatment is still mainly based on the assessment of the hormone receptors oestrogen receptor (ER) and progesterone receptor (PgR) by immunohistochemistry (IHC) and the cellular proliferation marker Ki-67. And by assessment of the protein human epidermal growth factor receptor 2 (HER2) by IHC or fluorescence in situ hybridisation (FISH). The results of this assessment help to categorise the cancer into the subtypes listed in **Table 1-1**.

Table 1 Breast cancer subtypes.

The current main molecular subtypes of breast cancer and their marker status. ER; oestrogen, PgR; progesterone, HER2; human epidermal growth factor receptor 2.

| Subtype | Hormone receptor | HER2 status | Prevalence |
|---------------|-----------------------|-------------|------------|
| Luminal A | ER+ and/or PgR+ | HER2- | 50-60% |
| Luminal B | ER+ and/or PgR+, Ki67 | HER2+/- | 15-20% |
| HER2 positive | ER/ PgR+/- | HER2+ | 10-15% |
| TNBC/ BLBC | ER-, PgR- | HER2- | 10-25% |

Treatment options based of these subtypes lead to enhanced survival rates for some subtypes as the receptors expressed present viable targets for anticancer therapeutics. 'Triple negative' breast cancer' (TNBC) accounts for around 10-25% of all breast cancers. It has either low or no levels of ER, PR and HER2, although the definitions of can vary from <1% of cells positive for receptors up to <10% of cells

positive [3]. It is characterised by an earlier age of onset, poorer prognosis and greater metastatic potential than the other breast cancer subtypes [4-8]. This is in part due to the lack of targeted therapies that are available to non-TNBC tumours. ER⁺/PgR⁺ breast tumours can be targeted with hormone treatments (tamoxifen, fulvestrant, aromatase inhibitors, including anastrozole, exemestane and letrozole) and HER2⁺ tumours with targeted therapies (e.g. trastuzumab).

One study of TNBC classification looked at the gene expression profiles of nearly 600 TNBC cases. The subsequent cluster analysis identified 6 subtype signatures. This included basal type1 and 2, immunomodulatory, mesenchymal, mesenchymal stem-like and luminal androgen receptor subgroups. Further analysis of these subgroups and their features may help act as future biomarkers to help triage patients for more targeted therapies [9].

Another subtype of breast cancer that is often wrongly interchanged with TNBC due to its similar histological features is Basal-like breast cancer (BLBC). Over 90% of BLBC are also TNBC according to histological classification [10]. But it is the molecular classification that differentiates BLBC from TNBC as cancer cells in the former typically expressing epidermal growth factor receptor (EGFR) and the cytokeratin gene KRT5, 14 and 17. Other genes that are heavily linked, but not exclusive to BLBC, are the mutated breast cancer gene 1 (BRCA1) and mutated breast cancer gene 2 (BRCA2) genes that are involved in DNA damage repair [11].

1.1.1. Current treatments for TNBC

With the lack of targeted therapies available for TNBC patients, the main options available are surgery, chemotherapy and radiotherapy. Treatment is dictated by the tumour size, location, stage, grade and spread of the tumour and how differentiated the tumour cells area.

Chemotherapy is often the main treatment for TNBC and is administered in the neoadjuvant (pre-surgery) and/or adjuvant (post-surgery) setting. Neoadjuvant therapy is often used to treat tumours considered to be at higher risk of metastasis or to improve surgical options for tumours that are considered unsuitable for resection. It also allows the initial assessment of tumour response to treatment, which can then inform later treatment as an adjuvant therapy in cases where poor initial responses are seen [12, 13]. The use of adjuvant chemotherapy post-surgery is used to attempt

to clear any remaining malignant cells in the general circulation and lymph nodes to reduce the risk of metastasis. Surgical resection is an integral part of most treatments, smaller tumours will undergo a wide local excision (WLE), to remove the cancer and a margin of healthy surrounding tissue. In cases with larger or more fragmented tumours, the complete removal of breast tissue may be required through a mastectomy. Following a WLE, radiotherapy is often given to target any remaining malignant cells remaining at the site of surgery, if the patient has undergone a mastectomy, radiotherapy would then be given to the chest [14].

1.1.2. Chemotherapeutic agents used in TNBC

A variety of chemotherapeutics are used in the neoadjuvant or adjuvant treatment of TNBC, including anthracyclines, taxanes, anti-metabolites, cyclophosphamide, and platinum agents which are summarised in **Table 1-2**.

Anthracyclines, including doxorubicin and epirubicin inhibit proliferation by blocking DNA and RNA synthesis through intercalation between the base pairs of DNA/RNA strands. Fluorouracil and methotrexate are antimetabolites which inhibit thymidylate synthase, this prevents the production of thymidine that is needed for DNA replication and repair [15]. Taxanes, including paclitaxel and docetaxel, inhibit cell division by disrupting microtubule function and thus preventing mitosis [16]. They are used as both single agents and in combination with other chemotherapeutic agents including anthracyclines and cyclophosphamide. [17]. Cyclophosphamide causes inter-strand and intra-strand DNA crosslinking, interfering with DNA replication. Metabolic activation of the drug is required by phosphamidase, an enzyme that is expressed at high levels by some cancerous cells. [18]. Within the UK, anthracyclines, antimetabolites, cyclophosphamide and taxanes are typically given as part of a FEC-T (fluorouracil, epirubicin, cyclophosphamide and docetaxel (taxotere) treatment regimens.

Platinum agents such as carboplatin and cisplatin work to interrupt the cell cycle with their metabolites binding to guanine, creating double strand breaks and preventing DNA transcription [19]. There is no single optimal treatment regimen for TNBC, although neoadjuvant chemotherapy regimens often include an anthracycline and taxane as they produce the highest response rates in this patient group [17, 20].

Table 2 Drugs used for the treatment of TNBC.

The current classes of chemotherapeutic agents used in TNBC treatment.

| Class of drug | Examples of drug | Mechanism of action |
|----------------------|----------------------------|--|
| Anthracycline | Doxorubicin, Epirubicin | Intercalation into DNA, blocking DNA synthesis |
| Antimetabolites | Fluorouracil, Methotrexate | Inhibit thymidylate synthase |
| Taxane | Paclitaxel, Docetaxel | Disruption of microtubule formation |
| Nitrogen mustard | Cyclophosphamide | Inter/intra-stand DNA crosslinking |
| Platinum agents | Carboplatin, Cisplatin | Generation of double strand DNA breaks |

1.1.3. Treatments beyond chemotherapy

There have been advances in treatment of TNBC with new and emerging therapies. One of these is the use of immune checkpoint inhibitors. Recently, Pembrolizumab, an antibody against programmed death 1 (PD-1) on T cells, has been approved for use in early, high-risk cases of TNBC. When given alongside neoadjuvant chemotherapy, it has been shown to reduce distant recurrence after 36 months from 13.1% to 7.7%, with the risk of disease progression 37% lower in the pembrolizumab treated group when compared to placebo and neoadjuvant therapy alone [21]. Treatment outcome was found to be independent of programmed death ligand 1 (PD-L1) expression. This was in contrast to another trial of pembrolizumab and chemotherapy within late stage metastatic TNBC, where patients with high levels of PD-L1 levels led to better improvement in progression free survival (PFS) [22]. This suggested that baseline PD-L1 levels in early TNBC play a different role to that seen in late stage TNBC tumours.

As well as this form of immunotherapy, targeted therapies such as PARP (poly-ADP ribose polymerase) inhibitors are likely to play a role in future treatments and currently undergoing trials [23]. PARP inhibitors block the role of the poly-ADP ribose polymerase in cell repair mechanisms. When paired with patients who have a mutated BRCA gene, it is an effective treatment and already proven to be effective in ovarian and fallopian tube cancers where BRCA1 and BRCA2 mutations are present. Up to 20% of TNBC tumours have been shown to have an altered BRCA1/2 genes [24], making PARP a great example of the new therapies that may be available to TNBC patients.

Antibody drug conjugates (ADCs) are also approved for the treatment of metastatic TNBC. ADCs work by combining monoclonal antibodies that are specific to a tumour antigen with a cytotoxic compound. This enables the efficient delivery of the cytotoxic compound to the tumour cells. Sacituzumab govitecan is an ADC that targets trophoblast cell-surface antigen 2 (TROP-2) a transmembrane signal inducer that is expressed on the surface on breast cancers. It is coupled to topoisomerase I inhibitor, SN-38. Within the phase III trial in metastatic TNBC, mean PFS was 5.6 months for Sacituzumab govitecan vs 1.7 months for single agent chemotherapy [25].

1.1.4. Response rates and survival in TNBC

Patients with TNBC often have distinctive clinico-pathological features compared to other forms of breast cancer including age at diagnosis (with TNBC patients characterised by a younger patient group), larger tumour sizes and higher tumour grades at diagnosis and an increased incidence amongst Black and Hispanic populations [4, 5].

Pathological complete response (pCR) is defined as the absence of remaining neoplastic cells (known as residual disease; 'RD') in the breast and axillary nodes after neoadjuvant treatment [26]. Women with TNBC who were treated with chemotherapy regimens that included anthracyclines or taxanes, had higher pCRs (22%) than those with receptor positive breast cancers (11%) [5]. This enhanced response is despite the typically larger size and higher grade of TNBCs mentioned earlier. However, patients who did not achieve pCR after receiving this form of neoadjuvant chemotherapy are at greater risk of recurrence within the first 3 years after diagnosis than those with receptor positive breast tumours [5, 6]. Indeed, in patients who had RD after receiving neoadjuvant chemotherapy, there was significantly reduced OS (68%) compared to patients with receptor positive breast cancers (88%) in the first three years post diagnosis. After this initial period, the risk of recurrence then became higher for receptor positive breast cancers than for TNBCs. All deaths in the TNBC group occurred within 10 years of diagnosis, whereas ER+ breast cancers had deaths linked to breast cancer up to 18 years after the original diagnosis [4, 5]. However, there are several limitations in these findings as there were differences between the TNBC and the ER+ groups in the number of

cycles of treatment administered, as well as the type of chemotherapy given. Also, as studies covered up to a 20-year period, during that timeframe, more efficient regimens were developed and used to treat patients. It is also stated within the studies that in some cases up to a third of patients were excluded due to a lack of information on the receptor status of their breast cancer.

1.1.5. Risk assessment in early breast cancer

To ensure the best outcomes can be achieved by patients, treatment is tailored to clinical features of the tumour, to aid with the slowing of disease progression, preventing recurrence, and improving overall survival. This is mainly done through the screening of tumour biopsies. Tumour node metastases staging (TMN) is a scoring system used to assess the initial tumour burden based on the tumour size (T), lymph node involvement (N) and the presence of metastases (M) (**Table 3**) and is used to aid treatment decisions within breast cancer, alongside hormone/HER-2 status to accurately inform on treatment decisions [27]. In a study looking at the clinical relevance of TNM staging related to RFS in breast cancer subtypes amongst 1879 patients. Variation was seen between the subtypes, with TNM staging of TNBC and HER-2 patients being less predictive of outcome compared to the other subtypes. Specifically, in TNBC, TNM staging did not correlate tumour stage with clinical outcome and could not differentiate between stages 1–3 [28].

| Stage | Criteria |
|-------|---|
| Tx | Primary tumour cannot be assessed |
| T0 | No evidence of primary tumour |
| Tis | Carcinoma in situ |
| T1 | Typically <2cm in greatest dimension; limited local invasion. |
| T2 | >2 cm but no more than >5 cm |
| T3 | Tumour over >5 cm |
| T4 | Tumour of any size, invading adjacent organs or tissues |
| N0 | No regional lymph node involvement |
| N1 | Metastasis in a small number of regional lymph nodes |
| N2 | Metastasis in multiple regional lymph nodes |
| N3 | Extensive regional lymph node involvement |
| M0 | No distant metastasis |
| M1 | Presence of distant metastasis |

Table 3 Summary of TMN tumour classification.

Adapted from Brierley et al 2017. TNM classification of malignant tumours [29].

As mentioned in section 1.1.4, the rates of pCR and RD within TNBC are indicators of the future prognosis and disease outcome. Across all breast cancers achieving pCR is associated with a significantly reduced risk of relapse and improved long-term survival, but this effect is seen to be stronger in TNBC and HER2-positive tumours [30]. In contrast, a higher burden of RD is strongly associated with an elevated risk of recurrence and poorer OS due to the treatment resistance/chemoresistance displayed by the remaining cancer cells [31]. This risk is particularly pronounced in TNBC, where even minimal residual disease can present a significantly worse prognosis due to the aggressive nature of the disease and the current lack of targeted post-neoadjuvant therapies [32].

1.1.6. Biomarkers in breast cancer

Biomarkers are measurable indicators of biological or pathological processes and are used for detecting disease, diagnosing conditions, predicting outcomes, and monitoring treatment responses [33]. The different kinds of biomarkers defined in

Table 4.

| Type of biomarker | Definition |
|-------------------|---|
| Diagnostic | Used to Identify the presence of a disease or condition. |
| Prognostic | Indicators of outcome irrespective of treatment. |
| Predictive | Predictors of response to specific treatments. |
| Pharmacodynamic | Reflect biological responses to a treatment |
| Susceptibility | Indicate the potential of developing a disease in the future. |
| Monitoring | Assess disease status or treatment effectiveness over time. |
| Safety | Indicate the likelihood of adverse effects from a treatment. |

Table 4 Definitions of biomarker types

Adapted from the biomarker Biomarker Working Group [34].

Within breast cancer the biomarkers available are broadly prognostic and/or predictive indicating likely outcomes and guiding treatment. Breast cancer biomarkers are summarised in **Table 5** and differ in their clinical applications and relevance to specific subtypes, particularly TNBC, highlighting an ongoing need for novel biomarkers to improve patient outcomes.

| Biomarker | Type | Relevance to TNBC | Testing Method | Refs |
|---|--|---|---|-------------|
| Oestrogen Receptor (ER) | Prognostic, Predictive ER-positive tumours generally have a better prognosis and respond to endocrine therapy. | Absent/low levels in TNBC. Present in most non-TNBC cases; ER positivity indicates hormonal sensitivity. | IHC on tumour tissue | [35] |
| Progesterone Receptor (PR) | Prognostic, Predictive PR positive tumours associated with a better outcome. | Absent/low levels in TNBC. | IHC on tumour tissue | [35] |
| Human Epidermal Growth Factor Receptor 2 (HER2) | Prognostic, Predictive Overexpression indicates more aggressive disease Predicts benefit from anti-HER2 therapies. | Absent/low levels in TNBC. | IHC and/or in situ hybridisation (ISH) on tumour tissue | [36] |
| Ki-67 | Prognostic High Ki-67 correlates with more aggressive disease; Used to distinguish between luminal A vs. luminal B subtypes. | Higher Ki-67 levels seen in TNBC | IHC on tumour tissue | [37-39] |
| PD-L1 (Programmed Death-Ligand 1) | Predictive PD-L1 positivity may predict response to checkpoint inhibitors in advanced TNBC. | More frequently expressed in TNBC. | IHC on tumour tissue | [40] |
| BRCA1/2 | Predictive Indicates sensitivity to PARP inhibitors. Highlights hereditary risk. | BRCA mutations more common in TNBC (20%) | Genetic testing | [24, 41] |
| p53 | Prognostic p53 mutations correlate with aggressive disease and poorer outcomes | p53 mutations are more common in TNBC | IHC on tumour tissue Genetic testing | [42, 43] |
| TILs (Tumour-Infiltrating Lymphocytes) | Prognostic, Predictive Higher TILs correlate with better prognosis and improved response to NAC. | Higher in TNBC, correlates with better survival and better chemotherapy responses. | Evaluation of TIL presence in H&E-stained tumour sections | [44-46] |

| | | | | |
|---------------------------------------|---|---|----------------------------|----------|
| CTCs (Circulating Tumour Cells) | Prognostic Higher CTC counts are associated with poorer survival. . | The presence of circulating tumour cells two years after adjuvant chemotherapy was associated with worse overall and disease-free survival in TNBC. | Blood test (liquid biopsy) | [47, 48] |
|---------------------------------------|---|---|----------------------------|----------|

Table 5 Summary of key biomarkers used within breast cancer

1.2. The tumour microenvironment

The tumour microenvironment (TME) is composed of many of many different cell types, including the malignant cancer cells that often form Tumour nests or tumour cell islands (TCI). These islands are often surrounded by the stroma, which is made up of the extracellular matrix (ECM) proteins such as collagen and fibrinogen. The stroma is also filled with many non-malignant cell types such as fibroblasts that help to produce the ECM, endothelial cells that help make up the vasculature and leukocytes that form the immune cell response [49]. Leukocytes have been shown to increase substantially within breast cancer when compared with non-malignant breast tissue [50]. Leukocytes express the cell surface marker CD45 and are made up of several types of immune cell, including CD3+ expressing lymphocytes (commonly referred to as T cells) which includes CD4+ T helper cells, CD8+ cytotoxic T cells and FOXP3+ T regulatory cells. Other leukocytes found in smaller number with the TME include CD19/CD20 expressing basophils, neutrophils and eosinophils and CD56 expressing natural killer cells (NK cells). These cells and their marker combinations are summarised in **Table 6**.

| Cell Type | Recognised Markers (Markers used) | Role in Breast Cancer |
|-------------|--------------------------------------|--|
| Macrophages | CD68+, CD163+ CD14 | Recruited into the tumour microenvironment, and shown to promote tumour progression, angiogenesis, and immunosuppression [51]. |
| CD8 T Cells | CD3+ CD8+ | Cytotoxic T cells can directly kill tumour cells; higher CD8+ T-cell infiltration often correlates with better prognosis [51]. |

| | | |
|-------------|--|---|
| CD4 T Cells | CD3+ CD4+ | Helper T cells modulate immune responses through cytokine release and help in the activation of B cells, cytotoxic T cells, and macrophages [51]. |
| Treg Cells | CD3+ CD4 FOXP3+ <i>CD25, CD127</i> | Treg cells suppress anti-tumour immune responses, enabling tumour immune evasion; higher Treg infiltration correlates with poor prognosis [52]. |
| NK Cells | CD3-, CD56, CD16+ | As innate immune cells, NK cells can kill tumour cells without prior sensitisation [53, 54]. |

Table 6 Summary of immune cell markers

Tumour infiltrating lymphocytes (TILs) are a grouping of lymphocyte populations including T helper cells, cytotoxic T cells and Tregs. The association between the frequency of TILs and relapse-free survival (RFS) in breast cancer was noted over 30 years ago where moderate or dense infiltration was associated with better relapse-free and overall survival compared to weak infiltration in a group of 489 breast tumours [55]. Within TNBC, there have been two large retrospective studies on archived tissue. The first study looked at 3771 breast tumours, of which 906 were TNBC. TILs were scored as low (0–10%), intermediate (11–59%), or high (60–100%) from H&E stains of core biopsies taken before NAC. From this it was found that high TIL numbers was associated with longer DFS in TNBC – something that was not seen in HER-2+ tumours [44]. The second study focused on early stage TNBC where they looked at 2148 tumours. Here, they found that stromal TILs were prognostics and that every 10% increment in stromal TILs corresponded with increased DFS. One issue noted was that the study contained no patients from the last 10 years, so no patients received platinum agents or immunotherapies to treatment strategies [45].

Regulatory T cells (Tregs) play a pivotal role in shaping the TME TNBC. These cells, primarily identified by their FOXP3 expression, accumulate in significant numbers within TNBC tumours, where they orchestrate multiple immunosuppressive mechanisms. By secreting anti-inflammatory cytokines such as interleukin-10 (IL-10) and transforming growth factor-beta (TGF- β), Tregs limit the activity of both CD4⁺ helper T cells and CD8⁺ cytotoxic T cells, limiting the efficacy of the immune

response [56]. The ability of Tregs dampen T cell function contributes to tumour progression, by reducing the potency of the immune response.

Elevated Treg infiltration in TNBC has been linked to poor clinical outcomes, including decreased overall survival, largely owing to the profound immunosuppressive environment these cells create [52]. Understanding how Tregs accumulate and function within TNBC tumours is critical for developing therapeutic strategies that are able to counteract their immunosuppressive effects and improve patient outcomes.

NK cells are a type of cytotoxic cell in the innate arm of the immune system. They are inhibited through the binding of MHC class I (MHC I) on normal cells, which allows them to target MHC I-deficient cancer cells [53]. NK cell cytotoxicity towards cancer cells utilises granzymes, perforin and apoptosis-inducing ligands such as TRAIL and FASL to kill tumour cells. They also coordinate the T cell response by facilitating the recruitment, activation, and proliferation of dendritic cells through the secretion of chemokines such as CCL5 and IFN γ [54].

There are limited data on the role of NK cells in TNBC. One study, using 278 TNBC tumours, showed that higher level of stromal NK cell infiltration - identified using an antibody to Nkp46, a marker of cytotoxic human NK cells, was associated with good clinicopathological features, whereas low infiltration was associated with shorter survival [57]. Another study though reported that NK cells were pro-tumourigenic when cultured with murine TNBC cells *in vitro*, and then found that higher numbers of immature NK cells (defined as CD56^{bright} when analysed by flow cytometry) were found within human TNBC (n=17) compared to other forms of breast cancer. High numbers in the TME of the TNBCs was linked to poor OS [58].

Of note though, CD68 or CD163 expressing macrophages have long been shown to associate with poor prognostic and progression in breast cancer and shape the TME [59, 60]. As will be discussed later in the chapter, macrophages are seen to aid tumour progression in multiple ways by promoting angiogenesis [61], immunosuppression and metastasis [62].

1.3. Origins of macrophages

Macrophages are a diverse type of myeloid cell found throughout all healthy tissues and organs (and some body fluids like the peritoneal fluid). They are often

responsible for tissue homeostasis, regulation of growth and regeneration. They also play a major role in the innate defence against pathogens and tumour response through cytokine production, inflammation, phagocytosis and antigen presentation, [63, 64].

There had been a long-held view that macrophages were recruited and derived from circulating blood monocytes, that are derived from haematopoietic stem cells (HSCs) in the bone marrow. However, this long held view has changed due to the advancement of cell lineage tracing methods in mice that allow that permanent tagging and tracking of cell types during development. These have indicated that macrophages originate from progenitors in the: (i) foetal yolk sac, (ii) foetal liver and (ii) bone marrow, or a mixture of these (**Figure 1-1**) [65-67].

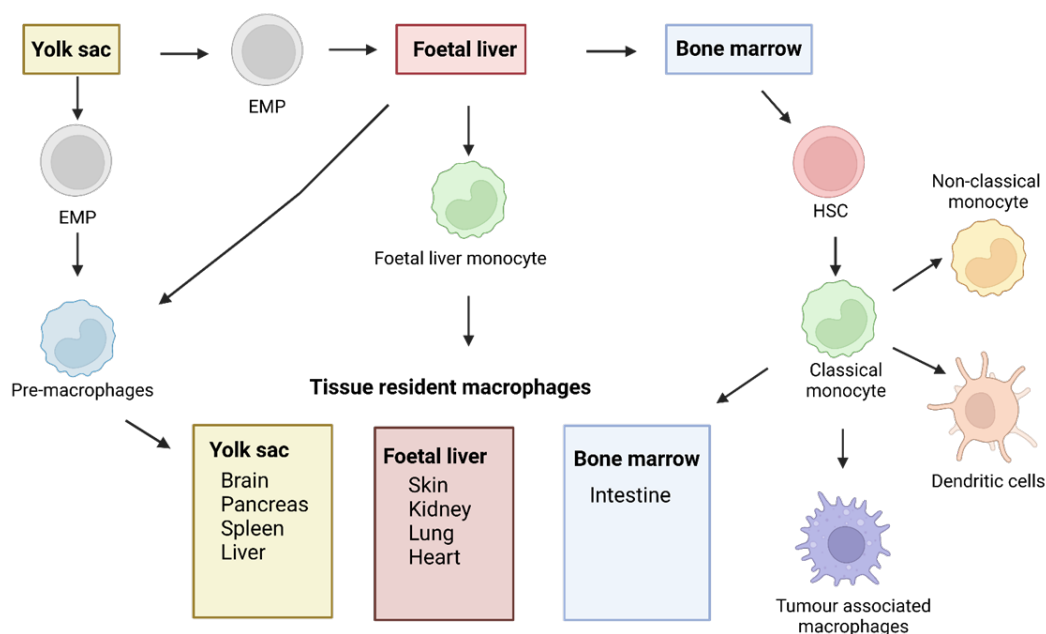


Figure 1-1 The origins of macrophages.

Macrophages have been shown to derive from three main sources, erythromyeloid progenitors (EMP) in the embryonic yolk sac and foetal liver, or haematopoietic stem cells (HSCs) in the adult bone marrow. Macrophages differentiate in response to local cues to become tissue-specific macrophages. Created with BioRender.com

Tissue resident macrophages (TRMs) are a type of macrophages that are found to permanently reside within different tissues in throughout the body such as

microglia in the brain, Kupffer cells in the liver, lung alveolar macrophages and Langerhans cells in the skin.

TRMs can originate from several sources, with those in the lung, brain and liver are derived from local erythromyeloid progenitors derived from the foetal yolk sac, rather than blood monocytes [66]. This TRM population is maintained through proliferation within tissues. Conversely, replenishment from blood monocytes is required to maintain TRM populations in the intestines, heart and mammary gland [61, 68, 69]. Some TRMs are primarily derived from once source only. For example, microglia in the brain are derived from yolk sac progenitors [70] whereas macrophages in intestinal mucosa are derived from the bone marrow [71].

It has been shown that there are potentially 3 TRM subpopulations that exist within tissues. TLF+ TRMs that are T-cell immunoglobulin and mucin domain 4+ (TIM4), lymphatic vessel endothelial hyaluronan receptor-1+ (LYVE1) and folate receptor beta+ (FOLR2). TLF+ TRMs that develop from foetal progenitor cells and are long lived. C-C chemokine receptor type 2+ (CCR2) TRMs that are replenished from the circulating monocyte pool and are short lived. And major histocompatibility complex class II^{high} (MHC class II) that have a mixed origin [72].

In healthy individuals, human blood monocytes are grouped into classical (CD14⁺⁺ CD16⁻) non-classical (CD14⁺ CD16⁺⁺) and intermediate (CD14⁺⁺ CD16⁺) subsets. Classical monocytes are shown to account for 80-90% of all blood monocytes, but all subsets have the ability to differentiate into macrophages *in vitro* [73, 74]. In mice there are only two populations, with classical monocytes distinguished as Cx3CR1^{LO}, CCR2⁺, Ly6CHI and non-classical Cx3CR1^{HI}, CCR2⁻, Ly6C^{LO} [75].

Although we know more about the early development stage of macrophages, it is still not known how ageing affects the longevity of TRM subpopulations. It also remains to be seen how macrophages derived from difference sources respond to the same signals within tissues or how these populations change through their life lifespan.

1.4. Macrophage activation

Plasticity is a hallmark of macrophages, allowing an adaptive response to the diverse microenvironment signals received in different tissues (normal and

diseased). Macrophage activation (sometimes referred to as 'polarisation') usually occurs in response to external stimuli such as cytokines, chemokines and microbial products, and result in distinct gene expression profiles that define certain macrophage activation states. A now outdated and simplistic model of this (**Figure 1-2**) is based on a spectrum with 'classically' activated (M1) and 'alternatively' activated (M2) activation states - at either end of a spectrum of macrophage activation [76, 77]. M1 skewed macrophages were defined as being polarised by the bacterial LPS and Th1- derived interferon- γ (IFN- γ), stimulating macrophages to express the IL-12^{high}, IL-10^{low} cytokine profile, and produce the Th1 attracting chemokines, CXCL9 and CXCL10. In contrast, M2 skewed macrophages are induced by Th2-derived IL-4, IL-13 and IL-33, stimulating macrophages to express the IL-12^{low}, IL-10^{high} cytokine profile, upregulate CCL17, CCL22 and CCL24 production, and recruit CCR4 and CCR3 expressing Th2 cells, T_{reg} cells, basophils and eosinophils [78]. M2 macrophages usually also express higher levels of scavenger receptors (CD163), mannose receptor (CD206) and TIE2 [76, 79, 80].

M1-like macrophages are better equipped for the clearing of microorganisms and tumour cells owing to their enhanced antigen presenting function, production of pro-inflammatory cytokines and ability to elicit a Th1 lymphocyte response. M2-like ones, on the other hand, are better suited to scavenging cellular debris, promoting angiogenesis and the remodelling and repair of tissue [78]. There are also subdivisions of the M2 activation state - described as M2a, M2b and M2c macrophages. M2a are induced through IL-4 or IL-13 with M2b induced by activation of the Toll like receptor and immune complexes while M2c is induced by IL-10 and glucocorticoid hormones. All three of these M2 subsets are involved in the Th2 responses with M2a taking part in inflammation, M2b involved in immune regulation and M2c involved in immune regulation and tissue remodelling [78, 81]. There will likely be many more subdivisions of the M1 and M2 activation states defined in the future reflecting the plasticity and diversity of macrophages in living organisms. Although this M1/M2 paradigm of macrophage activation had been used widely it is now generally considered to be an outdated oversimplification that under-represents the diversity of macrophages [82].

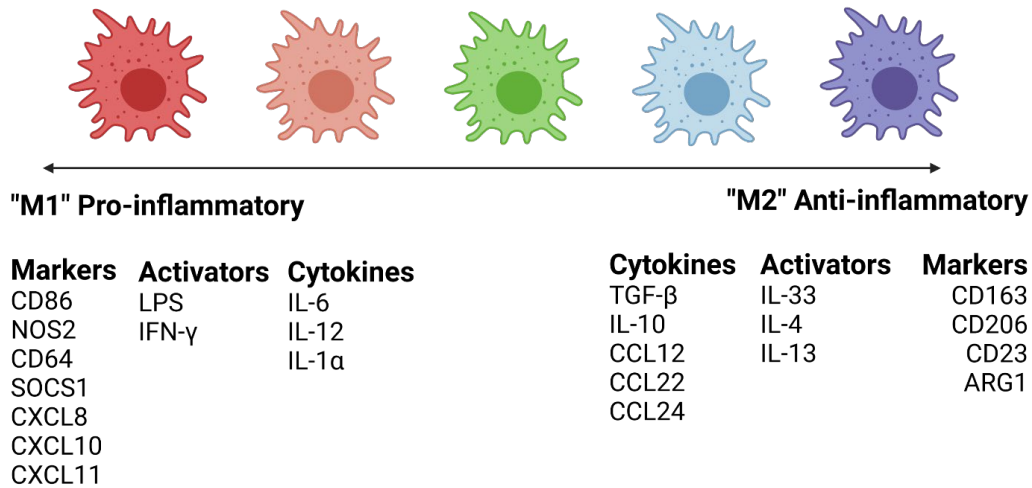


Figure 1-2 Simplified view of the different states of macrophage activation.

Macrophages were originally thought to be only M1 or M2 with classic markers such as NOS and ARG1 helping to differentiate their function. This spectrum is now known to be incredibly diverse, with macrophages known for their plasticity. Created with BioRender.com

1.5. Tumour-associated macrophages

Macrophages within tumours are commonly referred to as 'tumour associated macrophages' (TAMs) and are a major form of leukocyte in such tissues [44]. They are commonly identified using the pan macrophages markers CD68 and/or CD163.

The use of CD68 as a pan macrophages marker for macrophages is debated. CD68 is a transmembrane glycoprotein that is associated with the lysosomal/endosomal compartment of cells. It is part of the lysosomal-associated membrane proteins (LAMPs) family, which includes 5 other LAMPs that are similar in structure [83]. CD68 is highly expressed on macrophages and its expression is also seen amongst other myeloid cell types including monocytes and dendritic cells. But it is also seen to label non myeloid cell types including fibroblasts and endothelial cells [51, 84]. Its lack of specificity puts a question mark over the accurate identification and quantification of macrophages/TAMs within tissues and has the potential to misinterpret results.

High numbers of CD68+ TAMs correlate with a poorer prognosis in various forms of human cancer including breast cancer [44, 45], however this may depend on tumour type as it links with better prognosis in stomach cancers and non-small cell lung cancer [46]. Sometimes, different results are found when correlating TAM

density with prognosis in the same cancer type [44]. This may be down to factors like differences in the size and grade of tumours analysed, or the treatment the patients had received prior to surgical removal of the tumours. There may also be differences in the how the TAM analysis was conducted, with different macrophage-labelling antibodies used and thresholds set for determining high and low TAM counts [44].

The first study to look at the correlation between TAMs and clinical outcome in breast cancer [45] found that highly vascularised tumours had higher numbers of CD68+ TAMs, although the latter were mainly located in poorly vascularised tumour areas. A follow-on study by the same group then showed that TAMs in hypoxic areas of breast tumours express the pro-angiogenic cytokine, vascular endothelial growth factor A (VEGFA) [47]. Furthermore, a subsequent study in mice showed that TAMs are the major source of VEGFA in mammary tumours, not tumour cells [48].

Initially, TAMs in mouse tumours were also thought to be derived largely from blood monocytes [85], however, recent studies have shown that, in some mouse models of brain and pancreatic cancer, they are derived both from these cells in the circulation and the local proliferation of embryonic macrophages (**Figure 1-3**) [86, 87]. Further studies are now underway to see if this mixed ontogeny extends to other tumour types, and indeed, to any form of human tumour.

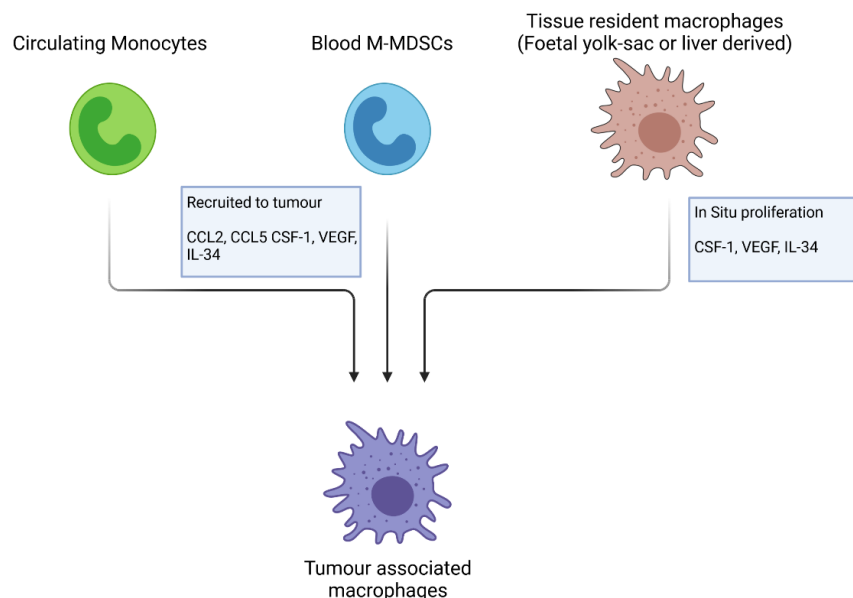


Figure 1-3 Precursors of Tumour-associated macrophages.

TAMs are derived from several sources including circulating monocytes, and monocyte-related myeloid-derived suppressor cells (M-MDSCs). Cytokines and chemokines including

CCL2, CSF-1, VEGF and IL-34 drive the recruitment and differentiation. They can also derive from tissue resident macrophages found within the tissues through in situ proliferation in response to IL-34 and CSF-1. Adapted from Mantovani et. al 2017 [88] Created with BioRender.com.

Blood monocytes are recruited to tumours by colony stimulating factor -1 (CSF-1), with high levels expressed by tumour cells and various stromal cell types [89]. IL-34 can also be expressed by tumours and act upon monocyte CSF-1R to recruit these cells into tumours [90]. Other recruitment factors include the chemokines, CCL2 [91] and C-X-C motif chemokine 12 (CXCL12) (also known as stromal derived factor; SDF-1). Targeting of CSF-1 in mouse tumour models, resulted in a reduced numbers of TAMs, which resulted in delayed tumour progression and reduced metastasis [89]. However when targeting CCL2, this did not result in a decrease of TAM numbers recruited to the tumour [91]. Once the blood monocytes have reached the tumour microenvironment, they mature into TAMs.

1.5.1. Tumour angiogenesis

Studies have linked a high number of TAMs and an increased vessel density within human tumours [59] and TAMs have been shown to promote tumour progression by stimulating the formation of new blood vessels through angiogenesis. Specially, they have been shown to play a major role in regulating an 'angiogenic switch', the expansion of a high-density vascular network that links the tumour to the rest of the circulation system. This is a crucial step with tumour progression, allowing the tumour to improve its oxygen supply, gain access to vital nutrients and the removal of metabolic waste from the tumour. It also helps to facilitate the seeding of tumour cells through metastasis.

Using the mouse mammary tumour model (MMTV-PyMT) during the early stages of tumour development, an influx of macrophages is seen that precedes the development of the tumour. When the macrophage population was depleted using CSF-1^{null} PyMT mice to stop the recruitment of TAMs, this resulted in a delay of the angiogenic switch and progression of the tumour to a malignant stage. When macrophage infiltration was stimulated, this accelerated the angiogenesis with the tumours and led to aggressive tumour progression [92]. Crucial to this process is the angiogenic factor Vascular endothelial growth factor (VEGF-A). Targeting of myeloid

derived VEGF-A, resulted in the inhibition of the angiogenic switch in mice, demonstrating how myeloid derived VEGFA is required to produce high-density vascular networks. However, this also resulted in accelerated tumour progression. This was linked to the increase in hypoxia, which is also a driver on angiogenesis, within the VEGFA depleted tumours [93].

A subset of circulating monocytes expressing the angiopoietin receptor, TIE2, referred to as TIE2 expressing monocytes (TEMs) have been shown to be selectively recruited to the tumours in mice where they stimulate angiogenesis. When these TEM cells were depleted using a suicide gene approach, it halted neovascularisation and resulted in tumour regression in human glioma xenografts [61]. TEMs are found within peripheral blood from both healthy human and cancer patient donors, with a higher frequency of TEMs seen in cancer patients (4.9% vs 3.3%) [94]. However, there was limited detection within nonneoplastic adjacent tissues. TEMs were also found within a range of different human tumour types including kidney, colorectal, lung, breast and pancreatic tumours where they were the dominant phenotype in the monocyte population and were distinct from TAMs. [94].

Further work by the group on TEMs examined their gene expression profiles of TEMs and TAMs isolated from murine mammary N202 tumours in TIE2-GFP transgenic mice by quantitative polymerase chain reaction (qPCR). Within this mouse model, TIE2 expressing cells were also green fluorescent protein + (GFP). TEMs were defined as F4/80⁺TIE2-GFP⁺CD11b⁺CD31^{low/-}, with TAMs defined as F4/80⁺ TIE2-GFP⁻ CD11b⁺CD31^{low/-}. Once isolated and the purity of the isolated population was checked by PCR, they looked at 280 genes that were known to be associated with angiogenesis, tissue, immune response, cell adhesion and tissue remodelling. Although both TEMs and TAMs shared many upregulated monocyte/macrophages genes, it was seen that TEMs upregulated a number of pro-angiogenic genes that included neuropilin-1 (NRP1), a VEGF co-receptor and ephrin-B2 (EFNB2), an ephrin ligand that binds to endothelial cells, regulating angiogenesis and angiopoietin-1 (ANGPT1), a TIE2 ligand that can stimulate the endothelial cell sprouting [95].

TEMs isolated from both tumours and peripheral blood are thought to be recruited into tumours where they promote angiogenesis [61, 96, 97]. Additional,

gene profiling of TEMs isolated from murine tumours revealed how they express a number of pro-angiogenic genes like *bfgf* [61, 68] *Vegfa*, *Vegfb*, *thymidine phosphorylase and placental growth factor* [80]. When TEMs were genetically eliminated from mouse tumours using a conditional 'suicide gene' approach, tumour angiogenesis was inhibited, resulting in slower tumour growth [68]. By targeting TIE2 on TAMs, or blocking ANG2 using an antibody to ANG2, the association of TIE2-expressing TAMs with the abluminal surface of tumour blood vessels was ablated. This resulted in reduced tumour angiogenesis and metastasis [98].

1.5.2. Immunosuppression in tumours

Suppression of anti-tumour immune responses by the host is another tumour-promoting function often exhibited by TAMs. IL-10 within the tumour microenvironment is expressed by a range of CD45⁺ leukocytes, although expression by TAMs can be 10 fold higher by other leukocytes [99]. The expression of IL-10 causes the downregulation of IL-12 from dendritic cells. As IL-12 promotes a Th1 response, its downregulation results in reduced numbers of CD8⁺ T cells within mouse tumours [99], which is significant as CD8⁺ T cells have been shown to correlate with a better prognosis in human breast cancers [90]. Furthermore, blocking of the IL-10 receptor, IL-10R allows the continued production of IL-12 and produce equivalent positive response in chemotherapy treated tumours as CSF-1 inhibitors [99].

Anti-tumour immunity is also inhibited by high expression of the negative checkpoint regulators (NCRs), including programmed death ligand 1 (PD-L1) and cytotoxic T lymphocyte-associated protein 4 (CTLA4). These NCRs are expressed by tumour cells and/or leukocytes like TAMs and T cell subsets and block the ability of antigen presenting cells in tumours to present tumour antigens, along with MHC, to cytotoxic T cells (for the activation of the latter). When the effects of CSF1 released by mouse pancreatic tumours on its receptor, CSF1R, was blocked using the CSF1R inhibitor, PLX3397, a decrease in myeloid populations was seen, including TAMs. The remaining TAMs were 'reprogrammed' by this treatment to be less immunosuppressive, which enhanced T cell number and cytotoxic activity in the tumours. However, it also led to an increase in CTLA4 on T cells and PD-L1 on tumour cells. So, CSF1/CSF1R inhibition was then combined with an anti-CTLA4 or

anti-PD1. This reduced tumour progression by over 90%, compared to treatment with either antibody alone or CSF1/CSF1R inhibition alone – all of which had only limited effects [100].

1.5.3. Metastases

Metastasis occurs when the tumour cells migrate from the primary tumour site, extravasate into the blood vessels, travel to distant sites in the body and remain undetected while a new metastatic tumour forms. TAMs have been shown to aid the formation of metastatic tumours through several mechanisms.

CSF-1 levels are elevated in breast tumours. When CSF-1^{null} PyMT mice were compared to WT strains, it was seen that neither the incidence or growth of primary tumours was not affected. However, the CSF-1^{null} mice did show a reduced progression to metastasis. Restoration of CSF-1 function within the mammary glands led to an increase in metastasis [101]. CSF-1 is linked to the recruitment of macrophages to the tumour. The depletion of TAMs in the absence of CSF-1 and its reduction in tumour progression and metastasis highlighted the role that TAMs play in metastatic disease.

The use of multiphoton microscopy in PyMT mice has shown that tumour cell intravasation only occurs after cell-to-cell interaction with perivascular macrophages at the blood vessels. Through the previously described a paracrine loop, of tumour cell-derived CSF-1 and TAM-derived endothelial growth factor (EGF), tumour cells were shown to migrate towards tumour blood vessels in the tumours and pass into circulation [102]. A subset of TAMs has also been linked to the subsequent escape of tumour cells into the systemic circulation. PV, TIE2⁺ TAMs attached to blood vessels control this when in contact with Mena⁺ tumour cells in such tumours. Once there, these TAMs aid the passage of tumour cells into the circulation by upregulating VEGFA which increases the permeability of blood vessels [103].

These TAM-Mena⁺ tumour cell-endothelial cell groupings in tumours are referred to as 'tumour microenvironments of metastasis' (TMEMs). High numbers of these TMEMs have been shown to correlate with increased risk of distant metastatic disease in human breast cancer [62]. However, it should be noted that a significant correlation between high TMEM score, and increased risk of distant metastasis was

only found in patients with ER⁺/HER2- tumours. Those with other subtypes, including TNBC, displayed no such association [104].

1.6. Macrophage function by location

It has been suggested that TAM function may also vary depending on the niche they occupy with solid tumours. Yang et al. [105] summarises the evidence from clinical reports and how their number and phenotypes link to overall survival and relapse free survival (RFS). These distinct niches within the TME include the invasive edge of the tumour, tumour nest, the surrounding stroma, the perivascular niche and areas of hypoxia and necrosis (**Figure 1-4**). Each environment has its own unique make up of cells type, chemokines/cytokines and ECM. This can build up a complex and often contradictory picture of TAMs within the TME, as TAMs are shaped by their surroundings, but at the same time help to influence the TME.

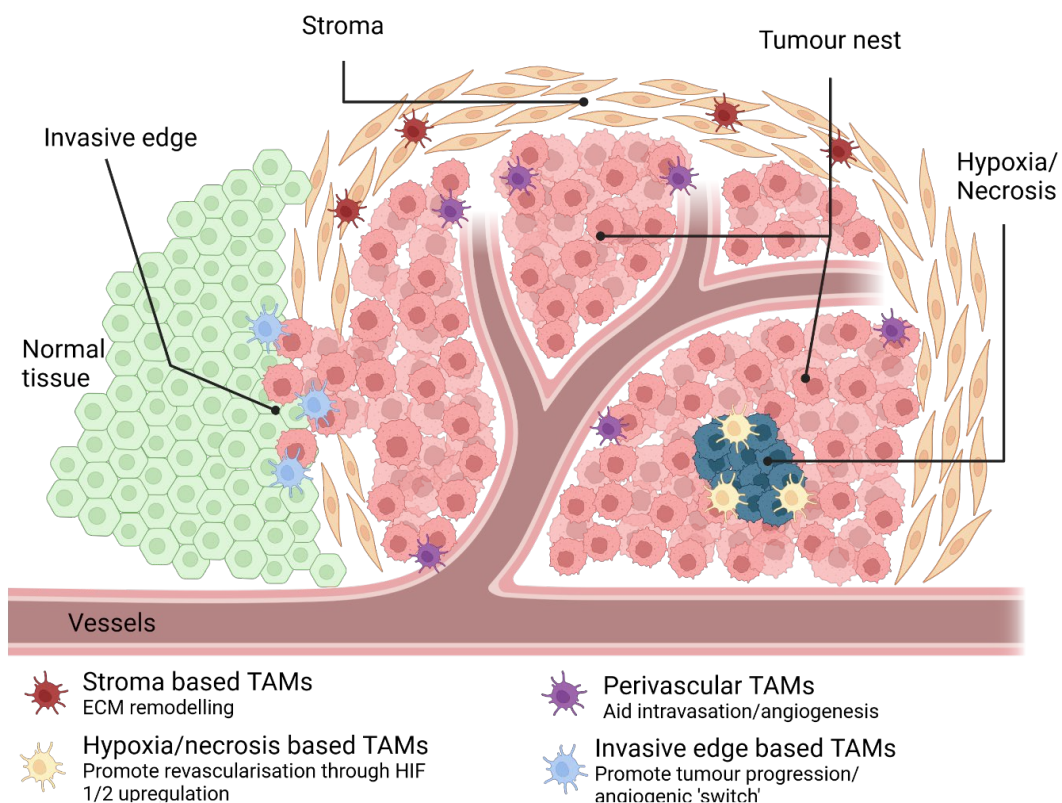


Figure 1-4 TAMs and the different compartment of the tumour microenvironment (TME).

The phenotype and the role of TAMs within different established regions of the TME. This includes the Tumour nests and the invasive edge of the tumour. The surrounding stroma, perivascular regions within proximity of the vasculature and the poorly oxygenated areas of

hypoxia and necrosis. The main functions of TAM subsets that are found within these regions have been listed. Created with BioRender.com.

1.6.1. Tumour nest

Where tumour cells pack together in tumour nest/cancer nests, TAMs within this microenvironment have shown a mixed response depending on the cancer type. Within endometrial and gastric cancer, high numbers within the tumour nest are associated with a favourable outcome. However, high numbers of TAMs within these nests has been correlated with a reduced overall survival within breast cancer of TAM infiltration the tumour nest and tumour stroma were associated with higher grade tumours and poor disease free survival [106]. One possible reason for this link in breast cancer may be due to the expression of CD47 on cancer cells that binds to signal regulatory protein alpha (SIRP α) on the surface of macrophages and acts as a 'don't eat me' signal and helping cancer cells evade the body's defences. When CD47 was blocked using an anti-CD47 antibody, this was shown to reduce metastasis and also inhibit tumour growth in an orthotopic MT1A2 mouse breast cancer model [107].

1.6.2. Tumour stroma

In the stromal regions that surround the tumour nest, extracellular matrix that has been produced by fibroblasts and are devoid of tumour cells. The components of the ECM including fibronectin, laminin and hyaluronan have been shown to regulate macrophage phenotype as well as macrophages playing a role in the constant remodelling of the ECM with collagen degradation and redistribution [108].

The composition of the ECM within breast tumours has also been shown to play a role in tumour grade and aggression. HER2+ and TNBC tumours were found to have a stiffer stroma, which correlated with a higher number of CD45+ immune cells (notably CD68+ CD163+ macrophages). Elevated TGF β signalling was also observed within these areas when compared to Luminal A and B tumours [109].

In studies looking at TAMs distribution in breast cancer, one study looking at 144 breast cancer patients (79% luminal A, 11% TNBC) found that high numbers of CD163 TAMs located in the stroma and not in the tumour nest were positively correlated with a higher tumour size and grade [110]. Within another study looking at

60 breast cancer patients (45% luminal A, 40% luminal B, 15% TNBC), CD163 TAMs located in the stromal regions showed a greater correlation to larger tumour sizes, increased nodal metastasis and vascular invasion, than CD163 TAMs located in the tumour nests did [111]. This correlation is not seen across all tumour types, as no correlation was seen in studies involving endometrial, lung and cervical cancer [105].

1.6.3. Perivascular niche

The perivascular niche are the highly oxygenated areas in close vicinity to the abluminal surface of blood vessel. This has been defined an expanded region anywhere between 15-150 μ m away from the blood vessels [112-114]. Macrophages found within this area have typically been shown to express higher level of M2 associated markers such as TIE2, MRC1 and CD163 where they promote angiogenesis, metastasis and relapse of tumours [61, 62, 113]. TAM upregulation of VEGFA within the perivascular niche helps to facilitate metastasis by increasing the permeability of local vessels [103]. This is backed up by higher numbers of TEM structures (macrophages in contact with blood vessels and MENA expressing tumour cells correlating with the increased risk of metastasis [62] and the early dissemination of tumour cells [115].

Within tumour relapse after chemotherapy treatment in mouse breast cancer models. The upregulation of CXCL12 specifically in the perivascular niche, recruits C-X-C motif chemokine receptor type 4+ (CXCR4+) TAMs to the site [113].

PV TAMs are also implicated in the immunosuppression of other leukocyte subsets. TEMs are seen to accumulate around the vasculature, partly due to ANG2, which is overexpressed by the tumour vasculature acting as a chemoattractant to TEMs. When TEMs were exposed to ANG2 *in vitro*, this resulted in the upregulation of MRC1 and IL-10 [116]. Further work *in vivo* work using *in vitro* using both TIE2+ and TIE2- human monocytes reiterated how ANG2 led to upregulation of IL-10 and resulted in the suppression of CD8+ T cell proliferation and caused the significant expansion of CD25^{high}FOXP3+ Tregs which suppress the activation of immune cells. This increased in Tregs was also seen *in vivo*, within MMTV-PyMT and N202 mouse model. It was confirmed that IL-10 was produced by TIE2+ and not TIE2- TAMs, and

that once TEMs were depleted, this significantly reduced the numbers of Tregs found within tumours [117].

Within MMTV-PyMT tumour bearing mice TAMs were depleted using an anti-CSF1 antibody given in combination with paclitaxel. When they checked the expression of immune related genes, IL-10 saw a decrease in expression. Macrophages expression of IL-10 was 10-fold higher than other leukocytes within the TME. This production of IL-10 was seen to regulate the production of IL-12 by dendritic cells, which in turn limited CD8+ T cell response [99].

Perivascular, TIE2+ CXCR4+TAMs have also been shown to express macrophage receptor with collagenous structure (MARCO), a scavenger receptor in an *in vivo* melanoma model. Treatment with an anti-MARCO antibody resulted in a change of TAM polarisation to a pro-inflammatory phenotype. It also resulted in the increase of interleukin 15 (IL-15) that has been shown to recruit and activate Natural killer (NK) cells into the tumours and increase tumour cell killing [118].

1.6.4. Invasive edge

The invasive edge of the tumour nest can occur at several points. In pre-invasive lesions, these will eventually break through the containing basement membrane. For established tumours, the invasive edge can occur at the invasive front, where tumour cells break through and invade into normal healthy tissue. And at the tumour-stroma border, invading into the ECM border that typically forms around the tumour nest.

The effect of the depletion of macrophages in delaying tumour progression with the mouse breast MMTV-PyMT model has already been discussed [101].

TAMs have also been shown to progress pre-invasive lesions in inducible fibroblast growth factor receptor-1 (iFGFR1) transgenic mice. Within this mammary model, induction of FGFR1 leads to the formation of buds on the mammary ducts, that develop into invasive lesions. Depletion of macrophages within the mode then inhibited proliferation of the epithelium when assess by Ki67 staining. And within the pre invasive lesions there was also reduce angiogenesis with significantly less small blood vessels [119].

At the invasive edge, *in vitro* studies showed that macrophage expression of EGF Once this loop was interrupted through blocking of EGF or CSF-1. This inhibited the tumour cell migration and invasion [120].

1.6.5. Hypoxic/Necrotic areas

Hypoxic areas develop within solid tumours, where the growth of the tumour and its oxygen demands outgrow the capabilities of the poorly formed tumour vasculature. As a result of this low oxygen concentration, there is an upregulation of hypoxia inducible factors (HIF) HIF-1 and HIF-2.

Despite the lack of oxygen and poor vascular infrastructure, hypoxia is not seen to alter TAMs to an M2 like phenotype. M2 like TAMs were recruited to areas of hypoxia in lung tumours within prolyl hydroxylase domain 2 (*PHD2*)-haplodeficient mice. But when the tumours were genetically oxygenated and hypoxic areas decreased, there were no changes in the TAM infiltration and their phenotypes. hypoxprolyl hydroxylase domain 2 (*PHD2*) haplodeficient mouse models that create genetic hypoxia. [121]

1.7. Multi-omic analysis of TAMs

Advances in technologies, bioinformatics and analytics have led to the rise of multi-omics studies, where a combination in data sets within studies generates a comprehensive view that can help determine biological processes and highlight therapeutic targets. Data obtained at several levels including genomic, epigenomic, transcriptome proteome and metabolomic can all be combined at a single cell level. along with spatial information.

The study of TAMs has moved on from studies quantifying CD68⁺ populations [59], with new protocols developed for the isolation of TAMs from human tumours [122] that have allowed the transcriptional mapping of TAMs, allowing them to be further characterised. Recent studies using RNA-sequencing [123] have shown how in human breast and endometrial cancer, that the TAM population found is significantly differs transcriptionally from the circulating monocytes and the tissue resident macrophages. With the TAM population expressing the monocyte chemoattractant, CCL8. This highlights how the cancer niche alters monocytes on recruitment to the tumour.

There has also been the development of multiplexing immunohistochemical protocols [124]. This has allowed the detection of an ever-increasing number of markers within paraffin embedded sections. Combined with improvements in machine learning and artificial intelligence (AI), this has enabled image cytometry to collect “big data”. This allows a multitude of information to be collected from stained sections including data on cell size, morphology and fluorescent intensity and can be combined with spatial information, including locational data of cell subtypes.

This has enabled the in-situ analysis of multiple cell subsets within tumours, with the simultaneous detection of 12 cell markers used to create both a lymphoid and myeloid biomarker panel. These panels were used to screen 24 pancreatic ductal carcinomas, where expression of PD-L1 on myeloid cells correlated with activated, granzyme B⁺ CD8⁺ T cells, leading to a more favourable prognosis [125].

Single cell RNA sequencing (scRNA-seq) that reveals the gene expression at the single cell level was used to analyse tumour infiltrating myeloid cells from 210 patients across 15 tumour types. When analysing TAM and monocyte subsets across the multiple cancer types, they found consistent populations of monocytes and macrophages, including, CD14⁺ and CD16⁺ tumour infiltrating monocytes (TIMs), LYVE1⁺ TAMs, secreted phosphoprotein 1⁺ (SPP1) TAMs, C1QC⁺ TAMs, Interferon-stimulated gene 15⁺ (ISG15) TAMs and Fibronectin 1⁺ (FN1) TAMs across multiple cancer types. The population of SPP1⁺ TAMs were also linked to tumour angiogenesis, making them a potential for future targeted treatments [126]. A study that looked at TAMs within human breast and colon cancers using single cell RNA sequencing (scRNA-seq) and multiplex imaging, found that there were 3 distinct macrophage niches that were not necessarily related to certain locations, but rather linked to areas with a similar tumour microenvironment (TME), such as areas of hypoxia, inflammation and cell death. They found that IL4I1⁺ TAMs were linked to areas of phagocytosis and cell death at the invasive tumour edge. Pro-angiogenic SPP1⁺ TAMs were found within hypoxic and necrotic regions of the TME and NOD-like receptor protein 3⁺ (NLRP3) TAMs were all linked to areas of acute inflammation and may drive neutrophil infiltration [127].

A recent review of recent RNA-seq based studies looking into macrophage diversity in the single cell omics era sought to clarify the nomenclature surrounding TAMs [128]. This looked at multiple cancer types and found there was a total of 7

subsets of TAMs were seemingly being preserved across different cancer types. These TAM subsets have been named, inflammatory cytokine enriched (Inflam-), interferon primed (IFN-), immune regulatory (Reg-), proliferating (Prolif-), resident tissue macrophage like (RTM-), pro-angiogenic (Angio-) and lipid associated (LA-) TAMS (Summarised in Table 1-3). Importantly, this newly proposed model is still a spectrum, with multiple markers/gene signatures spanning several subsets. This nomenclature proposed by Ma et.al is likely to change further.

The ability to accurately define macrophage subsets, their roles within the TME and tumour progression, will help to provide more viable therapeutic targets in future.

| TAM Subtype | Function | Key genes/Marker |
|-------------|---|--|
| Angio- | Characterised by high expression of pro-angiogenic markers and factors. Normally found within hypoxic regions of TME and shown to promote tumour progression. | VEGFA, SPP1, CD163, MACRO, CXCR4 |
| IFN- | Resemble M1 like macrophages due to expression of M1-like markers. But are shown to have immunosuppressive function by promoting T-reg recruitment to the tumour and expression of immune checkpoint inhibitors. | IDO, ISG15, CXCL8, 9, 10, PDL1, PDL2 MHCII, CCL2/3/4/7/8, CD40, LAMP3, CXCL2/3/9/10/11 |
| Inflam- | Recruitment and regulation of immune cells and promotion of inflammation through cytokines. | IL-1B, IL-6, CCL2/3/5/20, CXCL1/2/3/5/8, NLRP3 |
| LA- | Characterised by expression of lipid genes. TAM lipid catabolism linked with immunosuppression | APOC1, APOE, ACP5, FABP5 |
| Prolif- | Characterised by expression of proliferation marker KI-67 and cell cycle genes. May contribute to the expansion of other TAM subsets, acting as a precursor. | MKI67, CDK1, CDC45 |
| Reg- | Antigen presentation and Immune checkpoint, found abundantly within normal tissue. Similarity to M2-like macrophages | ARG1, MRC1, CD274, CX3CR1, CCL2, CD40, |
| RTM- | Resemble resident tissue macrophages from normal tissue. High expression of embryonic precursor markers least expression of monocytes markers and genes. Gene signatures also mimics distinct differences seen between RTM found in different organs such as Kupffer, Microglial and Alveolar RTMs. | LYVE1, HES1, FOLR2 |

Table 7 Subsets of TAMs based off single cell omics.

The increasing number of publications studying TAMs at a single cell level are building up a picture of defined TAM subsets that can be grouped based off their genetic signature and surface markers. Although there are 7 subsets proposed, the genes, markers and function are not exclusive to their subset, but continue with the idea that there is still an overlapping spectrum. Adapted from Ma et. al 2022 [128]

1.8. TAM responses to chemotherapy

Previous studies have shown that TAMs can also limit the efficacy of the various types of chemotherapeutic agent in mouse tumour models, both by reducing the initial response of tumours to such agents, and by stimulating their subsequent regrowth when the treatment has concluded.

1.8.1. Chemoresponsiveness of tumours

Initially, Mantovani and his colleagues discovered the effects of the host immune system on chemotherapy after inoculating Balb/c mice with leukemic cell lines that were known to be immunogenic or non-immunogenic. It was shown that the high immunogenic cells led to an increased efficacy of doxorubicin treatment compared to the non-immunogenic leukaemia. After receiving prior treatment with an immunosuppressant agent 5-(3,3-dimethyl-1-triazenyl)-1H-imidazole-4-carboxamide (DTIC), the efficacy of doxorubicin was reduced. Similar results were not seen when using another anthracycline, daunomycin, showing that the effects were specific to the type of chemotherapy agent used. When macrophages were targeted using silica and carrageenan, this resulted in reduced anti-tumour effects of doxorubicin but had little effect on the efficacy of daunomycin. This suggests that in tumours with high immunogenicity, macrophages are able to enhance the effects of chemotherapy and that the type of chemotherapeutic agent used is also important in maximising the host immune response [129].

An increase in the efficacy of chemotherapy was also seen when 4T1 mammary tumour-bearing mice are treated with the taxane, docetaxel [130]. After receiving treatment with docetaxel, the number of splenic leukocytes - termed myeloid derived suppressor cells (MDSCs), made up of monocytes, macrophages, dendritic cells and granulocytes - that stained for Th1 expressed IFN- γ and IL-12 was increased, while Th2 expression of IL-10 was decreased compared to untreated controls. The authors suggested that there was a shift from M2-like, immunosuppressive MDSCs to M1-like anti-tumour ones. This was supported by their higher expression of M1-associated C-C chemokine receptor 7 (CCR7), iNOS and lower expression of M2 associated MRC1 on MDSCs *in vitro* and *in vivo*. MRC1-expressing MDSC were seen to be selectively targeted by docetaxel, with the

majority of MRC1 expressing cells also expressing annexin-v, a marker for apoptosis, after treatment with docetaxel. Although the findings appear to rebalance the MDSC population from an M2-like state to a M1-like activation state, when Kodumudi et al looked at MDSCs as a whole, it was not clear how each cell type within the MDSCs had responded to docetaxel treatment. It was also not known what had occurred within the tumour microenvironment, as only splenic MDSCs were examined. It did, however, shed light on the mechanism for targeting MRC1 macrophages - through the inhibition of the transcription factor, STAT3. This is required for the expansion of MDSCs and the expression of macrophage polarising cytokines, IL-10, IL-14 and IL-13. Inhibition of STAT3 with JSI124 in MDSCs, resulted in similar results to those produced by docetaxel, polarising macrophages toward M1-like phenotypes [130].

Several studies have reported that chemotherapy increases the recruitment of monocytes into tumours in mouse models [51, 90, 131, 132]. Also, higher numbers of CD45⁺CD11b⁺CD14⁺ TAMs were present in human breast tumours after neoadjuvant chemotherapy, compared to those who had surgery alone [51]. The same response was also seen in MMTV-PyMT tumours following neoadjuvant treatment with paclitaxel, when an increase in CD45⁺ CD11b⁺ Ly6C^{low} Ly6G⁻ F4/80⁺ TAMs was evident [90]. Isolated tumour cells from these tumours showed increased expression of CSF1, CCL8 and IL-34 mRNA analysis. When an inhibitor of CSF-1R on TAMs (PLX3397) was given alongside paclitaxel treatment in such mice, the recruitment of TAMs was significantly reduced and tumour responsiveness to paclitaxel enhanced. This depletion of TAMs also reduces immunosuppression, allowing an increase in CD4⁺ and CD8⁺ T cells [90].

A second study showed that, after neoadjuvant treatment with paclitaxel, there was an upregulation of TAM-derived cathepsins within mouse mammary tumours – these are proteases involved in lysosomal protein degradation. Cathepsin-expressing TAMs were seen to reduce tumour cell death in response to paclitaxel *in vitro*. Addition of a pan cathepsin inhibitor, JPM-OEt (JPM), to these co-cultures reversed this effect and treatment of mice with mammary tumours with the same inhibitor significantly increased the anti-tumour efficacy of paclitaxel on tumour size [132].

TAMs were also seen to promote chemoresistance in MMTV-PyMT mice treated with doxorubicin. This led to an increase in both necrotic cell death and CCR2⁺ monocytes into the tumours. The latter correlated the CCR2 ligands, CCL2 and CCL12, being increased in tumours 48 hours after doxorubicin treatment. Doxorubicin induced lower levels of CCR2⁺ monocytes in tumours grown in CCR2 null than WT mice, and their tumours were more markedly reduced by this treatment. An increase in myeloid cell derived MMP9 was seen in tumours after chemotherapy which decreased vascular leakage. This, in turn, lowered the effectiveness of doxorubicin treatment. Genetic deletion of MMP9 in these cells increased both the expression the expression of endothelial adherence junctions, increased vascular permeability, and improved therapeutic response to doxorubicin [131].

1.8.2. Prevention of recurrence

There is now growing evidence that TAMs can also limit the ability of tumours to regrow and spread *after* chemotherapy.

M2-like (MRC1⁺ TIE2⁺ CXCR4⁺ VEGFA⁺) TAMs were shown to accumulate around blood vessels in syngeneic, implanted Lewis lung carcinoma (LLC1) tumours following cyclophosphamide treatment (and also in orthotopic 4T1 and MMTV-PyMT tumours treated with paclitaxel and doxorubicin respectively). This accumulation of these PV cells was shown to be dependent upon their expression of CXCR4, the receptor for CXCL12. The latter was upregulated in cyclophosphamide treated LLC1 tumours. When treated with CXCR4 inhibitor, AMD3100, tumour revascularisation and regrowth after cyclophosphamide was impaired in this tumour model [113].

Interestingly, cyclophosphamide is also known to induce oxidative stress and was seen to upregulate expression of the enzyme, heme oxygenase (HMOX-1), mainly in PV MRC1⁺ TAMs. This breaks down and recycles the components of heme into biliverdin, ferrous iron and carbon monoxide - the increase in which upregulates MRC1, VEGFA and CXCL12 expression by TAMs [133].

The ability of M2-skewed TAMs to promote relapse is also seen in mammary tumours treated with the vascular disrupting agent (VDA), combretastatin-A4P (CA4P) [134]. After treatment with this agent, vascular damage (and parallel increase in tumour hypoxia) resulted in the recruitment of PV TIE2⁺ TAMs in a CXCL12-dependent manner within 24h. Once again, targeting of this CXCL12-

induced recruitment of monocytes using a CXCR4 inhibitor resulted in increased tumour cell necrosis in response to CA4P and a significant reduction in mammary tumour (N202 and MMTV-PyMT) growth compared to CA4P alone [134]. After radiotherapy in mouse gliomas, bone marrow-derived CD11b+ cells are recruited to tumours, where they promote tumour angiogenesis and regrowth. When these myeloid cells were inhibited using an anti-CD11b neutralising antibodies, the anti-tumour efficacy of the radiotherapy was increased [135].

1.9. Therapeutic targeting of TAMs.

Due to the diverse functions of TAMs, they are open to different approaches to therapeutic targeting. This has led to various strategies being implemented within clinical trials that include preventing recruitment, depletion, proliferation, activation and the reprogramming of TAMs (**Table 1-4**).

| Target | Drug | Clinical trial identifier | Trial phase | Combination drug |
|------------------|-------------------|----------------------------|-------------|----------------------------|
| CSF1R- CSF | Axatilimab | NCT03238027 * | I | Anti-PD-L1 |
| | Sotuletinib | NCT02829723 [136] | I/II | Anti-PD-1 |
| | Cabiralizumab | NCT03502330 [137] | I | Anti-PD-1+ anti-CD40 |
| | Emactuzumab | NCT01494688 [138] | I | Chemotherapy, |
| | | NCT02760797 [139] | I | Anti-CD40 |
| | Pexidartinib | NCT03158103 [140] | I | MEK inhibitor, |
| | | NCT01525602 [141] | I | Chemotherapy |
| AMG820 | NCT02713529 [142] | I | Anti-PD-1 | |
| CXCL12- CXCR4 | Motixafortide | NCT02907099 [143], | I | Anti-PD-1, |
| | | NCT02826486,[144] | II | Anti-PD-1, |
| | | NCT02826486 [144] | II | Chemotherapy, Anti-PD-1 |
| | LY2510924 | NCT02652871 [145] | I | Anti-PD-L1 |
| | | NCT02737072 [146] | I | |
| Mavorixafor | NCT02823405 [147] | I | Anti-PD-1 | |
| CCR2- CCL2 | Carlumab | NCT01204996 [148] | I | Chemotherapy |
| | PF-04136309 | NCT01413022 [149] | I | Chemotherapy |
| CCR5- CCL5 | Leronlimab | NCT03838367 [150] [151] | I/II | Chemotherapy |
| | Maraviroc | NCT03274804 [152] | I | Anti-PD-1 |
| | Maraviroc | NCT01736813 [153] | I | Chemotherapy |
| ANG2 | Trebananib | NCT03239145 | I | Anti-PD-1, |

| | | | | |
|---|--------------|---------------------------|------------|-----------------------------|
| | | NCT01493505 | III | Chemotherapy |
| <i>CD47– SIRP1α</i> | AO176 | NCT03834948 [154] | I/II | Chemotherapy, Anti-PD-1 |
| | CC-90002 | NCT02367196 [155] | I | Rituximab |
| | Evorpaccept | NCT03013218 [156] | I | Anti-PD-1, |
| | | NCT03013218 [156] | I | Trastuzumab |
| | Magrolimab | NCT03558139 [157] | I | Anti-PD-1, |
| | | NCT03248479 [158] | I | Azacitidine, |
| | | NCT02953509 [159] | I | Rituximab, |
| | TTI-621 | NCT02953782 [160] | I/II | Cetuximab |
| | | NCT02663518 [161] | I | Rituximab |
| NCT03530683 [162] | | I | Anti-PD-1, | |
| <i>CD40</i> | Sotigalimab | NCT04996004 [163] | I | Chemotherapy |
| | | NCT03214250 [164] | I | Anti-PD-1, Chemotherapy, |
| | Selicrelumab | NCT03123783 [137] | I | Anti-PD-1, Anti- CSF1 |
| | | NCT00711191 [165] | I | Chemotherapy, |
| | | NCT00607048 [166] | I | Chemotherapy, |
| | | NCT01103635 [166] | I | Anti-CTLA4 |
| | | ACTRN12609000294257 [167] | I | Chemotherapy |
| | | NCT02760797 [139] | I | Anti-CSF1 |
| | | NCT02588443 [168] | I | Chemotherapy |
| | | NCT02304393 [169] | I | Anti-PD-L1 |

Table 8 Clinical trials targeting TAMs.

Summary overview of various drugs being tested, detailing their respective target pathways, the clinical trial identifiers, the current phase of the trial, and any drug combinations being utilised with the trials.

The CCL2/CCR2 pathway inhibition is another TAM targeting strategy. Inflammatory circulating monocytes express CCR2 and are recruited to tumours with high CCL2 expression. Targeting the pathway in pre-clinical models is seen to limit monocyte accumulation, delaying tumour progression and reducing metastasis [85].

In clinical trials blocking the CCL2/CCR2 pathway there has been little in the way of tumour response. Carlumab, a CCR2 inhibitor, was one of the first CCL2 targeting drugs to be tested in the clinic but failed to elicit a tumour response. It resulted in levels of CCL2 being only partially suppressed during treatment, which then increased 1000-fold from the baseline after therapy had ended [148]. In another phase I study using CCR2 inhibitor PF-0413639, in combination with the chemotherapy FOLFIRINOX in PDAC patients, it did prevent inflammatory monocytes from being recruited. This saw a reduction in the number of CD14^{high} TAMs from 9% down to 2% of total cells. Tumour response was seen in 16 of 33 patients (49%) and patients that had the best response were seen to have lower inflammatory monocytes in their baseline test, potentially indicating a biomarker to highlight patients that treatment is most likely to benefit [149]. This failure of CCR2 inhibition has been seen within a pre-clinical study. Using CCL2 monotherapy in several mammary tumour models, once CCL2 inhibition was interrupted, this resulted in monocyte recruitment to the tumour and led to increases in angiogenesis and metastasis [170].

CSF1R inhibitors have been used in combination to target the CSF1R chemokine receptor that is expressed by TAMs. This seeks to disrupt the signalling pathway that recruits macrophages to tumours.

The anti-CSF1R drug, emactuzumab was given as either a single agent (n=99) or in combination with paclitaxel (n=54) in advanced or metastatic tumours in a phase I study. This resulted in a reduction of CD163⁺ and CSF1R⁺ TAMs when biopsies were analysed by IHC. But importantly, there was no response to the single agent therapy and only a 7% response rate in the combination therapy [138].

Resistance mechanisms to CSF1R therapies are being uncovered which limit the efficacy of the therapy. In murine glioblastoma tumours subjected to prolonged CSF1R inhibitor treatment, tumour progression occurred in 50% of the mice, CSF1R inhibition in these mice resulted in elevated levels of phosphatidylinositol 3-kinase (PI3K) pathway activity, driven by macrophage-derived insulin-like growth factor-1 (IGF-1) and tumour-derived IGF-1 receptor (IGF-1R). When CSF1R inhibition was

combined with PI3K or IGF-1R inhibition, this resulted in prolonged survival [171]. These pathways may not be present in all cancers/patients, meaning that either further combinations therapies should be explored to inhibit all potential pathways, or biomarkers and tumour signatures should be identified in patients that will see the biggest benefit.

CXCR4 is a chemokine receptor that is often expressed by macrophages. It promotes the recruitment macrophage to tumours that express its ligand -CXCL12. When blocked in a pre-clinical model using the CXCR4 inhibitor plerixafor, it has been shown to stop TAM recruitment [113]. In a phase II trial using the CXCR4 inhibitor motixafortide, alongside the PD-1 inhibitor pembrolizumab, it was seen to increase the efficacy of treatment within pancreatic ductal adenocarcinoma (PDAC) with median overall survival of 7.5 months for those who received it as a second line therapy compared to the 6.1 months for the current approved second line therapy. In analysis of tumours after treatment, increases in CD8+ T cells were seen as well as a decrease in MSDCs [144]. Within melanoma, combination treatment of the CXCR4 inhibitor mavorixafor and pembrolizumab in a phase Ib study, again resulted in an increase of CD8+ T cells [147].

The CCR5 chemokine receptor is expressed by macrophages, myeloid cells and T cells. CCR5 is activated by its ligands CCL3, CCL4 and CCL5 which are over expressed by some tumour cells, including >95% in TNBC. This axis has been implicated in cancer progression and metastasis [172]. A phase 2 study of the CCR5 inhibitor, leronlimab in combination with carboplatin in metastatic TNBC patients has shown promise with patients, with 2 out of 7 achieving a partial response and 4 achieving stable disease [151].

Macrophages are also the main source of the cell surface receptor, SIRP α . This interacts CD47, a surface marker found on normal health cells acting as a 'don't eat me' signal that is overexpressed by some cancers [107]. Blockade of the CD47-SIRP α pathway has so far seen a mixed response, with tolerability being well reported amongst the trials. A phase one trial of CC-90002 within haematological cancers was discontinued, as all patients enrolled had died or had progressive disease [155]. Within another trial looking at magrolimab in combination with cetuximab – an EGFR inhibitor, there were limited responses, but tumour biopsies have shown a treatment related increase in macrophage infiltration [160].

The use of CD40 agonists works as CD40 stimulates TAMs, dendritic cells and B cells to drive a TH1 response through the release of IL-12. In a study combining CD40 agonist selicrelumab with anti-CSF1R drug emactuzumab, stable disease was achieved in 15 out of 37 patients. This resulted in a reduction of CD163+ TAMs compared to the baseline biopsy as well as an increase in CD8 T cells and reduction in FOXP3+ Treg cells [139].

1.10. Introduction to Methods

1.10.1. Multiplex immunofluorescence artificial intelligence segmentation

Multiplex immunofluorescence allows for the simultaneous detection of multiple biomarkers within a single tissue section, enabling the staining of up to 60+ markers [173] multiple cell population and panels of immuno-oncologic cells [174]. Compared to traditional IHC methods, which typically permits the assessment of only one or two markers per tissue section, this offers the advantage of being able to study numerous cell types in situ within the section as well as multiple surface markers per cell type that allow further data on activation status of cells.

Typically these multiplex methods work by sequential staining cycles, initially staining with the antibody and fluorophore followed by imaging and then either a quenching of the fluorophore or stripping of the antibody. However methods that involve repeated cycles of staining can result in increased tissue loss after each round of imaging [175]. A more advanced method of multiplex detection of antibodies is mass spectrometry imaging. This utilises mass spectrometry to detect multiple markers simultaneously as antibodies are conjugated to metal isotopes instead of fluorophores, which are then detected using mass spectrometry. However as this uses specialist mass spectrometry technology, utilising these methods for multiplex quantification comes at a much higher cost than using fluorescent microscope based methods used in multiplex immunofluorescence [176, 177].

As multiplex immunofluorescence can produce large datasets per sample, analysis has now moved far beyond traditional quantification methods. The use of artificial intelligence (AI) systems to train machine learning algorithms is a valuable tool in cell segmentation and quantification [178].

There can be limits to machine learning approaches, as developing machine learning models requires high-quality training datasets that are relevant to the

tissues being analysed. Variations in staining intensities, tissue morphology and the presence of staining artifacts can also challenge the accuracy of segmentation leading to the mislabelling of cells.

1.10.2. Immune microenvironment models of breast cancer

The immune microenvironment plays a key role in breast cancer development and response to treatment and is made up of varying components whose interactions can influence tumour growth, metastasis, and the efficacy of therapies.

Pre-clinical models, such as 3D cell culture and *in vivo* studies, help to study the interactions of immune cells with the rest of the TME. These models can be used at varying levels of complexity.

1.10.2.1. *In vivo* models of breast cancer

In vivo models, typically involving murine studies, enable the investigation of the immune microenvironment within the context of a whole, living organism, capturing factors and cell interactions that are not present *in vitro*. Within breast cancer, these models are useful tools that can help determine the roles of specific subsets of cells in different location and their role in dynamic events, such as therapy response [113]. However, typical *in vivo* models that use immortalised cell lines often fail to capture all the heterogeneity of cells, tissues and molecular changes found in the TME.

Patient derived xenograft (PDX) models are generated by implanting human tumour tissue into immunodeficient mice with the benefit that the histology of these tumours has a closer resemblance to the host. Although this preserves many aspects of the original tumour's heterogeneity, PDX models require immunosuppressed hosts, meaning that PDX models do not represent the role of the adaptive immune system in tumour progression [179, 180].

1.10.2.2. *Ex vivo* assays that attempt to preserve the TME integrity

Various *ex vivo* assay have been developed to preserve as many features of the TME as possible. Some have been used to investigate cell behaviour and others to predict tumour responses to various drugs. However, these often have limitations including loss of tissue architecture and cell viability over time.

Ex vivo assessment of breast tumour fragments in a perfusion bioreactor has been shown to maintain both tumour and immune cell viability for 7 days. They used 2mm³ chunks, cultured between a collagen scaffold and perfused at a constant flow rate with supplemented culture medium. Tumours were treated with Fulvestrant and pertuzumab, plus anti-PD-L1 and anti-CTLA4 antibodies. Higher cell viability was seen within the perfused cultures kept in the bioreactor when compared to the static cultures as assessed by apoptosis through caspase 3 staining. In the perfused culture, fulvestrant treatment of ER+ tumours, significantly reduced epithelial cell viability compared to untreated controls. With an effect also seen when HER2+ tumours that were treated with pertuzumab. Treatment with anti PD-L1 and anti-CTLA4 in assays using TNBC fragments led to immune activation with an increase T cells and a reduction in viable cancer cells (while adjacent healthy tissue in fragments remained unaffected by treatment) [181].

In a separate study, the effects of paclitaxel on 200um thick breast tumour slices were examined. The slices were cultured for 24h before being treated with vehicle or paclitaxel for up to 72h. Samples were then fixed embedded and stained using proliferation and viability markers. Paclitaxel treatment on tumour slices did not induce high levels of cell death during the experiment timeframe, but an increased uptake was seen in cancer cells, so it was suggested that cell death from paclitaxel would have occurred eventually, just not within the time limits of the assay [182].

Ex vivo assays involving slices of non-small lung cell lung carcinoma (NSCLC) have also been used for drug screening. Here fresh surgical tumour tissue was given a 'recovery phase'- where the tumour was cut into 2-3mm² pieces and cultured for 16-20 hours prior to treatment. Tumour pieces were then transferred to culture wells with the therapeutic compounds for 24h before being fixed, embedded and sectioned for analysis through IHC/IF. From 26 patients, the response of NSCLC to cisplatin using this assay saw a link to patient outcome. Using cPARP staining as a measure of cell death to the highest levels of cisplatin, they determined a cut-off for sensitive and resistant tumours. The sensitive samples identified were shown to correlate with patient survival, although there was no minimum follow-up period for the patient data [183].

1.10.2.2.1. Patient derived organoids

Patient derived organoids (PDOs), 3D structures derived from the primary tumours, also retain some genetic and histological features of primary tissues. They are typically generated from the partial dissociation of the primary tumour into microaggregates or are reformed into 3D structure from single cells. Breast PDOs have been shown to resemble the histology of the original tumour subtype, as well as retaining the hormone receptor and HER2 status [184, 185].

1.10.2.2.2. Dispersed methods

Keeping the tumour environment intact obviously has its advantages – for example some drug responses may depend on contact between cells - but if the same response to therapy is also seen when tumours are dispersed (and still correlates with tumour responses in patients), then this form of *ex vivo* assay is potentially a more flexible tool as it has greater scalability for drug screening assays.

1.10.2.2.3. Microfluidic models

Microfluidic models have been described as an ‘organ-on-chip’ assay as they aim to recapitulate at least some of the key features of tissue microenvironment. They are three-dimensional models that enable the user to control and study the cells in the specific tissue environment being studied. They are often manufactured out of glass or clear polymers such as polydimethylsiloxane (PDMS). They use precast channels to allow flowing fluids and extra cellular matrix (ECM) gels that can then be populated with cells from one or more sources to build complexity and recreate microenvironments that can be used to study live cell to cell interactions, as well as migration, intravasation extravasation events and angiogenesis [186, 187].

Microfluidics assays offer advantages over 2D *in vitro* cell cultures, as the latter do not attempt to replicate the 3D complexity of tissues. Co-cultures of multiple cell types in ECM substrates in microfluidics assays can replicate some features of tissues like a simplified form of the vasculature.

A microfluidic setup consisting of 3 parallel channels, a centre ECM gel containing channel, separated from the outer media channels by trapezium posts.

These held in the pre-polymerised hydrogel and stopped it leaking into the media channels. To produce a microvascular network, human umbilical vein endothelial cells (HUVECs) and human lung fibroblasts (HLFs) were seeded in a co-culture in a fibrin gel. Then over a 4/5-day period they formed vessel like structures with lumens that span the central gel region and connected the flanking media channels [188].

One variation of this model has been used to study the extravasation of breast cancer cells across microvessels into a bone-like microenvironment (modelling cancer cell seeding to form bone metastases). HUVECs were seeded with bone marrow-derived mesenchymal stem cells (BM-MSCs) in a fibrin gel to generate a microvascular network in a bone mimicking microenvironment. The human breast cancer cell line, MDA-MB-231, was then perfused through the microvascular network and observed in real time using confocal microscopy. In this study, they investigated the effect of blocking adenosine on the rate of MDA-MB-231 extravasation [189].

In a variation of this model, microvascular networks were generated in a fibrin gel and then these were infused with human derived monocytes. They then extravasated through the microvessels with many being retained <10um from microvessels (i.e. the PV areas). CCR2⁺ monocytes were more likely to extravasate through the microvessels compared to CCR2⁻ monocytes. Moreover, once CCR2⁺ monocytes extravasated, they began to upregulate MRC1. However, this was not linked to extravasation, as monocytes seeded directly into the fibrin gel, with HUVECs and HLFs also displayed the same levels of MRC1 upregulation [190].

1.11. Summary

TAMs are shown to play an important role in tumour progression with high numbers of TAMs linked to a poor prognosis and increase risk of recurrence in several cancer types, including breast cancer [191]. They play a major role within the tumour by promoting vascular growth through angiogenesis, helping the tumour to evade detection from the hosts defence mechanisms with immunosuppression and by aiding the detachment, migration and extravasation of tumour cells, enabling metastasis to occur.

The TNBC subtype of breast cancer currently lacks the targeted therapies that are available to other subtypes. Because of this, there is a reliance on chemotherapy for treatment options, which can prove to be very effective. Despite this, for those

whose still have residual disease after chemotherapy, there is a high risk of recurrence in TNBC within a 3 year period following treatment [5]. As TAMs have been shown to limit the efficacy of chemotherapy and drive recurrence [113], this seemingly makes TNBC tumours particularly susceptible to the effects of TAMs.

1.12. Project hypothesis and aims

PV TAMs have emerged recently as a major, tumour-promoting leukocyte population in tumours. Previous studies have shown this TAM subset to be present in treatment-naïve and chemotherapy-treated human breast tumours [113].

However, their presence/frequency in human TNBCs, and correlation with relapse after neoadjuvant chemotherapy has yet to be determined. In my PhD project, I will, therefore, investigate whether:

1. The number of PV MRC1⁺ TAMs in TNBCs is altered after neoadjuvant chemotherapy. To do this, I will quantify the number of PV MRC1⁺ TAMs in a cohort of human primary TNBCs after their treatment with neoadjuvant chemotherapy or surgery alone.
2. The number of PV MRC1⁺ TAMs after neoadjuvant chemotherapy correlates with metastasis in TNBCs. For this, I will compare the number of PV MRC1⁺ TAMs in human TNBCs from 2 cohorts of patients – those with or without the formation of distant metastases within 3 years of the surgical removal of their primary tumours.
3. The development of an *ex vivo* model to study the perivascular niche. This will involve growing microvessels in a fibrin gel preloaded with human fibroblasts and small tumour spheroids (made from primary human TNBC tumours), and then infusing various human macrophage subsets into the microvessels in the presence or absence of various chemotherapeutic agents. The extravasation of the latter through these microvessels, and subsequent retention near them or migration towards/into the tumour spheroids in the gel will then be quantified using confocal microscopy. Their phenotype will be assessed using fluorescent antibodies.

Chapter 2 Materials and methods

2.1 Materials and methods

2.1. Materials

2.1.1. List of reagents

| Reagent | Manufacturer |
|---|--------------------------|
| 4',6-Diamidino-2-Phenylindole, Dihydrochloride (DAPI) | Invitrogen, USA |
| Agarose | Sigma-Aldrich, USA |
| Anti-mouse peroxidase | Vector laboratories, USA |
| Bovine serum albumin | Sigma-Aldrich, USA |
| Bovine thrombin | Sigma-Aldrich, USA |
| Dextran, Oregon green 70 000 MW 488 | Invitrogen, USA |
| DPX mountant | Sigma-Aldrich, USA |
| Dulbecco's modified eagle medium (DMEM) | Lonza, Switzerland |
| Dulbecco's phosphate buffered saline (DPBS) | Lonza, Switzerland |
| Endothelial cell growth medium 2 (ECGM2) | Promocell, Germany |
| Endothelial cell growth medium MV2 (ECGM MV2) | Promocell, Germany |
| Eosin | Acros organics. USA |
| Ethanol | Fisher, USA |
| Ethylenediaminetetraacetic acid (EDTA) | Sigma-Aldrich, USA |
| Fibrinogen | Sigma-Aldrich, USA |
| Fibroblast growth medium 2 | Promocell |
| Haematoxylin, Gills no2 | Sigma-Aldrich, USA |
| Hydrogen peroxide | Fisher, USA |
| Hydrophobic barrier PAP pen | Vector laboratories, USA |
| Levamisole Solution | Vector laboratories, USA |
| Methanol | Fisher, USA |
| Normal Goat serum | Vector laboratories, USA |
| Normal Horse serum | Vector laboratories, USA |
| Phosphate buffered saline (PBS) | Lonza, Switzerland |
| ProLong Gold Antifade mountant | Invitrogen, USA |

| | |
|----------------------------------|--------------------|
| Pronase | Sigma-Aldrich, USA |
| Sodium chloride | Sigma-Aldrich, USA |
| Sodium citrate | Sigma-Aldrich, USA |
| Sudan B Black | Sigma-Aldrich, USA |
| Target retrieval solution pH 6.0 | Agilent Dako, USA |
| Tris base | Sigma-Aldrich, USA |
| Trypan blue solution (0.4%) | Sigma-Aldrich, USA |
| Trypsin/EDTA | Lonza, Switzerland |
| Tween-20 | Fisher, USA |
| Xylene | Fisher, USA |

2.1.2. List of commercial kits

| Kit | Manufacturer |
|--|--------------------------|
| AEC substrate kit | Vector laboratories, USA |
| Anti-mouse peroxidase | Vector laboratories, USA |
| CellTrace Carboxyfluorescein succinimidyl ester (CFSE) Proliferation Kit | Invitrogen, USA |
| CellTrace Far Red Cell Proliferation Kit | Invitrogen, USA |
| CellTrace Violet Cell Proliferation Kit | Invitrogen, USA |
| DAB Substrate kit, Peroxidase | Vector laboratories, USA |
| ImmPRESS Anti-rabbit alkaline phosphatase | Vector laboratories, USA |
| Streptavidin/biotin blocking kit | Vector laboratories, USA |
| Vector red alkaline phosphatase | Vector laboratories, USA |

2.1.3. List of materials

| Material | Manufacturer |
|-----------------|---------------------|
| DAX-1 chips | Aim Biotech, USA |

2.1.4. List of antibodies

| Antibody | Species | Final concentration | Manufacturer | Clone |
|-------------------------------------|----------------|----------------------------|--------------------------|--------------|
| Alexa fluor 555 anti-rabbit | Goat | 2.5 µg/ml | Life technologies | - |
| Alexa fluor 647 anti-mouse IgG1 | Rat | 5 µg/ml | Biolegend, USA | - |
| Alexa Fluor® 647 anti-human CD144 | Mouse | 13.3 µg/ml | Biolegend, USA | BV9 |
| Anti-mouse biotin | Goat | 7.5 µg/ml | Vector laboratories, USA | - |
| Anti-rabbit biotin | Goat | 7.5 µg/ml | Vector laboratories, USA | - |
| CD31 | Mouse | 1.25 µg/ml | Agilent Dako, USA | JC-70A |
| CD45 | Mouse | 10 µg/ml | Biolegend, USA | HI30 |
| CD68 | Mouse | 0.3 µg/ml | Agilent Dako, USA | PG-M1 |
| Dylight 488 streptavidin | - | 5 µg/ml | Vector laboratories, USA | - |
| MRC1 | Rabbit | 10.25 µg/ml | Abcam, UK | Polyclonal |
| Pan-Cytokeratin | Mouse | 0.05 µg/ml | Biolegend, USA | AE1/AE-3 |
| Purified mouse IgG1 Isotype control | Mouse | | Biolegend, USA | - |
| Purified mouse IgG3 Isotype control | Mouse | | Biolegend, USA | - |
| Streptavidin Alexa fluor 555 | - | 5 µg/ml | Life technologies | - |

2.1.5. List of Neogenomics antibodies

| Antibody | Source | Clone |
|-----------------|---------------------------------|------------|
| aSMA | Sigma-Aldrich, USA | 1A4 |
| CD11B | R&D systems, USA | 238439 |
| CD163 | Bio-rad, USA | EDHu-1 |
| CD3 | Agilent Dako, USA | F7.2.38 |
| CD31 | Cell Signalling Technology, USA | 89C2 |
| CD4 | Abcam, UK | ERP6855 |
| CD56 | Cell Marque, USA | MRQ-42 |
| CD68 | Biolegend, USA | KP1 |
| CD8 | Agilent Dako, USA | C8/144B |
| CXCR4 | Abcam, UK | UMB2 |
| FOXP3 | Biolegend, USA | 206D |
| LAG3 | Lifespan Biosciences, USA | 17B4 |
| Pan cytokeratin | Sigma-Aldrich, USA | PCK26 |
| PD1 | Abcam, UK | EPR4877 |
| PD-L1 | Abcam, UK | SP142 |
| TIM3 | R&D systems, USA | Polyclonal |

2.1.6. List of cell lines

| Cell line | Source |
|---|--------------------|
| Human lung fibroblasts (HLFs) | Promocell, Germany |
| Human umbilical vein endothelial cells (HUVECs) | Promocell, Germany |
| MDA-MB-231 | ATCC, USA |
| T47D | ATCC, USA |

2.1.7. List of equipment

| Equipment | Manufacturer |
|--|-----------------------------|
| AF600LX inverted widefield microscope | Leica Microsystems, Germany |
| Antigen retrieval pressure cooker | Prestige Medical, UK |
| Nanozoomer XR slide scanner | Hamamatsu photonics, Japan |
| Nikon A1 Confocal | Nikon, Japan |
| Nikon Ti Eclipse inverted widefield microscope | Nikon, Japan |
| RM2245 Microtome | Leica Biosystems, Germany |
| TC20 automated cell counter | Bio-rad, USA |

2.1.8. List of software

| Software | Developer |
|------------------|---|
| Fiji, Image J | https://imagej.net/Fiji [192] |
| GraphPad Prism 9 | GraphPad Software Inc |
| LAS X | Leica Microsystems, Germany |
| NIS-elements | Nikon, Japan |

2.1.9. List of breast cancer now TNBC samples

| | Treatment naïve, disease free | Treatment naïve, metastasis | Neoadjuvant therapy, disease free | Neoadjuvant therapy, metastasis |
|---|----------------------------------|--------------------------------|--------------------------------------|------------------------------------|
| Age at diagnosis | | | | |
| 21-39 | 2 (20) | 2 (20) | 1 (10) | 2 (28.6) |
| 40-59 | 3 (30) | 2 (20) | 7 (70) | 3 (42.8) |
| 60-79 | 3 (30) | 6 (60) | 2 (20) | 2 (28.6) |
| 80-99 | 2 (20) | 0 (0) | 0 (0) | 0 (0) |
| Tumour size | | | | |
| T1 | 4 (40) | 2 (20) | 2 (20) | 2 (28.6) |
| T2 | 6 (60) | 7 (70) | 7 (70) | 5 (71.5) |
| T3 | 0 (0) | 1 (10) | 1 (10) | 1 (14.3) |
| Tumour grade | | | | |
| 2 | 1 (10) | 2 (20) | 0 (0) | 0 (0) |
| 3 | 9 (90) | 8(80) | 10 (100) | 7 (100) |
| Time between end of treatment and surgery (days) | | | | |
| <30 | n/a | n/a | 3 (30) | 2 (28.6) |
| 30-40 | n/a | n/a | 4 (40) | 3 (42.8) |
| >40 | n/a | n/a | 3 (30) | 2 (28.6) |
| Lymph node status | | | | |
| Involved | 3 (30) | 7 (70) | 4 (40) | 7 (100) |
| Not involved | 6 (60) | 2 (20) | 5 (50) | 0 (0) |
| Not sampled | 1 (10) | 1 (10) | 1 (10) | 0 (0) |

| | Treatment naïve, disease free | Treatment naïve, metastasis | Neoadjuvant therapy, disease free | Neoadjuvant therapy, metastasis |
|--|----------------------------------|--------------------------------|--------------------------------------|------------------------------------|
| Neoadjuvant therapy received | | | | |
| FEC-T | 0 (0) | 0 (0) | 7 (70) | 3 (42.8) |
| FEC | 0 (0) | 0 (0) | 2 (20) | 1 (14.3) |
| Other | 0 (0) | 0 (0) | 1 (10) | 3 (42.8) |
| None | 10 (100) | 10 (100) | 0 (0) | 0 (0) |
| Metastases within 3-year follow-up? | | | | |
| Yes | 0 (0) | 10 (100) | 0 (0) | 7 (100) |
| No | 10 (100) | 0 (0) | 10 (100) | 0 (0) |
| Adjuvant therapy received | | | | |
| Radiotherapy only | 1 (10) | 0 (0) | 5 (50) | 6 (85.6) |
| Radiotherapy & Chemotherapy | 7 (70) | 6 (60) | 5 (50) | 1 (14.3) |
| Chemotherapy only | 1 (10) | 2 (20) | 0 (0) | 0 (0) |
| None | 1 (10) | 1 (10) | 0 (0) | 0 (0) |
| No data | 0 (0) | 1 (10) | 0 (0) | 0 (0) |
| Adjuvant chemotherapy received | | | | |
| Carboplatin | 0 (0) | 0 (0) | 2 (20) | 1 (14.3) |
| Carboplatin & Gemcitabine | 0 (0) | 0 (0) | 2 (20) | 2 (28.6) |
| Docetaxel | 0 (0) | 0 (0) | 0 (0) | 1 (14.3) |
| FEC-T | 5 (50) | 4 (40) | 0 (0) | 0 (0) |
| Other | 3 (30) | 4 (40) | 1 (10) | 2 (28.6) |
| None | 2 (20) | 1 (10) | 5 (50) | 1 (14.3) |
| No data | 0 (0) | 1 (10) | 0 (0) | 0 (0) |

2.2. Methods

2.2.1. Ethics

Studies involving human participants were reviewed and approved by the Ethics Review Boards of the Breast Cancer Now Tissue Bank in the UK and the Ottawa Health Sciences Network Research Ethics Board, Canada.

Samples were collected from Barts Health NHS Trust, UK and Nottingham University Hospitals NHS Trust, UK between 2011 and 2017 and obtained from the Breast Tissue Bank of the UK Charity, Breast Cancer Now, using ethical approvals 18/EE/0002 and 10/H1008/6. REB approval number 20160459-01H was issued by the Ottawa Health Sciences Network Research Ethics Board.

2.2.2. Optimisation of staining for perivascular macrophages

TNBC sections treated with neoadjuvant chemotherapy were used to optimise the triple stain protocols for CD31, CD68 and MRC1. These were then used for the quantification of MRC1+ PV macrophages in the sections received from the Breast Cancer Now tissue bank.

2.2.2.1. Optimisation of CD68, MRC1 and CD31 stains in TNBC

Sections from TNBCs were obtained from the Ottawa Hospital Research Institute, Canada. REB approval number 20160459-01H. These were confirmed as lacking ER, PR and HER2 at the OHRI and had all received neoadjuvant anthracycline or taxane prior to their surgical removal.

2.2.2.2. Haematoxylin and eosin (H&E) staining of TNBC sections

5µm thick, formalin fixed, paraffin-embedded (FFPE) sections were dewaxed in xylene and rehydrated using decreasing concentrations of ethanol (100-70%). The sections were rinsed in tap water for 1 min before staining with Gills No2 haematoxylin (Sigma-Aldrich) for 1 min. The slides were rinsed in tap water for 3 min before dehydration with increasing concentrations of ethanol (70%-100 %) for 3 min. The sections were stained with 95% eosin (Arcos) in ethanol for 30 s before rinsing with 100% ethanol to remove the residual eosin solution. Sections were cleared in

xylene before mounting in DPX mounting medium (Sigma-Aldrich). Representative images were acquired using a Nanozoomer-XR slide scanner (Hamamatsu).

2.2.2.3. Immunohistochemistry (IHC)

5 μ m thick FFPE sections were dewaxed with xylene, rehydrated using decreasing concentrations of ethanol, and rinsed in tap water. Following rehydration, endogenous peroxidase activity was blocked by incubation with 3% hydrogen peroxide in absolute methanol. Heat-induced antigen retrieval was performed using a target retrieval solution pH6.0 (Dako) and heated using a pressure cooker (Prestige Medical) for 20 min at 121°C. Sections were washed in tris buffered saline (0.5M tris base, 0.3M NaCl pH8.4) (TBS) and tissue surrounded using a hydrophobic barrier PAP pen (Vector Laboratories). A blocking step with 2.5% horse serum and 1% bovine serum albumin (BSA) (Vector) was performed for 20 min at room temperature. Unlabelled primary antibodies were diluted to the concentrations listed in Table 2 in TBS and added to the sections for 1 h. After washing with TBS, antibodies were detected using either an anti-mouse peroxidase or anti-rabbit alkaline phosphatase detection kit (Vector Laboratories). The sections were then washed before substrate detection with either DAB (Vector Laboratories) or Vector Red alkaline phosphatase. (Vector laboratories). Detection using Vector Red alkaline phosphatase included the addition of 1 drop of levamisole (Vector) per 5 ml of alkaline phosphatase substrate buffer to block endogenous alkaline phosphatase within the tissue sections. Sections were then washed in tap water, counterstained with Gills no2 haematoxylin, dehydrated through alcohol, and mounted with DPX. Representative images were acquired using a Nanozoomer-XR slide scanner (Hamamatsu) to capture whole slide images.

2.2.2.4. Immunofluorescence (IF) staining of TNBC sections.

Sections were dewaxed, rehydrated, antigen retrieval was performed, and sections were surrounded by a hydrophobic barrier PAP pen, as previously mentioned. A protein block prepared using 10% normal goat serum (Vector Laboratories) and 1% BSA was performed for 20 min at room temperature. Unlabelled primary antibodies were diluted in blocking serum at the concentrations given in section 2.1.4 and added to the sections for 1 h. The sections were washed

in TBS and incubated with fluorescent secondary antibodies for 1 h. To stain the two anti-mouse primary antibodies simultaneously, IgG-specific secondary antibodies were used to prevent cross-reaction between the primary antibodies. Sections were washed in TBS before the slides were mounted using prolong gold anti-fade with DAPI (Invitrogen). Slides were left to dry for 24 h before images were acquired using the Nikon inverted Ti Eclipse dual-cam widefield system and NIS-elements software (Nikon). All staining procedures were performed using IgG controls.

2.2.2.5. Biotin signal amplification

For biotin signal amplification, after incubation with the protein block, endogenous biotin was blocked using a streptavidin/biotin blocking kit (Vector) following the kit instructions. The first unlabelled primary antibody was diluted in protein blocking serum at the concentrations given in section 2.1.4 and added to the sections for 1 h. The sections were then incubated with anti-mouse biotin diluted in PBS for 30 min and washed in TBS. The sections were then incubated with streptavidin-bound fluorescent secondary antibodies for 1 h before washing with TBS. Additional markers were stained by incubation with protein-blocking serum for 20 min. The sections were then washed, mounted, and imaged as described previously for IF.

2.2.2.6. Image acquisition of perivascular staining

The IF-stained breast cancer sections were imaged using a Nikon inverted Ti Eclipse dual-cam widefield system. The DAPI channel was viewed at 20x magnification to manually scan sections. Regions of interest (ROIs) that contained approximately 50:50 tumour cell islands (TCI)/stroma were selected based on the morphology of the nuclear stains. Once a ROI had been selected, The CD31 channel was viewed. If no CD31 staining was present, the steps were repeated, randomly selecting another area of the section until an area containing CD31 labelled cells was found, and the image was captured.

2.2.2.7. Assessment of dual labelling

Following the acquisition of images from IF labelled slides, images were analysed using Fiji, ImageJ software [192]. The stain of interest was merged with the DAPI channel and using the cell counter plugin, only labelled cells that had nucleated DAPI⁺ events were marked. The marked image was then overlaid onto the second stain of interest and cells were marked using a second counter. The two counts then gave a percentage of co-localisation. If staining for any of the antibodies was considered sub-standard, then the sections was not counted.

2.2.2.8. Assessment of PV TAMs

Following the acquisition of images from IF labelled slides, images were analysed using Fiji, ImageJ software. Each channel containing a stain of interest was merged separately with the DAPI channel. Using the imaged of the merged DAPI and CD31 channels and using the ROI tool, overlays marking the surface area of CD31 labelled vessels were created and then measured. The CD31 overlays were then applied to the merged images of DAPI with CD68 and DAPI with MRC1. The CD31 overlays were then extended out by 10µm. Using the cell counter plugin, only CD68 labelled cells that had nucleated DAPI⁺ events were marked that fell with the extended CD31 overlay. The marked image was then overlaid onto the MRC1/DAPI image and MRC1⁺ labelled cells that had nucleated DAPI⁺ events were marked that fell with the extended CD31 overlay cells were marked using a second counter. The two counts then gave a percentage of co-localisation. If staining for any of the antibodies was considered sub-standard, then the sections was not counted.

2.2.2.9. Quality assurance of IHC

Breast tissue obtained in section **2.2.1** was checked alongside NHS pathologist, Patricia Verghani to identify areas of TCI and stroma regions and to avoid areas of necrosis and scarring that were present after neoadjuvant chemotherapy.

As part of the staining procedure, each antibody was substituted with its own isotype-matched, concentration-matched IgG control (listed in section **2.1.4**). Species-specific secondary antibodies conjugated to spectrally distinct fluorophores

were utilised. The selection of fluorophores was driven by the need to minimise spectral overlap and maximise signal-to-noise ratios and was checked using negative controls.

2.2.3. Multiplex analysis of TNBC sections

2.2.3.1. Human TNBCs

FFPE sections (3µm) from 37 primary human TNBCs (deetail in section **2.1.9**) were obtained from the Breast Tissue Bank of the UK charity, Breast Cancer Now under application number TR101. These were collected at the Barts Health NHS Trust Hospitals and Nottingham University NHS Trust Hospital in the UK between 2011 and 2017. Samples were split into 4 groups:

- Did not receive NAC and remained disease-free for a 3 year follow up period (Untreated DF).
- Did not receive NAC and then developed metastasis within a 3 year follow up period (Untreated Mets).
- Received NAC and remained disease free for a 3 year follow up period (NAC DF).
- Received NAC and then developed metastasis within a 3 year follow up period (NAC mets).

Follow-up data were used to correlate multiplex immunostaining results with the presence or absence of metastasis during this period.

2.2.3.2. Selection of ROIs

Prior to multiplexing, whole FFPE tumour sections were stained with H&E and examined by a pathologist to ensure the presence of malignant tumour.

ROIs across viable tumour areas were selected by an in-house pathologist (**Figure 2-1**). ROIs were selected to include both viable tumour cell islands (TCIs) and the surrounding stroma, with a particular focus on incorporating PanCK-rich regions that defined the TCIs.

Areas exhibiting necrosis or scarring were deliberately excluded to maintain the analytical integrity of the study, ensuring that only representative, viable tumour regions were analysed.

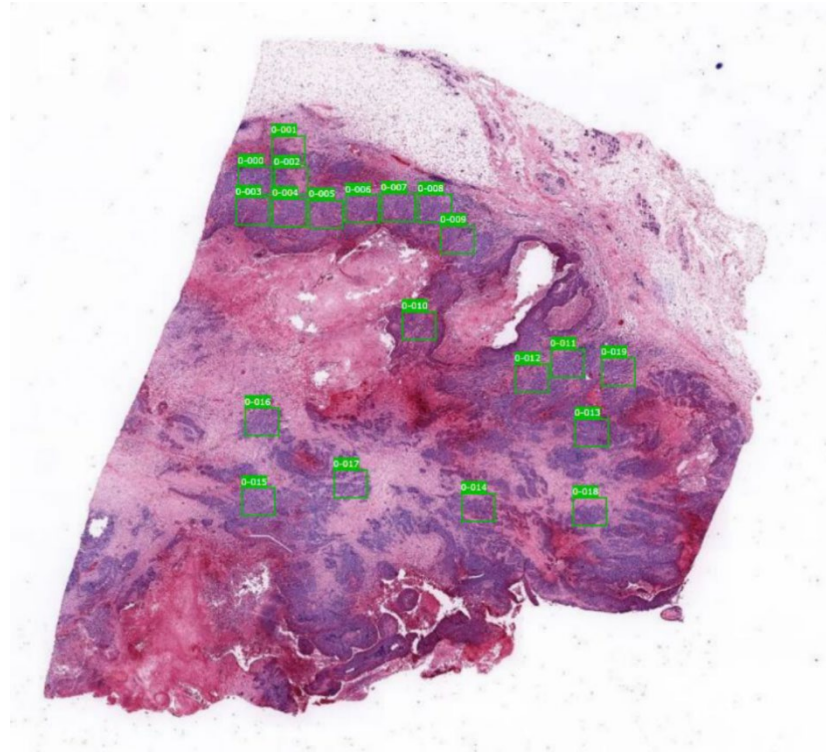


Figure 2-1 TNBC tumour H&E with 20 ROIs selected

A representative H&E stained TNBC with 20 ROIs (outlined by green boxes) selected by a pathologist, ensuring that ROIs contained regions of viable malignant tumour cells.

2.2.3.3. Multiplex staining of TNBC sections by NeoGenomics Labs (NGs)

Sections were then multiplexed with a custom panel, using the markers listed in section 2.1.5. This 'MultiOmyx™' procedure involved baking sections at 65°C for 1 h, deparaffinizing and treating them with a two-step antigen retrieval process. They were then blocked against nonspecific binding with 10% donkey serum and 3% BSA in PBS for 1h at RT and stained with DAPI for 15 min. Directly conjugated primary antibodies were diluted in PBS supplemented with 3% (wt/vol) BSA (to working concentrations optimized previously) and applied for 1h at RT on a Leica Bond III Stainer.

Several rounds of paired antibody staining were performed in sequence on each tumour section using the antibodies listed above. After each round of staining

with two antibodies, high resolution images were collected using a 20x objective on an INCell analyzer 2200 microscope (GE Healthcare Life Sciences) from 20 regions of interest (ROIs)

Following each staining round of the MultiOmyx™ staining procedure, all samples underwent and passed a quality control level check (**Figure 2-2**). The percentage of the original starting material present after each staining round was checked to ensure that a relative sample of cells was still present after all rounds of staining were complete. An internal quality control threshold level of 60% tissue retention was set by NeoGenomics Labs.

The mean value of a given parameter (e.g. TIM-3) was then calculated for each tumour section using these 20 ROIs, and the overall mean +/- SEM calculated for each tumour group using these values.

In between exposure to paired antibodies, slides were washed in PBS/0.3% TritonX-100 and dye inactivation performed by immersion in an alkaline solution containing H₂O₂ for 15 min with gentle agitation at room temperature. Slides were washed again in PBS, imaged to check the efficacy of the dye in-activation, and stained with the next pair of antibodies.

| Slide | Initial# Cells | Round 1 | Round 2 | Round 3 | Round 4 | Round 5 | Round 6 | Round 7 | Round 8 | Round 9 | Round 10 | Round 11 | Overall QC | QC passed # Cells |
|----------------|----------------|---------|---------|---------|---------|---------|---------|---------|---------|---------|----------|----------|------------|-------------------|
| S-190628-00060 | 57235 | 0.998 | 0.996 | 0.995 | 0.994 | 0.995 | 0.996 | 0.989 | 0.993 | 0.989 | 0.989 | 0.988 | 0.983 | 56254 |
| S-190628-00063 | 64934 | 1.000 | 0.999 | 0.999 | 0.999 | 0.999 | 0.999 | 0.997 | 0.997 | 0.997 | 0.997 | 0.995 | 0.994 | 64537 |
| S-190628-00066 | 52345 | 0.988 | 0.983 | 0.974 | 0.969 | 0.927 | 0.924 | 0.920 | 0.920 | 0.909 | 0.903 | 0.902 | 0.872 | 45659 |
| S-190628-00069 | 59626 | 0.998 | 0.989 | 0.988 | 0.988 | 0.987 | 0.983 | 0.983 | 0.978 | 0.971 | 0.966 | 0.964 | 0.951 | 56726 |
| S-190628-00072 | 56250 | 1.000 | 0.999 | 0.999 | 0.999 | 0.898 | 0.896 | 0.896 | 0.894 | 0.896 | 0.897 | 0.896 | 0.879 | 49450 |
| S-190628-00075 | 65168 | 0.999 | 0.999 | 0.998 | 0.998 | 0.994 | 0.993 | 0.993 | 0.992 | 0.992 | 0.992 | 0.991 | 0.987 | 64353 |
| S-190628-00078 | 60922 | 0.988 | 0.986 | 0.984 | 0.972 | 0.974 | 0.950 | 0.952 | 0.954 | 0.965 | 0.944 | 0.934 | 0.874 | 53246 |
| S-190628-00081 | 100856 | 1.000 | 1.000 | 0.999 | 0.996 | 0.996 | 0.995 | 0.996 | 0.981 | 0.981 | 0.978 | 0.979 | 0.974 | 98187 |
| S-190628-00084 | 105079 | 1.000 | 0.988 | 0.996 | 0.997 | 0.997 | 0.996 | 0.993 | 0.994 | 0.995 | 0.995 | 0.996 | 0.980 | 103009 |
| S-190628-00087 | 74984 | 1.000 | 1.000 | 0.999 | 0.999 | 0.996 | 0.996 | 0.995 | 0.994 | 0.995 | 0.994 | 0.995 | 0.991 | 74332 |
| S-190628-00090 | 85030 | 0.998 | 0.996 | 0.996 | 0.995 | 0.992 | 0.990 | 0.989 | 0.992 | 0.992 | 0.992 | 0.989 | 0.980 | 83324 |
| S-190628-00093 | 58034 | 0.996 | 0.992 | 0.993 | 0.994 | 0.994 | 0.994 | 0.993 | 0.993 | 0.992 | 0.992 | 0.992 | 0.986 | 57247 |
| S-190628-00096 | 87215 | 0.998 | 0.998 | 0.998 | 0.998 | 0.998 | 0.998 | 0.996 | 0.996 | 0.996 | 0.996 | 0.996 | 0.995 | 86739 |
| S-190628-00099 | 54760 | 0.998 | 0.997 | 0.994 | 0.991 | 0.991 | 0.990 | 0.988 | 0.987 | 0.988 | 0.984 | 0.983 | 0.978 | 53564 |
| S-190628-00102 | 82527 | 1.000 | 0.999 | 0.999 | 0.999 | 0.999 | 0.999 | 0.999 | 0.998 | 0.994 | 0.936 | 0.937 | 0.932 | 76940 |
| S-190628-00105 | 56572 | 0.998 | 0.991 | 0.991 | 0.978 | 0.948 | 0.946 | 0.945 | 0.946 | 0.945 | 0.944 | 0.944 | 0.937 | 52990 |
| S-190628-00108 | 55608 | 1.000 | 0.999 | 0.999 | 0.999 | 0.990 | 0.990 | 0.990 | 0.989 | 0.989 | 0.988 | 0.989 | 0.986 | 54837 |
| S-190628-00111 | 40473 | 0.995 | 0.996 | 0.995 | 0.995 | 0.994 | 0.995 | 0.992 | 0.993 | 0.992 | 0.990 | 0.991 | 0.984 | 39844 |
| S-190628-00114 | 90886 | 0.998 | 0.998 | 0.996 | 0.996 | 0.987 | 0.984 | 0.984 | 0.980 | 0.983 | 0.983 | 0.983 | 0.977 | 88754 |
| S-190628-00117 | 55447 | 0.871 | 0.870 | 0.845 | 0.857 | 0.876 | 0.855 | 0.795 | 0.812 | 0.803 | 0.802 | 0.773 | 0.734 | 40681 |
| S-190628-00120 | 64712 | 0.999 | 0.998 | 0.995 | 0.995 | 0.995 | 0.992 | 0.992 | 0.991 | 0.991 | 0.991 | 0.991 | 0.989 | 63984 |
| S-190628-00125 | 97784 | 1.000 | 1.000 | 0.999 | 0.999 | 0.999 | 0.999 | 0.999 | 0.998 | 0.995 | 0.995 | 0.995 | 0.994 | 97172 |
| S-190628-00128 | 57362 | 0.998 | 0.996 | 0.996 | 0.996 | 0.994 | 0.992 | 0.986 | 0.985 | 0.985 | 0.979 | 0.978 | 0.974 | 55879 |
| S-190628-00131 | 78713 | 1.000 | 1.000 | 1.000 | 1.000 | 0.966 | 0.966 | 0.967 | 0.967 | 0.968 | 0.968 | 0.967 | 0.958 | 75435 |
| S-190628-00134 | 70917 | 1.000 | 0.999 | 0.999 | 0.999 | 0.947 | 0.927 | 0.927 | 0.923 | 0.924 | 0.924 | 0.924 | 0.911 | 64634 |
| S-190628-00137 | 71843 | 0.998 | 0.997 | 0.996 | 0.996 | 0.994 | 0.994 | 0.994 | 0.994 | 0.993 | 0.992 | 0.991 | 0.987 | 70919 |
| S-190628-00140 | 106304 | 1.000 | 1.000 | 0.999 | 0.997 | 0.997 | 0.997 | 0.995 | 0.996 | 0.996 | 0.996 | 0.996 | 0.995 | 105746 |
| S-190628-00143 | 64117 | 0.999 | 0.998 | 0.998 | 0.997 | 0.996 | 0.996 | 0.996 | 0.994 | 0.995 | 0.994 | 0.994 | 0.992 | 63585 |
| S-190628-00146 | 51630 | 1.000 | 1.000 | 1.000 | 1.000 | 0.986 | 0.983 | 0.983 | 0.983 | 0.983 | 0.983 | 0.979 | 0.974 | 50295 |
| S-190628-00149 | 93701 | 1.000 | 0.999 | 0.999 | 0.999 | 0.999 | 0.998 | 0.998 | 0.998 | 0.997 | 0.998 | 0.998 | 0.996 | 93336 |
| S-190628-00152 | 65746 | 0.986 | 0.979 | 0.978 | 0.961 | 0.950 | 0.856 | 0.802 | 0.789 | 0.800 | 0.792 | 0.633 | 0.597 | 39271 |
| S-190628-00155 | 66306 | 0.994 | 0.997 | 0.989 | 0.996 | 0.996 | 0.999 | 0.992 | 0.981 | 0.988 | 0.991 | 0.991 | 0.972 | 64441 |
| S-190628-00158 | 83502 | 0.972 | 0.994 | 0.995 | 0.994 | 0.993 | 0.993 | 0.985 | 0.983 | 0.982 | 0.971 | 0.967 | 0.943 | 78729 |
| S-190628-00161 | 58012 | 0.977 | 0.998 | 0.998 | 0.998 | 0.998 | 0.997 | 0.995 | 0.994 | 0.980 | 0.992 | 0.993 | 0.970 | 56288 |
| S-190628-00183 | 102261 | 0.992 | 0.999 | 0.999 | 1.000 | 0.997 | 0.997 | 0.997 | 0.997 | 0.985 | 0.988 | 0.996 | 0.982 | 100452 |
| S-190628-00186 | 102749 | 0.973 | 0.999 | 0.999 | 0.997 | 0.997 | 0.998 | 0.997 | 0.998 | 0.986 | 0.995 | 0.997 | 0.969 | 99615 |
| S-190628-00189 | 77372 | 0.995 | 0.982 | 0.981 | 0.990 | 0.990 | 0.991 | 0.993 | 0.987 | 0.985 | 0.984 | 0.991 | 0.975 | 75406 |
| S-190628-00217 | 54956 | 0.996 | 0.996 | 0.981 | 0.983 | 0.982 | 0.980 | 0.979 | 0.980 | 0.972 | 0.978 | 0.977 | 0.962 | 52888 |
| S-190628-00226 | 53134 | 0.976 | 0.997 | 0.966 | 0.987 | 0.989 | 0.986 | 0.979 | 0.982 | 0.973 | 0.971 | 0.971 | 0.941 | 49982 |
| S-190628-00235 | 54957 | 0.998 | 0.997 | 0.972 | 0.985 | 0.984 | 0.982 | 0.979 | 0.963 | 0.975 | 0.974 | 0.973 | 0.953 | 52370 |

Figure 2-2 MultiOmyx™ tissue retention table

This table depicts the progression of tissue loss over the course of all staining rounds. Initial total cell was counted and recorded after each round of staining. Each row contains the combined data from all ROIs. Quality control level of at least 60% of cells in ROI pass.

2.2.3.4. Quantitative image analysis using AI

An AI-based, advanced analytics platform, proprietary to NeoGenomics Labs, called 'NEO Image Analysis', was used to quantify and analyse cell subsets in various tumour areas including algorithms that could differentiate between them in stromal and TCIs. PanCK was used as a marker of TNBC tumour cells and was used to define the TCI regions (**Figure 2-3 B**) and generate a binary tumour mask (**Figure 2-3 C**). Areas that were unstained outside if the TCI were defined as stroma regions.

For image analysis, study-specific datasets were generated by NeoGenomics Labs and with previously collected training datasets. Generally, datasets were not separated by tumour type, since expanding the training data tended to increase both accuracy and validity of the models.

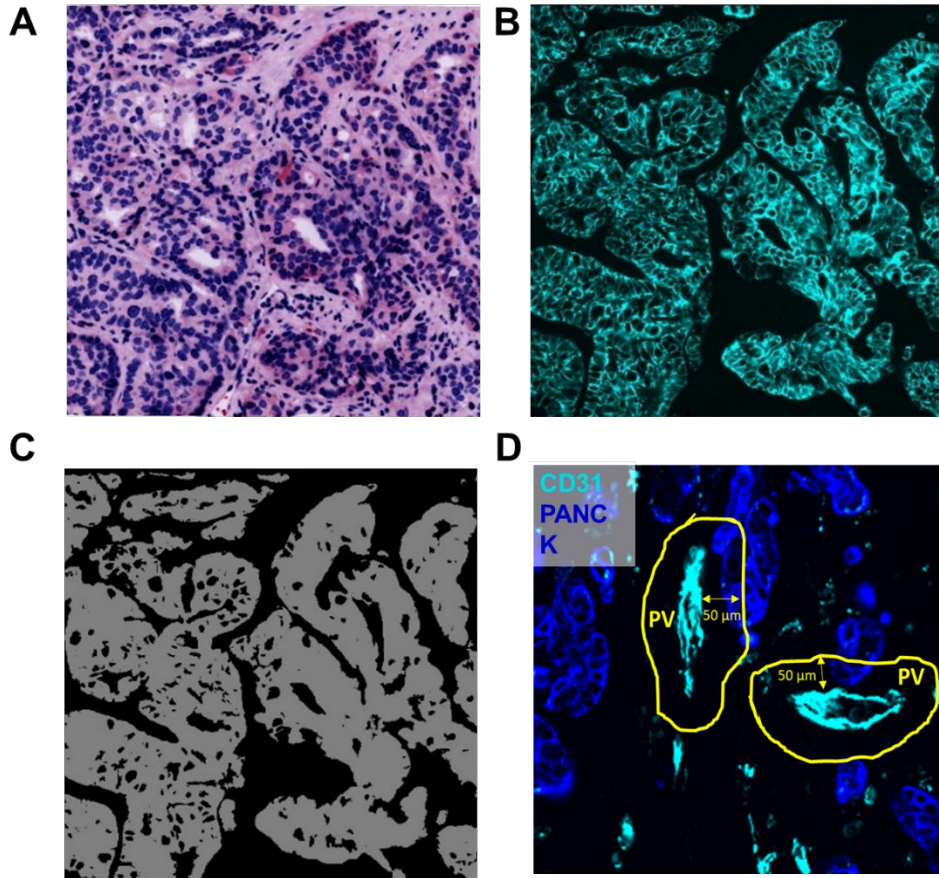


Figure 2-3 Defining the TCI, stroma and perivascular areas

A. H&E from a ROI. B. Tumour cell staining of PanCK staining to produce a tumour mask C. which can divide the section into tumour or outside tumour areas. D. Representative image of how PV regions are defined by expanding a 50µm region from a CD31+ blood vessel

Algorithms were developed as part of the NeoLYTX software, using CD31+ to mark blood vessels and the perivascular niche – defined as expanded 50µm region from the CD31+ blood vessels (**Figure 2-3 D**), in keeping with other published studies on the PV niche [112]. This was generated by radially expanding 50µm from the CD31+ cellular segmentation mask. This was then used to define the area 4 spatial regions - PV/stroma, PV/TCI, non-PV/stroma and non-PV/TCI.

Cells were segmented using this algorithm and tracked through each staining round, and deep learning models used to quantify positivity for each stain, as well as to classify regions as TCIs or stroma. A cell segmentation algorithm was trained on DAPI-stained images to detect and segment individual cells. This segmentation model was trained by manually annotated DAPI-positive objects in a representative set of images. These annotations were used to generate a labelled mask in which

pixels corresponding to each nucleus were assigned a unique identifier, providing the ground-truth data for the segmentation task.

After segmenting each nucleus, Cell positivity for each marker was assessed based on detectable signal above background. Marker-specific AI algorithms were trained to incorporate both stain intensity and stain morphology in order to differentiate between true stain and nonspecific background or image artifacts. For biomarker-specific binary (positive/negative) classification, a small image (100×100 pixels) was centred on the segmented nucleus. These patches were labelled as positive or negative for the given biomarker based on the observed staining pattern. Separate datasets were constructed for each biomarker, allowing the training of distinct classification models. Label maps for each biomarker underwent quality control for accuracy by the lead biologist and analyst at NeoGenomics Labs to ensure concordance between the algorithms and scientist.

The density of each cell type was calculated in each region of interest (ROI) (for both PV and non-PV areas of the stroma versus TCIs) by dividing the total cell count in a given area by the area itself (in mm²).

2.2.3.5. Quality assurance of MultiOmyx staining

ROI-level summary tables were generated for the whole study. These tables listed cell counts, densities, tissue, tumour and outside-tumour region areas. Images of the pathologist annotations for each ROI were provided (**Figure 2-1**). Label maps were generated for each biomarker for each ROI in the study. These binary images act as masks that show which cells are positive for a given biomarker

2.2.4. Generation of a microfluidic model

2.2.4.1. Subculture of human cell lines

Human Umbilical Vein Endothelial cells (HUVECs) were cultured in endothelial cell growth medium 2 (ECGM2) (PromoCell) supplemented with 10% foetal bovine serum (FBS) (0.05 ml/ml), endothelial cell growth supplement (0.0004 ml/ml), hEGF (10ng/ml), heparin (90µg/ml) and hydrocortisone (1µg/ml).

Human lung fibroblasts (HLFs) were cultured in fibroblast growth medium 2 (PromoCell) supplemented with FBS (0.02 ml/ml), hEGF (1ng/ml) and insulin (5 mg/ml). MDA-MB-231 cells were cultured in Dulbecco's modified Eagle's medium (DMEM) (Lonza) supplemented with 10% FBS (Gibco) and 2mM L-glutamine (Lonza). All the cell lines were incubated at 37°C and 5% CO₂.

For cell line passaging, cells were grown to 80% confluence. The growth medium was then removed and discarded. The cells were washed with Dulbecco's phosphate-buffered saline (DPBS) (Lonza), which was then removed and incubated with 0.2% trypsin/EDTA (Lonza). The detachment process was monitored using bright-field microscopy. Once the cells detached, trypsin was neutralised with FBS-containing medium. To remove the culture medium, the cells were pelleted by centrifugation. HUVECs and HLFs were centrifuged at 220 g for 3 min. MDA-MB-231 cells were centrifuged at 400 g for 5 min. The old medium was then removed from the cell pellet before the cell pellet was re-suspended at the desired seeding density and transferred to a T75 flask (ThermoFisher) in fresh media.

2.2.4.2. Cell counting

Cell counts were obtained by centrifugation of the cell lines to pellet the cells. The remaining medium was removed from the cell pellets before the pellets were re-suspended. Cells were either sampled from this suspension or diluted 1:10. The re-suspended cells were mixed 1:1 with 0.4% trypan blue solution. The cell suspensions were then counted using a TC20 automated cell counter (Bio-Rad).

2.2.4.3. Generation of fibroblast-conditioned medium

HLFs were seeded in T75 flasks and grown to 90% confluency. The old culture medium was removed from the flask and the cells were washed with DPBS. New supplemented fibroblast growth medium 2 was added to the cells and incubated for 24 h at 37°C with 5% CO₂. Fibroblast growth medium 2 was then removed from the cells, and the medium was centrifuged at 400 g for 10 min to remove any remaining cells/debris. This medium was then stored at -80°C until use.

2.2.4.4. Immunofluorescent labelling of live cells

For labelling of HUVECs, HLFs or MDA-MB-231 cultures, the cells were detached using 0.2% trypsin/EDTA and then pelleted by centrifugation. The supernatant was discarded, and the cells were resuspended at 1×10^6 cells/ml in DPBS containing 1 μ l of 5mM CellTrace Carboxyfluorescein succinimidyl ester (CFSE) dye, CellTrace Violet or CellTrace Far red. This was followed by incubation in the dark at 37°C for 20 min. Following incubation, supplemented media was added at five times the original staining volume and incubated at 37°C for 5 min. The labelled cells were pelleted by centrifugation at 220 g for 3 min and suspended in the supplemented media.

2.2.4.5. Generation of tumour spheroids

Tumour spheroids were generated using a 2% agarose solution (Sigma) in supplemented DMEM (Lonza). The solution was heated to its boiling point in a microwave until all the agarose had dissolved. The liquid solution was allowed to cool for 30 minutes, and 100 μ l of the DMEM/agarose solution was added to each well of a 96-well cell culture plate. The solution was then allowed to cool and solidify. The outer wells of the 96-well plate were filled with DPBS. Confluent MDA-MB-231 breast cancer cells were detached, centrifuged, counted, and seeded at varying densities ranging from 100 to 10,000 cells per well, and cultured in complete DMEM for 48 hours.

For co-cultured spheroids, confluent MDA-MB-231 breast cancer cells and HLFs were detached, centrifuged, and counted. The MDA-MB-231 and HLF cells were then mixed at a 1:1 ratio, seeded at varying densities ranging from 500 to 2000 cells per well, and cultured in fibroblast growth medium 2 for 48 hours. To determine the cellular composition during the growth of the spheroid, MDA-MB-231 and HLFs were labelled with CellTrace CFSE or CellTrace Violet as detailed in section **2.2.4.4**. This confirmed that outgrowths from the spheroids were fibroblast derived.

2.2.4.6. Generation of a microvascular network

Prior to use, bovine fibrinogen (Sigma) was dissolved in DPBS at a concentration of 6 mg/mL and incubated at 37°C for 3 hours. The fibrinogen solution

was then filtered using a 0.22µm sterile filter (Starlab), aliquoted and stored at 4°C. Bovine thrombin (Sigma) was diluted in DPBS to create 100U/mL stock solution and aliquoted for storage at -20°C until needed.

HUVECs and HLFs were each detached using 0.2% trypsin/EDTA, centrifuged at 220g for 3 minutes and counted using a TC20 automated cell counter. They were then centrifuged again at 220g for 3 minutes and the supernatant removed. HUVECs and HLFs were separately re-suspended in the re-suspension media – (40µl of Thrombin stock solution 1ml of Endothelial cell growth medium MV2 (Promocell) (ECGM MV2) - at four times the desired final density. HUVECs were suspended at $4-5 \times 10^6$ cells/ml and HLFs were suspended at $2-4 \times 10^6$ cells/ml. Re-suspension media was created by adding 40µl of thrombin 100U/ml stock to 1ml of ECGM MV2, supplemented with FBS (0.05ml/ml), hEGF (5ng/ml), hFGF (10ng/ml), IGF (20ng/ml), VEGF, ascorbic acid (1µg/ml) and hydrocortisone (0.2µg/ml). The HUVEC and HLF cell suspensions were then mixed 1:1, ensuring a homogenous mix (**Figure 2-4**).

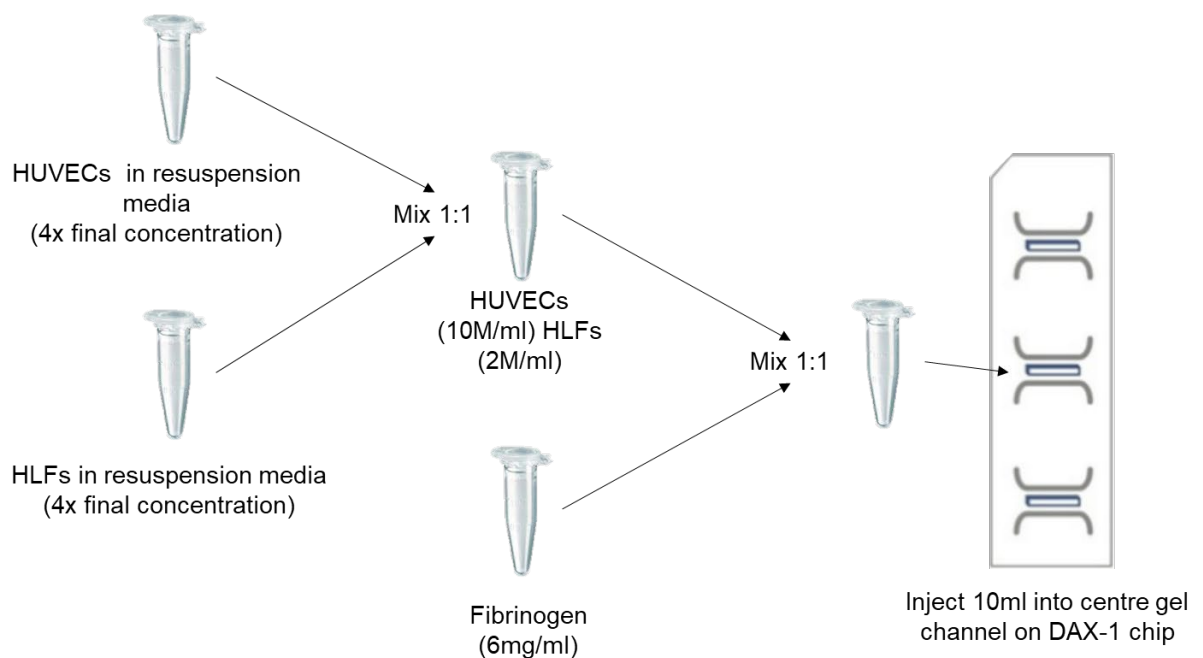


Figure 2-4 Mixing of cells and solutions prior to injection in the DAX-1 chip.

Generation of a vascular network. HUVECs and HLFs at 4x the desired final concentration, are suspended in ECGM MV2 media containing 4U/ml of thrombin are mixed together 1:1. This mix of cells is then mixed 1:1 with 6mg/ml fibrinogen solution injected into the centre gel inlet of the DAX-1 chip before the fibrin gel sets.

The HUVEC/HLF cell suspension was seeded by mixing 1:1 with 10 µl of 6mg/ml fibrinogen solution. The solutions were gently mixed 4-5 times by pipetting

before injection into gel inlet (**Figure 2-5 E**) of the DAX-1 chip (AIM Biotech). The DAX-1 culture chip was then placed in a humidified environment at 37°C for 15 mins to allow polymerisation of the fibrin gel. ECGM MV2 media complete with supplements was added to the media ports (**Figure 2-5 F**) and replaced every 24h. The chip was placed in a sterile 144mm petri dish (Fisher) containing a reservoir of sterile DPBS for humidity. After seeding of HUVEC/HLF cells, the 3D cell culture chips were checked under a phase contrast microscope to confirm a uniform distribution has been achieved and the gel had set.

To line the media channels with endothelial cells, a 60 µl suspension of 2×10^6 HUVEC cells in ECGM MV2 was added to the media reservoir at one end of each media channel (**Figure 2-5 B**), and allowed to , a vascular network would then form across the gel channel (**Figure 2-5 C**) within 4-6 days of seeding the chip.

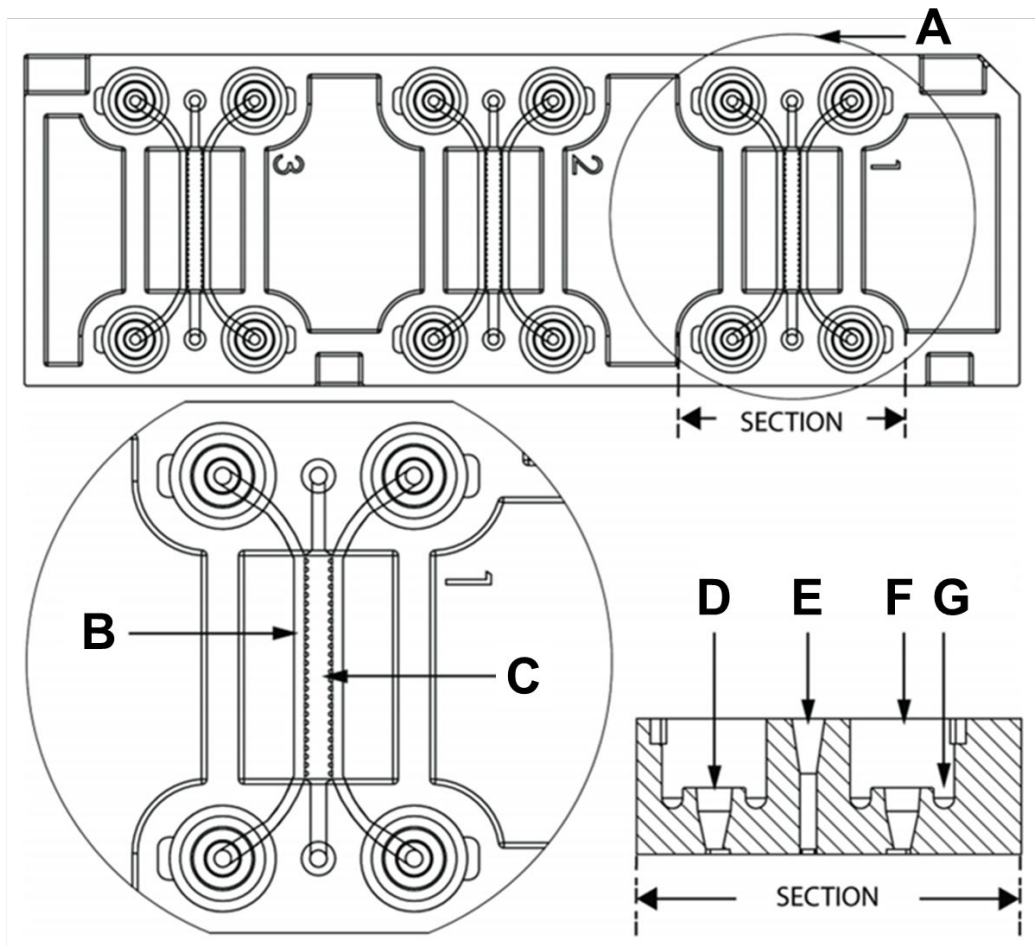


Figure 2-5 Schematic of the DAX-1 3D cell culture chip.

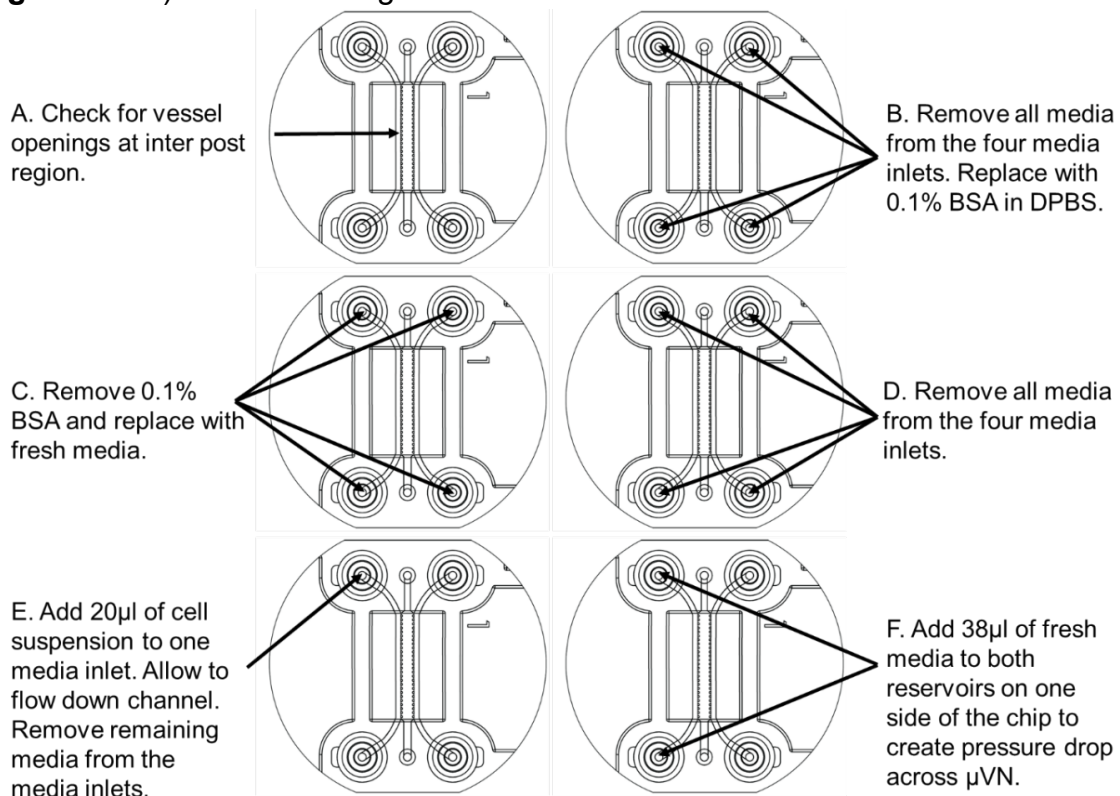
A. site. B. Shows the two media channels that flank either side of . C. gel channel. D. media inlet. E. the gel inlet which is the entry point to the gel channel. F. shows the port where media is added to media channels. G. media resevoirs.

2.2.4.7. Perfusion with tumour cells

After 4-5 days, the vascular network was checked for vessel openings at the inter-post regions on the DAX-1 3D cell culture chip (**Figure 2-6 A**). Prior to perfusion, confluent MDA-MD-231 cells were detached using 0.2% trypsin/EDTA and centrifuged at 400 g for 5 min. The supernatant was removed, and the cells were labelled using CellTrace CFSE dye, resuspended at 5×10^5 cells/ml, and stored on ice until perfusion.

Media reservoirs in the 3D cell culture chips were emptied and replaced with 0.1% BSA in DPBS for 20 min to minimise non-specific cell adhesion. Fresh ECGM MV2 medium was replaced in the media channels.

The media was then removed from all four media inlets, the suspended MDA-MD-231 cells were agitated to ensure a uniform cell suspension and 20 μ L was added to one of the media inlets and allowed to flow down the media channel (**Figure 2-6 E**). The remaining medium was removed from the media inlets. To allow



flow across the vascular network, a hydrostatic pressure drop was created by adding 38µl of fresh ECGM MV2 medium to both reservoirs on one side of the chip (**Figure 2-6 F**). Cell movements were then observed by both bright-field and fluorescence microscopy using a Leica AF600LX inverted microscope with a controlled environmental chamber. Images and time-lapse videos were captured using LAS AF software (Leica).

Figure 2-6 Perfusion of tumour cells through the vascular network.

Directions A-F of how to perfuse tumour cells through the DAX-1 chips once openings have formed at the inter-post regions.

2.2.4.8. Immunofluorescent staining of DAX-1 chips

At the end of the incubation period, all the media was removed from the media reservoir on the DAX-1 chip. The washing steps were performed by adding 100µl of PBS to the reservoirs on one side of the media channel only. This solution was allowed to flow through the media channels before being removed, and the washing step was repeated twice. 50µl of 4% PFA in PBS was then added the media reservoirs on one side of the media channel only. This solution was allowed to flow through and incubate for 10 min to allow fixation. The PFA was then removed from the channel reservoirs, and the PBS wash steps were repeated three times. Blocking steps were performed by adding 5% BSA/4% goat serum in PBS, allowing it to flow through, and incubating for 3 h at room temperature. After incubation, the protein block was removed before adding 50µl of primary antibody diluted in PBS, allowed to flow through the media channel, and left to incubate overnight in the dark at 4°C. The remaining primary antibody solution was then removed from the channel reservoirs, and the PBS washing steps were repeated three times. DAPI solution (300nM) in PBS was added to the medium channels for 2 min. The channels were washed a further three times with PBS. The stained DAX-1 chip was stored in the dark at 4°C before imaging.

2.3. Statistical analysis

Statistical analysis was carried out using GraphPad Prism V9 software (GraphPad Software) through the non-parametric Mann-Whitney U and Kruskal-

Wallis tests for unpaired data. Mean values and their standard errors of the mean (SEM) were plotted in graphs generated using GraphPad Prism. P values less than 0.05 were considered statistically significant. In cases where multiple testing was conducted, all P values were corrected for multiple testing using the Bonferroni or Dunn's test.

**Chapter 3 Establishment and validation of immunostaining protocols for
quantifying perivascular, tumour-promoting macrophages in human TNBCs
on of PV Macrophages by Histological Analysis**

3.1 Introduction

High numbers of CD68⁺ TAMs have long been associated with poor clinical outcome in breast tumours [191]. Macrophages though can display a wide range of phenotypes to cover their functions. As such, there can be several distinct populations of the cell type present in local tissue environments [193]. Furthermore, various studies reported differences in the number of perivascular (PV) MRC1⁺ TAMs between the TCIs and stroma in several tumour types [105] and they have been shown to drive relapse in pre-clinical models [113]. However, this has not yet been assessed in human TNBC, so the following study was conducted to see if PV MRC1⁺ TAMs are present in this tumour type, and whether more are present in the stroma than TCIs.

3.1. Results

3.1.1. Topography of triple negative breast cancers.

A number of published studies have reported the presence of distinct topography in human TNBC, consisting of tumour cell islands (TCIs, also sometimes known as tumour 'nests') and stroma [51, 194]. The presence of these 2 regions was confirmed in of a small cohort of TNBC biopsies (taken from patients treated with neoadjuvant chemotherapy) using haematoxylin and eosin (H&E) staining (see protocol described in section 2.2.2.2) (**Figure 3-1 A**). The stained sections were then examined with a breast pathologist, Dr Patricia Verghani, who provided training in how to identify TCIs and stroma areas.

On the rare occasions when TCIs were difficult to distinguish from healthy breast tissue, tumour cells in sections were stained using a pan-cytokeratin antibody, to identify epithelial cells (**Figure 3-1 B**). The nuclei of tumour cells exhibited a distinct size and morphology of the nucleus, being larger and more spherical (**Figure 3-1 red arrows**) than the nuclei of non-malignant cells, which were generally smaller (**Figure 3-1 yellow arrows**).

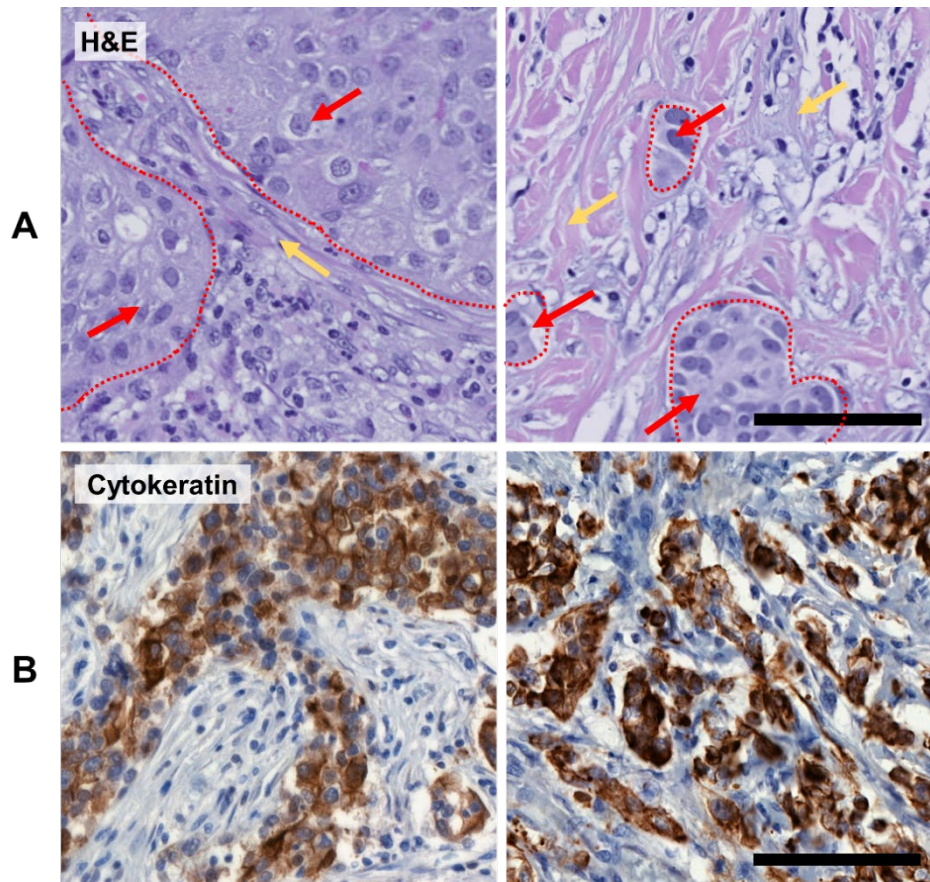


Figure 3-1 Identification of TCIs vs stromal areas in TNBC tumours.

A. examples of H&E staining in differing representative areas of TCIs (red arrows) and stroma (yellow arrows). Regions are separated by dotted line. B. IHC staining for pan cytokeratin (brown) to distinguish between epithelial TCIs and stroma. Regions are separated by dotted line. Scale bars 100 μ m.

The topography of the TNBC tumours varied, with cancer cells clustered into either small or large TCIs, but sometimes seen as single tumour cells occasionally in the stroma (**Figure 3-1 C**). Individual tumour cells or TCIs were identified in all TNBC sections and could be distinguished without the use of cytokeratin staining (i.e. using either H&E staining or the use of DAPI staining in IF staining protocols).

3.1.2. Optimisation of IHC protocol for MRC1⁺ perivascular TAMs in TNBC

To quantitatively assess the number and distribution MRC1⁺ CD68⁺ TAMs relative to blood vessels (i.e. to define them as PV or non-PV) in human TNBCs, a triple staining protocol for CD68, MRC1 and CD31 needed to be established and optimised. Furthermore, a previous paper suggested that CD68 can be expressed by

some fibroblasts in human breast tumours [51], so the pan-leukocyte marker, CD45, was also used to show that CD68 in the present study did not label fibroblasts (as these cells are CD45-).

Chromogenic detection had been chosen over fluorescence for several reasons - the occasional auto-fluorescence that occurs with some IF protocols on FFPE sections, the longer-term stability of chromogenic markers and the ability to amplify low antibody detection when necessary (e.g. biotin amplification of the CD68 staining), and the availability within the Department of scanning whole chromogenic-stained tissue sections. Due to the issues with detection dual labelling of markers on the same cells via the chromogenic approach, an IF staining method was used to stain and quantify the dual and triple labelling of TNBC sections.

Initially, each of the 4 markers was optimised as single stains on FFPE sections of human TNBCs (**Figure 3-2**) to demonstrate that the antibodies (listed in **2.1.4**) were working before moving onto the optimisation of dual stains and a triple stains. First, the recommended manufacturer's staining protocol was used to establish the single stains for each antibody (including the optimum retrieval method). Once a marker was optimised for a single stain and showed uniform staining across the section, the protocol for that marker was then tested on the remaining antibodies, until an optimal staining protocol (detailed in section **2.2.2.3**) was found to suit each CD68, MRC1, CD31 and CD45. A summary of the results for the different protocols tested for each single stain are shown in **Table 3-1**. As part of the optimisation procedure, each antibody was substituted with its own isotype-matched, concentration-matched IgG control. Due to the number of chromagens used for the detection of MRC1⁺ PV macrophages (MRC1, CD68 and CD31), it was not possible to include a stain for pan-cytokeratin in the IHC staining.

| Antibody (Species) | Dilution | Retrieval solution | Retrieval time (min) | Retrieval method | Buffer | Ab Incubation time (min) | Secondary Ab | Notes |
|--------------------|----------|--------------------|----------------------|------------------|--------|--------------------------|--------------|-----------------------|
| CD68 (mouse) | 1:60 | Sodium citrate | 30 | WB | PBS-T | 1 hr, RT | DAB | Good |
| | 1:60 | Tris/ EDTA | 10 | WB | PBS-T | 1 hr, RT | DAB | Non-specific staining |
| | 1:60 | Tris/ EDTA | 10 | WB | TBS-T | 1 hr, RT | DAB | Non-specific staining |
| | 1:60 | Tris/ EDTA | 10 | WB | TBS-T | 1 hr, RT | DAB | Good |
| | 1:60 | Tris/ EDTA | 10 | MW | TBS-T | 1 hr, RT | DAB | Good |
| | 1:100 | Sodium citrate | 20 | PC | PBS-T | 1 hr, RT | DAB | Good |
| | 1:100 | Dako pH 6.0 | 20 | PC | TBS | 1 hr, RT | DAB | Good |
| MRC1 (rabbit) | 1:800 | Tris/ EDTA | 10 | WB | TBS | 1 hr, RT | Vector Red | Non-specific staining |
| | 1:800 | Sodium citrate | 10 | WB | TBS | 1 hr, RT | Vector Red | Non-specific staining |
| | 1:800 | Sodium citrate | 20 | WB | TBS | 1 hr, RT | Vector Red | Non-specific staining |
| | 1:800 | Tris/ EDTA | 20 | WB | TBS | 1 hr, RT | Vector Red | Non-specific staining |
| | 1:800 | Tris/ EDTA | 10 | PC | TBS-T | 1 hr, RT | Vector Red | Good |
| | 1:800 | Sodium citrate | 20 | PC | PBS-T | 1 hr, RT | Vector Red | No staining |
| | 1:800 | Dako pH 6.0 | 20 | PC | TBS | 1 hr, RT | Vector Red | Good |
| CD31 (mouse) | 1:20 | Trypsin | 10 | Oven | TBS-T | 1 hr, RT | DAB | No staining |
| | 1:20 | Tris/ EDTA | 10 | MW | TBS-T | 1 hr, RT | DAB | No staining |
| | 1:20 | Sodium citrate | 20 | WB | TBS-T | 1 hr, RT | DAB | Good |
| | 1:20 | Sodium citrate | 20 | PC | PBS-T | 1 hr, RT | DAB | Good |
| | 1:20 | Dako pH 6.0 | 20 | PC | TBS | 1 hr, RT | DAB | Good |
| CD45 (mouse) | 1:50 | Dako pH 6.0 | 20 | PC | TBS | 1 hr, RT | DAB | Good |

Table 9 Single staining optimisation.

A summary of the conditions tested for the optimisation of 4 single antibodies (CD68, MRC1, CD31 and CD45). Ab (antibody), WB (water bath), MW (microwave), PC (pressure cooker).

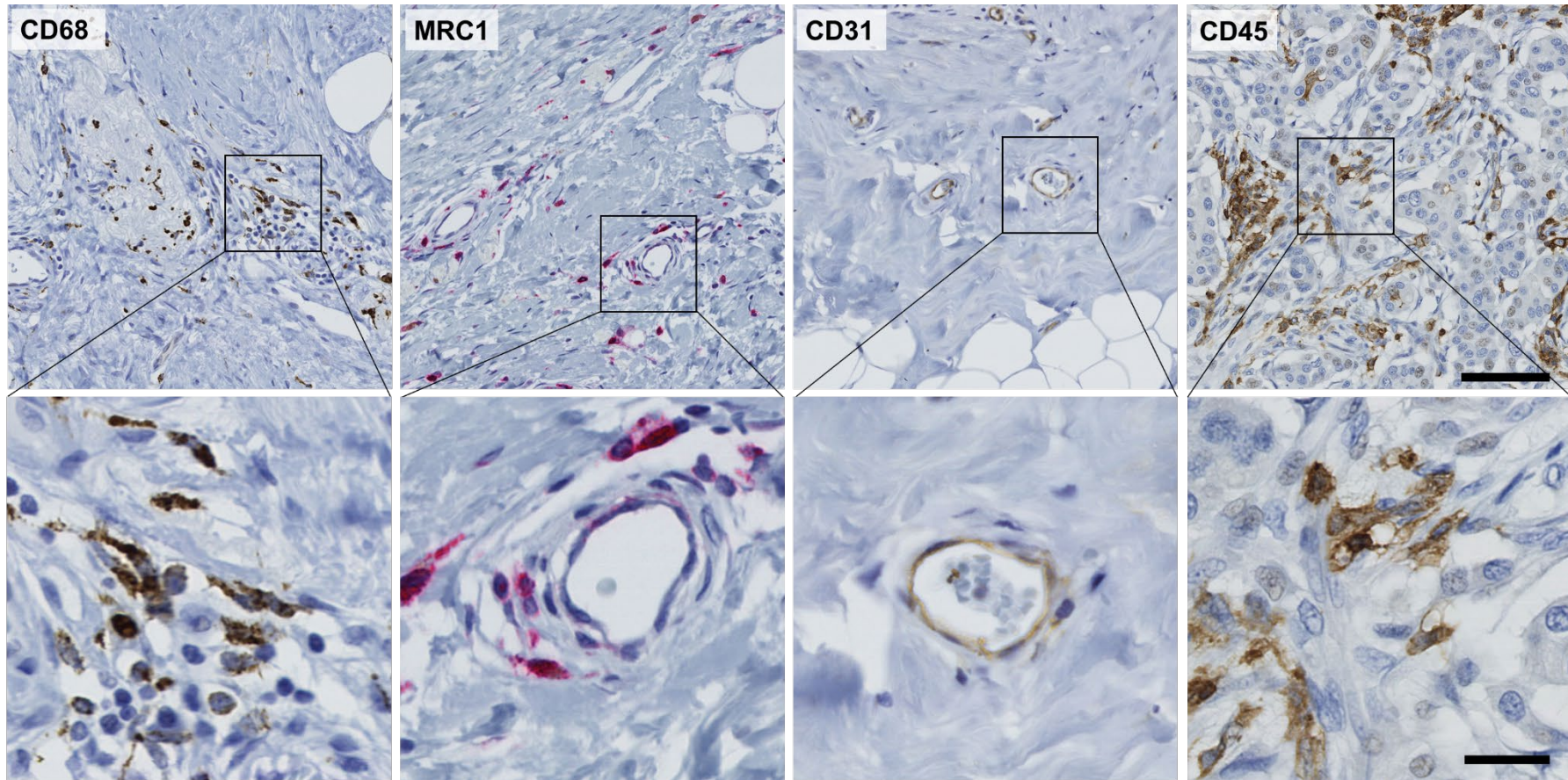


Figure 3-2 Optimised single stains using TNBC tumours.

Representative IHC staining for (left to right) CD68 (brown) detected by DAB stain, MRC1 (pink) detected by Vector red stain, CD31 (brown) and CD45 (brown) detected by DAB stain on human breast carcinomas. Enlarged insets on bottom row. Scale bar top row 100 μ m, bottom row 25 μ m.

3.1.3. Optimisation of dual and triple IHC stains

Once the single stains had been optimised, the antibodies for CD68, CD31 and MRC1 were tested for the tandem combinations CD68/MRC1 and MRC1/CD31. Optimisation of the dual stains for began by using the optimal staining protocol for the antibody raised in mouse (CD68 or CD31), as determined in section 3.1.2. The CD68 and CD31 antibodies were tested separately with the rabbit MRC1 antibody in a dual stain on the same sections. This made simultaneous staining of CD68/MRC1 or CD31/MRC1 a simpler process as the secondary antibodies were raised against different species of primary antibody and used different methods of detections (peroxidase based detect for mouse and alkaline phosphatase-based detection for rabbit).

Where staining did not work (a complete lack of staining), or was sub optimal (weak or patchy staining and over retrieval - signified by staining in the IgG isotype control for either antibody on the section), the staining process was repeated using the optimal conditions for the MRC1 antibody, as determined in section 3.1.2. If staining for the two antibodies was still sub optimal, then changes were made to the staining protocol in terms of the antigen retrieval time or method, antibody concentration, primary antibody incubation time, incubation of primary antibodies simultaneously in a cocktail or separately as sequential staining, the order antibodies were used in sequential staining and the type of buffer used for washing. A summary of the protocol changes made and assessed are in **Table 3-2**. A staining protocol was then generated for the dual combinations using IHC for CD68/MRC1 and CD31/MRC1 (**Figure 3-3 A-B**).

To optimise a triple stain IHC protocol, the antibodies against CD68, CD31 and MRC1 were combined by performing a sequential staining process- staining for one antibody at a time rather than staining for all antibodies together simultaneously in a cocktail. To prevent cross reaction during secondary peroxidase detection of the two antibodies raised in mice CD68 and CD31, additional protein blocking steps and a hydrogen peroxide blocking were performed to stop the staining of the first mouse raised antibody (CD68) being detected when staining for the second mouse raised antibody (CD31). To check the validity of the staining, each antibody was substituted

for the relevant IgG isotype control to check for non-specific detection from the secondary antibodies in the absence of the primary antibody.

Although this allowed the visualisation of the dual labelling in some limited areas of the tissue, co-staining of CD68 and MRC1 proved to be difficult in most areas using chromogenic detection. In other words, when they both appeared in the same areas of sections, the double labelled cells (red and brown chromogens on the same cell) were difficult to distinguish from the single stains (red or brown alone) (**Figure 3-3**). For the triple stain, the staining for the third marker – CD31 was not ideal due to the colour of the grey chromogen used, irrespective of staining intensity that made it difficult to detect against the H&E staining (**Figure 3-3 C**). Again, this was well stained in some areas of the tissue but was not providing strong staining throughout the section.

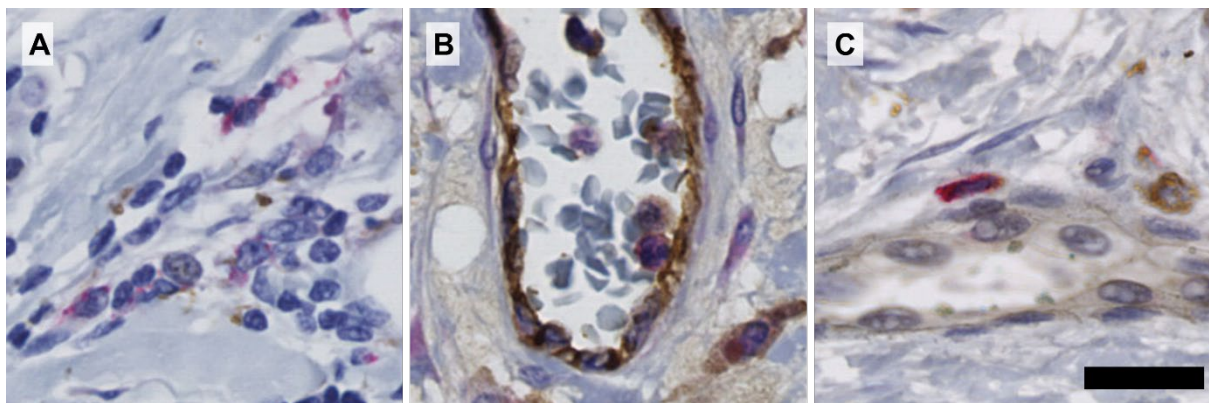


Figure 3-3 IHC staining of dual and triple stains on human TNBC tumours.

Examples dual and triple IHC staining using A. CD68 (brown) and MRC1 (Red). B. CD31 (brown) and MRC1 (red). C. CD68 (brown) CD31 (grey) MRC1 (red). Scale bar 25µm.

Table 10 Dual staining optimisation.

A summary of the conditions tested to optimise dual staining protocols for CD68 (mouse), MRC1 (rabbit), CD31 (mouse) and CD45 (mouse). Antibodies in bold show which antibody was incubated first when using a sequential staining protocol. WB (water bath), MW (microwave), PC (pressure cooker), RT (room temperature)

| Antibody | Dilution | Antibody incubation | Retrieval solution | Retrieval time (min) | Retrieval method | Ab incubation time (min) | Buffer | Secondary Ab | Notes |
|--------------------|--------------|---------------------|--------------------|----------------------|------------------|--------------------------|--------|-----------------|----------------------|
| CD68, MRC1 | 1:60, 1:800 | Cocktail | Tris/ EDTA | 10 | WB | 1hr, RT | PBS | DAB, Vector Red | No MRC1, good CD68 |
| CD68, MRC1 | 1:60, 1:800 | Cocktail | Tris/ EDTA | 10 | WB | 1hr, RT | TBS | DAB, Vector Red | No MRC1, good CD68 |
| CD68, MRC1 | 1:60, 1:800 | Cocktail | Tris/ EDTA | 5 | WB | 1hr, RT | TBS | DAB, Vector Red | Weak MRC1, good CD68 |
| CD68, MRC1 | 1:60, 1:800 | Cocktail | Tris/ EDTA | 1 | WB | 1hr, RT | TBS | DAB, Vector Red | No MRC1, good CD68 |
| CD68, MRC1 | 1:60, 1:800 | Cocktail | Tris/ EDTA | 5 | WB | 1hr, RT | TBS | DAB, Vector Red | No MRC1, good CD68 |
| CD68, MRC1 | 1:60, 1:800 | Cocktail | Pronase | 30 | Oven (37°C) | 1hr, RT | TBS | DAB, Vector Red | No MRC1, good CD68 |
| CD68, MRC1 | 1:100, 1:800 | Cocktail | Sodium citrate | 20 | WB | 1hr, RT | TBS-T | DAB, Vector Red | No MRC1, good CD68 |
| CD68, MRC1 | 1:100, 1:800 | Cocktail | Tris/ EDTA | 20 | WB | 1hr, RT | TBS-T | DAB, Vector Red | No MRC1, good CD68 |
| CD68, MRC1 | 1:100, 1:800 | Sequential | Sodium citrate | 20 | WB | 1hr, RT | TBS | DAB, Vector Red | Weak CD68, good MRC1 |
| CD68 , MRC1 | 1:100, 1:800 | Sequential | Sodium citrate | 20 | WB | 1hr, RT | TBS | DAB, Vector Red | Weak CD68, good MRC1 |
| CD68, MRC1 | 1:100, 1:800 | Cocktail | Sodium citrate | 20 | WB | 1hr, RT | PBS | DAB, Vector Red | Background staining |

| | | | | | | | | | |
|-----------------------|------------------|------------|----------------|----|-------------|---------------------------|-------|--------------------|------------------------------|
| CD68, MRC1 | 1:100, 1:1000 | Cocktail | Sodium citrate | 20 | PC | 1hr, RT | TBS | DAB, Vector Red | Good MRC1, weak CD68 |
| CD68, MRC1 | 1:100, 1:800 | Cocktail | Dako pH 6.0 | 20 | PC | 1hr, RT | TBS | DAB, Vector Red | Good MRC1, good CD68 |
| CD31, MRC1 | 1:40, 1:800 | Cocktail | Tris/ EDTA | 5 | WB | 1hr, RT | TBS-T | DAB, Vector Red | Weak CD31 |
| CD31, MRC1 | 1:20, 1:800 | Cocktail | Pronase | 30 | Oven (37°C) | 1hr, RT | TBS | DAB, Vector Red | No staining |
| CD31, MRC1 | 1:20, 1:800 | Cocktail | Tris/ EDTA | 1 | WB | 1hr, RT | TBS | DAB, Vector Red | No staining |
| CD31, MRC1 | 1:20, 1:800 | Cocktail | Tris/ EDTA | 5 | WB | 1hr, RT | TBS | DAB, Vector Red | No staining |
| CD31, MRC1 | 1:20, 1:800 | Cocktail | Tris/ EDTA | 10 | WB | 1hr, RT | TBS-T | DAB, Vector Red | No staining |
| CD31, MRC1 | 1:20, 1:800 | Cocktail | Tris/ EDTA | 10 | WB | 1hr, RT | TBS | DAB, Vector Red | No staining |
| CD31, MRC1 | 1:20, 1:800 | Cocktail | Tris/ EDTA | 10 | MW | 1hr, RT | TBS-T | DAB, Vector Red | No staining |
| CD31, MRC1 | 1:20, 1:800 | Cocktail | Tris/ EDTA | 10 | MW | 1hr, RT | TBS | DAB, Vector Red | No staining |
| CD31, MRC1 | 1:20, 1:800 | Cocktail | Sodium citrate | 20 | WB | 1hr, RT | TBS-T | DAB, Vector Red | Good CD31, no MRC1 |
| CD31, MRC1 | 1:20, 1:800 | Sequential | Sodium citrate | 20 | WB | 1hr, RT | TBS | DAB, Vector Red | No CD31, overstained MRC1 |
| CD31 , MRC1 | 1:20, 1:800 | Sequential | Sodium citrate | 20 | WB | 1hr, RT | TBS | DAB, Vector Red | No CD31, good MRC1 |
| CD31, MRC1 | 1:20, 1:800 | Sequential | Sodium citrate | 20 | WB | Overnight, 4°C 1hr, RT | TBS-T | DAB, Vector Red | Good CD31, poor MRC1 |
| CD31 , MRC1 | 1:20, 1:800 | Sequential | Sodium citrate | 20 | WB | Overnight, 4°C 1hr, RT | TBS | DAB, Vector Red | Good CD31, poor MRC1 |
| CD31, MRC1 | 1:20, 1:800 | Sequential | Sodium citrate | 20 | WB | 1hr, RT Overnight, 4°C | TBS | DAB, Vector Red | Weak CD31, weak MRC1 |
| CD31 , MRC1 | 1:20, 1:800 | Sequential | Dako pH 6.0 | 20 | PC | Overnight, 4°C 1hr, RT | TBS | DAB, Vector Red | Good CD31, good MRC1 |

3.1.4. Dual labelling with CD68 and MRC1 using IHC in sequential stained TNBC sections.

As mentioned above, the chromogenic detection of cells dual labelled for CD68 and MRC1 was problematic. If staining was too strong for one marker, this would make detection of the second marker difficult to confirm. One way to get around this issue and still use chromogenic detection, was to stain for each marker separately, on two sequentially cut sections, then perform the cell counts using these two images taken from each area.

So, using sequentially cut 4µm sections, these were stained for CD68 and MRC1 with the already optimised single stain protocols. One section was stained for CD68 while the other was stained for MRC1. To assess the results of the staining, common histological features were located in both sections such as blood vessels and TCI. In low power images (**Figure 3-4, top panel**) the staining for both antibodies looked to have labelled cells at the same area of the sections. However, when looking at higher powered images (**Figure 3-4, bottom panel**) there are many differences in the appearance of the two sections (highlighted by red arrows) where cells do not line up or are not present in the same areas in the next section. This would make it unsuitable to use to quantify dual labelled cells due to the number of cells that would only appear in one of the two sequential sections, even if the staining worked well for both CD68 and MRC1 antibodies.

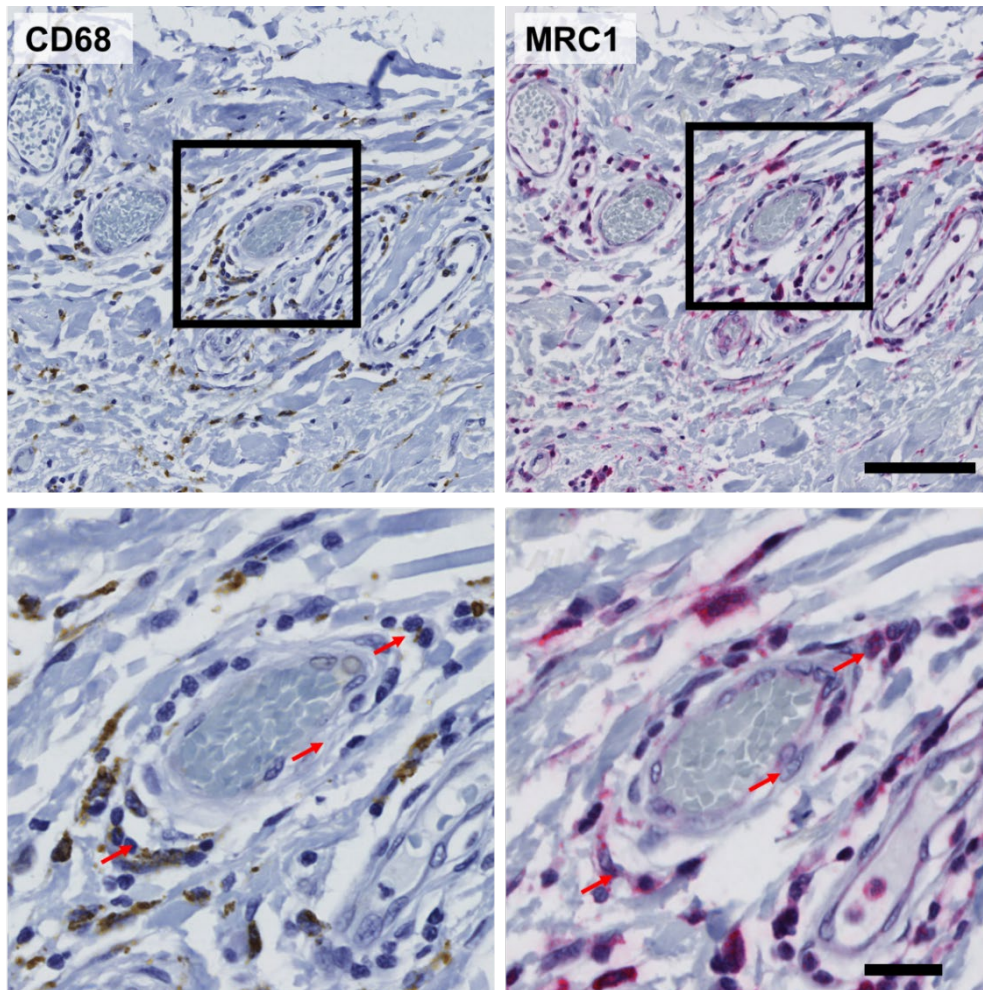


Figure 3-4 Detection of marker co-localisation in sequential sections.

Staining for of DAB stained CD68 (left) and Vector red stained MRC1 (right) using 4 μ m thick, sequentially cut breast tumour sections. Enlarged insets on bottom row. Arrows point to areas of histological difference between the sections. Scale bar top 100 μ m, bottom 25 μ m

3.1.5. Triple immunofluorescence

To enable triple staining to be conducted on the same sections for CD68, MRC1 and CD31, IF staining of FFPE TNBC sections was established, using the same conditions optimised for CD68, MRC1 and CD31 in the IHC protocols in section 2.2.2.3 and used the IF protocols detailed in section 2.2.2.4 containing additional IF specific blocking steps and secondary antibodies. By using IF methods, this allowed for clearer visualisation of dual labelling on single cells (**Figure 3-5 A**). The use of IF (**Figure 3-5 B**) also enabled better visualisation of all 3 markers compared to IHC (**Figure 3-3 C**) due to the diversity of fluorophores available as well as the number of excitation sources, filters and detectors accessible on widefield and confocal microscopes. However, it did encounter issue with auto-fluorescence. This

was mainly seen when using 488nm and 555nm excitation, 647nm excitation remained relatively clear of auto fluorescence. Auto fluorescence is mainly attributed to endogenous properties of the tissue sections such as collagen and lipofuscin and fixation of the tissues with formalin [195]. There were several options available to reduce the impact of auto fluorescence in the tissue. Photo bleaching samples with a UV light source for 30 mins prior saw no discernible difference in the sections being stained. The use of Sudan B black as a final step to the sections to reduce auto fluorescence but saw a reduction in the staining intensity of all 3 markers that were being stained for. As auto fluorescence was only an issue from 488nm excitation, biotin amplification was used of the CD68 marker being used at that wavelength. This increased the staining intensity of the marker allowing for the excitation laser to be turned down and reduce the exposure time on the shutter, reducing the levels of auto fluorescence being picked up while still picking up strong staining for CD68.

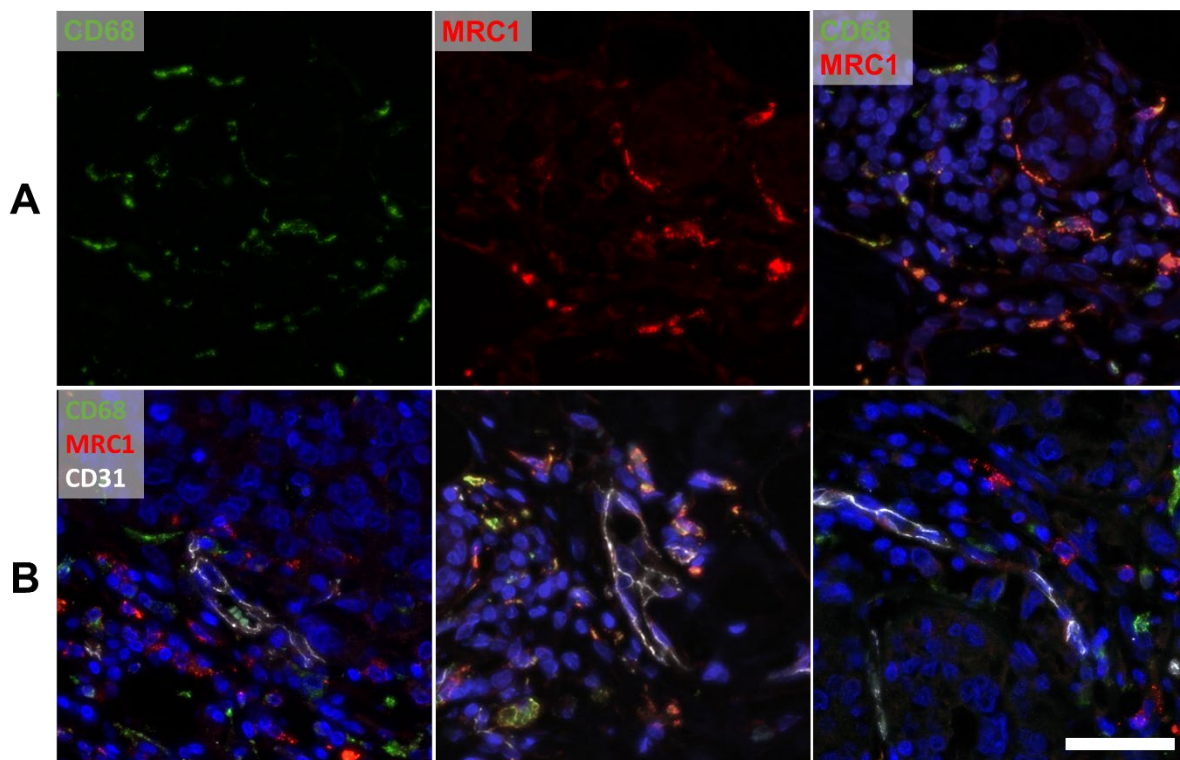


Figure 3-5 Use of IF methods for staining and quantification.

A. Dual labelling of CD68 an MRC1 marker on single cell in a representative TNBC section. B. Representative images of triple stains for CD68 MRC1 and CD31 using IF methods in separate TNBC sections. Scale bar 50 μ m.

As the detection methods for the primary antibodies varied from those used in IHC (peroxidase and alkaline phosphatase-based detection kits), to get around the issue of detecting the two antibodies raised in mice, staining was done sequentially, with the CD68 added first. CD68 staining was detected using anti-mouse biotin antibody and detected using streptavidin to amplify the signal of the stain. Additional blocking protein blocking steps were then included before staining for the second anti-mouse antibody, CD31 which was also detected using a specific IgG1 κ subclass secondary antibody that was different to that of CD68 (IgG3 κ subclass). This ensured there was no cross reactivity between the CD68 and CD31 antibodies and was also confirmed by using the relevant IgG isotype controls.

3.1.6. Validation of CD68 as a macrophage marker in TNBC sections using immunofluorescence staining.

As mentioned previously, it has been reported that some clones of the CD68 antibody label not only macrophages, but also fibroblasts in human breast carcinomas [51, 62]. The PG-M1 clone of CD68 was selected for my IF studies due to the reports of its high specificity for macrophages [196]. This was important to confirm the suitability of the PG-M1 clone for CD68 antibody as a selective macrophage marker IF staining of FFPE sections of TNBCs. So this was checked by seeing if the CD68⁺ cells were also positive for the leukocyte marker, CD45. A preliminary cohort of four TNBCs were IF stained for both CD68 and CD45 and imaged and counted in accordance with sections **2.2.2.6** and **2.2.2.7**. Briefly, regions of interest (ROIs) were selected that consisted of approximately 50:50 TCI and stroma (**Figure 3-6 A**). Quantification of dual labelling with CD68 and CD45 was performed as described in section 2.1.7. High levels of co-localisation were seen amongst the selected sections (**Figure 3-6 B**) with 93% (SEM \pm 2.1) of CD68⁺ dual staining for CD45. The data demonstrates that PG-M1 clone of CD68 was a suitable marker of macrophages in TNBC patient samples.

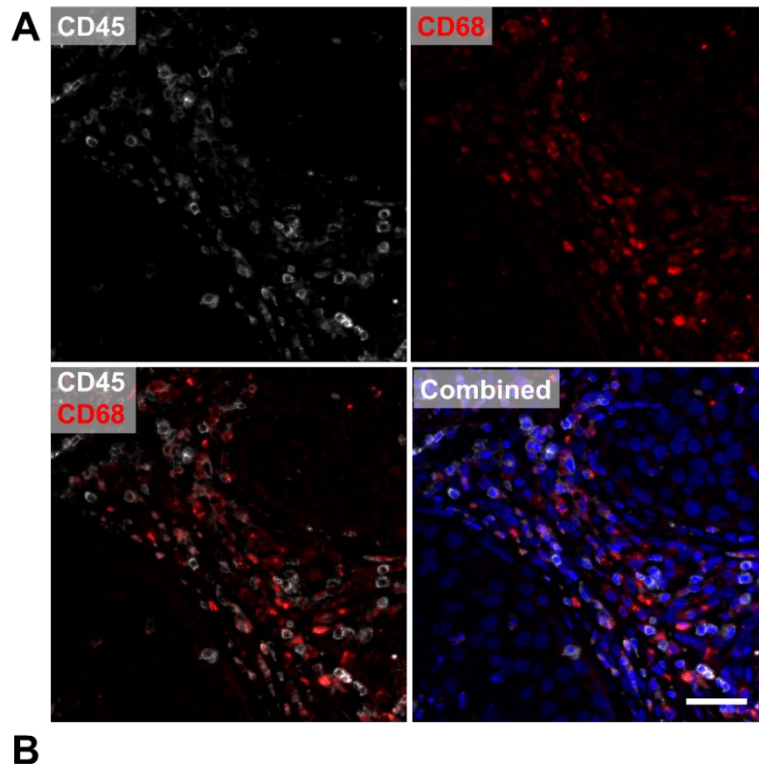


Figure 3-6 Co-localisation of CD68 with CD45.

A. Representative staining for CD68 (red) and CD45 (white) in TNBC tumours. Scale bar 50µm. B. Level of co-localisation of CD68+ cells with CD45+ amongst TNBC patients. Mean ±SEM.

3.1.7. Validation of MRC1 as a marker for PV TAMs in TNBCs

The next step was to quantify the co-localisation of CD68 with MRC1, the marker used in mouse tumour models to identify relapse-promoting TAMs [113]. There are reports in the literature that MRC1 is not solely limited to macrophages and is also expressed by immature dendritic cells and endothelial cells in some tissues [197, 198]. So, the extent to which MRC1 expression was limited to TAMs, or

even a macrophage subset, was examined in TNBCs. If it was found to be only expressed on CD68+ TAMs, then it could be used alone to identify MRC1+ TAMs in future IF labelling analyses (i.e. without the need for CD68 co-localisation).

Five human TNBCs were IF stained for CD68 and MRC1 (**Figure 3-7 A**). Across the whole tumour the proportion of MRC1+ cells dual labelling with CD68 was high (mainly >85%) (**Figure 3-7 B**). There were some cells present that were MRC1+ CD68-, although, these only represented a minor fraction of total MRC1+ cells (~7%) in these sections. The majority of MRC1+ CD68+ cells were present in the stroma between TCIs (see section below for more details). The number of MRC1+ cells/field of view varied between patients with large variations seen between patients (**Figure 3-7 C**).

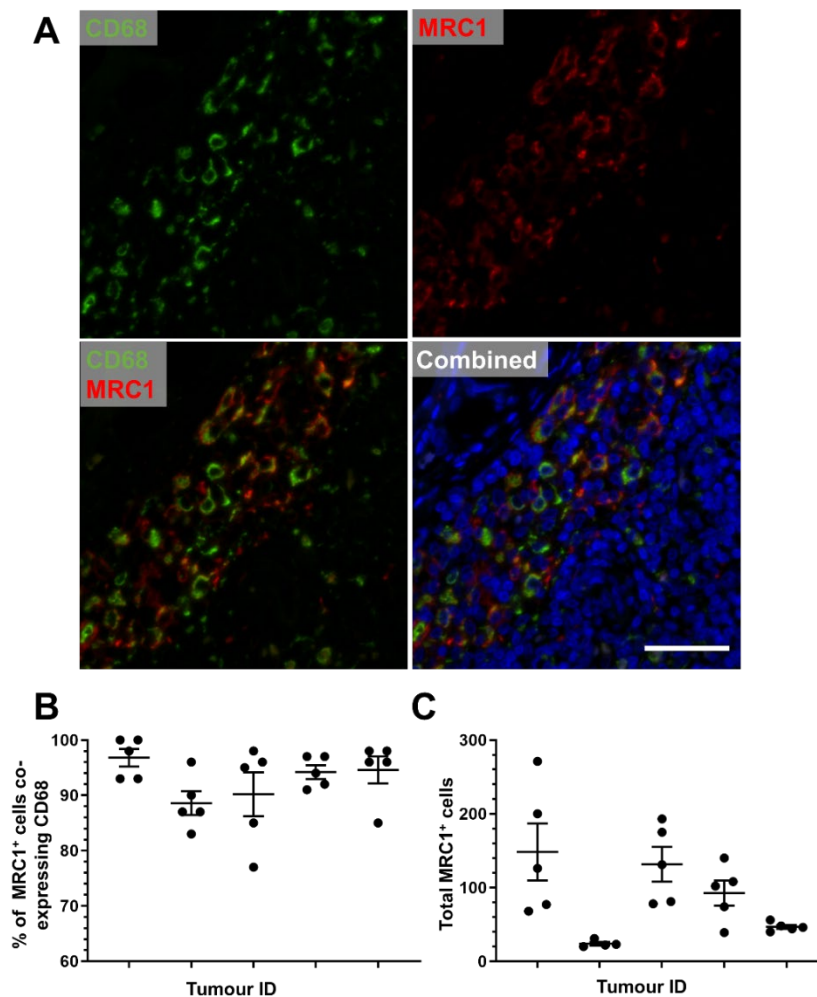


Figure 3-7 Co-localisation of MRC1 with CD68.

A. Representative IF staining for CD68 (green) and MRC1 (red) in triple negative breast cancer tumours that received neoadjuvant chemotherapy. Scale bar 50µm. B. The level of co-localisation of MRC1+ cells with CD68+. C. The difference in MRC1 counts between patients. Mean ±SEM.

3.1.8. MRC1+ TAMs are mainly located in the stroma compared to the TCIs.

The presence of MRC1 expressing CD68+ macrophages was then quantified (detailed in section 2.2.2.7) separately in TCIs and stromal areas in the preliminary cohort of 5 TNBC patients. The levels of MRC1 expression on CD68 TAMs was checked, showing the inter-sample variability with 2 samples close to 100% co-expression, but the remaining 3 samples at 80-90% co-expression (Figure 3-8 A). When combining the patient data, a significant difference was seen between the numbers of MRC1+ CD68+ cells in the TCIs (mean 25.6) versus the stromal areas (mean 76.9) (Figure 3-8 B) with CD68+ MRC1+ TAMs appearing more often in the stromal regions than in the TCIs within the sections. Although this wasn't normalised by cell density, FOV that were approximately 50:50 TCI and stroma were captured. Small variations were seen between the proportion of CD68+ cells co-staining for MRC1+ in tumour and stroma areas, with the stromal areas showing higher levels of CD68+ cells expressing MRC1 (90% SEM ± 0.04) than in the TCIs (75% SEM ± 0.12) (Figure 3-8 C). However, this did not achieve significance in this small cohort of TNBCs.

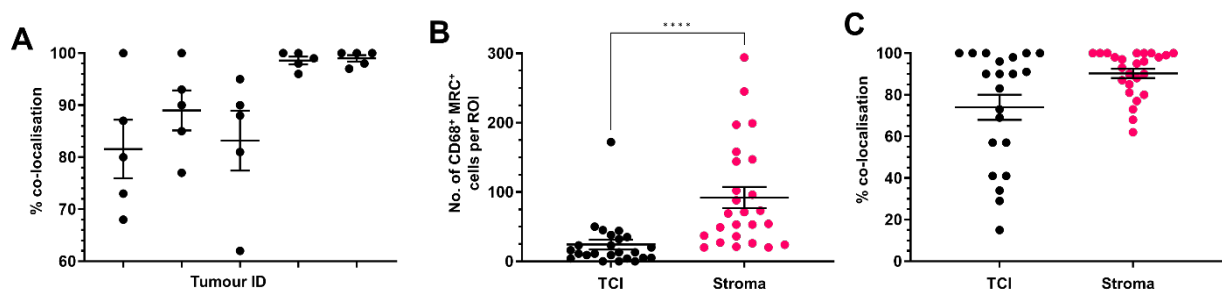


Figure 3-8 Expression of CD68 and MRC1 within TNBC tumours.

A. Shows the variation in co-localisation of MRC1 with CD68 amongst patients. B. The number of CD68+ MRC1+ cells per field of view when split into tumour and stromal regions. C. Levels of MRC1 expressed on CD68+ cells when split into TCIs and stromal areas. All data derived from triple negative breast cancer tumours that received neoadjuvant chemotherapy (n=5, 5 FOV for each patient). Mean ±SEM. *** p<0.0005

The triple stain IF protocol for CD68, MRC1 and CD31 was then optimised in section 3.1.5. This was used to stain a small cohort of primary TNBC sections from both untreated (n=3) and neoadjuvant chemotherapy-treated (n=7) patients.

In these sections, the mean length of CD31 vessels, the number of PV CD68⁺ cells in direct contact with, or within a cell diameter (10µm) of, CD31⁺ blood vessels, and the number and proportion of CD68⁺ cells that were MRC1⁺ were quantified (detailed in section 2.2.2.8). In this small cohort of tumours, no significant differences were seen between untreated patients vs. NAC treated patients in any of the parameters analysed (Figure 3-9 A-C). When looking at MRC1⁺CD68⁺ TAMs, although not significant, there is a tendency towards a lower number of MRC1⁺CD68⁺ TAMs, but higher percentage of CD68⁺ TAMs expressing MRC1⁺, in NAC than untreated tumours (Figure 3-9 B & D). There were no significant differences between the standardised numbers of PV CD68⁺ or CD68⁺ MRC1⁺ TAMs (i.e. normalised to vessel length) between the two treatment groups (Figure 3-9 E-F).

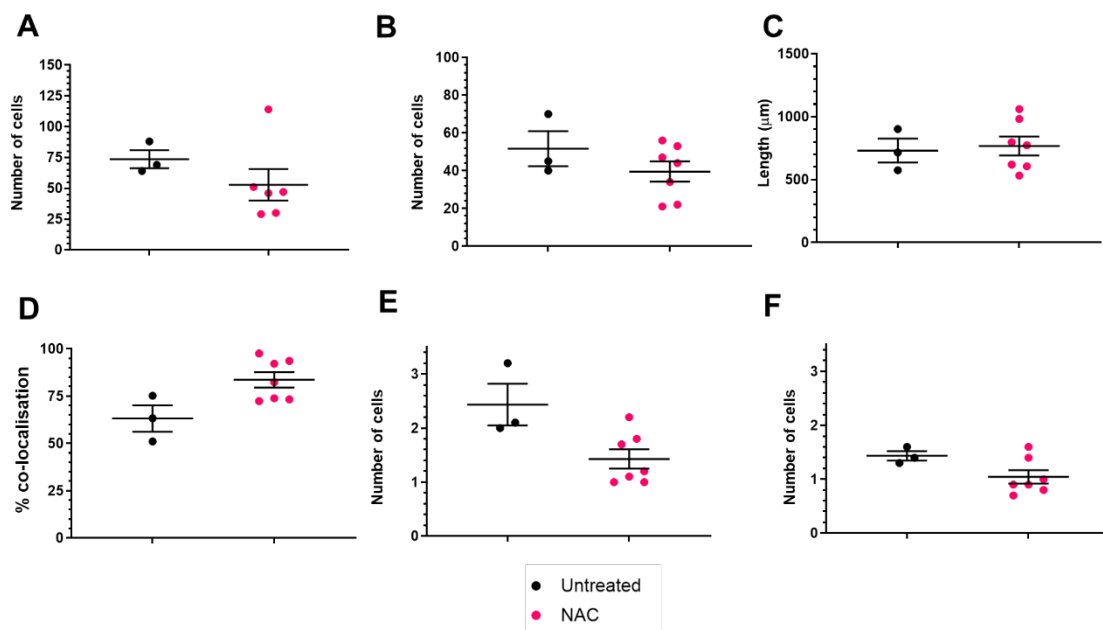


Figure 3-9 The characteristics of PV macrophages in treatment naïve vs. neoadjuvant chemotherapy treated TNBC tumours.

A. The total number of perivascular CD68⁺ cells per tumour. B. Total number of perivascular CD68⁺ MRC1⁺ cells per tumour. C. Total measured vessel length per tumour. D. The % of CD68⁺ TAMs that are MRC1⁺ per tumour. E. Number of PV CD68⁺ cells per 1000µm of vessel. F. Number of PV CD68⁺ MRC1⁺ cells per 100µm of vessel. Treatment naïve n=3, Neoadjuvant n=7.

3.2. Discussion

PV MRC1⁺ TAMs - previously identified as relapse-promoting in mouse tumours [113] - have been identified in TNBC sections using triple stain IF for MRC1, CD68 and CD31. Initially IHC was the preferred immunostaining method due to the stability of the stains in sections, and the absence of issues like auto fluorescence in FFPE tissue sections. Dual staining IHC worked well when antibodies were not labelling the same cells, but when they did, it was difficult to see them clearly (i.e. the colours on top of one another) so dual labelled cells were often difficult to identify. Further, dual labelling was made far harder when the staining intensity of one of the chromogens used was stronger than the other.

Moving to IF staining made the detection of cells dual-labelled for CD68 and MRC1 far easier as they were imaged using separate detection filters, allowing for the colour channels to be split for analysis. The biggest issue using IF methods for staining though was the presence of autofluorescence. This was mainly seen when using 488nm and 555nm excitation, 647nm excitation remained relatively clear of auto fluorescence. Auto fluorescence is mainly attributed to endogenous properties of the tissue sections such as collagen and lipofuscin and fixation of the tissues with formalin [195]. There were several options available to reduce the impact of auto fluorescence in the tissue with photo bleaching of samples with a UV light source and quenching of autofluorescence using Sudan B black. Biotin signal amplification of the markers used on the 488nm detection wavelength where autofluorescence was highest, resulted in increased the staining intensity and allowed for clean images to be captured with a clear difference between the background and cell stain.

It was determined that the CD68 antibody clone, PG-M1, was a selective marker for macrophages in the protocols described in this chapter. As mentioned earlier, the use of another CD68 antibody to label macrophages in breast tumour sections had been called into question [51]. When immunostaining macrophages in sections, these authors saw a population of CD68⁺ cells within the stroma that were CD45⁻ and CSF1R⁻. They, therefore, suggested that these cells were not macrophages [51]. From their morphology in sections, it was postulated by the authors that these cells may have been fibroblasts (may be even fibroblasts derived from TAMs or their precursors, monocytes) and that these may account for the previously high number of macrophages reported previously within tumours [90,

191]. Interestingly they use the KP1 clone of CD68 antibody, which is reported to also stain for fibroblasts [84, 199, 200]. So, the PG-M1 clone of CD68 was selected for the analyses conducted in this chapter, as this is reportedly more selective for staining macrophages than other clones of antibodies for CD68 [196]. However, the PG-M1 clone was found to be a good marker for macrophages in TNBC as these cells were dual labelled with the leukocyte marker CD45, ruling out the possibility of CD68 staining of fibroblasts. It is possible that PG-M1 may have also labelled other CD45⁺ leukocyte subsets like dendritic cells [201], although it has already been ruled out staining for granulocytes and myeloid precursors [196].

The higher number MRC1-expressing CD68⁺ TAMs in the stroma than the TCIs may be significant, as it may indicate that this TAM subset are prevented from migrating into the TCIs and are being retained in the stromal areas of tumours after being recruited. This could then have further implications if the immunosuppressive functions of TAMs are acting upon T cell infiltration and preventing their infiltration into the TCIs.

A small population of MRC1⁺ CD68⁻ cells was also seen within TNBCs, MRC1 has long been considered to be a marker of alternatively (M2) activated macrophages but it could be that some TAMs downregulate/lose their expression of CD68 (and so appear to be CD68⁻).

After optimising the triple staining protocol for CD68, MRC1 and CD31, a method for quantifying PV TAMs was established in preliminary cohort of TNBC tumours. Of the 10 TNBCs analysed, an unexpected finding was that treatment-naïve tumours had higher numbers of PV CD68⁺ TAMs and CD68⁺ MRC1⁺ TAMs than those surgically removed after NAC. Although not significant, the same trend was present in the number of PV TAMs was normalised to vessel length, with treatment naïve tumours again displaying slightly higher number of CD68⁺ and CD68⁺ MRC1⁺ cells compared to those treated with neoadjuvant chemotherapy.

These normalised numbers of PV CD68⁺ cells are similar to the number reported previously for breast cancer in a previous study by the Condeelis lab [62]. However, there are several distinct differences to the study, as the Condeelis group focuses on a 3-cell structure made up of a CD68 TAM, CD31 vessel and MENA expressing tumour cell, termed the tumour microenvironment of metastasis (TMEM). But it does not look at the relevance of MRC1⁺ expression on TAMs. Further differences are that they only looked at PV TAMs within the TCI, not the stroma, so

the area where TAMs are most abundant were not analysed. And finally when they looked at the correlation of the TMEM and TNBC no correlation was seen, suggesting that TMEM may only be relevant to non-TNBC breast tumours [104].

Interestingly, NAC appeared to cause a non-significant increase in the proportion of CD68⁺ TAMs expressing MRC1 across TNBCs compared to the treatment-naïve cohort. Two possible explanations for this preliminary result could be that either chemotherapy activated MRC1 expression on a group of previously MRC1⁻ TAMs, or it caused a turnover of TAMs, with some MRC1⁻ TAMs undergoing cell death in the tumour microenvironment during the chemotherapy and being replaced by newly recruited monocytes, maturing to MRC1⁺ TAMs.

Regarding the vascularisation of the tumours, both the treatment naïve and neoadjuvant tumours exhibited similar total vessel length. This is in contrast to what is seen in LLC1 tumour models, where a decrease in vessel length was after cyclophosphamide, suggesting their destruction during the treatment [113]. However, the latter was seen 48 hours after the last treatment when the tumours were still recovering, whereas the TNBCs used in the present study were resected 30-60 days after the last cycle of neoadjuvant chemotherapy. So, any disrupted vessels may undergo angiogenesis and recover. This may also have implications for the numbers of PV MRC1⁺ TAMs seen here in chemotherapy treated TNBC tumours. As patients recover from neoadjuvant chemotherapy for 30-60 days, immune cell numbers may also return to pre-treatment levels in tumour residues. So, the initial influx of TAMs (and/or the tumour conditioning of their MRC1 expression and PV accumulation) may have receded in tumours. Ideally, tumours resected earlier after neoadjuvant chemotherapy would have been used but these were not available.

It is also important to remember that these results, and any that looked at NAC treated TNBC tumours are already skewed. As those patients with the best outcomes have already had a pCR to NAC and as such, have no residual disease to study. In these cases, analysis of a pre-NAC biopsy may help to highlight why these patients respond so well to NAC in the first instance.

3.3. Concluding remarks

Within this first, small TNBC cohort, perivascular macrophages that were directly in contact with the vasculature were not seen to increase after NAC or directly link to metastasis, although there was a difference in the expression of MRC1 after NAC with higher expression seen in the NAC treated group.

Chapter 4 Quantitative analysis of leukocytes and CXCR4 expression in human TNBC: Changes after neoadjuvant chemotherapy and correlation with metastasis

4.1 Introduction

In Chapter 3, a quantitative immunofluorescence (IF) method was established to assess the density of perivascular (PV) MRC1+CD68+ TAMs in sections of primary human TNBCs. However, the number of TNBCs available for those early studies was too small to compare these PV cells in untreated versus neoadjuvant chemotherapy (NAC)-treated TNBCs. So, in this follow-on study, sections from a larger cohort of 37 TNBCs were obtained from the Breast Cancer Now Tissue Bank along with associated, anonymous clinical data about patient age, tumour size and grade, and details of all treatments (see full list of Breast Cancer Now TNBC samples, section **2.1.9**).

Briefly, the sections were from primary TNBCs from 4 groups of patients who:

1. Did not receive NAC and remained disease-free for a 3 year follow up period.
2. Did not receive NAC and then developed metastasis within a 3 year follow up period.
3. Received NAC and remained disease free for a 3 year follow up period.
4. Received NAC and then developed metastasis within a 3 year follow up period.

As a detailed analysis of the phenotype and distribution of TAMs (and their interactions with other immune cell types) was to be conducted in these TNBC sections (including analysis of TCIs and stroma separately in each section), a collaboration was set up with the US-based Company, Neogenomics Laboratories. They had already established an automated platform, MultiOmyx™, to perform multiplex IF staining on human tissue sections (**Figure 4-1**). This utilises their proprietary AI-based, cell segmentation software, 'NEO image analysis', to conduct spatial analysis of specific cell types in IF stained sections (including the direct contacts made by cells in specific tumour areas like the PV niche).

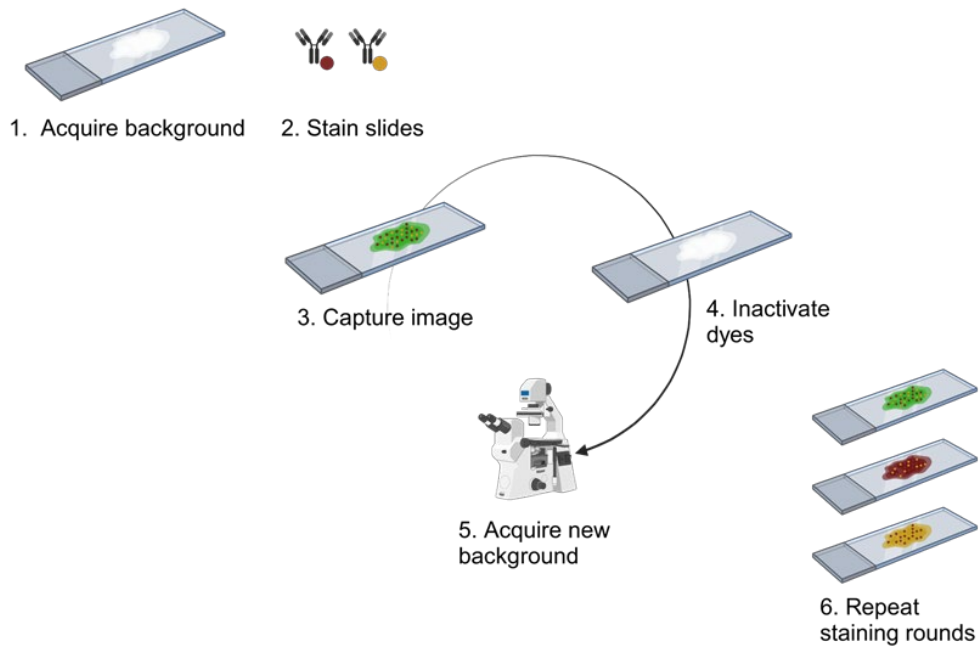


Figure 4-1 MultiOmyx™ Assay Workflow

After initial slide preparation: 1. A background image is obtained, 2. The section is then stained with a pair of Cy3 and Cy5 labelled antibodies. 3. The slide is imaged. 4. The dyes are inactivated. 5. A new background signal of the slide is obtained. 6. The cycle is then repeated using 2 more antibodies. This repeated until all the pairs of antibodies have been applied to each section.

. MultiOmyx™ Assay Workflow, Neogenomic Laboratories.

The sequential steps in the MultiOmyx™ protocol are shown in **Figure 4-1**. Briefly, these include a series of rounds in which paired antibodies (labelled with Cy3 and Cy5) are added to sections, then washed off, the resultant staining imaged, reagents added to inactivate/strip antibodies, and 2 new antibodies added, and so on. Multiple images are layered on top of one another for each section to include the multiple stains with panels of antibodies that can detect up to 60+ markers [173]. AI-based cell segmentation is then applied to the images. AI algorithms that incorporate deep learning and neural networks can be trained using data sets to recognise cell structures and then use this information to segment cell structures or markers based on their staining patterns. In this way, PV and non-PV cells could be quantified in both TCIs and stromal areas.

The initial aim here was to apply the optimised IF staining protocol for CD68, MRC1 and CD31 developed in Chapter 3 into the MultiOmyx™ platform so it could be applied to our larger cohort of 37 TNBCs. Although CD68 and CD31 antibodies

were validated for use together in MultiOmyx™ platform it did not prove possible to validate the MRC1 antibody in time for its inclusion in the IF staining of the TNBC sections by Neogenomics Labs. Fortunately, the Company had already validated 40 other antibodies suitable for studying the TME, 16 of these were selected for this study (**Table 4-1**).

These included antibodies against pan cytokeratin (expressed by cancer cells), CD31 for blood vessels, the receptor for the CXCL12 chemokine, CXCR4, various myeloid cell markers (CD11b, CD68, CD163), T cell markers (CD3, CD4, CD8 and FOXP3), NK cells (CD56), negative checkpoint regulators (PD-1, PD-L1, TIM3, LAG3) and alpha smooth muscle actin (α SMA, to label pericytes and fibroblasts). The company's proprietary, AI-based cell segmentation system carried out the requested image analysis of the MultiOmyx™ staining as described in section **2.2.3.1**.

| MultiOmyx™ marker panel. | | | |
|---------------------------------|--------------|-------|-------|
| CD3 | CD31 | CXCR4 | CD56 |
| CD4 | PanCK | PD-1 | CD11b |
| CD8 | α SMA | PD-L1 | LAG-3 |
| FOXP3 | CD68 | TIM-3 | CD163 |

Table 11 MultiOmyx™ multiplex antibody panel

The pan cytokeratin (PanCK) antibody was included so that cancer cells (i.e. in TCIs) [202] could be clearly identified in sections. This meant that a 'TCl mask' could be generated for image analysis of TCIs versus stromal areas of TNBCs. An antibody to CD31, a common marker of endothelial cells [203] was used to identify the vasculature - and enable PV and non-PV areas to be defined in tumour sections. As previously defined [112], PV areas were defined as the region within 50 μ m of CD31+ vessels and non-PV areas defined as beyond 50 μ m. For the identification of myeloid cells, CD11b was used [204], and for TAMs, antibodies against CD68 and the scavenger receptor, CD163 were applied [205, 206]. α SMA was used to identify pericytes and cancer associated fibroblasts (CAFs) [207, 208]. The latter was partly

included to see if the CD68 antibody used labelled any fibroblasts in TNBC sections , as this has been reported previously [51].

In the studies described in this chapter, antibodies against various well-established markers of TILs were used including those for T helper cells, (CD3+ CD4+ FOXP3-), cytotoxic T cells (CD3+ CD8+) and regulatory T cells (CD3+ CD4- FOXP3+). CD56 is an Fc receptor found on natural killer (NK) cells (so these cells are defined as CD3- CD56+). The negative checkpoint regulators (NCRs) listed in Table 4-1 are expressed by T cells and include T cell immunoglobulin and mucin domain-containing protein 3 (TIM-3) [209], Lymphocyte-activation gene 3 (LAG-3) [210], and PD-1 (plus it's ligand PD-L1) [211]. Their inclusion in the multiplex staining of TNBCs allowed the activation status of CD4+ and CD8+ T cells to be assessed.

NCRs normally play a vital role in limiting T cell activation in immune response so that autoimmunity does not occur. However, NCRs also suppress anti-tumour immunity. Once bound by PD-L1 on cancer cells or antigen presenting cells like dendritic cells or macrophages, PD-1 on T cells suppress T cell proliferation and activation, facilitating tumour immune evasion. Antibodies to PD-1 (and PD-L1) have offered new treatment options for TNBC [21, 22] but a substantial proportion of patients fail to respond or develop resistance. Often, this is because activated T cells can become exhausted (i.e. no longer cytotoxic) and start to express the markers, TIM-3 and LAG-3. TIM-3 is also expressed by myeloid cells and NK cells, where its functions have yet to be fully elucidated. Likewise, LAG-3, can also be expressed by Tregs, engages with major histocompatibility complex (MHC) class II molecules to inhibit T cell activation and proliferation [210]. Within breast cancer, single cell-RNA sequence analysis has shown that, in fact, myeloid cells are the predominant expressors of TIM-3, while PD-1, PD-L1 and LAG-3 are mainly expressed by T cells [212].

Contrasting prognostic outcomes have been shown with TIM-3 within breast cancer that seemingly link to the subtype. High levels of TIM-3 in 109 TNBCs tissue microarrays (TMA) analysed by IHC, were shown to link to a significantly better prognosis with better DFS and OS survival levels than TIM-3^{low} tumours [213]. This contrasts with a study of 42 breast cancer samples analysed by IHC in which high levels of TIM-3 were shown to link to a worse 5 year OS, compared to TIM-3^{low} tumours [214].

Lastly, the present study also included an analysis of CXCR3 expression in TNBCs as high expression of CXCR4 by cancer cells has been shown to correlate with metastasis in some forms of breast cancer [215]. This chemokine receptor is expressed by various cell types in human tumours and selectively binds to CXCL12 (also known as SDF-1). Both primary breast tumours and their metastases express CXCR4 more highly than healthy breast tissue [215]. The possible role of CXCR4 in metastatic seeding has been shown in a landmark study that found its ligand, CXCL12 to be highly expressed at organ sites known to host metastasis in breast cancer: lymph nodes, lungs, the liver and bone marrow. And that pharmacological blocking of the CXCR4/CXCL12 axis *in vivo* in nude mice bearing MDA-MD-231 tumours markedly reduced metastasis [216].

4.1. Hypothesis

The main hypotheses being tested in the studies conducted in this chapter were that:

- 1) A high density of PV TAMs in the stroma and/or TCIs of TNBCs would promote metastasis – and that this might be more prominent in NAC-treated than untreated tumours.
- 2) The close interaction of TAMs with other immune effectors like Tregs, and CD4+ and CD8+ T cells in the PV niche of tumours would suppress on anti-tumour immunity, and thus promote metastasis.
- 3) A high density of NK cells in the stroma and/or TCIs of TNBCs would hinder metastasis – in both untreated and NAC-treated TNBCs.
- 4) TNBC tumours with high expression of CXCR4 in TCIs or the stroma are more likely to develop metastasis within 3 years in both untreated and NAC-treated tumours.

[Please note that the first two hypotheses were tested in a paper that has now been published in 2023 in the peer-reviewed journal, '*Frontiers in Immunology*' – so those studies appear in this chapter in the format of a published paper]

4.2. Results

4.2.1. Defining the spatial characteristics of TNBCs using AI-based image analysis

Using the TNBC sections obtained from Breast Cancer Now (defined in section 2.2.3.1), these were split into 4 groups based on treatment and outcome:

1. Untreated and did not develop metastasis within a 3 year follow up period (Untreated DF),
2. Untreated and developed metastasis within a 3 year follow up period (Untreated Mets),
3. Received NAC and did not develop metastasis within a 3 year follow up period (NAC DF),
4. Received NAC and developed metastasis within a 3 year follow up period (NAC Mets).

Following the MultiOmyx™ staining protocol carried out by Neogenomics Labs (defined in section 2.2.3.2) using the TNBC sections obtained from the Breast Cancer Now Tumour Bank (section 2.2.3.1), all sections met the quality control threshold, retaining >60% of their starting material. Two samples had noticeable tissue loss, with one on the cut-off point at 59.7. No stained sections had any significant tissue loss compared to the other groups. Overall, the mean level of tissue retention was 95%±1.08%.

Initially, the total area (defined in mm²) for the TCI and stroma was assessed for the untreated and NAC treated groups by comparing the total area for the TCI and stroma in each of 20 ROIs imaged in each tissue section. No significant differences were seen when comparing these areas in all 4 groups of TNBCs (**Figure 4-3 A**). It would be expected that there would be less TCI area in tumours that received NAC compared to untreated tumours. However, each of the 20 ROIs for the sections was selected by a pathologist (**Figure 2-1**) who ensured that ROIs contained areas of viable tumour for analysis. When looking at the cell density for the TCI and stromal areas (total area of region mm²/total cell count of region), there was a significantly higher density of cells in the stroma than TCI (**Figure 4-3 B**) in both the untreated (8026 cells/mm SEM ± 382.1 vs 36737 cells/mm SEM ± 5190) and the NAC treated samples (8052 cells/mm SEM ± 479.6 vs 27334 cells/mm SEM ± 2326

$P < 0.0001$). When this was broken down according to outcome (i.e. with or without metastases), it was seen that there was a significant difference between the cell density of the tumour and stroma in the disease-free/untreated, metastatic/untreated and disease-free/NAC treated groups, but not in the metastatic/NAC treated group (**Figure 4-3 C**). No significant differences were seen between the disease-free and metastatic groups or untreated vs NAC treated. Algorithms were developed as part of the NeoLYTX software, using CD31+ to mark blood vessels and the PV niche – defined as expanded region, 50mm from the CD31+ blood vessels (**Figure 2-3 D**). This was then used to define the area 4 spatial regions - PV/stroma, PV/TCI, non-PV/stroma and non-PV/TCI. There were no significant differences between the 4 spatial regions in the Untreated vs NAC treated tumours. But within the untreated group, the PV stroma region made up the largest area (**Figure 4-3 D**).

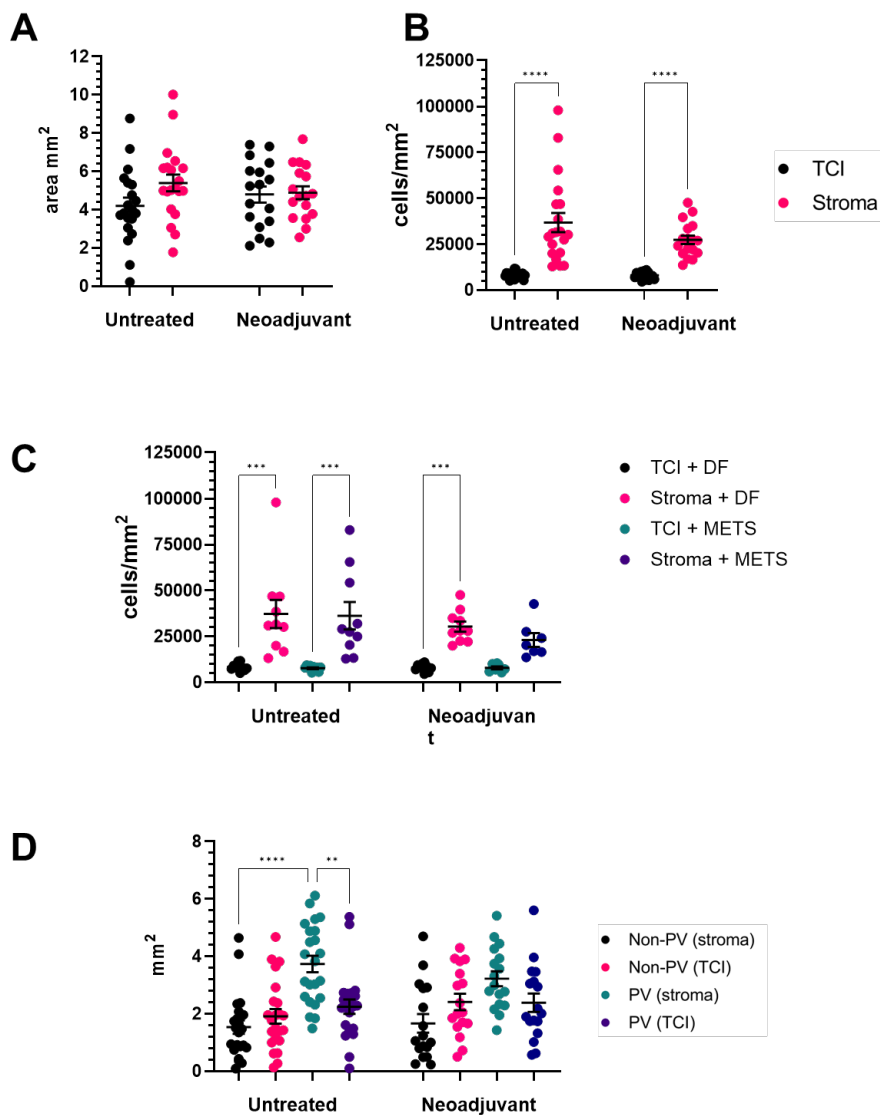


Figure 4-2 Area and cell density of the TCI, stroma and perivascular regions.

A. The total area (in mm²) of the TCI and stroma regions in untreated and NAC treated TNBC tumour sections. B. The cell density for each of the TCI and stroma regions in untreated and NAC treated TNBC tumour sections. C. The total cell density for each of the TCI and stroma regions in untreated and NAC treated for patients who did or did not develop metastases D. The area (mm²) of the PV And Non-PV regions in both the TCI and stroma regions in untreated and NAC treated TNBC tumour sections (METS). Error bars \pm SEM. ** $P < 0.01$ *** $P < 0.001$ **** $P < 0.0001$.

4.2.2. The stroma is more vascularised than TCIs in TNBCs.

As part of the analysis conducted, the vascular component of the TCIs and stromal regions was examined (**Figure 4-4 A**). There were significant differences in the density of CD31+ vessels (vessel count per region/region area) with a higher density of vessel in the stroma compared to TCIs in both untreated and NAC treated tumours. Treatment with NAC did not alter vessel density, area, counts or length (i.e. compared to the untreated tumours) (**Figure 4-4 B-E**).

A reduction in tumour vascularity would be anticipated after treatment with NAC due to the vascular disruption caused by chemotherapeutics [113], however when comparing the vessel counts, mean vessel areas and mean vessel length, no differences were seen in the untreated compared to NAC treated tumours. When vessel density was examined relative to disease outcome, there was a significant difference between the tumour and stroma in the disease free/untreated, metastatic/untreated and disease free/NAC treated groups, but not the metastatic/NAC treated group (**Figure 4-4 F**).

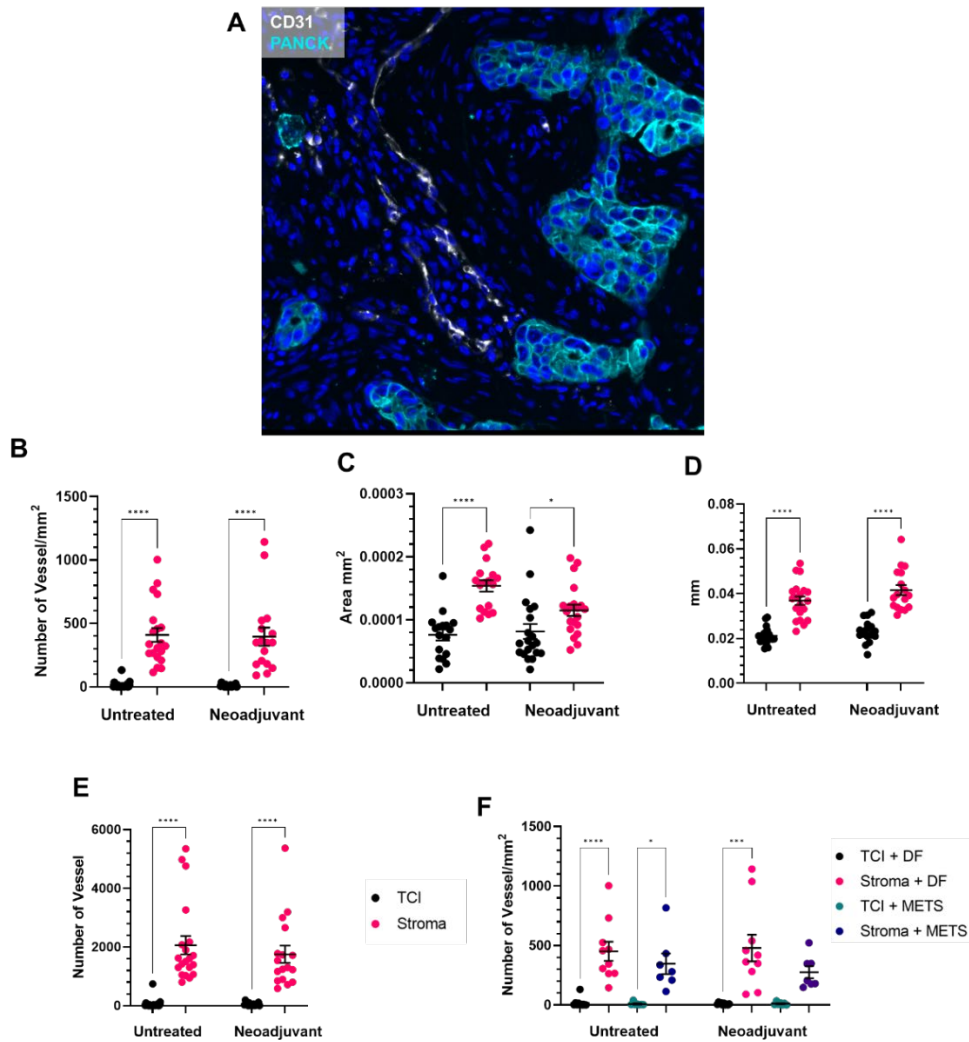


Figure 4-3 Vessel characteristics in untreated vs NAC treated TNBCs

*A. Representative image of CD31⁺ vessels in the stromal regions of a TNBC. B. vessel density C. vessel area D. vessel length E. vessel count for TCI and stromal regions in untreated and NAC treated TNBC tumour sections F. Vessel density for the disease outcomes in the TCI and stroma regions. Means±SEM. *P>0.05, **** P<0.0001.*

4.2.3. Macrophage staining characteristics in TNBC sections.

It was noted that there were abnormal patterns of staining with some of the antibodies used to pick up the CD11B, CD68 and CD163 in TNBC sections. It is anticipated that there would be higher numbers of the myeloid cell marker, CD11B than of the CD68⁺ cells and CD163⁺ cells, as all TAMs are myeloid cells and so expected to be CD11B⁺. When looking at the cell counts for the single markers or colocalised, it was seen that the colocalised counts of CD11B⁺CD68⁺ and CD68⁺ and CD163⁺ were much lower than the individual counts (**Figure 4-2 A**). To investigate this discrepancy, we looked that the number of CD68⁺ that also

expressed the commonly used fibroblast marker α SMA, as CD68 labelling of fibroblasts is commonly observed [51, 84] (**Figure 4-2 B**). This showed that the percentage of total CD68+ cells that were α SMA positive across the whole tumour was on average 12.5%, with a small difference seen in the levels of the TCI and stroma (13.5% vs 12.5%).

This did not seem to account for the differences in the cell counts between the individual markers and the co-localised cell counts. We looked at the cell segmentation maps for each of the markers (**Figure 4-2 C, D**). Here it was seen that the segmentation masks were not capturing a representative proportion of the CD11B and CD68 staining due to the background staining, however the staining for CD163 was much cleaner, allowing the segmentation algorithms to accurately segment the marker staining.

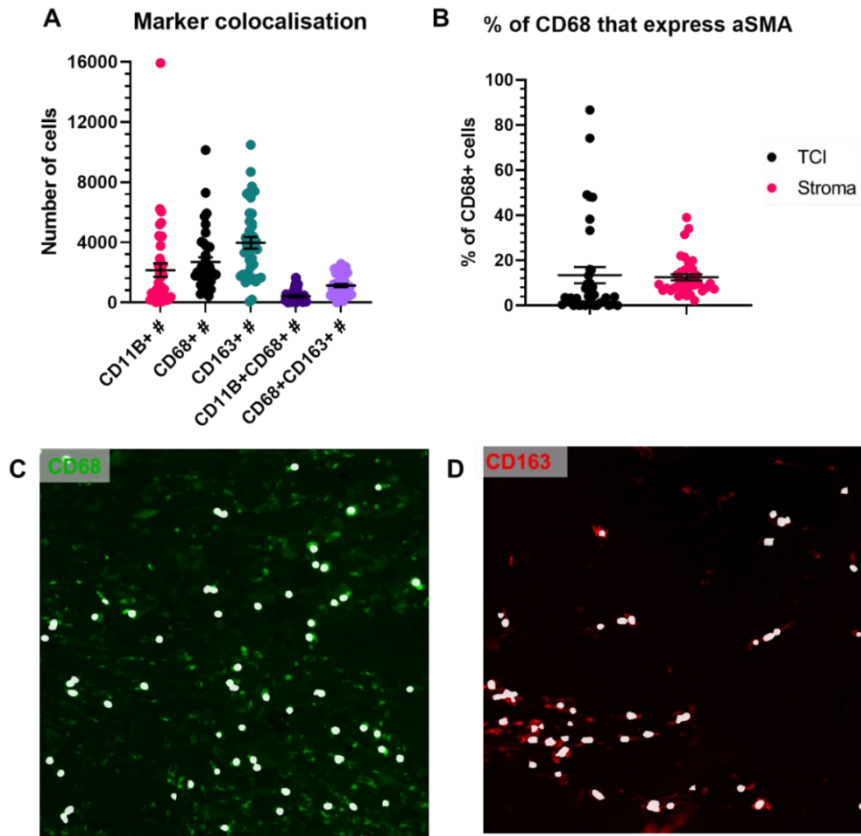


Figure 4-4 Macrophage marker co-localisation and detection using CD68 and CD163.

A. Total cell counts for each of the macrophage associated markers. B. The percentage of Total CD68 cells that express the fibroblast associated marker α SMA. Representative image of antibody staining C. CD68 (green) and D. CD163 (red) with the AI segmentation mask (White).

4.2.4. Effect of neoadjuvant chemotherapy on the distribution and activation status of TAMs, CD4+ and CD8+ T cells, and Tregs

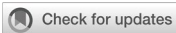
As mentioned previously, this part of the chapter was compiled into a paper published in 2023 in the journal, *Frontiers in Immunology* (PMID: 38090569). This shown in full within the next section, followed by the supplementary materials.

This is an open access publication, published under the creative commons licence CC-BY, version 4.0 (<https://creativecommons.org/licenses/by/4.0/>). Permission has been granted from the publisher and from the co-authors to include this manuscript within this thesis submission.

4.2.5. Declaration of contribution

My contributions to this publication were in:

- Helping to formulate the scientific questions being addressed in this chapter (e.g. examining immune cells like macrophages, etc in PV versus non-PV areas of TCIs v stroma).
- Identification and definition of the TNBC samples characteristics and required follow up data from the Breast Cancer Now Tissue Bank and obtaining the TNBC sections required for the study (Application No. TR101),
- Establishing and validating the IF staining methods for PV TAMs.
- Selection of the 16 markers to be used and cells to be identified in the MultiOmyx™ staining process.
- Liaising with Neogenomics Laboratories to guide them as to how they needed to apply their 'NEO Image Analysis' (and arrange the raw data for analysis in Sheffield).
- Requesting of marker analysis data from Neogenomics Laboratories. Drawing up the raw data into figures and applying statistical analysis.
- Helping to write the paper, review it prior to submission, and revise it after peer review.
- **Generation of the data and the statistical analysis for Figures 1, 2, and 4, and Supplementary Figures 1, 3, 5a, and Supplementary Table 1.**



OPEN ACCESS

EDITED BY
Felix Marsh-Wakefield,
Royal Prince Alfred Hospital, Australia

REVIEWED BY
Ravi K. Patel,
San Francisco, United States
Keyue Ma,
Zai Lab, China

*CORRESPONDENCE
Claire Elizabeth Lewis
✉ Claire.lewis@sheffield.ac.uk

RECEIVED 09 September 2023
ACCEPTED 23 October 2023
PUBLISHED 09 November 2023

CITATION

Moamin MR, Allen R, Woods SL, Brown JE, Nunns H, Juncker-Jensen A and Lewis CE (2023) Changes in the immune landscape of TNBC after neoadjuvant chemotherapy: correlation with relapse.
Front. Immunol. 14:1291643.
doi: 10.3389/fimmu.2023.1291643

COPYRIGHT

© 2023 Moamin, Allen, Woods, Brown, Nunns, Juncker-Jensen and Lewis. This is an open-access article distributed under the terms of the Creative Commons Attribution License (CC BY). The use, distribution or reproduction in other forums is permitted, provided the original author(s) and the copyright owner(s) are credited and that the original publication in this journal is cited, in accordance with accepted academic practice. No use, distribution or reproduction is permitted which does not comply with these terms.

Changes in the immune landscape of TNBC after neoadjuvant chemotherapy: correlation with relapse

Mohammed Ridha Moamin¹, Richard Allen¹, Steven Leslie Woods¹, Janet Elizabeth Brown¹, Harry Nunns², Anna Juncker-Jensen² and Claire Elizabeth Lewis^{1*}

¹Division of Clinical Medicine, School of Medicine & Population Health, Faculty of Health, Sheffield, United Kingdom, ²Neogenomics Labs., Aliso Viejo, CA, United States

Introduction: Patients with high-risk, triple negative breast cancer (TNBC) often receive neoadjuvant chemotherapy (NAC) alone or with immunotherapy. Various single-cell and spatially resolved techniques have demonstrated heterogeneity in the phenotype and distribution of macrophages and T cells in this form of breast cancer. Furthermore, recent studies in mice have implicated immune cells in perivascular (PV) areas of tumors in the regulation of metastasis and anti-tumor immunity. However, little is known of how the latter change during NAC in human TNBC or their impact on subsequent relapse, or the likely efficacy of immunotherapy given with or after NAC.

Methods: We have used multiplex immunofluorescence and AI-based image analysis to compare the immune landscape in untreated and NAC-treated human TNBCs. We quantified changes in the phenotype, distribution and intercellular contacts of subsets of tumor-associated macrophages (TAMs), CD4+ and CD8+ T cells, and regulatory T cells (Tregs) in PV and non-PV various areas of the stroma and tumor cell islands. These were compared in tumors from patients who had either developed metastases or were disease-free (DF) after a three-year follow up period.

Results: In tumors from patients who remained DF after NAC, there was a marked increase in stromal CD163+ TAMs, especially those expressing the negative checkpoint regulator, T-cell immunoglobulin and mucin domain 3 (TIM-3). Whereas CD4+ T cells preferentially located to PV areas in the stroma of both untreated and NAC-treated tumors, specific subsets of TAMs and Tregs only did so only after NAC. Distinct subsets of CD4+ and CD8+ T cells formed PV clusters with CD163+ TAMs and Tregs. These were retained after NAC.

Discussion: Quantification of stromal TIM-3+CD163+ TAMs in tumor residues after NAC may represent a new way of identifying patients at high risk of relapse. PV clustering of immune cells is highly likely to regulate the activation and function of T cells, and thus the efficacy of T cell-based immunotherapies administered with or after NAC.

KEYWORDS

triple negative breast cancer (TNBC), multiplex optical bioassays, encoding, bioimaging and biodetection, diagnostics, neoadjuvant chemotherapy (NAC), macrophages, TIM-3

1 Introduction

Triple negative breast cancer (TNBC) is a type of breast cancer that lacks oestrogen and progesterone receptors, as well as human epidermal growth factor receptor 2 (HER2). TNBC is associated with earlier age of onset, aggressive clinical course, rapid relapse after treatment, and worse prognosis compared to hormone receptor positive and HER2-positive breast carcinomas (1). TNBC also has more limited treatment options, with the mainstay being chemotherapy administered in the neoadjuvant and/or adjuvant/metastatic settings. Neoadjuvant chemotherapy (NAC) is being increasingly used for patients with high-risk TNBC but the majority fail to show a complete pathological response and relapse within three years (2). In an attempt to increase response rates and patient survival, attention has now turned to the use of immune checkpoint inhibitors (ICIs) in combination with NAC. Indeed, various clinical trials have showed that the addition of an ICI to NAC reduces relapse in some patients (3, 4).

Robust biomarkers are needed to predict relapse after NAC and inform patient selection for treatment with ICIs. Despite considerable effort to characterise the molecular and cellular features of TNBCs, very few have led to changes in treatment or improved outcomes for patients (5). So, there is now considerable focus on how the immune landscape of TNBCs is altered by NAC, and how this might help to predict subsequent relapse. Changes in this could also help to explain why some patients respond well to NAC administered with ICIs, while others do not.

Various studies have used single-cell transcriptomics and proteomics to demonstrate the presence of multiple subsets of immune effector cells like T cells and tumor-associated macrophages (TAMs) in human TNBCs (6–9). More recently, spatially resolved methods like digital spatial profiling, imaging mass cytometry, multiplexed ion beam imaging, and multiplex immunofluorescence have started to map important features of the immune landscape in this type of breast cancer. These studies have shown the importance of local signals and intercellular interactions in the regulation of immune cell function in specific compartments within tumors (10, 11). For example, they highlighted marked differences in immune cell functions in the tumor stroma versus the tumor cell islands ('TCIs', sometimes referred to as tumor 'nests') (12, 13).

There is also increasing evidence in mouse tumor models that some immune cells like TAMs, T cells and regulatory T cells (Tregs) may accumulate around tumor blood vessels, in what is often termed the 'perivascular niche' (PVN, usually defined as within 50µm from the abluminal surface of vessels) (14). This alters their pattern of gene expression and function(s) due to their exposure to endothelial-derived factors like angiopoietin-2 and interleukin-6 (15–17). For example, perivascular (PV) TAMs inhibit anti-tumor immunity and stimulate tumor angiogenesis and metastasis (14, 18). Furthermore, they have been shown to limit the efficacy of chemotherapy in mouse tumors, in part by blocking T cell recruitment across the tumor vasculature, and then promoting tumor angiogenesis and regrowth after the cessation of treatment (17, 19). This TAM subset also promote relapse by helping cancer cells to escape into the circulation during chemotherapy and form distant metastases (20, 21). However, recent evidence has emerged for functional diversity amongst PV TAMs as some appear to be able to augment rather than inhibit T-cell-mediated immunity in tumors (22, 23).

CD4+ T cells and Tregs have also been shown to accumulate around blood vessels in human glioma, and that this is an independent predictor of relapse-free survival (24). Additionally, a subset of CD4+ T cells aggregate around blood vessels in human breast carcinomas and correlate with poor prognosis (25). When it comes to the impact of PV CD8+ T cells, this appears to be dependent on cancer type as high numbers of these cells correlate with improved disease-free (DF) survival in resected hepatocellular carcinomas (26), but not in metastatic melanoma (27).

How the density, distribution and function of such immune cells as TAMs, Tregs, and T cells are altered in human TNBCs by NAC have yet to be fully defined. So, in this study we have used multiplex immunofluorescence and AI-based image analysis to analyse these features for the following four immune cell types in the stroma and TCIs of human TNBCs in untreated versus NAC-treated tumors: (i) CD163+ TAMs, (ii) CD3+CD4+FOXP3+ T regs, (iii) CD3+CD4+FOXP3- ('CD4+') T cells, and (iv) CD3+CD8+ ('CD8+') T cells. We included an assessment of PV and non-PV sites in these areas to allow PV immune changes to be defined for the first time.

Our data indicate that all four immune cell types studied showed the phenomenon of 'immune exclusion' as they were found mainly in the tumor stroma in both untreated and NAC-

treated TNBCs. Of note, PV TAMs, T cells and Tregs often made direct contact with one another to form distinct, three-cell clusters. We discuss the implications of these observations for relapse after NAC alone, and the likely success of combining ICIs with chemotherapy in the neoadjuvant setting. We also identified a specific subset of TAMs which, when increased during NAC, correlated with the absence of metastasis over a three year follow up period.

2 Material and methods

2.1 Human TNBCs

FFPE sections (3µm) from 36 primary human TNBCs (age, size and grade-matched, anonymised) were from the Breast Tissue Bank of the UK charity, Breast Cancer Now. These were collected at the Barts Health NHS Trust Hospitals and Nottingham University NHS Trust Hospital in the UK between 2011 and 2017. Nineteen of these were from patients who did not receive NAC before definitive surgery (the 'untreated' group) and the other seventeen were from those given NAC followed by surgery. Approximately half of each of these two patient groups developed distant metastases within three years of surgery. These follow-up data were used to correlate multiplex immunostaining results with the presence or absence of metastasis during this period (ie. the '+Mets' or 'disease-free', 'DF', groups respectively) (Supplementary Table 1). Power calculations were performed using data from our previous human multiplex immunofluorescence studies to ensure that sufficient tumors were included in each of the above four groups.

2.2 Multiplex immunofluorescence staining

Prior to multiplexing, whole FFPE tumor sections were stained with H&E and examined by a pathologist to ensure the presence of malignant tumor. Sections were then multiplexed with a custom panel, including the 10 markers listed below, as described previously (28). This 'MultiOmyx' procedure involved baking sections at 65°C for 1h, deparaffinizing and treating them with a two-step antigen retrieval process. They were then blocked against nonspecific binding with 10% donkey serum and 3% BSA in PBS for 1h at RT and stained with DAPI for 15 min. Directly conjugated primary antibodies (list below) were diluted in PBS supplemented with 3% (wt/vol) BSA (to working concentrations optimized previously) and applied for 1h at RT on a Leica Bond III Stainer.

Antibodies used were: mouse anti-LAG-3 (17B4, LifeSpan Biosciences), mouse anti-PanCK (PCK26, Sigma-Aldrich/AE1, BioScience), mouse anti-CD31/PECAM-1 (89C2, Cell Signaling), mouse anti-CD3 (F7.2.38, Dako), rabbit anti-CD4 (EPR6855, Abcam; Cat# ab196372, RRID : AB_2889191), mouse anti-CD8 (C8/144B, Dako), mouse anti-FoxP3 (206D, BioLegend), rabbit anti-PD-1 (EPR4877, Abcam), rabbit anti-PD-L1 (SP142, Abcam), mouse anti-TIM-3 (polyclonal, R&D Systems) and mouse anti-CD163 (EDHu-1, Bio-Rad).

TAMs were identified using an antibody to CD163 rather than the commonly used alternative, CD68, as the latter has been shown to label other cells such as fibroblasts in human breast tumors (29). We also examined TAM expression of two negative checkpoint regulators (NCRs), PD-L1 (programmed cell death ligand 1) and TIM-3 (T cell immunoglobulin and mucin domain-containing protein 3) as these have been linked to improved relapse free survival and/or survival in untreated TNBC (30, 31). Furthermore, the effect of NAC on TAM expression of these two cell surface receptors has yet to be defined.

The density and distribution of three other immune cell types were also quantified: Tregs identified using CD3, CD4 and FOXP3; CD4+ T cells using CD3 and CD4 and FOXP3 negativity (herein called 'CD4+ T cells'); and cytotoxic T cells using CD3 and CD8. Finally, the activation status of CD4+ and CD8+ T cells was defined using a combination of the above markers with the T cell activation marker, PD-1 (programmed cell death protein 1) and T cell exhaustion marker, LAG-3 (lymphocyte-activation gene 3) (32). So, non-activated (naïve) T cells are PD-1-; activated T cells, PD-1+LAG-3-; and exhausted T cells, PD-1+LAG-3+.

Several rounds of paired antibody staining were performed in sequence on each tumor section using the antibodies listed above. After each round of staining with two antibodies, high resolution images were collected from 20 regions of interest (ROIs) across viable tumor areas using a 20x objective on an IN Cell analyzer 2200 microscope (GE Healthcare Life Sciences). ROIs included both PanCK-rich areas (TCIs) and PanCK-negative areas (stroma). The mean value of a given parameter (eg. TIM-3) was then calculated for each tumor section using these 20 ROIs, and the overall mean +/- SEM calculated for each tumor group using these values.

In between exposure to paired antibodies, slides were washed in PBS/0.3% TritonX-100 and dye inactivation performed by immersion in an alkaline solution containing H₂O₂ for 15 min with gentle agitation at room temperature. Slides were washed again in PBS, imaged to check the efficacy of the dye in-activation, and stained with the next pair of antibodies.

2.3 Quantitative image analysis

An AI-based, advanced analytics platform, proprietary to NeoGenomics Labs, called 'NEO Image Analysis', was used to quantify and analyse subsets of TAMs, T cells and Tregs in various tumor areas. This included algorithms that could differentiate between them in stromal and TCIs, and within PV (within 50µm from a CD31+ blood vessel) and non-PV areas (>50µm) of TCIs and the tumor stroma (Figure 1A). Cells were segmented and tracked through each staining round, and deep learning models used to quantify positivity for each stain, as well as to classify regions as TCIs or stroma. The density of each cell type was calculated in each region of interest 'ROI' (for both PV and non-PV areas of the stroma versus TCIs) by dividing the total cell count in a given area by the area itself (in mm²).

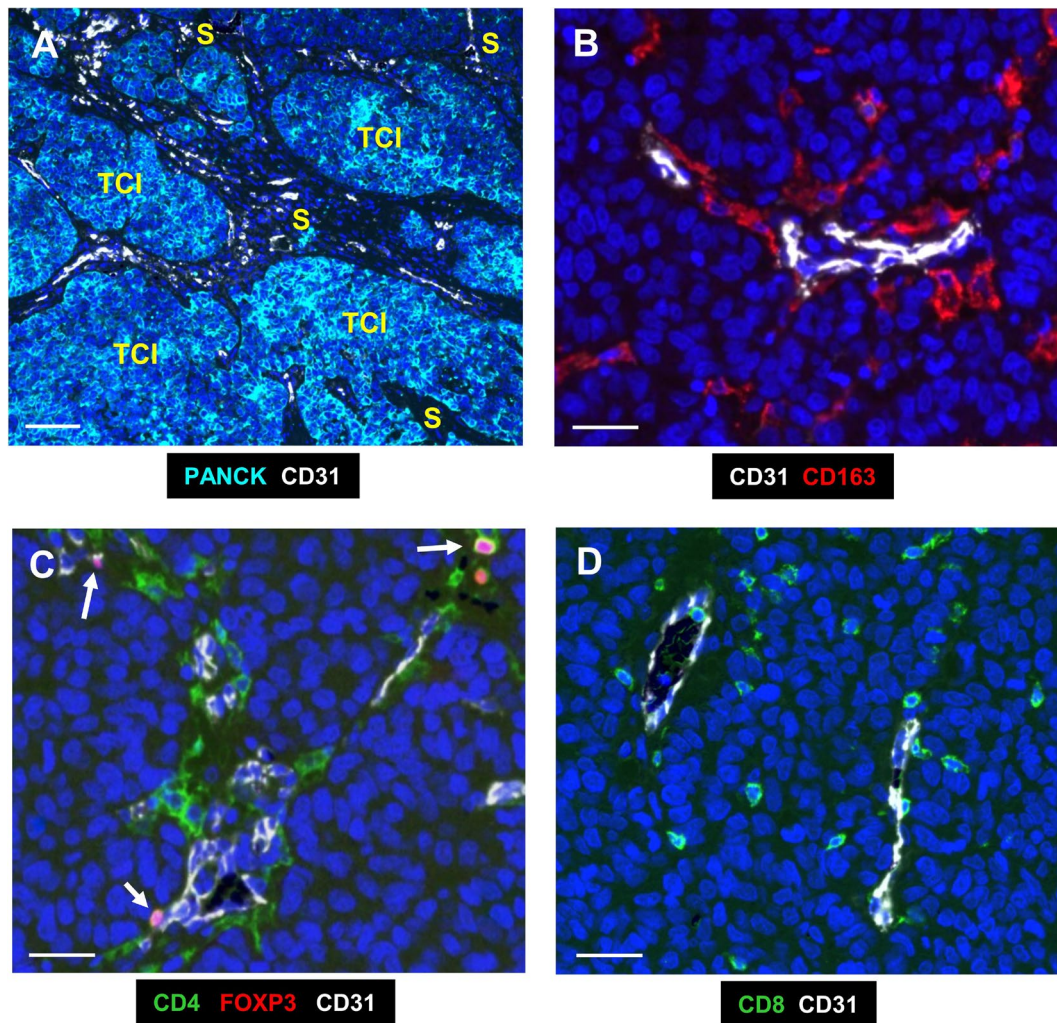


FIGURE 1

Representative fluorescence images of the two main compartments and immune cells analysed in human TNBC. (A) The 2 main compartments, tumor cell islands (TCIs) containing PANCK+ cancer cells, and the stroma which has most of the CD31+ blood vessels; white). (B) CD163+ TAMs (red) in the PV niche (PVN), the area within 50µm from the abluminal surface of a blood vessel. (C) CD4+ T cells (green) were mainly around CD31+ blood vessels, with some also expressing nuclear FOXP3. These are Tregs (pink; arrows). (D) CD8+ T cells (green) were more widely distributed across the stroma. Blue = DAPI staining of nuclei. Bar in (A) = 200 µm; bars in (B-D) = 50 µm.

Cell positivity for each marker was assessed based on detectable signal above background. Marker-specific AI algorithms were trained to incorporate both stain intensity and stain morphology in order to differentiate between true stain and nonspecific background or image artifacts. All analytical results (for every single image for each stain) were checked by a trained scientist to ensure concordance between the algorithms and scientist.

2.4 Statistical analysis

All data shown are means±SEMs and were analysed using GraphPad Prism (RRID : SCR_002798). Data analysis was done blind (ie with the four groups only identified after each analysis). Statistical analysis between groups was performed using the Mann-

Whitney U-test with P values of ≤ 0.05 considered to be significant. All p values were corrected for multiple testing using the Bonferroni test. Pearson's correlation analysis was used to assess the correlation between two groups of data.

The receiver operating characteristic (ROC) curve analysis graphically represents the ability of an observation to predict an outcome. It is a plot of the true positive rate (the rate at which the test accurately predicts the outcome), versus the false positive rate (the rate at which the test predicts the outcome incorrectly), at various threshold values of the observation. The performance of a test is often expressed as the Area Under Curve (AUC), which has a value of 1.0 for a test which is both 100% accurate and totally sensitive. An AUC of >0.7 is considered a "good" test result, whereas 0.5 or less indicates a test which gives random results.

3 Results

3.1 Distribution of CD163+ TAMs and their correlation with metastasis after NAC.

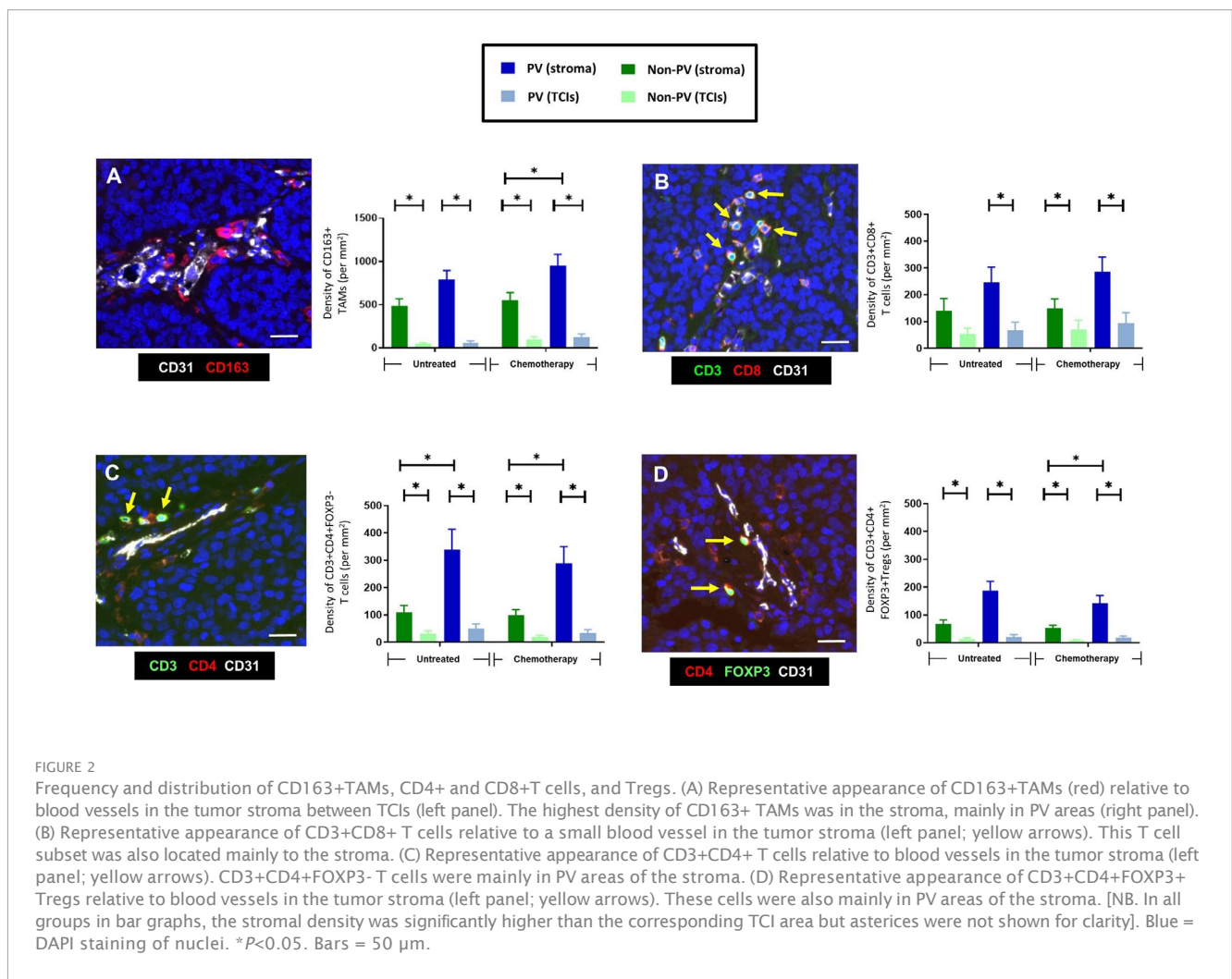
Figure 1A illustrates the two main compartments analysed in this study; the TCIs in which cancer cells were labelled using a panCK antibody, and the stroma in between them. Both CD31+ blood vessels and the 4 groups of immune cells assessed (CD163+TAMs, CD4+ and CD8+ T cells and CD4+FOXP3+Tregs) were present mainly in the stroma (Figures 1, 2). As mentioned previously, the PV area is defined as being within 50µm of the abluminal surface a given CD31+ blood vessel (8). It excludes the area of CD31 staining for blood vessels as well as their lumens.

CD163+ TAMs (Figures 1B, 2A) and Tregs (Figures 1D, 2D) were preferentially located in PV areas of the stroma after NAC. By contrast, CD4+ T cells were mainly PV in untreated as well as NAC-treated tumors (Figures 1C, 2C), and CD8+T cells were evenly distributed across the stroma (Figures 1D, 2B). The density of PV and non-PV CD163+ TAMs showed a trend towards a reduction in the stroma of the NAC +Mets group compared to the NAC DF group although this

achieved significance only in the non-PV group (Supplementary Figure 1A). Links with metastasis were not seen with the other three immune cell types studied, although stromal T regs were significantly ($p= 0.01$) lower in the PV '+Mets' group after NAC than the PV +Mets group in untreated tumors (Supplementary Figures 1B-D).

3.2 Most CD163+ TAMs lack expression of PD-L1

In this study, the majority of TNBCs were found to contain at least some cancer cells and CD163+ TAMs expressing detectable PD-L1 although there was considerable heterogeneity in this between tumors (Supplementary Figures 2A, B, D). When we examined PD-L1 expression specifically by CD163+ TAMs, the majority (77-80%) of stromal CD163+TAMs were found to lack detectable PD-L1 expression and to be preferentially located in PV areas in the stroma after NAC (Figures 3A, B, D). By contrast, CD163+ TAMs that expressed PD-L1 were evenly distributed across the stroma and unaffected by NAC. Neither PD-L1+ nor PD-L1- CD163+TAMs correlated with metastasis (Figures 3C, E).



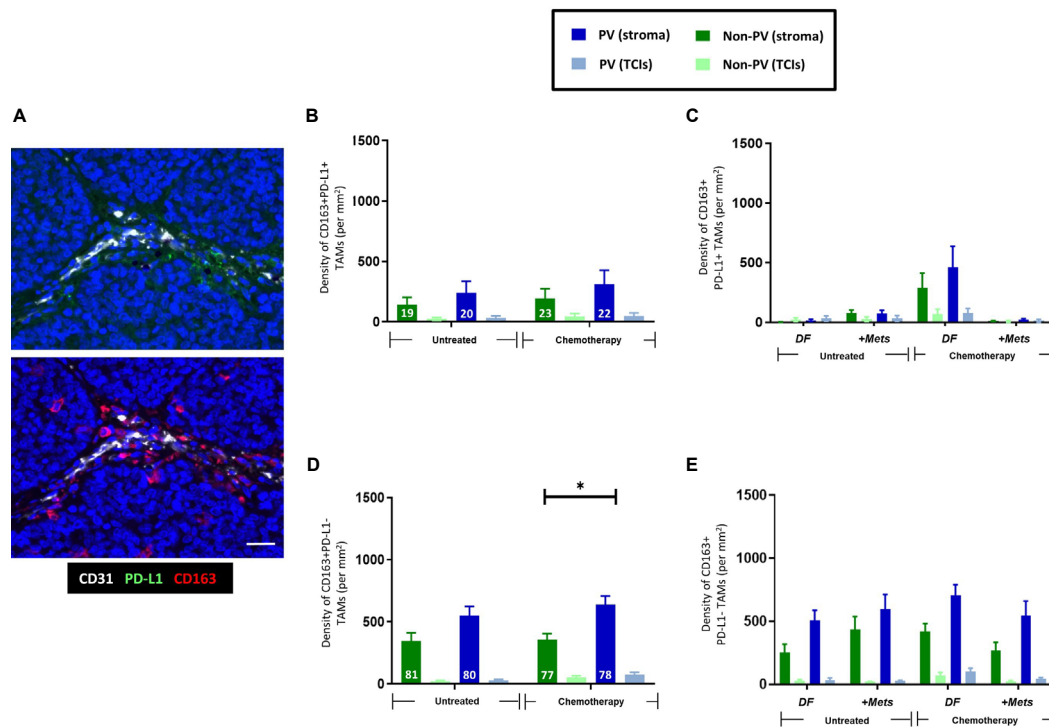


FIGURE 3

Expression of PD-L1 by CD163+TAMs. (A) Representative appearance of sparse stromal PD-L1 staining (top panel; green) and greater density of CD163+ TAMs in the same area (bottom panel; red) in the tumor stroma. Bar = 50 μ m. The majority of stromal CD163+ TAMs do not express PD-L1. Blue = DAPI staining of nuclei. (B) PD-L1+CD163+ TAMs are evenly distributed across the stroma and generally exist at lower density than PD-L1-CD163+ TAMs (D). (C) The density of PV PD-L1+CD163+ TAMs exhibited a non-significant trend towards being lower in PV areas of the stroma in the '+Mets' group than the DF one after NAC, a feature not seen with PD-L1-CD163+ TAMs (E). (D) Unlike PD-L1+ CD163+ TAMs, PD-L1- CD163+ TAMs preferentially locate to PV areas after NAC. The white figures at the base of each bar are the % of CD163+ TAMs in each group that were either PD-L1+ (B) or PD-L1- (D). [NB. In all groups in bar graphs, the stromal density was significantly higher than the corresponding TCL area but asterisks for this were not shown for clarity]. * P <0.05 (ns = not statistically significant).

3.3 TIM3+CD163+ TAMs increased after NAC in tumors from patients who did not develop metastases

As with CD163+ TAMs (Figure 2A), NAC induced an increase in PV TIM3+CD163+TAMs (Figures 4A, B). There was also a significant ($p=0.008$) increase in the proportion of CD163+TAMs in all tumor areas expressing TIM-3 after NAC in the DF group compared to the untreated, DF group (Figure 4C). Taken together these two findings suggest that NAC leads to TIM-3 upregulation by existing CD163+ TAMs in the DF group and/or the recruitment of TIM-3-expressing TAMs into the stroma in the DF group. Figure 4D also shows that, after NAC, the DF group contained a significantly ($p=0.0015$) higher density of non-PV TIM-3+CD163+ TAMs than in non-PV areas of the +Mets group. None of the above features were seen with TIM-3-CD163+ TAMs (Supplementary Figure 3).

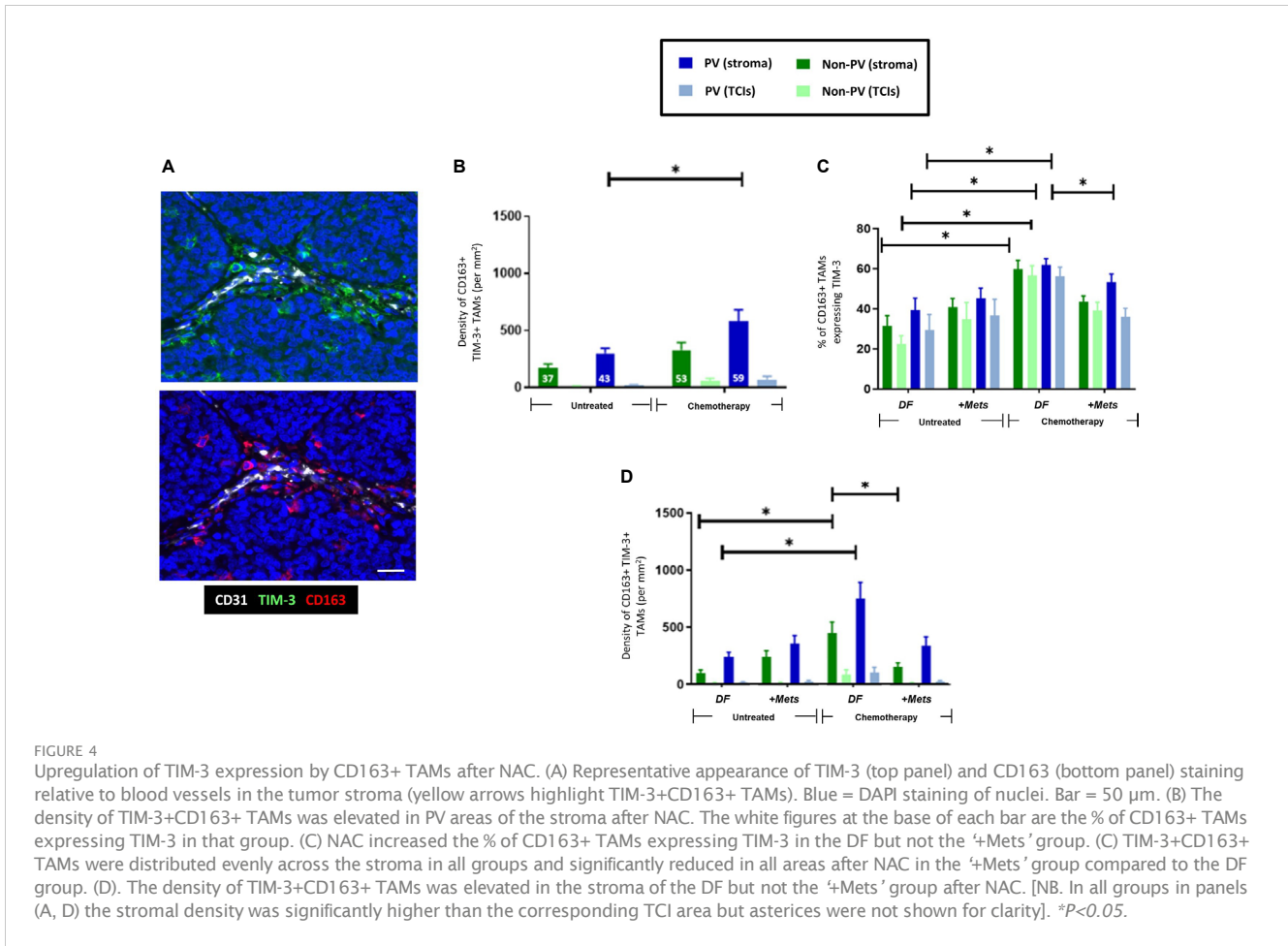
To interrogate the ability of stromal CD163+ TAMs or TIM3+CD163+ TAMs to predict relapse in NAC-treated TNBC patients, we then conducted ROC curve analyses of the density of these two TAM subsets (DF v '+Mets'). We also included an analysis of TIM-3-CD163+ TAMs for comparison. These analyses showed that both CD163+ and TIM-3+CD163+ TAMs were strongly predictive of metastasis (area under the curve, 'AUC', values: CD163+ TAMs, 0.8143 ($p=0.0318$); TIM-3+CD163+ TAMs, 0.800 ($p=0.0404$)).

(Supplementary Figures 4A-C). We also demonstrated that this

predictive power resided in both PV or PV subsets CD163+ and TIM-3+CD163+ TAMs (i.e. in cells across the entire stroma) (Supplementary Figures 4D-F). By contrast, the AUC value for TIM-3-CD163+ TAMs showed a weaker predictive power with metastasis, 0.6857 ($p=0.2046$). The latter accords well with the absence of any significant differences in TIM-3-CD163+ TAMs between the NAC DF and +Mets groups (Supplementary Figure 3B).

Although TIM-3 is known to be expressed by various cell types in human tumors our study demonstrated that CD163+ TAMs were the main cell type expressing this protein in TNBCs (Supplementary Figure 5A). Our finding that TNBC patients with high levels of stromal TIM-3-expressing CD163+ TAMs after NAC were less likely to develop metastasis within three years was supported, albeit inferentially, by data from a previously published dataset. These showed that when 153 TNBC patients were divided into those with high or low TIM-3 expression after NAC, the latter group had significantly worse relapse free survival (Supplementary Figure 5B) (33).

Interestingly, over 75% of TIM-3+CD163+TAMs were PD-L1- (Figure 5A) and NAC significantly ($p=0.001$) increased the proportion of PD-L1-CD163+TAMs expressing TIM-3 (Figure 5B). The density of PD-L1-TIM-3+CD163+ TAMs was significantly ($p=0.002$, non-PV; $p=0.005$, PV) increased in stromal areas of tumors after NAC, being highest in PV areas (Figures 5C, D). This effect was restricted to this specific TAM subset as it did not occur in other CD163+TAM subsets: PD-L1+TIM-3+,



PD-L1+TIM-3- or PD-L1-TIM-3- (Supplementary Figure 6). Of note, when TIM-3+CD163+ TAMs were divided up into PD-L1- or PD-L1+ (Figure 5D, Supplementary Figure 6D), the significant correlation of TIM3+CD163+ TAMs with metastasis was lost.

3.4 Effect of NAC on stromal PV Tregs

CD3+CD4+FOXP3+ Tregs located preferentially to PV areas of the stroma in both untreated ($p=0.045$) and NAC-treated ($p=0.036$) '+Met' groups. However, their density in these PV areas was significantly ($p=0.01$) lower in the NAC +Mets' group than in the untreated '+Mets' group (Supplementary Figure 1D).

3.5 Activation status of CD4+ and CD8+ T cells in the PVN

The activation status of CD4+ and CD8+ T cells was assessed using antibodies to the activation marker, PD-1, and exhaustion marker, LAG-3 (ie. naïve T cells are PD1-LAG3-; active T cells are PD1+LAG3-; exhausted T cells are PD1+LAG3+). Figure 6 shows that only naïve CD4+ (top row) and CD8+ T cells (bottom row) preferentially located to PV areas of the stroma in untreated tumors. This persisted in NAC tumors for CD4+ T cells. By contrast, both

active and exhausted CD4+ and CD8+ T cells were evenly distributed across tumors (although active subsets of both CD4+ and CD8+ T cells showed a non-significant trend towards a more stromal distribution). Exhausted CD4+ T cells were only present at low density in all areas whereas exhausted CD8+ T cells showed greater variation between tumors with some containing a similar density in the stroma to naïve CD8+ T cells. Taken together, these data suggest that PV areas of tumors contain mainly naïve and active CD4+ T cells, and naïve and exhausted CD8+ T cells.

Interestingly, correlation analysis of the density of the above subsets of T cells (as well T regs) with the PD-L1+ and PD-L1- CD163+ TAM subsets showed that PD-L1+CD163+ TAMs showed a highly significant, positive correlation with all 3 activation subsets of CD4+ T cells, CD8+ T cells (and Tregs). This correlation was not seen with PD-L1-CD163+ TAMs (Supplementary Table 2, Supplementary Figure 7).

3.6 Perivascular clustering of distinct subsets of T cells with Tregs and CD163+ TAMs

Distinct, 3-cell clusters were seen in the PV areas of the stroma of untreated and NAC-treated tumors. These consisted of CD163+TAMs, either a CD4+ (FOXP3-) or a CD8+ T cell and a

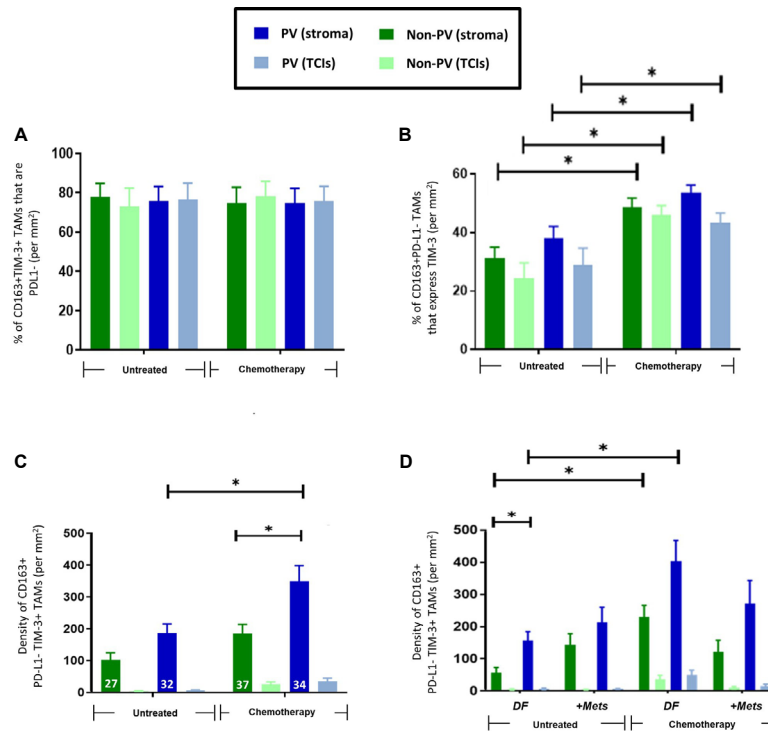


FIGURE 5

Frequency and distribution of PD-L1-TIM-3+CD163+TAMs. (A) 75-85% of CD163+TIM-3+ TAMs in all tumor areas failed to express detectable PD-L1. (B) NAC significantly increased the % of PD-L1-CD163+TAMs expressing TIM-3 (throughout tumors). (C) PD-L1-TIM-3+TAMs were mainly PV and exhibited increased numbers in all areas of NAC-treated compared to untreated tumors. The white figures at the base of each bar are the % of CD163+ TAMs that were both PD-L1- and TIM-3+ in that group. (D) The increased density of this TAM subset after NAC occurred mainly in PV areas of both treatment groups. [NB. in all groups in panels (B, C) stromal PV and non-PV groups were significantly higher than corresponding groups in TCIs, asterisks not shown for clarity]. $P < 0.05$. [NB. None of the TAM features shown in panels B-D were exhibited by the 15-25% of CD163+TIM-3+ TAMs that expressed PD-L1 (data not shown)].

CD4+FOXP3+ Treg (Figure 7). In keeping with the relatively high levels of naïve and active CD4+ T cells (along with naïve and exhausted CD8+ T cells) in the PV niche (Figure 6), the main types of PV 3-cell clusters were those containing naïve and active CD4+ and naïve and exhausted CD8+T cells (40-60%). The proportion of clusters containing active CD8+ T cells was significantly ($p < 0.0001$) lower than those with active CD4+ T cells but the opposite was true when clusters contained exhausted T cells (Figures 8A, B). When PD-L1 expression by CD163+ TAMs in these PV clusters was interrogated, both PD-L1- and PD-L1+ ones were found to be present but significantly ($p = 0.002$, untreated CD4; $p = 0.003$, NAC CD4; $p = 0.003$, untreated CD8; $p = 0.0004$, NAC CD8) more PD-L1- CD163+ TAMs were present in clusters containing naïve T cells. This was also the case for active CD4+ T cells ($p = 0.008$). (Figures 8C, D).

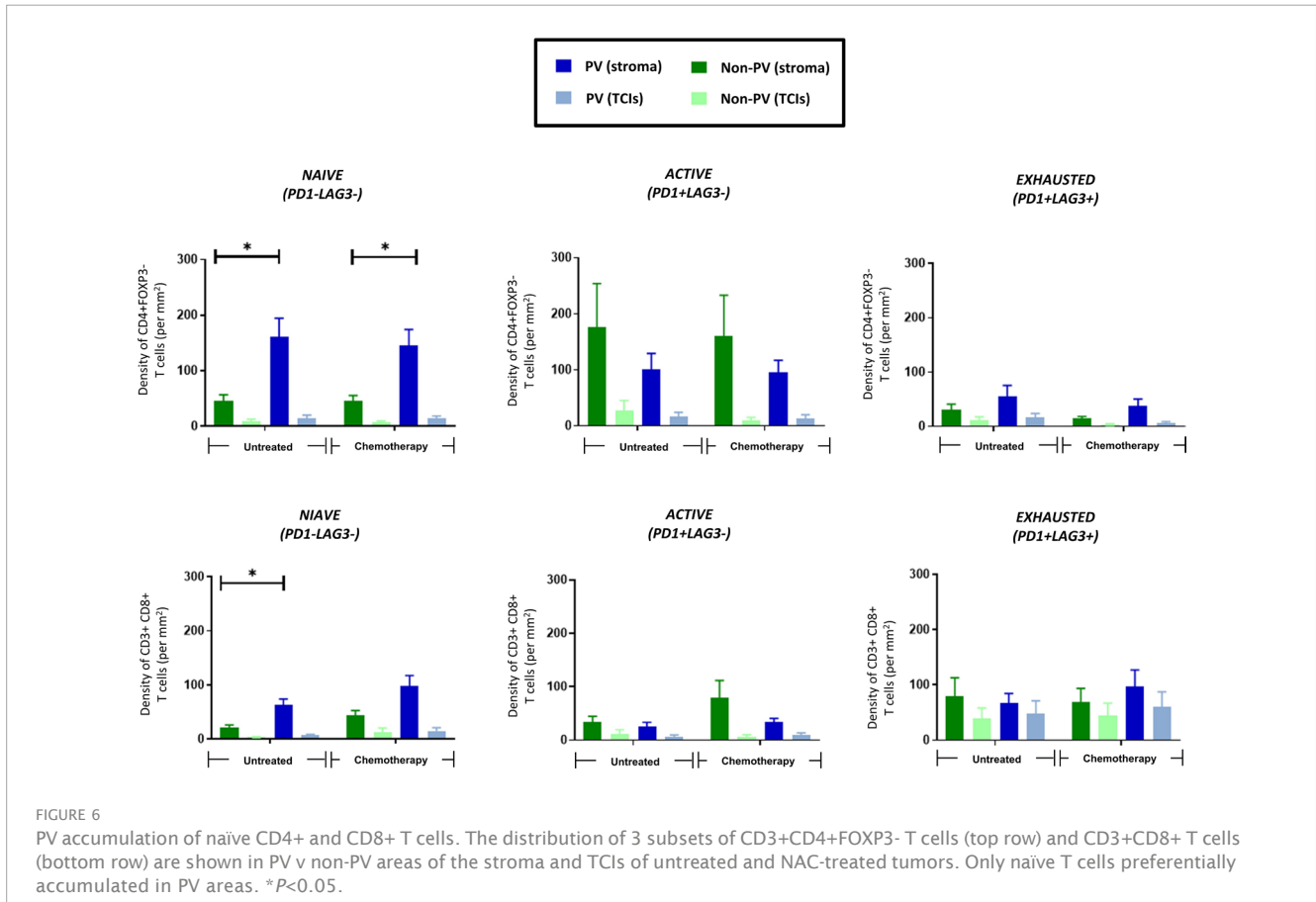
4 Discussion

Our finding that all four of the immune cell groups studied here reside mainly in the stroma of TNBC, accords well with other reports of such 'immune exclusion' from TCIs in both mouse and human tumors (34, 35). Indeed, several stromal cell types, such as TAMs, Tregs, MDSCs and cancer-associated fibroblasts (CAFs) have been shown to limit T cell infiltration into TCIs (35). Although

high levels of T cells in the stroma correlate with improved survival in breast cancer (36), their accumulation away from TCIs also limits the efficacy of T cell-based immunotherapies, as cytotoxic T cells require close contact with cancer cells to kill them (37). So, the retention of T cells in the stroma after NAC is likely to limit the efficacy of immunotherapy administered with or after NAC.

Somewhat surprisingly, our data showed that high levels of stromal CD163+ TAMs in NAC-treated tumor residues correlated with the absence of metastasis within three years of primary surgery. This TAM subset also appeared to have utility as a predictive biomarker for metastasis in our ROC analyses, although this awaits validation in a larger, independent cohort of NAC-treated TNBCs. A number of studies have shown that high CD163+ TAMs in pre-NAC biopsies correlate with worse treatment responses (38, 39) but our data suggest that opposite is the case in post-NAC TNBCs. This is supported by the finding that high CD163+ TAMs in NAC-treated human pancreatic tumors correlate with improved disease-free progression compared to tumors with low levels (40).

When we then divided CD163+ TAMs by their TIM-3 expression we found that the link with metastasis resided with the TIM-3-expressing subset. This raises the possibility that this TAM subset is amplified in the stroma during NAC where it exerts an anti-metastatic effect. They could limit metastases by inhibiting the escape of cancer cells through tumor blood vessels and/or their



ability to form metastases at distant sites. They could also phagocytose cancer cells and present their antigens to naïve T cells in PV tumor areas (or draining lymph nodes) to activate their tumoricidal functions. The latter could result in increased intra-tumoral or systemic immunity to metastasizing cancer cells.

At first glance, the link between this TAM subset and reduced metastasis appears to contradict the finding that high levels of TIM-3+ TAMs correlate with increased metastasis and/or reduced survival in other tumor types like untreated human non-small cell lung cancer and clear cell renal carcinomas (41, 42). However, the opposite appears to be the case for stromal TIM-3+ TILs (including TAMs) in untreated TNBC (31) so this appears to be context-dependent. Furthermore, to our knowledge the present study is the first to report specifically on the prognostic significance of stromal TIM-3+ TAMs after NAC.

Interestingly, cancer cell-derived TGFβ is known to stimulate the expression of both TIM-3 by TAMs (43, 44) and is upregulated by chemotherapeutic agents (45). However, it remains to be seen whether TGFβ contributes to the abundance and/or the possible anti-metastatic function(s) of stromal TIM-3+ TAMs, within the complex milieu of NAC-treated tumors.

Various immune cells were seen to preferentially accumulate in PV areas of TNBCs after NAC including CD163+ TAMs (both PD- L1- and TIM-3+), naïve CD4+ T cells and Tregs. This contrasted with CD4+ T cells which were also located mainly around blood vessels in untreated tumors, and CD8+ T cells that were widely distributed across the stroma under both conditions.

When it comes to PV TAMs, Arwert et al. (46) showed in a mouse model of mammary cancer that immature TAMs can be stimulated by cancer cells to upregulate CXCR4. This then causes them to traffic towards CXCL12 expressed by fibroblasts around vessels. As mentioned earlier, various studies have reported that PV TAMs promote tumor resistance to chemotherapy, as well as tumor regrowth and metastatic spread after this treatment (14, 17–19, 21). As multiple subsets of macrophages are present in untreated tumors (6–8), the possibility of more than one TAM subset existing in PV areas untreated or NAC-treated TNBCs exists. Indeed, two recent studies have highlighted the presence of TAM subsets in the PVN with apparently opposing effects on tumor immunity. Sharma and colleagues (47) demonstrated the presence of a subset of PV, CD163hi TAMs that interact closely with T cells and Tregs in the PVN of human colorectal tumors and suppress T cell activation. This appears to be similar to our observation of these 3 cells forming PV clusters in TNBCs and suggests that they may inhibit anti-tumor immunity. Their presence in TNBCs after NAC could, therefore, limit the efficacy of ICIs given during or after NAC. However, it should be noted that Ramos et al. (22) recently described a subset of PV CD163+ that clustered at high density with CD8+ T cells, expressed genes that stimulate the cytotoxic function of T cells, and correlated with favourable clinical outcome in human breast cancer. The latter finding is supported by the demonstration that activated TAMs (as well as dendritic cells) colocalize with CD8+ T cells in mouse colorectal and pancreatic tumors, and that a high frequency of these PV TAM-T cell clusters

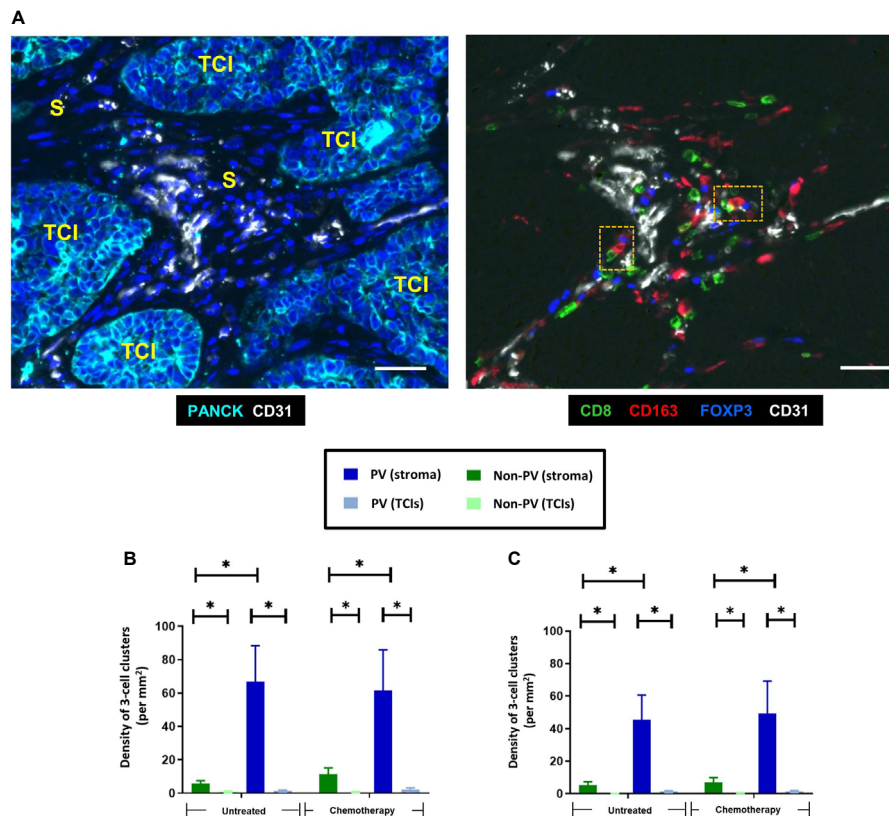


FIGURE 7
 Distinct clusters of three immune cell types (CD163+ TAMs, CD8+ T cells and FOXP3+ Tregs) accumulate around blood vessels in both untreated and NAC-treated TNBCs. (A) Representative appearance of PV 3-cell clusters present around blood vessels in the stroma. Left panel: stromal areas (S) containing blood vessels are present between PANCK+ TCIs. Blue = DAPI staining of nuclei. Right panel: Close interaction between CD163+ TAMs, CD8+ T cells and FOXP3+ Tregs around blood vessels in the same tumor area shown in panel (A). The orange dashed boxes in the right panel show two, 3-cell clusters, each containing a CD163+ TAM, a CD8+ T cell and FOXP3+ Treg. Bars = 50 μ m. Density of 3-cell clusters containing either CD4+ T cells (B) or CD8+ T cells (C). They exist mainly in PV areas of the stroma. *P < 0.05.

correlated with improved tumor responses to immunotherapy (23). These latter findings raise the possibility that the PV clusters we describe could actually augment T cell activation and thus the efficacy of immunotherapy.

Using quantitative, multi-parameter imaging, such PV immune cell clusters in other mouse tumor models have been shown to contain a specific subset of CD8+ T cells called 'resource' CD8+ T cells (ie. a subset of non-exhausted, PD-1-expressing cells with the capacity for enhanced proliferation) (23). It was proposed that the close interaction leads this subset to proliferate and rapidly develop into terminally differentiated, cytotoxic CD8+ T cells (23). This may accord with our finding that the main form of T (albeit CD4+) cells present in PV clusters in TNBCs were active (PD1+LAG3-) or naïve (ie. PD-1-) ones. The active ones may be analogous to the 'resource T cells' reported above in PV clusters in the mouse tumors (23). However, it should be noted that the above was not seen for CD8+ T cells in our cohort of TNBCs. In their case, the main form in clusters was naïve, with very few in an active state. The reason for the difference between CD4 and CD8+ cells is presently unclear.

It is possible that incorporation of naïve T cells into PV clusters is simply a way to retain them in an inactive state as soon as they enter tumors across the vasculature. It remains a possibility that

these structures can regulate T cell function in a number of ways. Over 40% of PV clusters contained active CD4+ T cells which may have stemmed from naïve CD4+ T cells in clusters that were activated by antigen presented to them by CD163+ TAMs. Moreover, some or all of the Tregs present in clusters may have formed from naïve CD4+ T cells as the intra-tumoral generation of Tregs from CD4+ T cells has recently been reported (48). It is noteworthy though that, in human breast cancer xenografts grown in humanized mice, blocking the recruitment of naïve CD4+ T cells into PV areas of tumors resulted in reduced numbers of intra-tumoral Tregs, and inhibited tumor progression (25). Maintaining newly formed Tregs (and/or those recruited from the peripheral blood) in PV clusters close to other immune effectors in TNBC would be likely to have a suppressive effect on the latter - unless PV Tregs are in an immature, non-functional state. Our study shows that CD163+ TAMs in PV clusters containing either naïve or active CD4+ T cells, or naïve CD8+ T cells, lacked expression of PD-L1. Of note, the immunostimulatory PV TAM subset described recently in mouse colorectal tumors also lacked PD-L1 expression (23). However, further analysis of the phenotype of such 'cluster TAMs' is now needed to help understand the effect of such PV clusters on T-cell mediated immunity in TNBC.

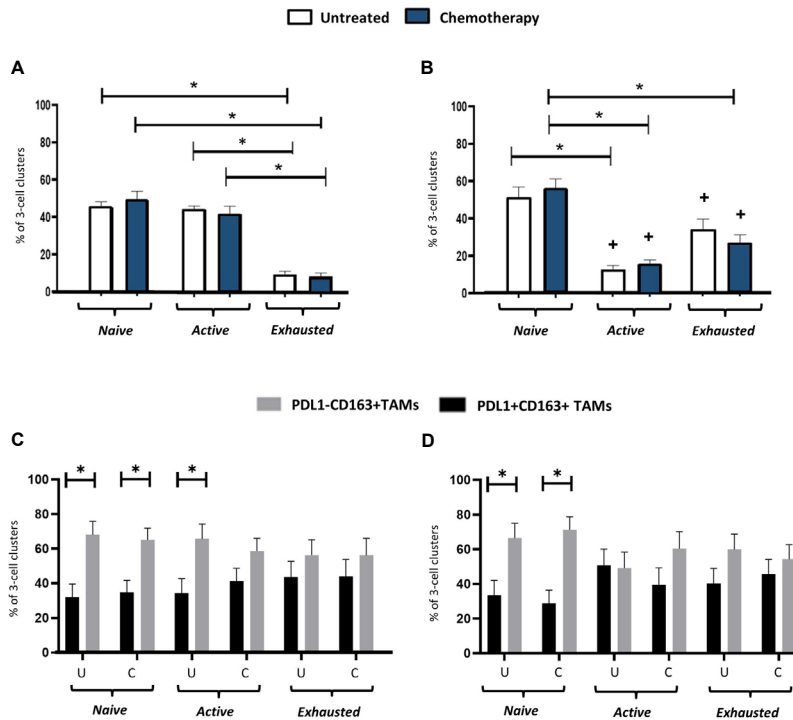


FIGURE 8
 Activation status of T cells in PV, 3-cell clusters: correlation with PD-L1 status of CD163+ TAMs. The proportion of PV 3-cell clusters in the stroma containing either naïve, active or exhausted CD3+CD4+FOXP3- T cells (A, C) or a CD3+CD8+ T cells (B, D) (top row), or PD-L1- or PD-L1+ TAMs (bottom row). The ratio of TIM-3+:TIM-3- TAMs in PD-L1-TAMs in these clusters with 1:1 (data not shown). U, untreated; C, NAC-treated. *P<0.05. *P<0.05 w.r.t the same group in (A).

Of course, it remains a possibility that T cells could also influence the phenotype of TAMs or Tregs in PV clusters. For example, naïve T are unable to release interferon (IFN)- γ (49), an important stimulus for PD-L1 expression by macrophages in tumors (50). This could help to explain to our finding that CD163+ TAMs in clusters with naïve T cells were predominantly lacking in PD-L1 expression. Taken together, our data have identified a distinct subset of TAMs that correlates inversely with metastasis after NAC. As such, they could be a new biomarker for relapse. They also show that a number of important immune effectors form intimate contacts with one another in PV areas of TNBCs, a feature retained after NAC. These clusters are highly likely to impact on T cell function and thus the success of immunotherapy administered with NAC.

Data availability statement

The original contributions presented in the study are included in the article/Supplementary Material. Further inquiries can be directed to the corresponding author.

Ethics statement

The studies involving humans were approved by Breast Cancer Now's ethics review committee. The studies were conducted in

accordance with the local legislation and institutional requirements. The participants provided their written informed consent to participate in this study.

Author contributions

MM: Conceptualization, Data curation, Formal Analysis, Methodology, Writing – review & editing. RA: Conceptualization, Formal Analysis, Investigation, Methodology, Writing – review & editing. SW: Formal Analysis, Writing – review & editing. JB: Formal Analysis, Writing – review & editing. HN: Data curation, Formal Analysis, Methodology, Software, Writing – review & editing. AJ: Conceptualization, Data curation, Formal Analysis, Funding acquisition, Methodology, Project administration, Software, Supervision, Writing – review & editing. CL: Conceptualization, Data curation, Formal Analysis, Funding acquisition, Investigation, Methodology, Project administration, Supervision, Validation, Visualization, Writing – original draft, Writing – review & editing.

Funding

The author(s) declare financial support was received for the research, authorship, and/or publication of this article. This study was funded by a grant to CEL from the UK charity, Team Verrico.

Acknowledgments

The authors acknowledge the role of the Breast Cancer Now Tissue Bank in the UK in collecting and making available the samples and/or accompanying anonymised patient data, as well as the patients who have generously donated their tissues and shared their with the Breast Cancer Now Tissue Bank for research purposes.

Conflict of interest

AJ-J and HN are employees of Neogenomics Laboratories in the USA. The remaining authors declare that the research was conducted in the absence of any commercial or financial relationships that could be constructed as a potential conflict of interest.

Publisher's note

All claims expressed in this article are solely those of the authors and do not necessarily represent those of their affiliated organizations, or those of the publisher, the editors and the reviewers. Any product that may be evaluated in this article, or claim that may be made by its manufacturer, is not guaranteed or endorsed by the publisher.

Supplementary material

The Supplementary Material for this article can be found online at: <https://www.frontiersin.org/articles/10.3389/fimmu.2023.1291643/full#supplementary-material>

SUPPLEMENTARY FIGURE 1

Reduced density of stromal CD163+ TAMs correlate inversely with metastasis. Distribution of CD163+ TAMs (A), CD3+CD8+ T cells (B), CD3+CD4+FOXP3- T cells (C) and CD3+CD4+FOXP3+ Tregs (D) in PV and non-PV areas of the stroma and TCIs in untreated and NAC-treated groups (subdivided into those that did or did not develop metastases within 3 years of primary surgery. 'DF' = DF; ie. no metastases; '+Mets' = developed metastases). * $P < 0.05$.

References

1. Bianchini G, De Angelis C, Licata L, Gianni L. Treatment landscape of triple-negative breast cancer - expanded options, evolving needs. *Nat Rev Clin Oncol* (2022) 19:91–113. doi: 10.1038/s41571-021-00565-2
2. Marra A, Curigliano G. Adjuvant and neoadjuvant treatment of triple-negative breast cancer with chemotherapy. *Cancer J* (2021) 27(1):41–9. doi: 10.1097/PPO.0000000000000498
3. Cortes J, Cescon DW, Rugo HS, Nowecki Z, Im SA, Yusof MM, et al. Pembrolizumab plus chemotherapy versus placebo plus chemotherapy for previously untreated locally recurrent inoperable or metastatic triple-negative breast cancer (KEYNOTE-355): a randomised, placebo-controlled, double-blind, phase 3 clinical trial. *Lancet* (2020) 396(10265):1817–28. doi: 10.1016/S0140-6736(20)32531-9
4. Xin Y, Shen G, Zheng Y, Guan Y, Huo X, Li J, et al. Immune checkpoint inhibitors plus neoadjuvant chemotherapy in early triple-negative breast cancer: a systematic review and meta-analysis. *BMC Cancer* (2021) 21(1):1261. doi: 10.1186/s12885-021-08997-w
5. Ferrari P, Scatena C, Ghilli M, Bargagna I, Lorenzini G, Nicolini A. Molecular mechanisms, biomarkers and emerging therapies for chemotherapy resistant TNBC. *Int J Mol Sci* (2022) 23(3):1665. doi: 10.3390/ijms23031665
6. Chung W, Eum HH, Lee HO, Lee KM, Lee HB, Kim KT, et al. Single-cell RNA-seq enables comprehensive tumor and immune cell profiling in primary breast cancer. *Nat Commun* (2017) 8:15081. doi: 10.1038/ncomms15081
7. Jiang K, Dong M, Li C, Sheng J. Unraveling Heterogeneity of tumor cells and microenvironment and its clinical implications for triple negative breast cancer. *Front Oncol* (2021) 11:557477. doi: 10.3389/fonc.2021.557477

SUPPLEMENTARY FIGURE 2

Representative appearance of PD-L1 expression by CD163+ TAMs and PANCK+ cancer cells in high/moderate PD-L1-expressing TNBCs. PD-L1+CD163+ TAMs were most frequent at the interface between TCIs and the stroma. Bar = 50 μ m.

SUPPLEMENTARY FIGURE 3

Frequency and distribution of TIM-3-CD163+TAMs. (A) TIM-3-CD163+ TAMs were present throughout the stroma in untreated and NAC-treated tumors. The white figures at the base of each bar are the % of CD163+ TAMs in each group that were TIM-3-. (B) The density of this TAM subset did not correlate with metastasis. [NB. in all groups, stromal PV and non-PV groups were significantly higher than corresponding groups in TCIs, asterics not shown for clarity]. $P < 0.05$.

SUPPLEMENTARY FIGURE 4

Receiver Operating Characteristic (ROC) curve analysis of the ability of three stromal TAM subsets to predict the development of metastasis in NAC-treated patients within 3 years of surgical removal of primary tumors (ROC analysis of data at the level of whole tumor sections). (A) all CD163+ TAMs; (B) all TIM3-3+CD163+ TAMs; (C) all TIM-3-CD163+ TAMs; (D) PV v non-PV CD163+ TAMs; (E) PV v non-PV TIM-3+CD163+ TAMs; (F) TIM-3-CD163+ TAMs.

SUPPLEMENTARY FIGURE 5

Expression of TIM-3 in human TNBC: correlation with relapse free survival after NAC. (A) CD163+ TAMs and alpha smooth muscle actin-positive cells ('ASMA'; pericytes and fibroblasts) are the predominant cell types expressing TIM-3 - and the proportion of these cells expressing this cell surface protein increases after NAC. ASMA = alpha smooth muscle actin. * $P < 0.05$. (B) Significant correlation between TIM-3 expression levels in 153 TNBCs (taken from women administered NAC) and DFS (using online dataset: <http://kmpplot.com/analysis/index.php?p=service&cancer=breast#>) (33).

SUPPLEMENTARY FIGURE 6

No effect of NAC on various CD163+ TAM subsets. Three CD163+ TAM subsets (A, D) PD-L1+TIM-3+; (B, E) PD-L1+TIM-3-; (C, F). PD-L1-TIM-3- were evenly distributed throughout the stroma of tumors at significantly higher density than in corresponding areas of TCIs (asterics not shown). There was no effect of NAC on the density or distribution of these cells, nor did they correlate with metastasis. (ns = not statistically significant).

SUPPLEMENTARY FIGURE 7

Correlation graphs for significantly different comparisons seen in Supplementary Table 2. R = correlation coefficient.

SUPPLEMENTARY TABLE 1

Clinical parameters for the four patient groups analysed in this study. Parentheses indicate percentage data. NAC = neoadjuvant chemotherapy (3-8 cycles). DF = DF (no metastasis within 3 years of primary surgery), '+Mets' = developed metastases within 3 years. FEC = 5 fluorouracil, epirubicin, cyclophosphamide. FEC-T - 5 = fluorouracil, epirubicin, cyclophosphamide, docetaxel. 'Other' NACs included FEC-T + Carboplatin, EC (epirubicin cyclophosphamide) and ECD (epirubicin cyclophosphamide & docetaxel).

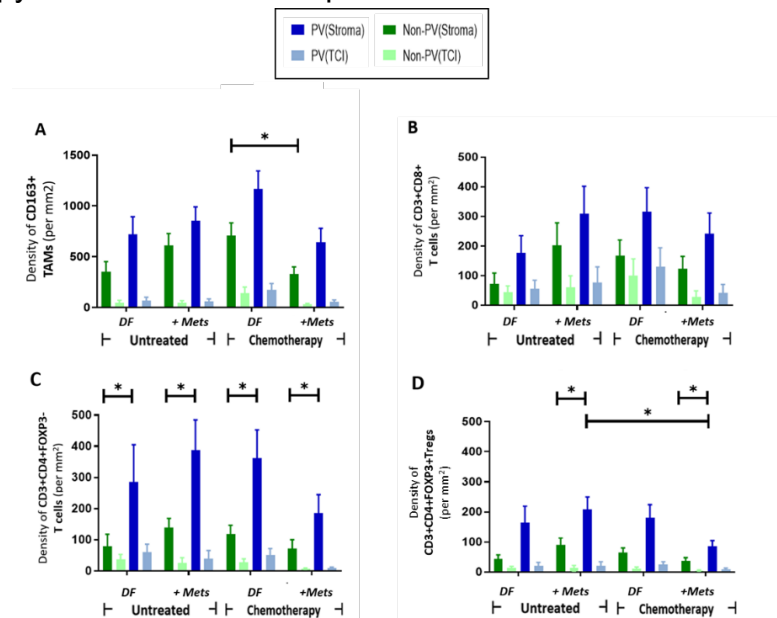
SUPPLEMENTARY TABLE 2

Correlation of the overall density of PD-L1+ CD163+TAMs with CD4+ T cells, CD8+ T cells and Tregs.

8. Azizi E, Carr AJ, Plitas G, Cornish AE, Konopacki C, Prabhakaran S, et al. Single-cell map of diverse immune phenotypes in the breast tumor microenvironment. *Cell* (2018) 174(5):1293–308. doi: 10.1016/j.cell.2018.05.060
9. Wu SZ, Roden DL, Wang C, Holliday H, Harvey K, Cazet AS, et al. Stromal cell diversity associated with immune evasion in human triple-negative breast cancer. *EMBO J* (2020) 39(19):e104063. doi: 10.15252/embj.2019104063
10. Wang G, Yao Y, Huang H, Zhou J, Ni C. Multiomics technologies for comprehensive tumor microenvironment analysis in triple-negative breast cancer revealed under neoadjuvant chemotherapy. *Front Oncol* (2023) 13:1131259. doi: 10.3389/fonc.2023.1131259
11. Keren L, Bosse M, Marquez D, Angoshtari R, Jain S, Varma S, et al. A structured tumor-immunomicroenvironment in triple-negative breast cancer revealed by multiplexed ion beam imaging. *Cell* (2018) 174(6):1373–87. doi: 10.1016/j.cell.2018.08.039
12. Carter JM, Chumsri S, Hinerfeld DA, Ma Y, Wang X, Zahrieh D, et al. Distinct spatial immune microlandscapes are independently associated with outcomes in triple-negative breast cancer. *Nat Commun* (2023) 14(1):2215. doi: 10.1038/s41467-023-37806-0
13. Gruosso T, Gigoux M, Manem VSK, Bertos N, Zuo D, Perlitch I, et al. Spatially distinct tumor immune microenvironments stratify triple-negative breast cancers. *J Clin Invest* (2019) 129(4):1785–800. doi: 10.1172/JCI96313
14. Lapenna A, De Palma M, Lewis CE. Perivascular macrophages in health and disease. *Nat Rev Immunol* (2018) 18:689–702. doi: 10.1038/s41577-018-0056-9
15. Coffelt SB, Tal AO, Scholz A, De Palma M, Patel S, Urbich C, et al. Angiopoietin-2 regulates gene expression in TIE2-expressing monocytes and augments their inherent proangiogenic functions. *Cancer Res* (2010) 70:5270–80. doi: 10.1158/0008-5472
16. Coffelt SB, Chen YY, Muthana M, Welford AF, Tal AO, Scholz A, et al. Angiopoietin 2 stimulates TIE2-expressing monocytes to suppress T cell activation and to promote regulatory T cell expansion. *J Immunol* (2011) 186:4183–90. doi: 10.4049/jimmunol.1002802
17. Anstee JE, Feehan KT, Opzoomer JW, Dean I, Muller HP, Bahri M, et al. LYVE-1⁺ macrophages form a collaborative CCR5-dependent perivascular niche that influences chemotherapy responses in murine breast cancer. *Dev Cell* (2023) 58(17):1548–61. doi: 10.1016/j.devcel.2023.06.006
18. Lewis CE, Harney AS, Pollard JW. The multifaceted role of perivascular macrophages in tumors. *Cancer Cell* (2016) 30(1):18–25. doi: 10.1016/j.ccr.2016.07.009
19. Hughes R, Qian BZ, Rowan C, Muthana M, Keklikoglou I, Olson OC, et al. Perivascular M2 macrophages stimulate tumor relapse after chemotherapy. *Cancer Res* (2015) 75(17):3479–91. doi: 10.1158/0008-5472.CAN-14-3587
20. Karagiannis GS, Pastoriza JM, Wang Y, Harney AS, Entenberg D, Pignatelli J. Neoadjuvant chemotherapy induces breast cancer metastasis through a TME-mediated mechanism. *Sci Transl Med* (2017) 9(397):eaa0026. doi: 10.1126/scitranslmed.aan0026
21. Karagiannis GS, Bianchi A, Sanchez LR, Ambadipudi K, Cui MH, Anampa JM, et al. Assessment of MRI to estimate metastatic dissemination risk and prometastatic effects of chemotherapy. *NPJ Breast Cancer* (2022) 8(1):101. doi: 10.1038/s41523-022-00463-5
22. Ramos R, Missolo-Koussou Y, Gerber-Ferder Y, Bromley CP, Bugatti M, Núñez NG, et al. Tissue-resident FOLR2⁺ macrophages associate with CD8⁺ T cell infiltration in human breast cancer. *Cell* (2022) 185(7):1189–207. doi: 10.1016/j.cell.2022.02.021
23. Stoltzfus CR, Sivakumar R, Kunz L, Olin Pope BE, Menietti E, Speziale D, et al. Multi-parameter quantitative imaging of tumor microenvironments reveals perivascular immune niches associated with anti-tumor immunity. *Front Immunol* (2021) 12:726492. doi: 10.3389/fimmu.2021.726492
24. Mu L, Yang C, Gao Q, Long Y, Ge H, DeLeon G, et al. CD4⁺ and perivascular Foxp3⁺ T cells in glioma correlate with angiogenesis and tumor progression. *Front Immunol* (2017) 8:1451. doi: 10.3389/fimmu.2017.01451
25. Su S, Liao J, Liu J, Huang D, He C, Chen F, et al. Blocking the recruitment of naive CD4⁺ T cells reverses immunosuppression in breast cancer. *Cell Res* (2017) 27:461–82. doi: 10.1038/cr.2017.34
26. Schoenberg MB, Hao J, Bucher JN, Miksch RC, Anger HJW, Mayer B, et al. Perivascular tumor-infiltrating leukocyte scoring for prognosis of resected hepatocellular carcinoma patients. *Cancers (Basel)* (2018) 10(10):389. doi: 10.3390/cancers10100389
27. Erdag G, Schaefer JT, Smolkin ME, Deacon DH, Shea SM, Dengel LT, et al. Immunotype and immunohistologic characteristics of tumor-infiltrating immune cells are associated with clinical outcome in metastatic melanoma. *Cancer Res* (2012) 72:1070–80. doi: 10.1158/0008-5472.CAN-11-3218
28. Gerdes MJ, Sevinsky CJ, Sood A, Adak S, Bello MO, Bordwell A, et al. Highly multiplexed single-cell analysis of formalin-fixed, paraffin-embedded cancer tissue. *Proc Natl Acad Sci U.S.A.* (2013) 110(29):11982–7. doi: 10.1073/pnas.1300136110
29. Ruffell B, Au A, Rugo HS, Esserman LJ, Hwang ES, Coussens LM. Leukocyte composition of human breast cancer. *Proc Natl Acad Sci U.S.A.* (2012) 109:2796–801. doi: 10.1073/pnas.1104303108
30. Wang J, Browne L, Slapetova I, Shang F, Lee K, Lynch J, et al. Multiplexed immunofluorescence identifies high stromal CD68⁺PD-L1⁺ macrophages as a predictor of improved survival in triple-negative breast cancer. *Sci Rep* (2021) 11(1):21608. doi: 10.1038/s41598-021-01116-6
31. Byun KD, Hwang HJ, Park KJ, Kim MC, Cho SH, Ju MH, et al. T-cell immunoglobulin mucin 3 expression on tumor-infiltrating lymphocytes as a positive prognostic factor in triple-negative breast cancer. *J Breast Cancer* (2018) 21:406–14. doi: 10.4048/jbc.2018.21.e61
32. Dutta S, Ganguly A, Chatterjee K, Spada S, Mukherjee S. Targets of immune escape mechanisms in cancer: basis for development and evolution of cancer immune checkpoint inhibitors. *Biol (Basel)* (2023) 12(2):218. doi: 10.3390/biology12020218
33. Györfy B. Survival analysis across the entire transcriptome identifies biomarkers with the highest prognostic power in breast cancer. *Comput Struct Biotech J* (2021) 19:4101–9. doi: 10.1016/j.csbj.2021.07.014
34. Pai SI, Cesano A, Marincola FM. The paradox of cancer immune exclusion: immune oncology next frontier. *Cancer Treat Res* (2020) 180:173–95. doi: 10.1007/978-3-030-38862-1_6
35. Vonderheide RH, Bear AS. Tumor-derived myeloid cell chemoattractants and T cell exclusion in pancreatic cancer. *Front Immunol* (2020) 11:605619. doi: 10.3389/fimmu.2020.605619
36. Denkert C, von Minckwitz G, Darb-Esfahani S, Lederer B, Heppner BI, Weber KE, et al. Tumor-infiltrating lymphocytes and prognosis in different subtypes of breast cancer: a pooled analysis of 3771 patients treated with neoadjuvant therapy. *Lancet Oncol* (2018) 19(1):40–50. doi: 10.1016/S1473-2045(17)30904-X
37. Peranzoni E, Lemoine J, Vimeux L, Feuillet V, Barrin S, Kantari-Mimoun C, et al. Macrophages impede CD8 T cells from reaching tumor cells and limit the efficacy of anti-PD-1 treatment. *Proc Natl Acad Sci U.S.A.* (2018) 115(17):E4041–50. doi: 10.1073/pnas.1720948115
38. Ye JH, Wang XH, Shi JJ, Yin X, Chen C, Chen Y, et al. Tumor-associated macrophages are associated with response to neoadjuvant chemotherapy and poor outcomes in patients with triple-negative breast cancer. *J Cancer* (2021) 12:2886–92. doi: 10.7150/jca.47566
39. van den Ende NS, Nguyen AH, Jager A, Kok M, Debets R, van Beurzen CHM. Triple-negative breast cancer and predictive markers of response to neoadjuvant chemotherapy: A systematic review. *Int J Mol Sci* (2023) 24:2969. doi: 10.3390/ijms24032969
40. Reddy SM, Reuben A, Barua S, Jiang H, Zhang S, Wang L, et al. Poor response to neoadjuvant chemotherapy correlates with mast cell infiltration in inflammatory breast cancer. *Cancer Immunol Res* (2019) 7:1025–35. doi: 10.1158/2326-6066.CIR-18-0619
41. Zhang C, Xu L, Ma Y, Huang Y, Zhou L, Le H, et al. Increased TIM-3 expression in tumor-associated macrophages predicts a poorer prognosis in non-small cell lung cancer: a retrospective cohort study. *J Thorac Dis* (2023) 15(3):1433–44. doi: 10.21037/jtd-23-227
42. Komohara Y, Morita T, Annan DA, Horlad H, Ohnishi K, Yamada S, et al. The coordinated actions of TIM-3 on cancer and myeloid cells in the regulation of tumorigenicity and clinical prognosis in clear cell renal carcinomas. *Cancer Immunol Res* (2015) 3(9):999–1007. doi: 10.1158/2326-6066.CIR-14-0156
43. Yan W, Liu X, Ma H, Zhang H, Song X, Gao L, et al. Tim-3 fosters HCC development by enhancing TGF- β -mediated alternative activation of macrophages. *Gut* (2015) 64(10):1593–604. doi: 10.1136/gutjnl-2014-307671
44. Trebaska-McGowan K, Chaib M, Alvarez MA, Kansal R, Pingili AK, Shibata D, et al. TGF- β alters the proportion of infiltrating immune cells in a pancreatic ductal adenocarcinoma. *J Gastrointest Surg* (2022) 26(1):113–21. doi: 10.1007/s11605-021-05087-x
45. Bholra NE, Balko JM, Dugger TC, Kuba MG, Sánchez V, Sanders M, et al. TGF- β inhibition enhances chemotherapy action against triple-negative breast cancer. *J Clin Invest* (2013) 123(3):1348–58. doi: 10.1172/JCI65416
46. Arwert EN, Harney AS, Entenberg D, Wang Y, Sahai E, Pollard JW. A Unidirectional transition from migratory to perivascular macrophage is required for tumor cell intravasation. *Cell Rep* (2018) 23(5):1239–48. doi: 10.1016/j.celrep.2018.04.007
47. Sharma A, Seow JJW, Dutertre CA, Pai R, Blériot C, Mishra A, et al. Oncofetal reprogramming of endothelial cells drives immunosuppressive macrophages in hepatocellular carcinoma. *Cell* (2020) 183(2):377–94. doi: 10.1016/j.cell.2020.08.040
48. Li C, Jiang P, Wei S, Xu X, Wang J. Regulatory T cells in tumor microenvironment: new mechanisms, potential therapeutic strategies and future prospects. *Mol Cancer* (2020) 19(1):116. doi: 10.1186/s12943-020-01234-1
49. Wu CY, Kirman JR, Rotte MJ, Davey DF, Perfetto SP, Rhee EG, et al. Distinct lineages of T(H)1 cells have differential capacities for memory cell generation. *in vivo Nat Immunol* (2002) 3(9):852–8. doi: 10.1038/cr.2017.34
50. Chung B, De M, De A, Bankey PE. Interferon-gamma induces PD-L1 expression in macrophages and neutrophils. *J Am Coll Surg* (2011) 213:S63. doi: 10.1016/j.jamcollsurg.2011.06.141

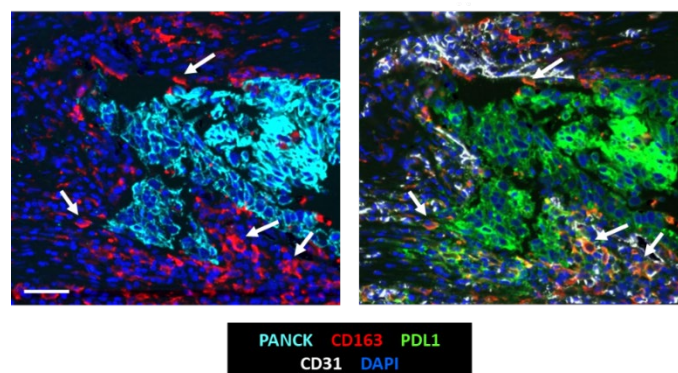
Supplementary figures and tables

The figures and tables here are the supplementary materials from the manuscript, 'Changes in the immune landscape of TNBC after neoadjuvant chemotherapy: correlation with relapse.



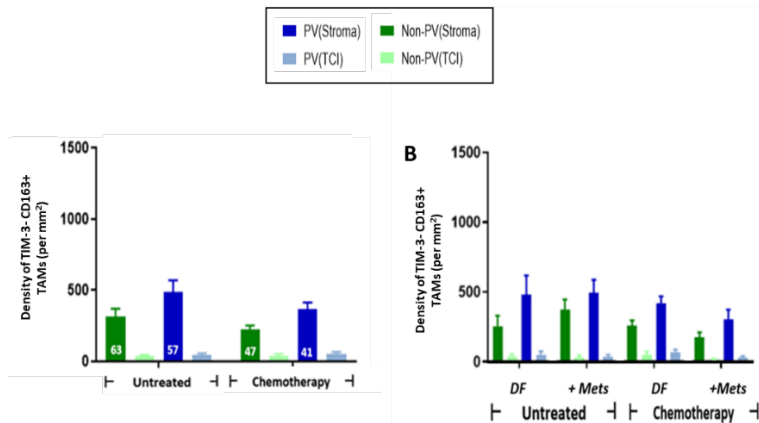
Suppl. Figure 1 Reduced density of stromal CD163+ TAMs correlate inversely with metastasis.

Distribution of CD163+ TAMs (A), CD3+CD8+ T cells (B), CD3+CD4+FOXP3- T cells (C) and CD3+CD4+FOXP3+ Tregs (D) in PV and non-PV areas of the stroma and TCIs in untreated and NAC-treated groups (subdivided into those that did or did not develop metastases within 3 years of primary surgery. 'DF' = DF; ie. no metastases; '+Mets' = developed metastases). * $P < 0.05$.



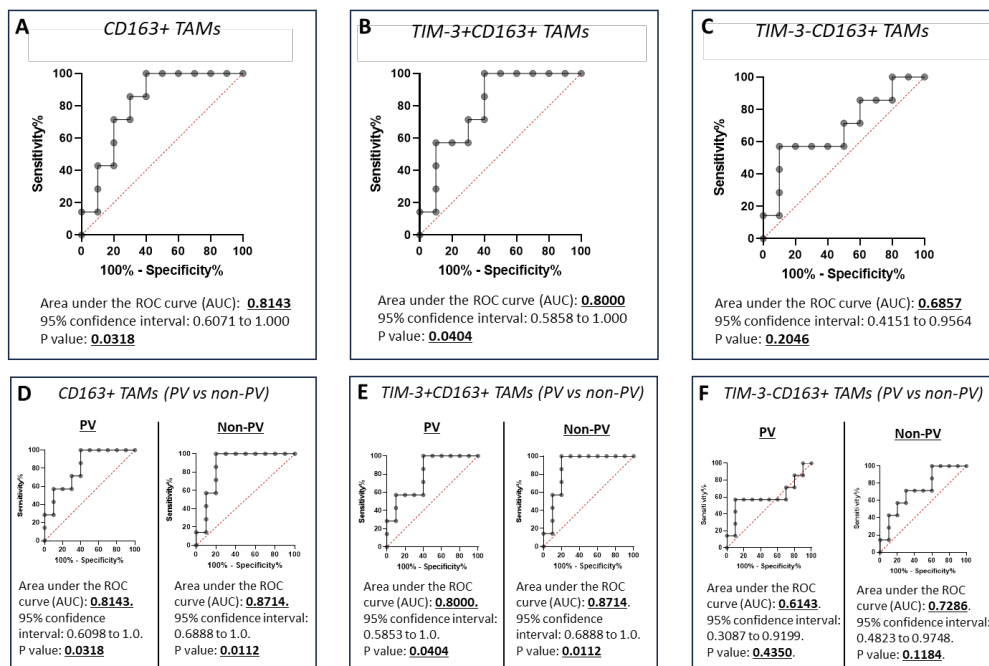
Suppl. Figure 2 Representative appearance of PD-L1 expression by CD163+ TAMs and PanCK+ cancer cells in high/moderate PD-L1-expressing TNBCs.

PD-L1+CD163+ TAMs were most frequent at the interface between TCIs and the stroma.
Bar = 50 μ m.



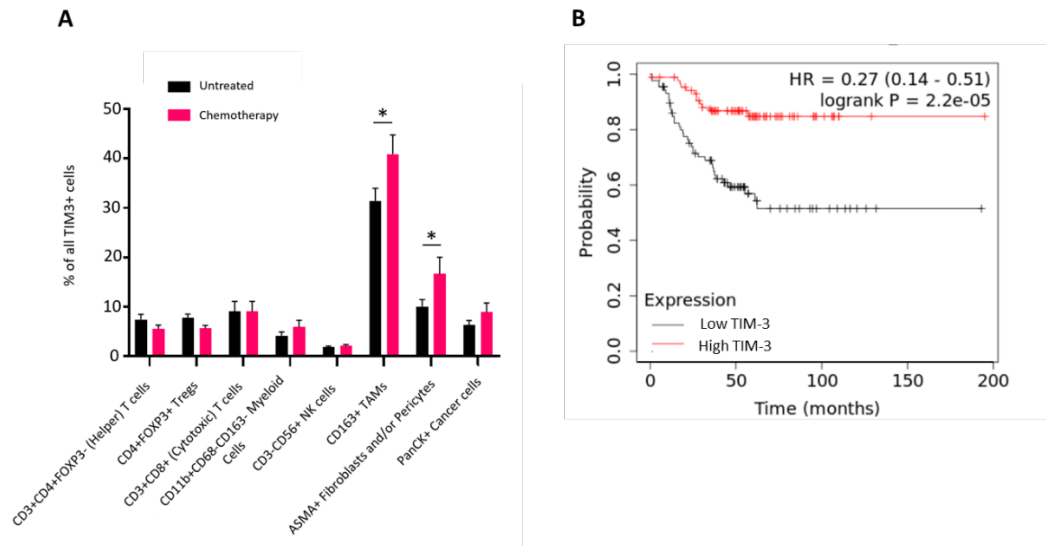
Suppl. Figure 3 Frequency and distribution of TIM-3-CD163+ TAMs. (A) TIM-3-CD163+ TAMs were present throughout the stroma in untreated and NAC-treated tumors.

The white figures at the base of each bar are the % of CD163+ TAMs in each group that were TIM-3-. (B) The density of this TAM subset did not correlate with metastasis. [NB. in all groups, stromal PV and non-PV groups were significantly higher than corresponding groups in TCIs, asterices not shown for clarity]. $P < 0.05$



Suppl. Figure 4 Receiver Operating Characteristic (ROC) curve analysis of the ability of three stromal TAM subsets to predict the development of metastasis in NAC-treated patients within 3 years of surgical removal of primary tumors (ROC analysis of data at the level of whole tumor sections).

(A) all CD163+ TAMs; (B) all TIM-3+CD163+ TAMs; (C) all TIM-3-CD163+ TAMs; (D) PV v non-PV CD163+ TAMs; (E) PV v non-PV TIM-3+CD163+ TAMs; (F) TIM-3-CD163+ TAMs.

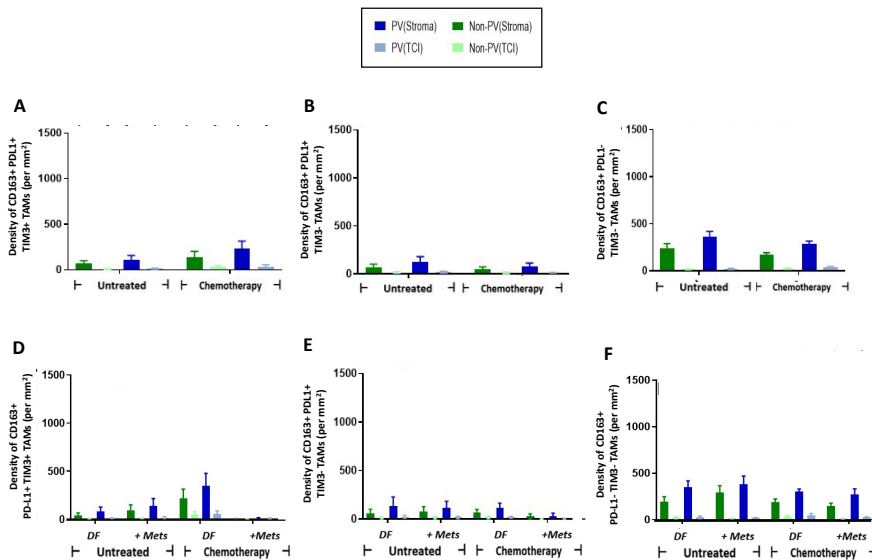


Suppl. Figure 5 Expression of TIM-3 in human TNBC: correlation with RFS after NAC.

(A) CD163+ TAMs and alpha smooth muscle actin-positive cells ('ASMA'; pericytes and fibroblasts) are the predominant cell types expressing TIM-3 - and the proportion of these cells expressing this cell surface protein increases after NAC. ASMA = alpha smooth muscle actin.

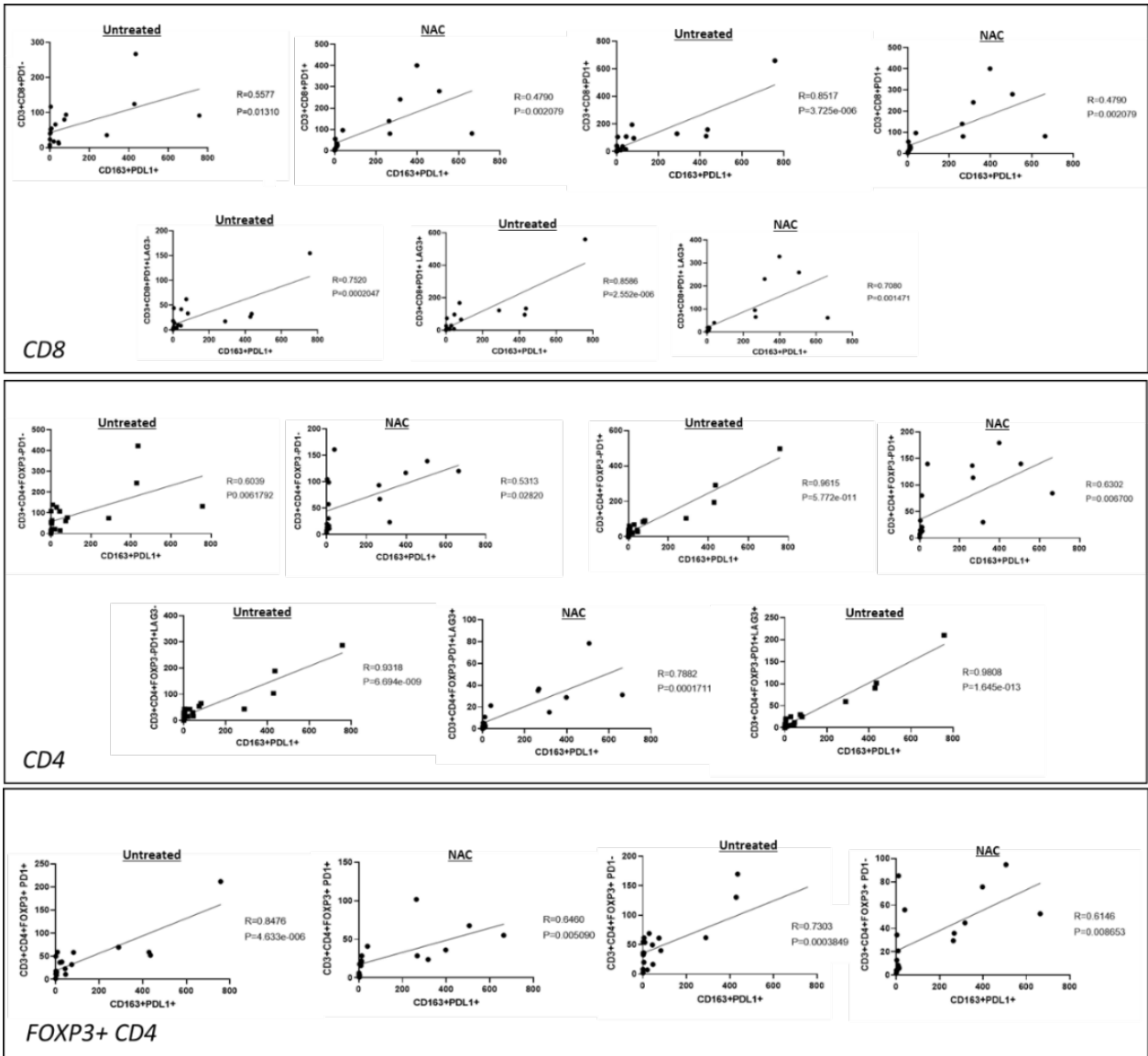
* $P < 0.05$. (B) Significant correlation between TIM-3 expression levels in 153 TNBCs (taken from women administered NAC) and DFS (using online dataset

[:http://kmplot.com/analysis/index.php?p=service&cancer=breast#](http://kmplot.com/analysis/index.php?p=service&cancer=breast#)) [217]



Suppl. Figure 6 No effect of NAC on various CD163+ TAM subsets.

Three CD163+ TAM subsets (A, D) PD-L1+TIM-3+; (B, E) PD-L1+TIM-3-; (C, F). PD-L1-TIM-3) were evenly distributed throughout the stroma of tumors at significantly higher density than in corresponding areas of TCIs (asterices not shown). There was no effect of NAC on the density or distribution of these cells, nor did they correlate with metastasis. (ns = not statistically significant).



Suppl. Figure 7 Correlation graphs for significantly different comparisons seen in Suppl. Table 2.

R = correlation coefficient.

| | Untreated - DF | Untreated + Mets | NAC - DF | NAC+ Mets |
|---|----------------|------------------|----------|-----------|
| Age at diagnosis | | | | |
| 21-39 | 2 (22.2) | 2 (20) | 1 (10) | 2 (28.6) |
| 40-59 | 2 (22.2) | 2 (20) | 7 (70) | 3 (42.8) |
| 60-79 | 3 (33.3) | 6 (60) | 2 (20) | 2 (28.6) |
| 80-99 | 2 (22.2) | 0 (0) | 0 (0) | 0 (0) |
| Tumour size | | | | |
| T1 | 4 (44.4) | 2 (20) | 2 (20) | 2 (28.6) |
| T2 | 5 (55.5) | 7 (70) | 7 (70) | 5 (71.5) |
| T3 | 0 (0) | 1 (10) | 1 (10) | 1 (14.3) |
| Tumour grade | | | | |
| 2 | 1 (11.1) | 2 (20) | 0 (0) | 0 (0) |
| 3 | 8 (88.8) | 8(80) | 10(100) | 7 (100) |
| Time between end of treatment and surgery (days) | | | | |
| <30 | n/a | n/a | 3 (30) | 2 (28.6) |
| 30-40 | n/a | n/a | 4 (40) | 3 (42.8) |
| >40 | n/a | n/a | 3 (30) | 2 (28.6) |
| Lymph node status | | | | |
| Involved | 3 (33.3) | 7 (70) | 4 (40) | 7 (100) |
| Not involved | 5 (55.5) | 2 (20) | 5 (50) | 0 (0) |
| Not sampled | 1 (11.1) | 1 (10) | 1 (10) | 0 (0) |
| Neoadjuvant therapy received | | | | |
| FEC-T | 0 (0) | 0 (0) | 7 (70) | 3 (42.8) |
| FEC | 0 (0) | 0 (0) | 2 (20) | 1 (14.3) |
| Other | 0 (0) | 0 (0) | 1 (10) | 3 (42.8) |
| None | 9(100) | 10 (100) | 0 (0) | 0 (0) |
| Metastases within 3-year follow-up? | | | | |
| Yes | 0 (0) | 10 (100) | 0 (0) | 7 (100) |
| No | 9(100) | 0 (0) | 10(100) | 0 (0) |
| Adjuvant therapy received | | | | |
| Radiotherapy only | 1 (11.1) | 0 (0) | 5 (50) | 6 (85.6) |
| Radiotherapy & Chemotherapy | 6 (66.6) | 6 (60) | 5 (50) | 1 (14.3) |
| Chemotherapy only | 1 (11.1) | 2 (20) | 0 (0) | 0 (0) |
| None | 1 (11.1) | 1 (10) | 0 (0) | 0 (0) |
| No data | 0 (0) | 1 (10) | 0 (0) | 0 (0) |
| Adjuvant chemotherapy received | | | | |
| Carboplatin | 0 (0) | 0 (0) | 2 (20) | 1 (14.3) |
| Carboplatin & Gemcitabine | 0 (0) | 0 (0) | 2 (20) | 2 (28.6) |
| Docetaxel | 0 (0) | 0 (0) | 0 (0) | 1 (14.3) |
| FEC-T | 5 (55.5) | 4 (40) | 0 (0) | 0 (0) |
| Other | 2 (22.2) | 4 (40) | 1 (10) | 2 (28.6) |
| None | 2 (22.2) | 1 (10) | 5 (50) | 1 (14.3) |
| No data | 0 (0) | 1 (10) | 0 (0) | 0 (0) |

Suppl. Table 1 Clinical parameters for the four patient groups analysed in this study. Parentheses indicate percentage data. NAC = neoadjuvant chemotherapy (3-8 cycles). DF = DF (no metastasis within 3 years of primary surgery), '+Mets' = developed metastases within 3 years. FEC = 5 fluorouracil, epirubicin, cyclophosphamide. FEC-T - 5 = fluorouracil, epirubicin, cyclophosphamide, docetaxel. 'Other' NACs included FEC-T & Carboplatin, EC (epirubicin cyclophosphamide) and ECD (epirubicin cyclophosphamide & docetaxel).

| Correlation | Untreated | | Chemotherapy | |
|---|------------------|----------------|---------------------|----------------|
| | <i>R</i> | <i>p value</i> | <i>R</i> | <i>P value</i> |
| <u>Cytotoxic (CD8+) T Cells</u> | | | | |
| CD163+PDL1- TAMs v CD3+CD8+PD1- | 0.27 | NS | 0.20 | NS |
| CD163+PDL1- TAMs v CD3+CD8+PD1+ | -0.15 | NS | -0.002 | NS |
| CD163+PDL1+ TAMs v CD3+CD8+PD1- | 0.56 | 0.01 | 0.4 | NS |
| CD163+PDL1+ TAMs v CD3+CD8+PD1+ | 0.84 | <0.0001 | 0.48 | 0.002 |
|LAG3- (active) | 0.75 | <0.0001 | 0.52 | 0.03 |
|LAG3+ (exhausted) | 0.86 | <0.0001 | 0.70 | 0.001 |
| <u>Helper (CD4+FOXP3-) T Cells</u> | | | | |
| CD163+PDL1- TAMs v CD3+CD4+FOXP3-PD1- | 0.15 | NS | 0.22 | NS |
| CD163+PDL1- TAMs v CD3+CD4+FOXP3-PD1+ | -0.15 | NS | 0.23 | NS |
| CD163+PDL1+ TAMs v CD3+CD4+FOXP3-PD1- | 0.60 | 0.006 | 0.53 | 0.03 |
| CD163+PDL1+TAMs v CD3+CD4+FOXP3-PD1+ | 0.96 | <0.0001 | 0.63 | 0.007 |
| ...LAG3- (active) | 0.93 | <0.0001 | 0.46 | NS |
|LAG3+ (exhausted) | 0.98 | <0.0001 | 0.79 | <0.0001 |
| <u>Regulatory (CD4+FOXP3+) T cells</u> | | | | |
| CD163+PDL1- TAMs v CD3+CD4+FOXP3+PD1- | 0.24 | NS | 0.06 | NS |
| CD163+PDL1- TAMs v CD3+CD4+FOXP3+PD1+ | -0.25 | NS | 0.42 | NS |
| CD163+PDL1+ TAMs v CD3+CD4+FOXP3+PD1- | 0.73 | 0.0004 | 0.61 | 0.009 |
| CD163+PDL1+ TAMs v CD3+CD4+FOXP3+PD1+ | 0.85 | <0.0001 | 0.65 | 0.005 |

Suppl. Table 2. Correlation of the overall density of PD-L1+ CD163+TAMs with CD4+ T cells, CD8+ T cells and Tregs.

4.2.6. NK cell infiltration is not altered by NAC and does not correlate with metastasis.

The distribution of CD56+ NK cells in TNBCs (untreated v NAC-treated) was not included in the above paper, so is described below. Overall, there was a significantly higher density of NK cells within the stroma than the TCI regions (**Figure 4-5 A**), but no significant differences were seen between TCIs and the stromal regions of TNBCs in the 4 groups (**Figure 4-5 B-C**). There was, however, a non-significant trend towards a higher stromal NK cell density in the disease-free groups (untreated and NAC-treated) (**Figure 4-5 C**). but no significant differences were seen between the untreated and NAC treated groups. Furthermore, significant differences were seen when looking at the PV and non-PV regions. (**Figure 4-5 D**).

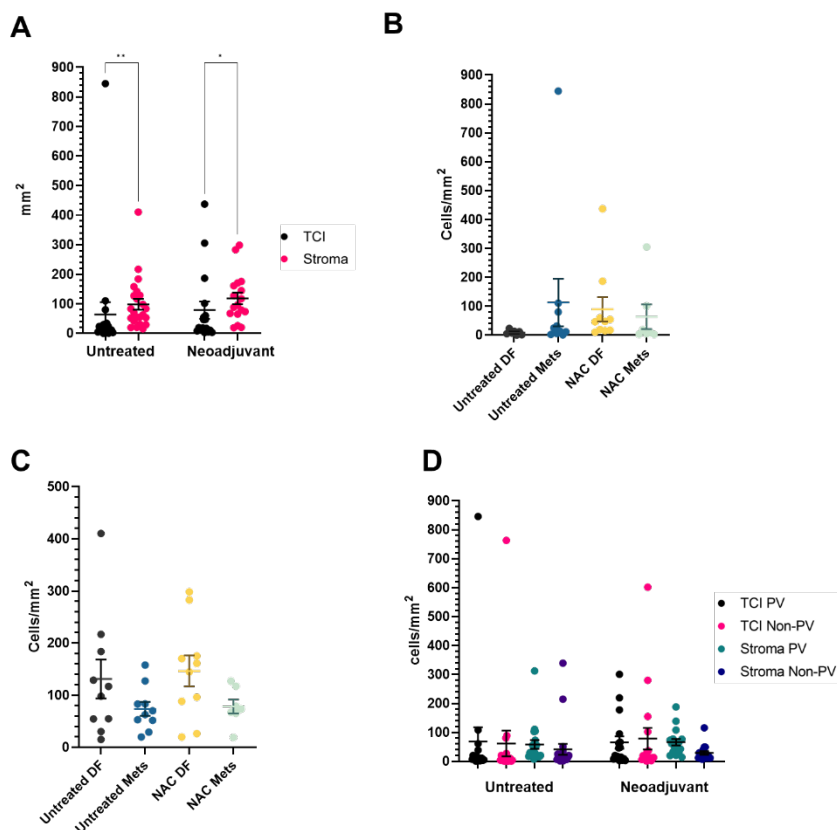


Figure 4-5 NK cells density within the TME

The density of NK cells: A, within the TCI and stromal regions in the Untreated vs NAC treated tumours. B. TCI and C. Stromal regions for each of the treatment and 4 disease outcome subgroups. D. The density within the PV vs non-PV areas Error bars \pm SEM. * $P > 0.05$. ** $P < 0.01$.

4.2.7. CXCR4 expression by cancer cells does not correlate with metastasis in untreated or NAC-treated TNBC

High expression of CXCR4 has been shown previously to correlate with metastasis in breast cancer [215], but there is inconclusive evidence when it comes to CXCR4 expression in human TNBC [218]. So, the overall density and expression of CXCR4 across all cell types in the tumour groups was examined within our cohort of 37 TNBCs - to see if high levels of CXCR4 linked to relapse (**Figure 4-6 A-B**). No significant difference was seen between the disease-free groups and the metastatic groups (untreated or NAC-treated), with both groups showing similar levels of CXCR4 within the TCIs and stroma.

Tumours are sometimes described in publications as being 'negative' or 'positive' for CXCR4 if the cancer cells overexpress CXCR4 compared to normal breast tissue [219]. However, there is no standard definition of CXCR4 positivity, so a >5% cut-off level of CXCR staining in tumours was set to define CXCR4 positive tumours (**Figure 4-6 A&B**). However, no significant difference was seen between the disease-free groups and the metastatic groups when this cut off was applied (**Figure 4-6 AC**).

As most of the CXCR4 staining was seen within TCIs, expression by PanCK+ cancer cells alone were investigated (**Figure 4-6 D**). Again, there were no significant differences seen in the expression between the tumours that remained disease free or developed metastasis within 3 years.

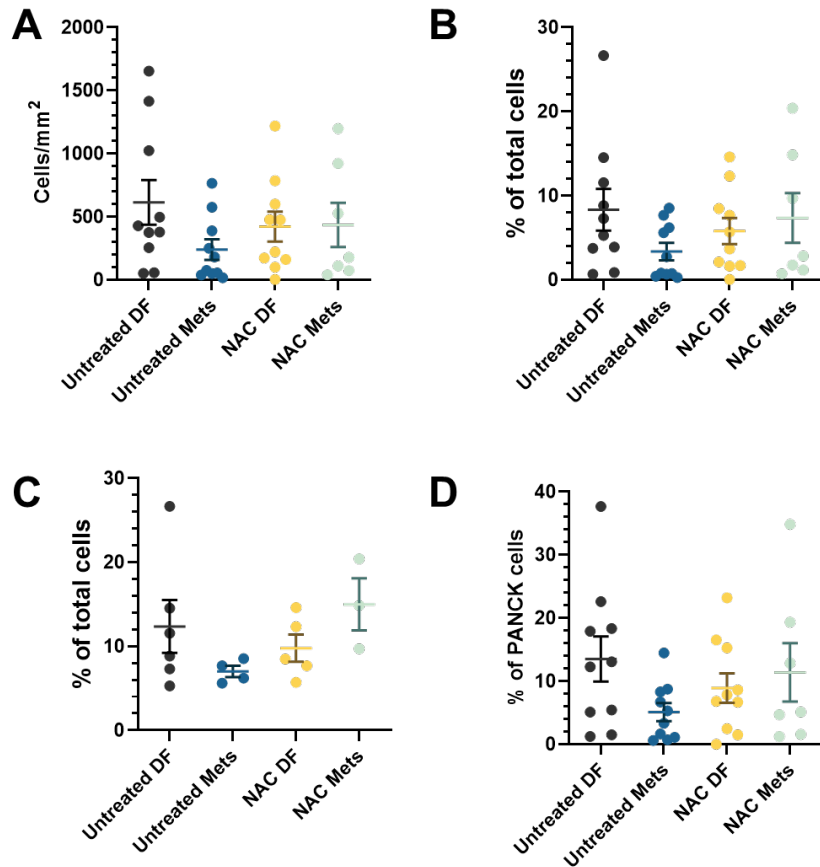


Figure 4-6 Overall CXCR4 density within TNBC

A. The density of overall CXCR4 between the 4 groups and B. the % of total cells in each subgroup that express CXCR4. C. CXCR4 positive tumours (>5% of total cells CXCR4 expression) in each group. D. The percentage of PanCK+ tumour cells that express CXCR4 in each treatment/outcome group. Error bars \pm SEM.

4.2.8. CXCR4 expression does not increase after NAC.

Across the tumours there was no difference in the overall density of CXCR4 between untreated vs NAC tumours (**Figure 4-7 A**). We then investigated on whether there were any differences in TCI v stromal regions (**Figure 4-7 B-C**). No differences were seen between the untreated vs NAC tumours. But the density of CXCR4 was seen to be significantly higher in the TCI compared to the stroma in both untreated and NAC treated tumours.

When looking at the source of CXCR4 across the whole tumours, PanCK+ tumours cells were seen to be the main source, expressing on average over 77% of the total CXCR4, with only a fraction of the overall total of CXCR4 expression from the leukocytes (Figure 4-7 D).

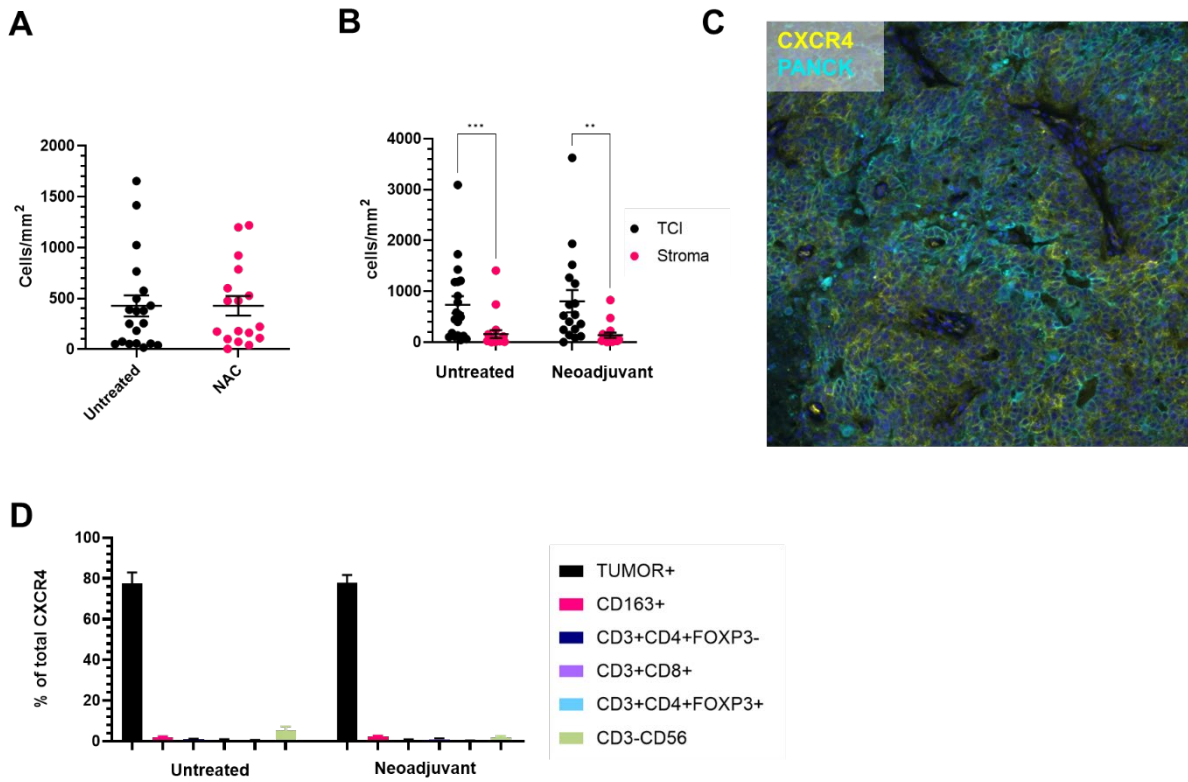


Figure 4-7 Differences in CXCR4 in Untreated vs NAC treated tumour

A. The density of overall CXCR4 and B. the Density of overall CXCR4 across the TME in untreated vs NAC treated tumours. C. A representative image of CXCR4 staining in the TCI. D. Comparison of the source of CXCR4 between cells types across the whole tumour in untreated vs NAC treated tumours. Error bars \pm SEM. ** $P < 0.01$ *** $P < 0.001$.

4.2.9. TAM expression of CXCR4

In LLC1 tumours in mice, CXCR4 is seen to be expressed on TAMs (98% of all CXCR4 expressing cells in NAC treated tumours) and that these TAMs accumulated around the vasculature and drive relapse after NAC [113], with limited data available on the TAM expression in TNBC.

Overall mean levels of TAM derived CXCR4 across TNBC tumours was only 2.3% and 2% of total CXCR4 expression in untreated and NAC treated groups respectively (**Figure 4-8 A**). In the stromal compartment, TAMs were the main immune cell source of CXCR4, but no difference was seen in the expression levels between untreated and NAC treated tumours (**Figure 4-8 B**). Overall density of CD163+ CXCR4+ cells showed no differences amongst the treatment outcome groups, or when broken down into the TCI/stroma PV/Non-PV regions (**Figure 4-8 B-C**). This indicates that within TNBC, the numbers of CD163+ CXCR4+ TAMs are not directly linked to disease outcome.

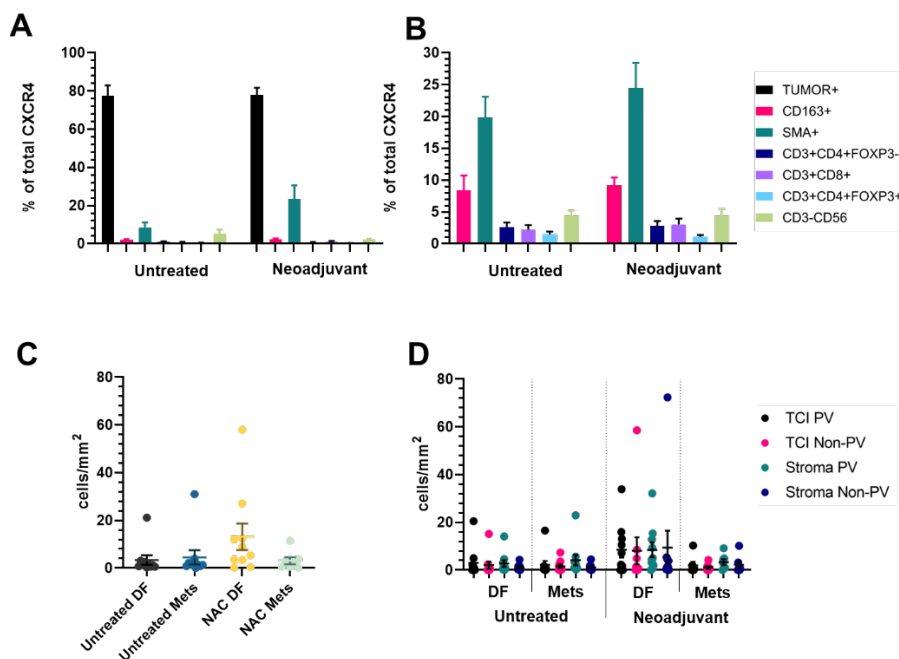


Figure 4-8 Stromal/TAM expression of CXCR4

The cellular sources of total CXCR4 expression found within the A. Tci B. stroma regions in the untreated and NAC treated TNBC tumours. C. The overall density of CD163+ CXCR4+ cells amongst the disease outcome groups. D. The density of CD163+ CXCR4+ cells in the TCI/stroma PV/Non-PV regions across the disease out come groups. Error bars \pm SEM.

4.3. Discussion

In this chapter, we first investigated the effects of NAC on the immune landscape of TNBC (i.e. TAMs, T cells, Tregs and NK cells). This uncovered significant alterations in the distribution of CD163+ TAMs and various T-cell subsets (**Figure 4-10**). These findings may shed some light into the roles these immune cells play within the TME post-NAC. One interesting early finding is that all the immune cell types studied preferentially located to either the stroma generally or PV areas within the stroma, a potential result of immune exclusion from the TCI. This observation that immune cells, are often found in the surrounding stroma but not within the TCI themselves present a challenge for immunotherapy. This phenomenon is attributed to a combination of physical barriers such as features of the extra cellular matrix and cytokines and chemokines production by the TCI and stroma that deter or retain immune cell infiltration. Addressing immune exclusion is vital for improving the efficacy immunotherapies [220].

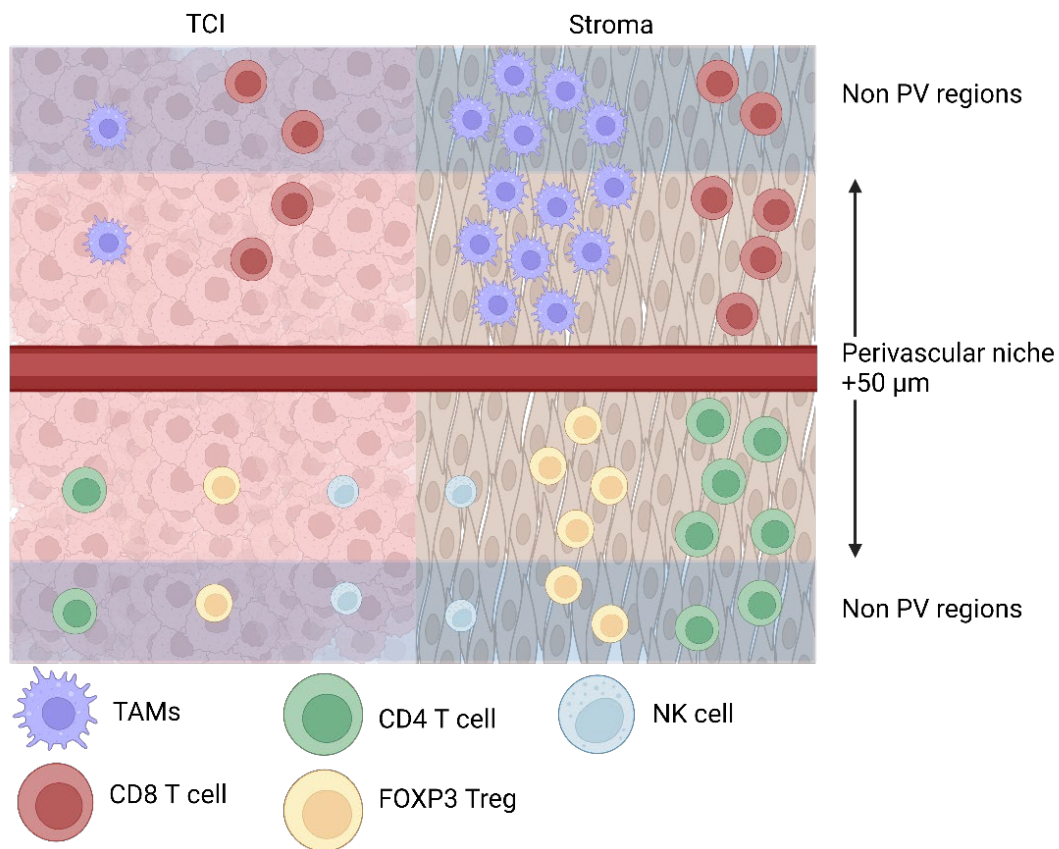


Figure 4-9 Location of immune cell subsets within the TME in TNBC.

Overview of the location of immune cells found within TNBC TME showing TCI and stroma regions as well as the perivascular niche (non-shaded)(within 50 μ m of blood vessels) and the non PV regions (shaded) (beyond 50 μ m of blood vessels).

Of note, is the observation of high CD163+ TAM levels in patients who remained disease-free post-NAC. This presents a challenge the traditional view of TAMs as they are often associated with an anti-inflammatory and immunosuppressive response, aiding tumour progression and relapse [221, 222] .

Also contrary to our initial hypothesis, TAMs in close proximity to the vasculature did not exhibit the anticipated increase following NAC, or correlate with relapse after NAC, in the same way that has been seen in other studies looking at PV TAMs in breast cancer [62, 104]. This lack of correlation with outcome after NAC suggests that PV TAMs might not be the primary drivers of metastasis in TNBC during NAC.

Most of the CD163 TAMs in the TME were also seen to lack expression of PD-L1. The apparent disconnect between PD-L1 expression on TAMs and metastatic outcomes raises questions about the predictive value of PD-L1 as a biomarker for therapy response or disease progression. In contrast to our findings, a recently published paper has linked PD-L1+ TAMs with a better clinical outcome within breast cancer by showing them to be immunostimulatory. scRNA sequencing of PD-L1+/- TAMs uncovered expression profiles that suggested PD-L1+ TAMs are more activated and immunostimulatory with higher levels of CD83, CD74, HLA-DRA/B, and HLA-DQA/B, with pro-inflammatory cytokines/chemokines IL1B, CXCL2/3/8, and CCL3/4/18. While PD-L1- TAMs were immunosuppressive and pro-tumour with expression of anti-inflammatory genes CD9, CD52, IL1RN, osteopontin, MMP9, and SPARC. These findings were shared across both luminal and TNBC tumour types [223].

One population of cells that did see significant differences in the untreated and NAC treated groups was TIM-3+ TAMs. Which was significantly higher within the stromal areas of patients who remained disease free after NAC and seen in both the PV and non-PV areas. Approximately 75-80% of these TAMs also remained PD-L1-. Traditionally, TAMs, and specifically the M2-like CD163+ subset, have been associated with immunosuppressive activities that promote tumour growth and

metastasis in various cancers, including breast cancer. Studies have frequently reported a correlation between high densities of CD163+ TAMs and poor prognosis in BC, suggesting these cells facilitate a tumorigenic environment [82, 99]. Future studies are warranted to unravel the mechanisms behind these observations and to assess the potential of targeting CD163+ TIM-3+ in TNBC.

The data on NK cells was limited as it lacked additional markers that could identify activated subsets such as CD69 [224]. A recently published study has demonstrated how NK cells can lose their cytotoxicity towards cancer cells within 24h of entering solid tumours, something that could impact upon the efficacy of CAR NK therapy [225]. Data shown in this chapter suggests that this could be, in part, because NK cells locate to the stroma when they infiltrate TNBCs and so fail to come into contact with cancer cells in the TCIs. This could be due to inhibitory crosstalk between NK cells and immune cells in the TME which has been demonstrated with TAMs expression of TGF- β , IL-10 and IL-1 β [226] and Treg expression of TGF- β and IL-2 [227], which were seen at higher levels within the stromal regions.

Finally, a number of reports have established a link between tumour CXCR4 and metastasis in various tumour types [228], But the lack of correlation between CXCR4 expression and metastasis in the small cohort of TNBCs studied in this chapter was unexpected. While neither cancer cell nor TAM expression of CXCR4 correlated with metastasis in untreated or NAC-treated tumours, the data may not be conclusive for various reasons. The in-house pathologist at Neogenomics Labs selected ROIs for analysis that were only in viable areas of tumour, rather than randomly selected areas across the whole tumour section. Hypoxia has been shown to induce CXCR4 in various cell types [229], so a different picture may have emerged had hypoxic/necrotic tumour areas been included in the ROI selection.

Previous studies have not shown conclusive data on the role of CXCR4 in TNBC. Within TNBC, a study using transcriptomic analysis looked at 115 post-NAC samples with residual disease, 38 of which had developed metastasis. They developed a transcriptomic 8 gene signature that was linked to immune cell infiltration and included CXCR4, CXCR6 and CCL4. High expression of the genes in this signature was able to predict RFS, with a high number of tumour infiltrating leukocytes (TILs), indicating the role of the chemokine in recruiting the immune infiltrate [230]. Another study using 163 TNBC tumours compared the gene

expression profiles of these from 4 public databases and compared these to 60 healthy breast samples. CXCR4 and CXCL10 were found to be overexpressed in TNBC tumours and linked RFS [231]. Neither of these studies were able to link CXCR4 expression on its own to metastasis.

Blocking of the CXCR4/CXCL12 axis to reduce metastasis has been demonstrated in several TNBC *in vivo* studies though using MDA-MD-231 [232, 233] and 4T1 [215] models. Interestingly though, another study found that CXCR4 inhibitors AMD3100 and TN14003 impaired tumour growth in HER2 patient derived xenograft models (PDX) models. But it did not reduce tumour growth in TNBC PDX models and even increased metastatic spread in a quarter of cases [218]. The relevance of this study is debatable, as although the PDX models captured the TC/stroma compartments seen within human tumours, they were developed in immunodeficient Swiss nude mice that lack mature T cells, thus the role of adapted immune cells in response to these therapies is absent.

However, there are still a limited number of studies that link protein expression of CXCR4 to the clinical outcomes. One study that looked 151 TNBC tumour cores taken at the time of surgery and analysed CXCR4 levels by western blot. Positive samples were defined as >6-fold elevation compared to CXCR4-negative CRL6509 control cells. 30 tumours were defined as high CXCR4, but these has a worse 5-year DFS when compared to low CXCR4 tumours (46% vs 61%) [234].

Using immunostaining of CXCR4 in TNBC, one study looked at 37 TNBC tumours and correlated positive CXCR4 tumours with histological grade and were negative for lymph node metastasis. However the effects of NAC or the source of CXCR4 were not investigated [235]. Another study using tissue microarrays (TMAs) looked at 184 TNBC tumours, 97 of which scored positive for CXCR4 (4-point scale used. Negative - no staining, weak - 1+ intensity, intermediate - 2+ intensity and strong immunoreactivity - 3+ intensity). However, no link was made to any clinical outcomes [233].

None of these studies distinguish between the different cellular sources of CXCR4 in TNBC or changes in CXCR4 expression after NAC. Other than tumour cells, TAMs are seen to be the main source of CXCR4, where they increased after NAC and played a critical role in promoting relapse *in vitro* using a model where tumour cells do not express CXCR4 [113].

Arguably, the quantification of CXCR4 on its own may not be enough and pairing quantification data with its ligand, CXCL12 would provide a better overview of the role of the CXCR4-CXCL12 axis. It is CXCL12 driven chemotaxis that attracts CXCR4 cells, so a lack of or low signalling from CXCL12 within areas of the TME may result in an absence of correlation with metastasis- regardless of CXCR4 levels in TNBC. Recently published results that utilise the novel multichannel immunofluorescence methods to quantify chemotactic gradients have shown that high CXCL12 gradients around the vasculature caused by CXCL12+ TAMs in pre-clinical models of breast cancer [236].

The selection of ROIs for the study may have had a wider impact on the observed findings of the other cell types. As our initial goal was to study the role of macrophages with the perivascular environment, we chose to select areas that contained viable tumour areas that also contained stromal region. This was so comparisons could be made in the tumour vs stroma regions and in the perivascular regions within these. This allowed for a comparison of the untreated vs the NAC treated tumours but did not consider factors present across the whole tissue section such as a reduced TCI, vascular changes or increased hypoxic and necrotic regions that are seen as a result of NAC treatment.

One notable limitation of the multiple IF study reported in this chapter was the omission of other immune cell types that also play a significant role in anti-tumour immunity like dendritic cells [237], B cells [238], and neutrophils [239]. At the time the multiplex IF staining was carried out by Neogenomics Labs, validated antibodies to identify these cell types were not available on their MultiOmyx platform. Had they been, it would have been good to use their AI-based imaging system to generate a picture of the complex interplay between multiple immune cell types in the stroma, especially the stromal PV niche, and how this was affected by NAC and could drive metastasis.

The methodology for analysing cell frequency and distribution in this chapter is also not without its limitations. The use of multiplex IF staining and AI-based image analysis allows for much greater scalability and reproducibility compared to the manual counting methods in Chapter 3. Moreover within the subsets analysed here, AI segmentation provided individual data on 2.5 million cells in total across the 37 tumours, compared to manual counts of <500 perivascular TAMs in counted in

Chapter 3. However, there are several limitations in the application of AI for segmentation. One significant issue is that the variability of cell staining patterns and morphologies across sections, the presence of IF staining artefacts and background, and/or clustering of cells can reduce segmentation accuracy. Overcoming these limitations requires continued algorithm development at Neogenomics Labs, mainly using increasing numbers of relevant training datasets to ensure that AI segmentation is being used in an accurate and reproducible manner.

An additional methodological consideration is the use of unpaired samples for comparing untreated and NAC treated TNBCs. This approach implies that any observed differences in the immune landscape between untreated and NAC-treated samples are due to the NAC alone. When, in fact, in such small group sizes, differences may be due, in part, to inter-tumoral variability. The use of paired pre- and post-treatment samples (i.e. from the same patients) would have been preferable. However, these were not available at the time of this study.

Interestingly, TILs and their expression of PD-1, TIM-3 and LAG-3 were looked at in another study using 66 paired pre- and -post NAC treated TNBC tumours to see how expression levels linked to disease progression. The study used pre-NAC treatment biopsies and matched with the post NAC samples from the patients. TILs were quantified using H&E staining with PD-L1, TIM-3 and LAG-3 quantified using IHC. Although this study used different methods to stain and quantify its markers, its use of paired tumour samples is of particular interest as it provides a directly comparable baseline pre-NAC.

A recent study [240] used IHC to examine TILs and their expression of PD-1, TIM-3 and LAG-3 in 66 paired pre- and -post NAC treated (i.e. matched) TNBCs. Although this study used different methods to stain and quantify these markers, it's use of paired tumour samples is of particular interest as it provides assessment of the direct effects of NAC on individual tumours. Interestingly, they reported that the number of TIM-3 positive TNBCs (defined as $\geq 1\%$ of stromal cells stained for TIM-3) was found to increase following NAC. This confirmed similar results to what we observed, with significantly higher TIM-3 levels seen in CD163+ TAMs and α SMA+ cells, in NAC-treated tumours compared to untreated (**Suppl. Figure 5**). They also saw more TIM-3 positive tumours after NAC in the non-pCR group compared to the pCR group. The number of LAG-3 positive tumours (defined as >0 staining), saw no

significant change after NAC. TIL response to NAC overall showed no change, but when this was broken down into response groups, they were found to have decreased in the pCR group and increased in the non-pCR group when compared to baseline levels found in the pre-NAC biopsies. An interesting finding from this study, was that the only significant prognostic marker that was seen in the pre-NAC tumours, was TIL counts of >10% relating to a better 3-year OS compared to counts <10%. Indicating that for PD-L1, TIM-3 and LAG-3 expression, it is the changes in expression that are induced by NAC that correlate with pCR and OS [240].

There are also several limitations to the data within this chapter. One of the main constraints of the work carried out was being able to access the necessary patient sample numbers with the relevant associated data. Although we used the largest breast cancer tissue bank in the UK which has been collecting samples since 2010, there were still issues such as incomplete/missing paired clinical data. For example, many of the early samples collected by the tissue bank only had basic clinical data linked to it, such as ER/PR/HER2 receptor status. Because we were asking for a minimum of 3 years follow up data, this ruled out any recently collected samples and many samples where the follow up data wasn't collected or missing. In future, human tissue banks will be an increasingly valuable resource for carrying out retrospective clinical studies, as more samples are added to repositories with a complete clinical data profile that researchers can utilise.

Leading on from this, the small sample size of TNBC patients used within this study is another major limitation. Small study sizes can be useful and, as in this case, can help to generate preliminary information. However, a small sample size can lack the statistical power that is required to uncover true effects and minimise the chance of type I and type II errors. Although the statistical power required for this study was worked out based on previous research this was specific to the original question posed about perivascular macrophages and not powered towards the additional analysis that was carried out.

As a result of the smaller sample size, this can lead to an increased risk of bias. The TNBC samples used in this study were obtained from Barts Health NHS Trust, UK and Nottingham University Hospitals NHS Trust, UK between 2011 and 2017. This may have led to demographic bias, as the local populations of these 2 trusts may not be fully representative of the population at a national level. Risk factors that

are present at a local level, may not play as much or play even more of a role at a national level. This may include factors such as affluency, access to healthcare, number of smokers or levels of air pollutants. Selection bias can be overcome, but it would require a larger study to be carried out, with enough patient samples to be considered representative of the population.

A final point tied to the sample size is the reproducibility of the findings, the findings from the multiplex analysis need to be validated in a study using a larger cohort of TNBC samples that would help to reinforce or dispute any findings from this initial study.

To ensure a potential new biomarker remains independently predictive in TNBC after multivariate analysis with other recognised risk factors key recognised risk variables—such as patient age, tumour size, tumour grade, lymph node involvement, and the specific neoadjuvant chemotherapy regimen. Although we sought to control some of these parameters as much as possible in the sample selection, there are differences seen across the patient cohorts. As a result these factors can mask the apparent predictive value of the biomarker. Additionally tumours with initially higher immune infiltration may respond differently to certain NAC regimens compared to those that had lower baseline infiltration.

Another area of the study that has limitations is that bias may have been introduced using AI that was used to segment the cells. The images and training data that are used to first teach the AI need to be representative of the general population. If training data sets are used which aren't representative of the population being analysed, then this may potentially have issues during the segmentation process if the cells have different morphology characteristics. If certain cell types are underrepresented and/or poorly defined within the data training set, then these cell types are more likely to be missed/mislabelled during the segmentation process. Although this is not an issue with the cell types looked at within this study, when looking for rare cell types of clinical significance, this presents a larger issue. To counter these potential AI issues, the TNBC image dataset obtained within this study could also be used with other AI-based cell segmentation programs. This would help to identify what level of variability is introduced by using different source of AI in the segmentation process.

One issue with the use of stained FFPE sections to determine the effects of NAC on the TME, is that the average time between the last treatment and surgery for the TNBC samples used in this study was 35 days. By this timepoint, the snapshot of the TME taken so long after the last chemotherapy treatment, will not be representative of the TME containing the initial influx of immune cells. Responses to NAC within murine tumours were seen 48hrs after last chemotherapy does [113]. This is an issue that can be overcome in murine tumours, with live imaging allowing an in depth look at the TME [103]. But it is a challenge that will not be easily overcome to study the immediate effects of NAC on the TME within human tumours.

The areas defined as perivascular are also open to question. The FFPE sections used within the study were all 3-5 μm in thickness, resulting in a clear 2D, XY plane image. The perivascular area is then defined from the vascular staining present within the image. However, tumours are very much indeed a 3D structure. By using FFPE tissue sections in the way they have been used within this study, we are ignoring what is happening 50 μm above and below the section in the Z plane. As such, it may be that the majority of a tumour could end up being classed as perivascular. This could be achieved by reconstructing stacks of serial stained sections to reconstruct a 3D section of the tissue or methods that study much thicker tumour sections/slices. This then presents challenges within the staining processes due to the penetration of the antibodies, image acquisition and subsequent analysis.

4.4. Concluding remarks

Despite the study limitations listed above, this study appears to be the first to show that the density of stromal CD163+TIM3+ TAMs in TNBCs after NAC correlates with the onset of metastases after surgery. This suggests this could be a novel biomarker for predicting relapse although a larger study of this in TNBC is now warranted to validate this as a biomarker. Various immune cell types accumulated preferentially, and made direct contact with one another, in PV areas of both untreated and NAC-treated tumours. This infers a close pattern of communication between them that could impact on tumour immunity. This also now awaits further study. Higher levels of the chemokine receptor CXCR4 are often associated with metastasis, but they did not appear to be directly linked to metastasis in TNBC. This

challenges previous assumptions about the role of CXCR4 in TNBC progression, suggesting that alternative mechanisms may drive metastasis in this typically more aggressive form of breast cancer.

Chapter 5 Use of a microfluidics assay to model the stromal perivascular niche in TNBC.

5.1 Introduction

The previous chapter examined the distribution and phenotype of CD163+ TAMs, CD4+ T cells, CD8+ T cells and regulatory T cells (Tregs) relative to blood vessels in untreated and chemotherapy treated TNBCs. These immune cell types were found to locate preferentially to the tumour stroma, with the highest density of some subsets of these seen in perivascular (PV) stromal areas after chemotherapy (e.g. TIM3+PD-L1-CD163+ TAMs). Furthermore, distinct 3-cell clusters of CD163+ TAMs, Tregs and predominantly naïve T cells formed in stromal PV areas, suggesting that T cells may be maintained in a naïve state in these PV clusters.

Moving forward, the goal was to see if these events in the perivascular niche (PVN) could be modelled in an *ex vivo* model that simulates the complexities of the stroma and PVN. *Ex vivo* models use primary tissue to bridge between *in vitro* studies and clinical research. They include a diverse range of systems including precision-cut tissue slices, organotypic cultures and ‘organ-on-a-chip’ technologies, each tailored to mimic specific aspects of the physiological or disease environment outside the living organism with its own benefits and scalability (**Figure 5-1**).

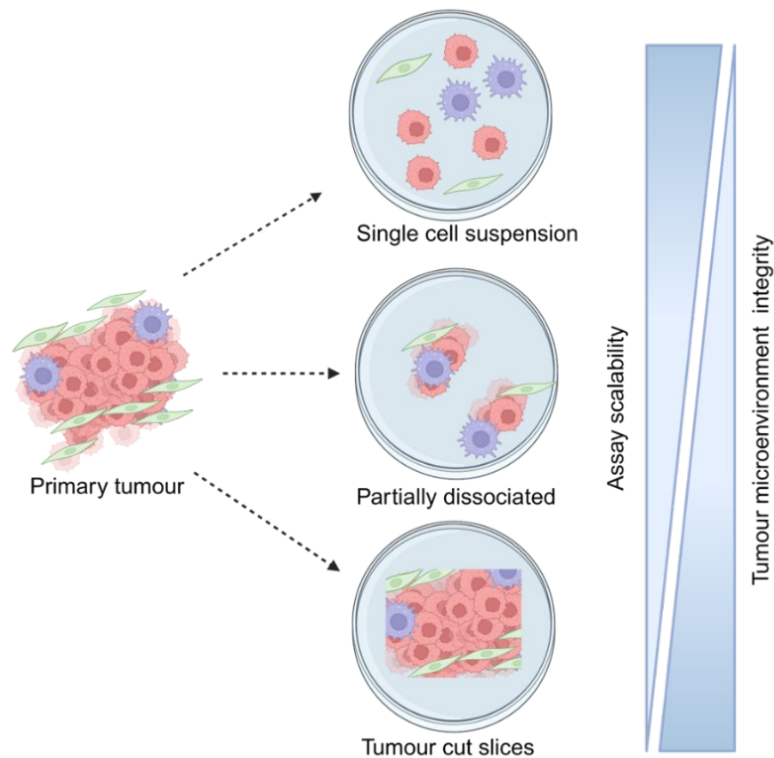


Figure 5-1 Different approaches to using primary tumours in an ex vivo setting.

Patient derived material from sources such as primary tumours can be used in several ways. The structures can be kept intact to preserve the TME and allow in situ observations. Partial dissociation disrupts the overall TME, but still maintains some cell-cell interactions while fully dissociated single cell suspension lose all spatial context.

5.2. Aims

The aim of the work described in this chapter was to generate a microfluidics assay using DAX-1 chips (Aim Biotech) (**Figure 5-2 A**) that simulated TCIs and stromal areas in human tumours, with flow-carrying microvessels and small tumour spheroids in a fibrin gel, to produce a model for studying the phenotype and interaction of immune cells in PV areas of TCIs and stromal regions in response to chemotherapy in breast cancer. The plan was to use human cell lines to set up the basic assay - and then to infuse the model with human PBMCs (i.e. into the microvessels) so that their extravasation and interaction in PV and non-PV regions of the fibrin stroma could be imaged (**Figure 5-2 B-C**). If this was successful, the next step that tumour spheroids could be replaced with small TNBC fragments derived from patients at elective surgery. This approach aimed to replicate the biological processes and changes seen within the perivascular environment to better understand the immune response to treatment in TNBC.

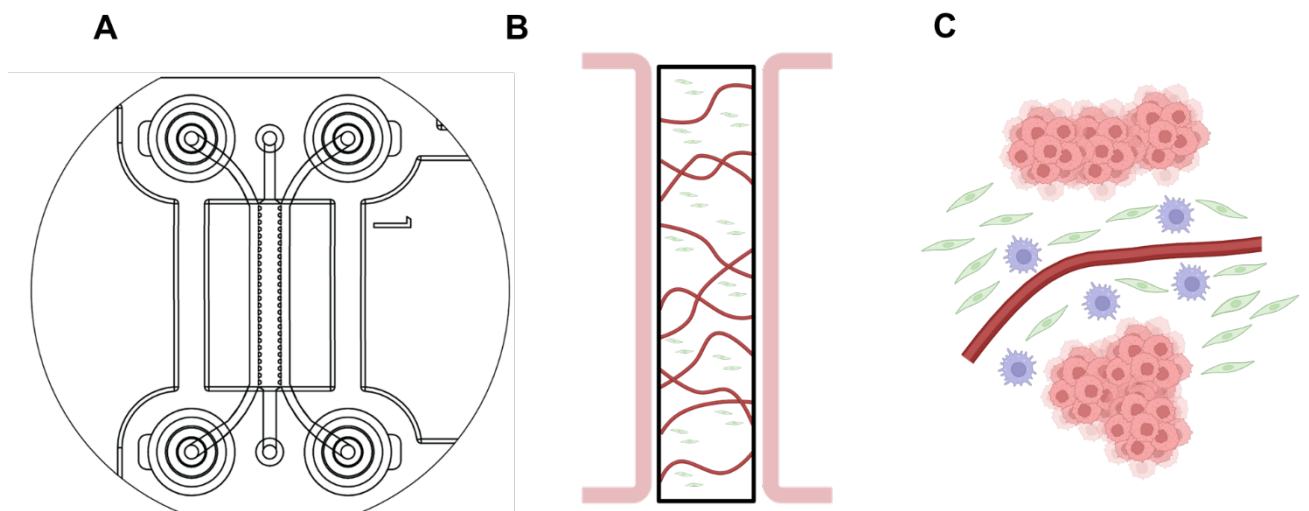


Figure 5-2 Microfluidic model setup of the TME

Overview of the microfluidic model to be used that shows A. a schematic overview of the microfluidic site in a DAX-1 chip. B The central gel containing channel, flanked by 2 media channels. Flow carrying vessels develop across the central gel channel. C. Planned setup of the model to contain regions of TCI/stroma and perivascular/non-vascular regions. Immune cells such as macrophages can be added during set-up or seeded into the media channels to extravasate through the vessels.

5.2.1. Impacted Aims

Arrangements were made with the Breast Cancer Now Tumour Bank (Prof Angie Cox) and the Sheffield teaching hospitals breast multidisciplinary team to collect fresh breast tumours (preferably TNBC where possible) from surgery under the following ethical approval (STH ref. STH15545, BCN REC Ref. 09/H1308/138).

Once obtained, these tumours would have been used to:

- Isolation of primary breast tumour cells or tumour cell fragments for use within the fibrin hydrogel of the microfluidic assays.

Following surgical acquisition, fresh tumour tissue would be mechanically and enzymatically dissociated into a single-cell suspension. Cancer cells would then be isolated using either FACS or magnetic bead separation. The colony-forming ability of these isolated cells in the fibrin region of the DAX-1 chip would be compared with the growth and viability of small tumour fragments derived from TNBC tumours. The optimal method—defined by the method that yields the most viable TCI within the assays and maintain the formation of the microvessels network—would be selected.

- Isolation of cancer-associated fibroblasts to replace human lung fibroblasts for use within the microfluidic assay.

To replicate the stromal microenvironment, cancer-associated fibroblasts (CAFs) would be isolated from human breast tumours using FACS or magnetic bead techniques. These cells would then be incorporated into the gel during the initial setup of the microfluidics assay, replacing the human lung fibroblasts previously used. The impact of using CAFs on the formation and viability of both microvessels and tumour cells would be assessed to determine whether they provide a more physiologically relevant alternative.

- Isolation of CD163+ TAMs for use within the microfluidic assay.

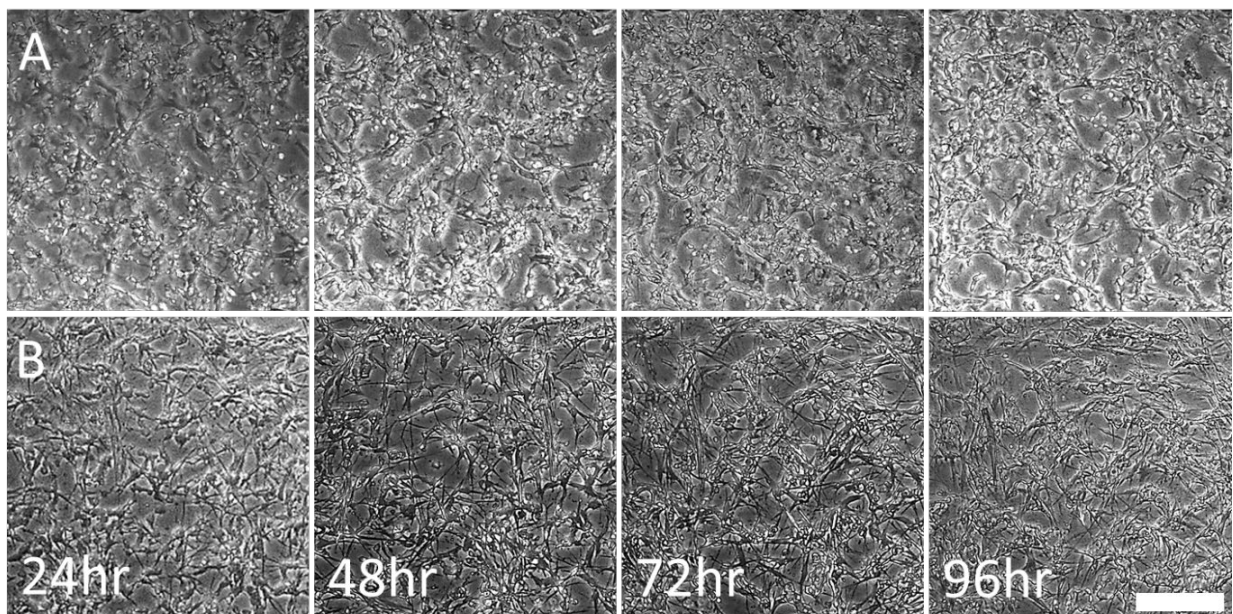
To study the role of CD163+ TAMs within the assay, Monocytes isolated from waste buffy coats were to be fluorescently labelled for identification and introduced into the microfluidics assay via the microvessel network. Once the microfluidic model was established using primary human cells or tumour fragments, clinically relevant treatments were infused through the microvessel network. The subsequent analysis focused on the impact of these treatments on cancer cell viability, as well as the migration and phenotype of macrophages within the gel.

Unfortunately, this study was negatively impacted by the covid pandemic, affecting its progress and work towards its aims.

5.3. Results

5.3.1. Generating a microvascular network in the MFAs

To achieve this, the DAX-1 chips (supplied by AIM Biotech specifically for microfluidics assays), were used as described earlier in section 2.2.4.6. Human umbilical vein endothelial cells (HUVECs) were seeded alone within the central fibrin gel of these chips. Following advice from AIM Biotech, it was suggested to try using these cells at concentrations from 4-6 x10⁶ cells/ml. To make up the fibrin gel that would contain the cells in the centre channel of the DAX-1 chips, fibrinogen is cleaved into fibrin by thrombin, which allows a liquid solution to be injected into the DAX-1 gel channel where it polymerises into harder gel. Starting concentrations of thrombin and fibrinogen used were 4 U/ml and 6 mg/ml respectively to form the fibrin



gel, as advised by AIM Biotech. Decreasing the concentration of the fibrinogen has been shown to increase the number of endothelial branches and decrease their diameter as the fibrin gel becomes more porous [188]. In the end, HUVECs were found to produce a microvascular network in the chips at densities of $4-6 \times 10^6$ cells/ml. The vessel-like structures began to form 48-72 hrs after seeding (**Figure 5-3 A**). After culturing for 5 days however, the network began to regress. By this time, lumen openings had not formed as no infiltration was seen into the network when MDA-MB-231 cells were added to the media to flow through the microvessels.

Figure 5-3 Generation of a microvascular network

A. Formation of a vascular network over 4 days using HUVECs only B. formation of a vascular network over 4 days using HUVECs and HLFs. Scale bar 250 μ m.

Previous studies had shown that microvessel stability could be enhanced by both physical contact with, and soluble mediators released by, fibroblasts in the gel [188]. To test this, vascular networks were established containing either HUVECs alone in endothelial ECGM MV2 medium, HUVECs with fibroblast-conditioned medium (detailed in section **2.2.4.3**) or HUVECs grown in direct co-culture with HLFs within the gels at a 1:5 HLF/HUVEC ratio. This resulted in the formation of the microvessel network which maintained its viability for up to 10 days (**Figure 5-3 B**).

The addition of fibroblasts and fibroblast conditioned media to the DAX-1 chip A vascular network was seen spanning the fibrin gel channel in the 2-3 days following seeding, in all conditions (**Figure 5-4 A-B**). Although the vascular network was stable for up to 10 days, signs of deterioration started as early as day 8.

Initially, there were technical issues with the fibrin gel not setting properly in the AIM chips. This meant that HUVECs formed monolayers within 24h of seeding rather than microvessels within the 3D fibrin scaffold. It was found that this was due to heparin in the culture media preventing the thrombin from cleaving fibrinogen into a fibrin so it could not form a gel in the assay. There were also issues with the uniformity of HUVEC distribution with vast differences seen in the cell density in one end of the chip site compared to the other end. To correct this, rather than filling the whole gel channel from one end only, it was filled only halfway and then using the opposite gel port, the remaining half was filled.

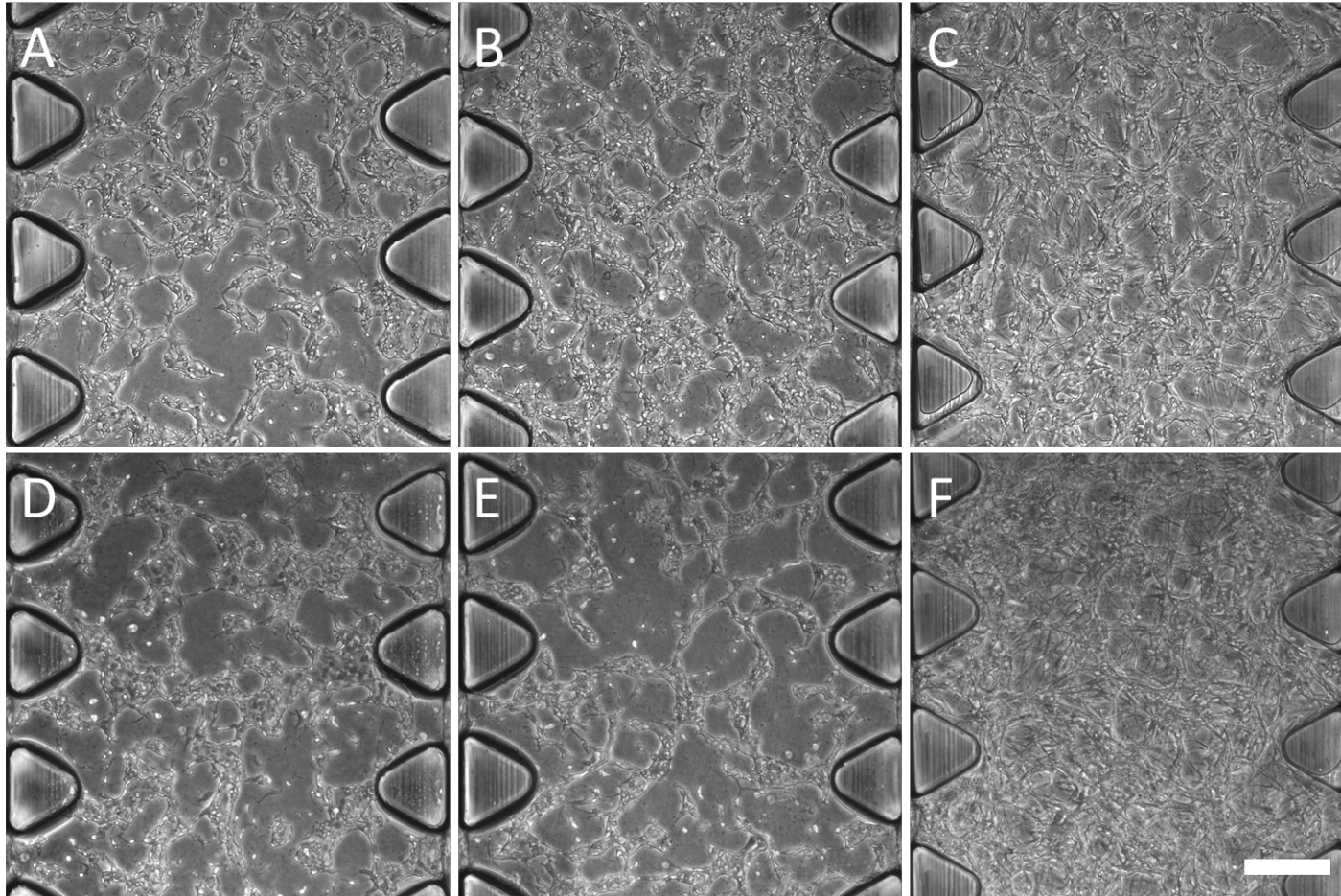


Figure 5-4 Effects of fibroblasts on microvessel formation in MFAs

Formation of microvessel network formed by HUVECs after 4 days in MFAs with: A. Endothelial medium (ECGM MV2) alone, B. Fibroblast-conditioned medium, and C. HLFs in the gel from the start of the assay. D-F shows the deterioration of the vascular network after 8 days of culturing D ECGM MV2 medium. E. Fibroblast conditioned medium and F. Addition of HLFs in the gel. Scale bar 250 μ m

5.3.2. Assessment of microfluidic flow

To check the entire microvascular network was carrying flow through the lumen, multiple duplicate DAX-1 chips were set-up containing HUVECs co-cultured with HLFs until a microvascular network had grown. Once lumen openings had been observed (**Figure 5-5 A-B**), fluorescently labelled dextran was added to media channels on one side of the fibrin gel to create a pressure drop. Ten minutes after adding the dextran, the chips were imaged to view the spread through the device. All of the devices tested allowed flow throughout the microvascular network (**Figure 5-5 C**) that appeared to be contained within the HUVEC formed vessels (**Figure 5-5 D**). Vessel distribution was even throughout the fibrin gel, but not all the vessel structures appeared to carry flow. When looking at the number of flow carrying lumen, differences were seen between the 'entry' channels of the fibrin the 'exit' channels (**Figure 5-5 E**). The stability of the microvascular network was also seen to remain very stable up until day 10 of culturing (**Figure 5-5 F**). Also assessed was the average diameter of the PV spaces outside of the vessels. The mean (\pm SEM) of the diameter of these spaces was 99.4 ± 5.5 μ m.

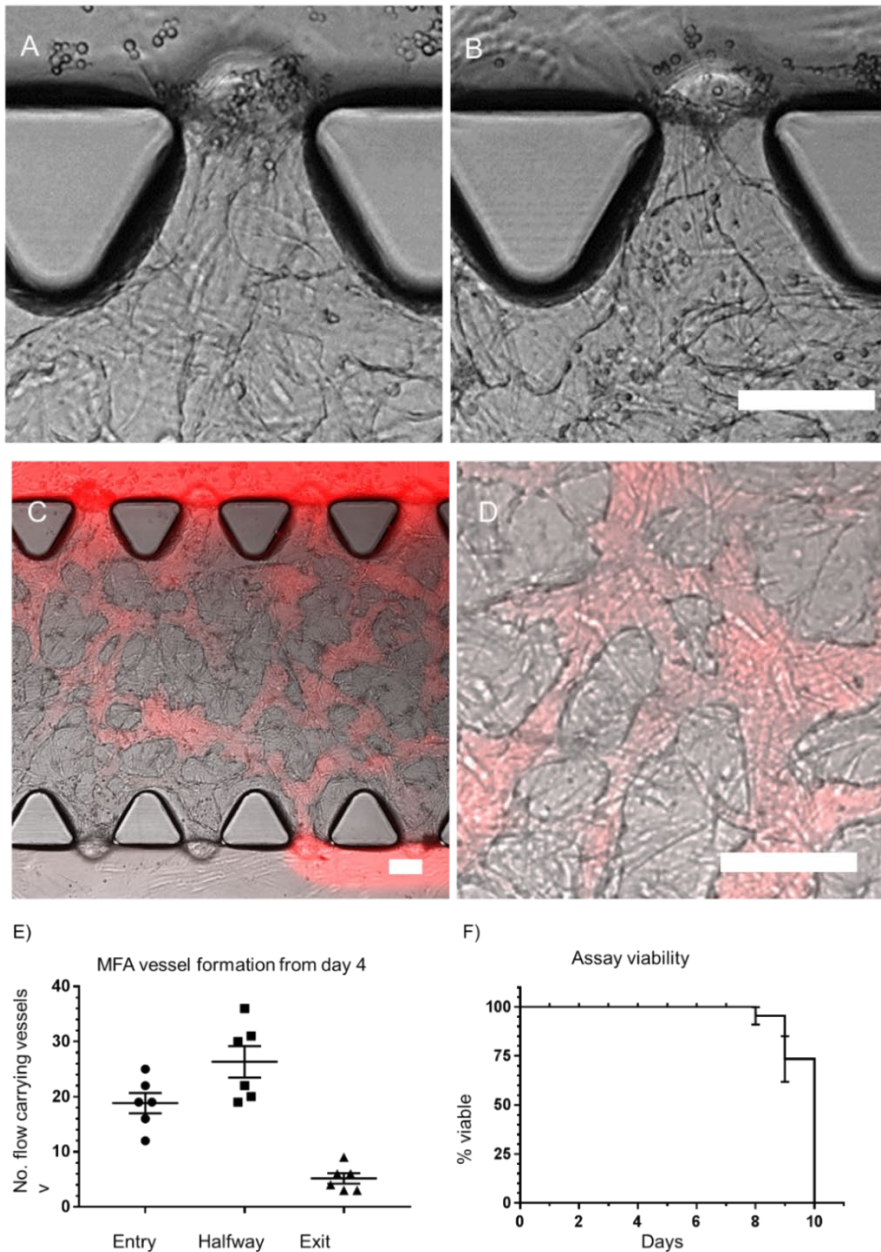


Figure 5-5 Microfluidic assay characteristics.

Representative images A. A vessel opening and B. Vessels that have not created openings. C. Flow of dextran (red) through the microvascular network D. Dextran (red) contained within the HUVEC network. Scale bar 100 μ m. E. The number of flow carrying lumen the carry flow on entry through the fibrin gel, halfway through the gel and exited the gel into the opposite media channel. F. The length of time assay remains viable before the network collapses when co-culturing HUVECs and HLFs (n=7).

5.3.3. Perfusion of tumour cells

Before introducing tumour spheroids into the assay, it was decided to examine the movement through the gel and survival of single tumour cells following their extravasation across the microvessels. This also served the purpose of showing that microvessels could carry cells not just medium. So, tumour cells were perfused into the device once open lumen had been observed within the microvascular network (**Figure 5-5 A**). A pressure drop created by selectively filling the media reservoirs on one side of the chip, created flow through the microvessels in the chip [241]. MDA-MB-231 breast tumour cells were labelled with Carboxyfluorescein succinimidyl ester (CFSE) (detailed in section 2.2.4.4) and were added to these media reservoirs as (detailed in section 2.2.4.7) at a density of 5×10^5 cells/ml. Widefield imaging (Leica AF6000) imaging of cells took place within 10 mins of adding the MDA-MB -231 cells. The use of a fluorescent label made it possible to visualise the passage of cells in microvessels through widefield immunofluorescence microscopy. These cells were seen to immediately flow down the media channel and into the centre region through open lumen contained with the microvascular network (**Figure 5-6**) (**Supplementary video 1**).

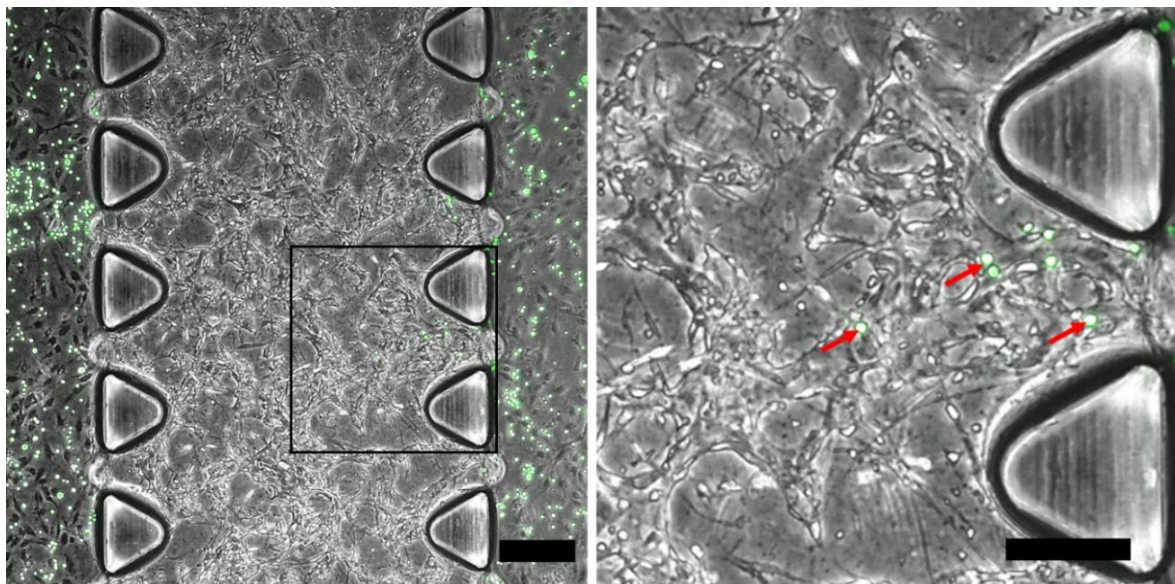


Figure 5-6 Perfusion of CFSE-labelled, MDA-231 tumour cells through the microvascular network

Left image. Labelled tumour cells were introduced through the media channel on one flank the microvessel network in the centre gel region. Square inset defines region. Right image. Inset

region, Red arrows indicate green CFSE-labelled MDA-MB-231 cells contained within the HUVE microvessel network. Scale bar left 250µm, right 150µm.

Cells were carried by the initial flow generated by the pressure drop created by filling the media channels on one side of the gel, but soon came to rest once the flow media had equalised on both sides of the gel channel. To check that lumen were being generated by HUVECs and not HLFs or by channels in the gel, chips containing fibrin gel or HLFs alone were also used. Tumour cells were only seen to pass into the centre gel region in gels containing HUVECs only or HUVECs co-localised with HLFs, with no infiltration seen in HLF only or fibrin only conditions.

5.3.4. Co-culture with tumour spheroids

The overall aim of the model is to begin to add in cells derived from primary tumours to mimic the TCI and stroma region and the PV areas found within the TME to study the immune response in the different spatial compartments in response to therapies. As we did not yet have access to patient derived material, 3D tumour spheroids were generated from cell lines (section **2.2.4.5**). Initial spheroids consisted of MDA-MB-231 cells only, which lacked sufficient strength within their structure to withstand the procedure of transferring from the well plate where the spheroids were initially cultured, to the DAX-1 chip where they were mixed with the HUVEC/HLF thrombin/fibrinogen constituents. To get around this, MDA-MB-231 spheroids were cultured 1:1 with HLFs which formed a stable spheroid (**Figure 5-7 A**). These were successfully added and contained in the fibrin gel during the set-up (**Figure 5-7 B**) of the DAX-1 chip. Spheroids grew within the device for up to 8 days, with fibroblast sprouts emerging from the spheroids.

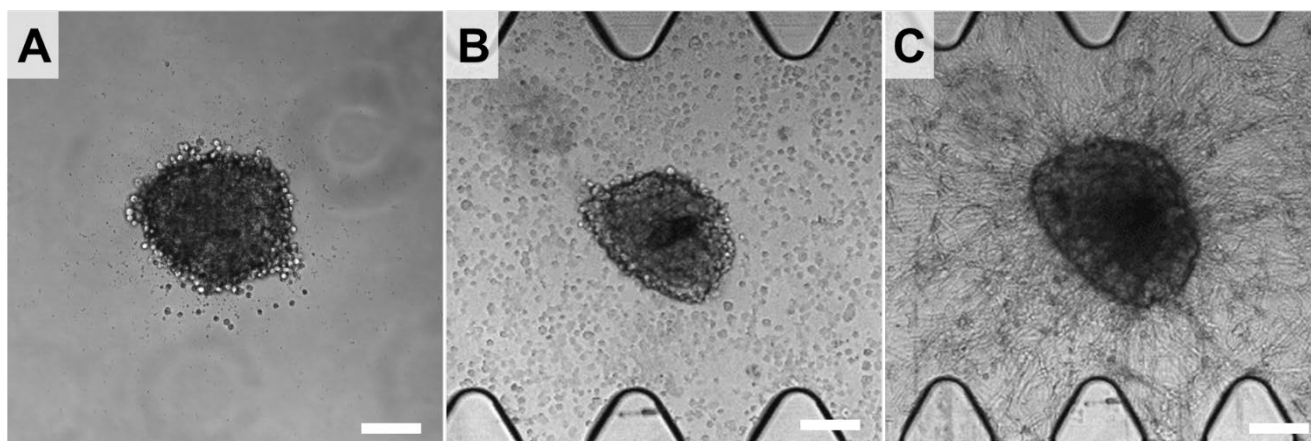


Figure 5-7 Generation of tumour spheroids.

A. Pre-cultured spheroid generated from MDA-MD-231 cells and HLFs. B. Spheroid remained intact immediately after seeding into DAX-1 chip centre well. C Growth of spheroid lasted upto 8 days. Scale bar 150 μ m

5.4. Discussion

Microfluidic models have been utilised now in the study of cellular behaviour, biomolecular interactions, and disease mechanisms [242]. These allow micro-TMEs to be recreated *in vitro* and then cell behaviour (like migration, proliferation, differentiation and interaction with other cells) to be examined on a single-cell level using microscopy. They have also been used for drug screening [243, 244] and provide insights into drug toxicity (as they can mimic the physiological complexity of a given human organ).

In studies described in this chapter, a microfluidics model was established in order to study the phenotype and interaction of immune cells in PV areas of TCIs and stromal regions (using human PBMCs and human TNBC cell lines – then replacing the latter with fragments of primary human TNBCs).

Although the pandemic meant it was not possible to obtain human blood samples or TNBC fragments, an assay with a functioning microvascular network in a fibrin gel containing fibroblasts (HLFs) was established. This was the first time that such an assay had been established/used at the University of Sheffield. It was interesting to see that the addition of fibroblasts to the assay improved the longevity of the microvascular network and stability of tumour spheroids in the fibrin gel. It was previously reported that fibroblasts have a stabilising effect upon such networks in the microfluidics assay, due to paracrine signalling between the cells involving

angiopoietin-1, platelet-derived phospholipids phosphatidic acid and sphingosine 1-phosphate [245].

Fluorescently labelled MDA-MB-231 tumour cells were able to pass through media channels into the microvascular network which demonstrated that they had lumen large enough to carry cells. However, cells did not flow in all parts of the network and could reflect both the absence of lumen forming microvessels in some parts of the gel, and the limited flow of media through some vessels. As the latter is only created by a pressure drop generated by loading the media wells on one side of the DAX-1 chips, it may not be sufficient to create flow throughout the vascular network. The DAX-1 chips have the capacity to be attached to a peristaltic pump system to increase/control the flow rate in the assay. A lack of conformity in the size of the vessels and their lumen across the network may also be an issue. Staining the endothelial cells with a fluorescent CD31 antibody and performing Z stack imaging on the confocal microscope could help to characterise the vessels across the network. It would also enable the cross-sectional dimensions of the lumen to be visualised to see if the microvessels are maintaining their structure or collapsing over time.

Although there is considerable excitement about the various ways that microfluidics assays can be used to image single cells in a 3D microenvironment, they have also been criticised for failing to model the more complex aspects of tissue biology and dysfunction in disease. This is confirmed by the fact that novel microfluidics models are more usually published in engineering journals than biological or medical ones [246]. Although the Aim biotech DAX-1 chips are flexible and can accommodate multiple cell types in the assay, in order to produce a microvascular network in the DAX-1 chips, a fibrin gel had to be used [188]. This detracts from a more physiological relevant ECM such as collagen type IV [247]. Finally, due to the tiny volumes of cells, gel and medium used in microfluidic devices it makes them more susceptible to environmental changes like small changes such as media evaporation and inefficient gas exchange.

There remained several other challenges to overcome when using the microfluidics assay for my planned studies. Although a flow-carrying network was generated, the flow rate through these vessels was still too low to carry cells. So, a

peristaltic pump mimicking the flow of blood through small blood vessels in tumours would be needed.

The model also requires the addition of tumour cells or spheroids to the central gel region to model the presence of TCIs in tumours. The number and ratio of tumour cells to HUVECs and HLFs would have to be optimised to prevent the cancer cells from growing out into the gel and potentially disrupting the microvascular network. This could be achieved by testing a panel of human TNBC cell lines and seeding them at various ratios with HUVECs and HLFs in the centre gel region. Further work is also needed to see how long small tumour spheroids survive in the gel (in order to replicate the TCIs seen in TNBCs). Once these steps have been addressed, human PBMCs could then be added to the assay in order to study their extravasation into, and function in the PV space under various conditions such as infusing different forms of chemotherapy into the assays.

Beyond microfluidic approaches, 3D in vitro and in vivo models present alternative strategies for investigating spatial specific immune responses in cancer. Spheroid and organoid platforms recapitulate tumour architecture more accurately than traditional 2D methods and can be co-cultured with immune cells to better mirror complex cell–cell interactions *ex vivo*. As previously mentioned, patient-derived xenograft (PDX) mouse models preserve original tumour characteristics, though they are primarily established in immunocompromised mice—a key drawback that can be mitigated by adopting humanised PDX models carrying functional human immune components. Each of these models brings distinctive advantages in terms of physiological relevance and complexity providing suitable alternative to using microfluidic-based models [179].

Chapter 6 General discussion

6.1 Wider considerations of the perivascular niche in tumours

One of the main aims of this thesis was to employ multiplex immunofluorescence to investigate the impact of neoadjuvant chemotherapy on the density and characteristics of different immune cells, such as TAMs, in the perivascular niche (PVN) of primary TNBCs. Additionally, it explored potential associations between these immune cell characteristics and metastasis during a three-year post-surgery period. Growing evidence highlights the perivascular niche in tumours as a dynamic, evolving microenvironment, that is densely populated not only with leukocytes like TAMs, T cells, and regulatory T cells (as discussed in Chapter 4) but also with alpha-smooth muscle actin-positive (α SMA+) cells, including pericytes and fibroblasts (**Figure 6-1**). Other immune cells like neutrophils, B cells, gamma delta T cells, and NKT cells, may also preferentially localise to these perivascular (PV) areas in TNBC.

The close proximity between such diverse cell types in PV areas suggests significant intercellular communication. Chapter 4 presents data showing that CD163+ TAMs, regulatory T cells, and CD4+ and CD8+ T cells can make direct contact in the PVN, forming tri-cellular clusters. Mathematical and AI modelling is now required to elucidate the patterns of communication among these PV cell types and to assess the implications of this for tumour responses to chemotherapy and the development of metastasis. Notably, interactions between TAMs and CD8+ T cells in PV tumour regions have been shown to diminish the effectiveness of chemotherapy in mouse models of mammary tumours [248] and immunotherapy in melanoma models [118].

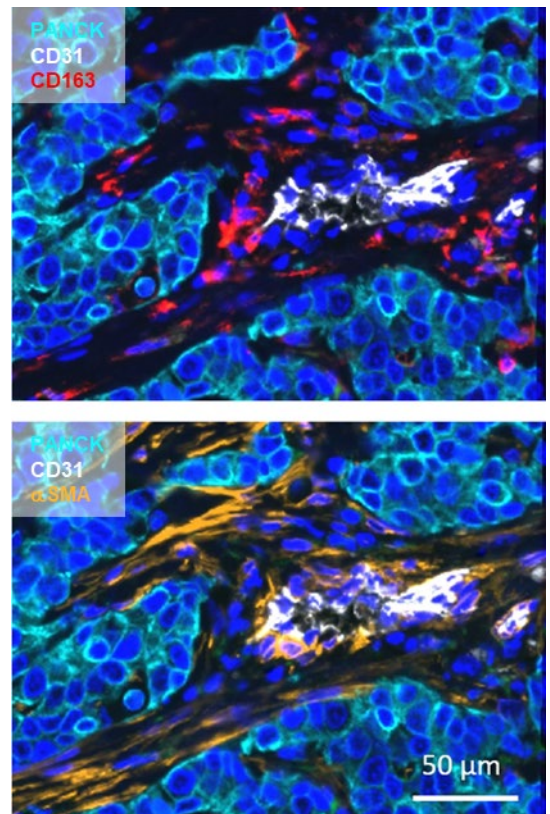


Figure 6-1 Microenvironment crosstalk
Images from the TNBC stroma show the close proximity of TAMs and fibroblast, a potential route of future targeting?

Furthermore, PV TAMs influence the prevalence of fibroblasts in mammary tumours [112], while selectively eliminating PV fibroblasts enhances the effectiveness of CAR-T cell immunotherapy [249]. These findings suggest that PV TAMs and fibroblasts could potentially undermine the effectiveness of various frontline therapies. It remains to be determined whether these cell types are individually primed by signals within the PVN to perform such tumour-promoting functions, and whether they communicate in the PVN to coordinate these functions. It is important to note that the above insights have been almost entirely derived from the use of mouse tumour models, necessitating validation in human tumours. Although mouse based *in vivo* studies are a crucial tool for research, there are biological, genetic, and physiological differences that affect the translation from animal models to human clinical applications. This discrepancy can lead to promising preclinical results that fail to materialize in human trials. This gap is closing with methods such as patient-derived xenografts or organoid cultures, that more accurately model human cancer biology, but these methods often require the use of immunocompromised mouse strains with no adaptive immune system.

For this study, we chose to use multiplex immunofluorescent staining coupled to AI-based image analysis that would not have been possible 10 years ago. It enabled the simultaneous detection of multiple proteins within a single tumour section, and then the analysis of the frequency, phenotype and interaction of various cell types. Panels of markers can be built in the same way they are utilised for flow cytometry, but with the added benefit of providing their spatial context. In comparison, techniques like single-cell RNA sequencing (scRNA-seq) and spatial transcriptomics offer an insight of mRNA expression at the level of single cells. scRNA-seq offers a high-resolution look at the transcriptome of a cell and can be used to compare this in different subsets of the same cell. However, this technique fails to provide spatial information on where cells were in the tumour microenvironment. Spatial transcriptomics can bridge the gap between single cell transcriptome analysis and multiplex immunofluorescence, as it provides information on gene expression patterns across discrete tissue regions. However, it is often difficult to examine gene expression by single cells rather than groups of cells in a given region of a tissue section.

Using the approach taken in chapter 4, it was possible to show that higher levels of CD163+ TAMs (especially those expressing the immune checkpoint regulator, TIM-3) that were found in the tumour stroma, where they correlated with a reduced risk of metastasis in TNBC patients treated with neoadjuvant chemotherapy (NAC). This correlation was not seen in untreated tumours, so further studies are now warranted to see if this stromal TAM subset exhibits anti-metastatic functions in NAC-treated TNBCs, and how this is regulated. These cells could be isolated from TNBCs by fluorescence activated cell sorting and used in a range of *in vitro* mechanistic assays. Migration based assays such as scratch assay, Boyden chambers and the developed microfluidic platform could all be used to test isolated CD163+ TIM3+/- TAMs and their effects on cancer cell motility/migration and intravasation.

6.2. Clinical implications

Importantly, low levels of stromal CD163+TIM3+ TAMs may represent a new potential biomarker for identifying patients at higher risk of relapse after NAC. TNBC represents around 10-25% of all breast cancer cases and lacks the targeted treatment options available to receptor positive breast cancers. As such, NAC is still a main therapeutic option for the treatment of TNBC. Of those TNBC patients who receive NAC, 22% will have a complete pathological response (pCR). For the majority who still have residual disease post-NAC, there is almost a 33% chance of them dying within the following 3-year period due to disease progression [5]. This highlights the need to identify the group of post-NAC TNBC patients who have residual disease and are at a heightened risk of disease progression.

6.3. Further work and directions

There are several areas of work in this thesis that it would have been beneficial to carry forward, had time (and the covid pandemic) permitted.

The finding that CD163+ TIM-3+ TAMs present in TNBC residues after NAC correlate with development of metastasis over a 3-year follow-up period after surgery, now needs to be confirmed in larger, separate cohort of TNBC samples. If it validated in this way, it could have clinical implications. Identifying patients who are less likely to benefit from NAC, could lead to their closer monitoring during follow-up

after surgery, and could help to personalise and improve decisions about subsequent treatments. The study conducted in chapter 4 was relatively small-scale and underpowered for many areas of analysis that were considered. Expanding the sample size studied in chapter to include a more diverse and representative TNBC population is crucial. This would enhance the statistical power of the study and allow for the assessment of the biomarker's prevalence across different demographics and clinical subtypes that is more representative of the general population could yield more biological and clinical insights. A larger cohort would also allow for multivariate analyses to control for potential confounding factors, strengthening the evidence for the prognostic value of the biomarker.

It would have been good to use matched pre- and post -NAC tumours to analyse changes in the tumours induced by NAC. Although we compared differences in untreated and NAC treated tumours within this study, it would have been better to assess these in the same tumours before and after NAC.

Spatial transcriptomic analysis of TNBCs after NAC would also add an extra layer of genomic data that could further highlight differences between immune cells after this treatment in TCIs, stroma, PV/non-PV, and hypoxic and necrotic areas. Some recent studies have taken this approach. For example, in TNBC, spatial profiling has shown differences in immune profiles between TCIs and stromal regions in 44 untreated TNBC tumours (22 recurred, 22 disease free). Here they showed that stromal regions containing high levels of CD68+ TAM contained higher levels and CTLA-4, B7-H3 and TIM-3, compared to CD45 enriched regions that were high for B and T cells related proteins. However there were no differences seen that linked to relapse between the CD68 or CD45 enriched regions [250].

Since the start of this PhD project, the main neoadjuvant treatment for TNBC has changed from NAC alone to NAC with immunotherapy (specifically a PD-L1 antibody) if patients have PD-L1+ tumours. So, it is important now to see if the density of stromal CD163+TIM3+ TAMs is also predictive of metastasis after this combined treatment.

Regarding the development of a microfluidics model, devices similar to the one used in chapter 5 have the potential to help direct personalised treatment options and are being assessed in clinical trials [180]. Developing a model using DAX-1 chips and patient-derived material, would not only provide a valuable research tool,

(e.g. for investigating cellular behaviour and interactions in diseases like cancer), but can also be used as a tool for personalised medicine.

With the microfluidics model described in chapter 5, progression towards a more comprehensive model, encompassing cells derived from primary TNBCs would help to recreate 3D areas of the TME. At present, the model uses HUVECs to generate the microvessel network, but it would be good to use endothelial cells derived from human TNBCs along with pericytes. It would be good to see if, once established using cells from individual patients, the model is able to predict the efficacy of various forms of treatment in each one.

In summary, these studies have generated novel insights into the way that various subsets of TAMs, T cells and Tregs are distributed across, and interact with one another, in untreated and NAC-treated TNBCs. This has highlighted a potential new biomarker for metastasis in the NAC-treated group. Furthermore, this thesis shows that microfluidics assays have the potential to simulate some aspects of the complex spatial features of tumours, so their influence on tumour immunity can be investigated at the single cell level.

References

1. ONS. *Cancer Registration Statistics, England - Office for National Statistics*. 2017; Available from: <https://www.ons.gov.uk/peoplepopulationandcommunity/healthandsocialcare/conditionsanddiseases/bulletins/cancerregistrationstatisticsengland/latest>.
2. Russnes, H.G., et al., *Breast Cancer Molecular Stratification*. The American Journal of Pathology, 2017. **187**(10): p. 2152-2162.
3. Foulkes, W.D., I.E. Smith, and J.S. Reis-Filho, *Triple-Negative Breast Cancer*. New England Journal of Medicine, 2010. **363**(20): p. 1938-1948.
4. Dent, R., et al., *Triple-negative breast cancer: Clinical features and patterns of recurrence*. Clinical Cancer Research, 2007. **13**(15): p. 4429-4434.
5. Liedtke, C., et al., *Response to neoadjuvant therapy and long-term survival in patients with triple-negative breast cancer*. Journal of Clinical Oncology, 2008. **26**(8): p. 1275-1281.
6. Carey, L.A., et al., *The triple negative paradox: Primary tumor chemosensitivity of breast cancer subtypes*. Clinical Cancer Research, 2007. **13**(8): p. 2329-2334.
7. Bauer, K.R., et al., *Descriptive analysis of estrogen receptor (ER)negative, progesterone receptor (PR)-negative, and HER2-negative invasive breast cancer, the so-called triple-negative phenotype - A population-based study from the California Cancer Registry*. Cancer, 2007. **109**(9): p. 1721-1728.
8. Gao, B., et al., *Mammographic and clinicopathological features of triple-negative breast cancer*. The British Journal of Radiology, 2014. **87**(1039): p. 20130496.
9. Lehmann, B.D., et al., *Identification of human triple-negative breast cancer subtypes and preclinical models for selection of targeted therapies*. Journal of Clinical Investigation, 2011. **121**(7): p. 2750-2767.
10. Cheang, M.C.U., et al., *Defining Breast Cancer Intrinsic Subtypes by Quantitative Receptor Expression*. The Oncologist, 2015. **20**(5): p. 474-482.
11. Bianchini, G., et al., *Triple-negative breast cancer: challenges and opportunities of a heterogeneous disease*. Nature Reviews Clinical Oncology, 2016. **13**(11): p. 674-690.
12. Schott, A.F. and D.F. Hayes, *Defining the Benefits of Neoadjuvant Chemotherapy for Breast Cancer*. Journal of Clinical Oncology, 2012. **30**(15): p. 1747-1749.

13. Asselain, B., et al., *Long-term outcomes for neoadjuvant versus adjuvant chemotherapy in early breast cancer: meta-analysis of individual patient data from ten randomised trials*. *The Lancet Oncology*, 2018. **19**(1): p. 27-39.
14. Kaufmann, M., et al., *Recommendations from an international expert panel on the use of neoadjuvant (primary) systemic treatment of operable breast cancer: new perspectives 2006*. *Annals of Oncology*, 2007. **18**(12): p. 1927-1934.
15. Longley, D.B., D.P. Harkin, and P.G. Johnston, *5-Fluorouracil: Mechanisms of action and clinical strategies*. *Nature Reviews Cancer*, 2003. **3**(5): p. 330-338.
16. Gelmon, K., *THE TAXOIDS - PACLITAXEL AND DOCETAXEL*. *Lancet*, 1994. **344**(8932): p. 1267-1272.
17. von Minckwitz, G. and M. Martin, *Neoadjuvant treatments for triple-negative breast cancer (TNBC)*. *Annals of Oncology*, 2012. **23**: p. 35-39.
18. Emadi, A., R.J. Jones, and R.A. Brodsky, *Cyclophosphamide and cancer: golden anniversary*. *Nature Reviews Clinical Oncology*, 2009. **6**(11): p. 638-647.
19. Sikov, W.M., *Assessing the Role of Platinum Agents in Aggressive Breast Cancers*. *Current Oncology Reports*, 2015. **17**(2).
20. Oakman, C., G. Viale, and A. Di Leo, *Management of triple negative breast cancer*. *Breast*, 2010. **19**(5): p. 312-321.
21. Schmid, P., et al., *Event-free Survival with Pembrolizumab in Early Triple-Negative Breast Cancer*. *New England Journal of Medicine*, 2022. **386**(6): p. 556-567.
22. Cortes, J., et al., *Pembrolizumab plus Chemotherapy in Advanced Triple-Negative Breast Cancer*. *New England Journal of Medicine*, 2022. **387**(3): p. 217-226.
23. NCT03150576. *Platinum and Polyadenosine 5'Diphosphoribose Polymerisation Inhibitor for Neoadjuvant Treatment of Triple Negative Breast Cancer and/or Germline BRCA Positive Breast Cancer (PARTNER)*. [cited 2023 11/03/2023]; Available from: <https://clinicaltrials.gov/ct2/show/NCT03150576?term=Jean+Abraham&cond=Breast+Cancer&cntry=GB&draw=2&rank=1>.
24. Gonzalez-Angulo, A.M., et al., *Incidence and Outcome of <i>BRCA</i> Mutations in Unselected Patients with Triple Receptor-Negative Breast Cancer*. *Clinical Cancer Research*, 2011. **17**(5): p. 1082-1089.
25. Bardia, A., et al., *Sacituzumab Govitecan in Metastatic Triple-Negative Breast Cancer*. *New England Journal of Medicine*, 2021. **384**(16): p. 1529-1541.

26. von Minckwitz, G., et al., *Definition and Impact of Pathologic Complete Response on Prognosis After Neoadjuvant Chemotherapy in Various Intrinsic Breast Cancer Subtypes*. *Journal of Clinical Oncology*, 2012. **30**(15): p. 1796-1804.
27. Veronesi, U., et al., *Rethinking TNM: Breast cancer TNM classification for treatment decision-making and research*. *The Breast : official journal of the European Society of Mastology.*, 2006. **15**(1): p. 3-8.
28. Park, Y.H., et al., *Clinical relevance of TNM staging system according to breast cancer subtypes*. *Annals of Oncology*, 2011. **22**(7): p. 1554-1560.
29. Brierley, J., M.K. Gospodarowicz, and C. Wittekind, *TNM classification of malignant tumours*. 2017.
30. Cortazar, P., et al., *Pathological complete response and long-term clinical benefit in breast cancer: the CTNeoBC pooled analysis*. *The Lancet*, 2014. **384**(9938): p. 164-172.
31. Luen, S.J., et al., *Prognostic implications of residual disease tumor-infiltrating lymphocytes and residual cancer burden in triple-negative breast cancer patients after neoadjuvant chemotherapy*. *Annals of Oncology*, 2019. **30**(2): p. 236-242.
32. Lejeune, M., et al., *Prognostic Implications of the Residual Tumor Microenvironment after Neoadjuvant Chemotherapy in Triple-Negative Breast Cancer Patients without Pathological Complete Response*. *Cancers*, 2023. **15**(3): p. 597.
33. Califf, R.M., *Biomarker definitions and their applications*. *Experimental Biology and Medicine*, 2018. **243**(3): p. 213-221.
34. *BEST (Biomarkers, EndpointS, and other Tools) Resource*.
35. Allison, K.H., et al., *Estrogen and Progesterone Receptor Testing in Breast Cancer: ASCO/CAP Guideline Update*. *Journal of Clinical Oncology*, 2020. **38**(12): p. 1346-1366.
36. Wolff, A.C., et al., *Human Epidermal Growth Factor Receptor 2 Testing in Breast Cancer: American Society of Clinical Oncology/College of American Pathologists Clinical Practice Guideline Focused Update*. *Archives of Pathology & Laboratory Medicine*, 2018. **142**(11): p. 1364-1382.
37. Nielsen, T.O., et al., *Assessment of Ki67 in Breast Cancer: Updated Recommendations From the International Ki67 in Breast Cancer Working Group*. *Journal of the National Cancer Institute : JNCI.*, 2021. **113**(7): p. 808-819.
38. Jones, R.L., et al., *The prognostic significance of Ki67 before and after neoadjuvant chemotherapy in breast cancer*. *Breast Cancer Research and Treatment*, 2009. **116**(1): p. 53-68.

39. Davey, M.G., et al., *Ki-67 as a Prognostic Biomarker in Invasive Breast Cancer*. *Cancers*, 2021. **13**(17): p. 4455.
40. Tan, Q., et al., *Potential Predictive and Prognostic Value of Biomarkers Related to Immune Checkpoint Inhibitor Therapy of Triple-Negative Breast Cancer*. *Frontiers in Oncology*, 2022. **12**.
41. Tutt, A.N.J., et al., *Adjuvant Olaparib for Patients with
<i>BRCA1</i>
- or
<i>BRCA2</i>
-Mutated Breast Cancer*. *New England Journal of Medicine*, 2021. **384**(25): p. 2394-2405.
42. Silwal-Pandit, L., A. Langerød, and A.-L. Børresen-Dale, *<i>TP53</i>Mutations in Breast and Ovarian Cancer*. Cold Spring Harbor Perspectives in Medicine, 2017. **7**(1): p. a026252.
43. Koboldt, D.C., et al., *Comprehensive molecular portraits of human breast tumours*. *Nature*, 2012. **490**(7418): p. 61-70.
44. Denkert, C., et al., *Tumour-infiltrating lymphocytes and prognosis in different subtypes of breast cancer: a pooled analysis of 3771 patients treated with neoadjuvant therapy*. *Lancet Oncology*, 2018. **19**(1): p. 40-50.
45. Loi, S., et al., *Tumor-Infiltrating Lymphocytes and Prognosis: A Pooled Individual Patient Analysis of Early-Stage Triple-Negative Breast Cancers*. *Journal of Clinical Oncology*, 2019. **37**(7): p. 559-569.
46. Salgado, R., et al., *The evaluation of tumor-infiltrating lymphocytes (TILs) in breast cancer: recommendations by an International TILs Working Group 2014*. *Annals of Oncology*, 2015. **26**(2): p. 259-271.
47. Trapp, E., et al., *Presence of Circulating Tumor Cells in High-Risk Early Breast Cancer During Follow-Up and Prognosis*. *Journal of the National Cancer Institute : JNCI.*, 2019. **111**(4): p. 380-387.
48. Thomas-Bonafos, T., et al., *Circulating tumor cells in breast cancer: clinical validity and utility*. *npj Breast Cancer*, 2024. **10**(1).
49. Quail, D.F. and J.A. Joyce, *Microenvironmental regulation of tumor progression and metastasis*. *Nature Medicine*, 2013. **19**(11): p. 1423-1437.
50. Ruffell, B., N.I. Affara, and L.M. Coussens, *Differential macrophage programming in the tumor microenvironment*. *Trends Immunol*, 2012. **33**(3): p. 119-26.

51. Ruffell, B., et al., *Leukocyte composition of human breast cancer*. Proceedings of the National Academy of Sciences of the United States of America, 2012. **109**(8): p. 2796-2801.
52. Jiang, D., et al., *Clinicopathological and prognostic significance of FOXP3+ tumor infiltrating lymphocytes in patients with breast cancer: a meta-analysis*. BMC Cancer, 2015. **15**(1).
53. Wolf, N.K., D.U. Kissiov, and D.H. Raulet, *Roles of natural killer cells in immunity to cancer, and applications to immunotherapy*. Nature Reviews Immunology, 2023. **23**(2): p. 90-105.
54. Vivier, E., et al., *Functions of natural killer cells*. Nature Immunology, 2008. **9**(5): p. 503-510.
55. Aaltomaa, S., et al., *LYMPHOCYTE INFILTRATES AS A PROGNOSTIC VARIABLE IN FEMALE BREAST-CANCER*. European Journal of Cancer, 1992. **28A**(4-5): p. 859-864.
56. Huang, P., et al., *Regulatory T cells are associated with the tumor immune microenvironment and immunotherapy response in triple-negative breast cancer*. Frontiers in Immunology, 2023. **14**.
57. Tian, W., et al., *A prognostic risk model for patients with triple negative breast cancer based on stromal natural killer cells, tumor-associated macrophages and growth-arrest specific protein 6*. Cancer Science, 2016. **107**(7): p. 882-889.
58. Thacker, G., et al., *Immature natural killer cells promote progression of breast cancer*. Science Translational Medicine, 2023. **15**(686): p. 15.
59. Leek, R.D., et al., *Association of macrophage infiltration with angiogenesis and prognosis in invasive breast carcinoma*. Cancer Research, 1996. **56**(20): p. 4625-4629.
60. Volodko, N., et al., *Tumour-associated macrophages in breast cancer and their prognostic correlations*. Breast, 1998. **7**(2): p. 99-105.
61. De Palma, M., et al., *Tie2 identifies a hematopoietic monocytes required for tumor lineage of proangiogenic vessel formation and a mesenchymal population of pericyte progenitors*. Cancer Cell, 2005. **8**(3): p. 211-226.
62. Robinson, B.D., et al., *Tumor Microenvironment of Metastasis in Human Breast Carcinoma: A Potential Prognostic Marker Linked to Hematogenous Dissemination*. Clinical Cancer Research, 2009. **15**(7): p. 2433-2441.
63. Mantovani, A., et al., *Macrophage plasticity and polarization in tissue repair and remodelling*. Journal of Pathology, 2013. **229**(2): p. 176-185.

64. Wynn, T.A., A. Chawla, and J.W. Pollard, *Macrophage biology in development, homeostasis and disease*. Nature, 2013. **496**(7446): p. 445-455.
65. Schulz, C., et al., *A Lineage of Myeloid Cells Independent of Myb and Hematopoietic Stem Cells*. Science, 2012. **336**(6077): p. 86-90.
66. Perdiguero, E.G., et al., *Tissue-resident macrophages originate from yolk-sac-derived erythro-myeloid progenitors*. Nature, 2015. **518**(7540): p. 547-551.
67. Hoeffel, G., et al., *C-Myb+ Erythro-Myeloid Progenitor-Derived Fetal Monocytes Give Rise to Adult Tissue-Resident Macrophages*. Immunity, 2015. **42**(4): p. 665-678.
68. De Palma, M., et al., *Targeting exogenous genes to tumor angiogenesis by transplantation of genetically modified hematopoietic stem cells*. Nature Medicine, 2003. **9**(6): p. 789-795.
69. Franklin, R.A., et al., *The cellular and molecular origin of tumor-associated macrophages*. Science, 2014. **344**(6186): p. 921-925.
70. Bruttger, J., et al., *Genetic Cell Ablation Reveals Clusters of Local Self-Renewing Microglia in the Mammalian Central Nervous System*. Immunity, 2015. **43**(1): p. 92-106.
71. Bain, C.C., et al., *Constant replenishment from circulating monocytes maintains the macrophage pool in the intestine of adult mice*. Nature Immunology, 2014. **15**(10): p. 929-937.
72. Dick, S.A., et al., *Three tissue resident macrophage subsets coexist across organs with conserved origins and life cycles*. Science Immunology, 2022. **7**(67).
73. Boyette, L.B., et al., *Phenotype, function, and differentiation potential of human monocyte subsets*. Plos One, 2017. **12**(4).
74. Metcalf, T.U., et al., *Human Monocyte Subsets Are Transcriptionally and Functionally Altered in Aging in Response to Pattern Recognition Receptor Agonists*. Journal of Immunology, 2017. **199**(4): p. 1405-1417.
75. Geissmann, F., S. Jung, and D.R. Littman, *Blood monocytes consist of two principal subsets with distinct migratory properties*. Immunity, 2003. **19**(1): p. 71-82.
76. Mantovani, A., et al., *Macrophage polarization: tumor-associated macrophages as a paradigm for polarized M2 mononuclear phagocytes*. Trends in Immunology, 2002. **23**(11): p. 549-555.
77. Mills, C.D., et al., *M-1/M-2 macrophages and the Th1/Th2 paradigm*. Journal of Immunology, 2000. **164**(12): p. 6166-6173.

78. Mantovani, A., et al., *The chemokine system in diverse forms of macrophage activation and polarization*. Trends in Immunology, 2004. **25**(12): p. 677-686.
79. Gordon, S. and P.R. Taylor, *Monocyte and macrophage heterogeneity*. Nature Reviews Immunology, 2005. **5**(12): p. 953-964.
80. Pucci, F., et al., *A distinguishing gene signature shared by tumor-infiltrating Tie2-expressing monocytes, blood "resident" monocytes, and embryonic macrophages suggests common functions and developmental relationships*. Blood, 2009. **114**(4): p. 901-914.
81. Martinez, F.O. and S. Gordon, *The M1 and M2 paradigm of macrophage activation: time for reassessment*. F1000prime reports, 2014. **6**: p. 13.
82. Qian, B.-Z. and J.W. Pollard, *Macrophage Diversity Enhances Tumor Progression and Metastasis*. Cell, 2010. **141**(1): p. 39-51.
83. Chistiakov, D.A., et al., *CD68/macrosialin: not just a histochemical marker*. Laboratory Investigation, 2017. **97**(1): p. 4-13.
84. Gottfried, E., et al., *Expression of CD68 in non-myeloid cell types*. Scandinavian Journal of Immunology, 2008. **67**(5): p. 453-463.
85. Qian, B.Z., et al., *CCL2 recruits inflammatory monocytes to facilitate breast-tumour metastasis*. Nature, 2011. **475**(7355): p. 222-5.
86. Chen, Z.H., et al., *Cellular and Molecular Identity of Tumor-Associated Macrophages in Glioblastoma*. Cancer Research, 2017. **77**(9): p. 2266-2278.
87. Zhu, Y., et al., *Tissue-Resident Macrophages in Pancreatic Ductal Adenocarcinoma Originate from Embryonic Hematopoiesis and Promote Tumor Progression*. Immunity, 2017. **47**(2): p. 323-+.
88. Mantovani, A., et al., *Tumour-associated macrophages as treatment targets in oncology*. Nature Reviews Clinical Oncology, 2017. **14**(7): p. 399-416.
89. Lin, E.Y., et al., *Colony-stimulating factor 1 promotes progression of mammary tumors to malignancy*. Journal of Experimental Medicine, 2001. **193**(6): p. 727-739.
90. DeNardo, D.G., et al., *Leukocyte complexity predicts breast cancer survival and functionally regulates response to chemotherapy*. Cancer Discov, 2011. **1**(1): p. 54-67.
91. Fridlender, Z.G., et al., *CCL2 Blockade Augments Cancer Immunotherapy*. Cancer Research, 2010. **70**(1): p. 109-118.
92. Lin, E.Y., et al., *Macrophages regulate the angiogenic switch in a mouse model of breast cancer*. Cancer Research, 2006. **66**(23): p. 11238-11246.
93. Stockmann, C., et al., *Deletion of vascular endothelial growth factor in myeloid cells accelerates tumorigenesis*. Nature, 2008. **456**(7223): p. 814-818.

94. Venneri, M.A., et al., *Identification of proangiogenic TIE2-expressing monocytes (TEMs) in human peripheral blood and cancer*. *Blood*, 2007. **109**(12): p. 5276-5285.
95. Pucci, F., et al., *A distinguishing gene signature shared by tumor-infiltrating Tie2-expressing monocytes, blood "resident" monocytes, and embryonic macrophages suggests common functions and developmental relationships*. *Blood*, 2009. **114**(4): p. 901-14.
96. De Palma, M., et al., *Tumor-targeted interferon-alpha delivery by Tie2-expressing monocytes inhibits tumor growth and metastasis*. *Cancer Cell*, 2008. **14**(4): p. 299-311.
97. Murdoch, C., et al., *Expression of Tie-2 by Human Monocytes and Their Responses to Angiopoietin-2*. *The Journal of Immunology*, 2007. **178**(11): p. 7405-7411.
98. Mazziere, R., et al., *Targeting the ANG2/TIE2 axis inhibits tumor growth and metastasis by impairing angiogenesis and disabling rebounds of proangiogenic myeloid cells*. *Cancer Cell*, 2011. **19**(4): p. 512-26.
99. Ruffell, B., et al., *Macrophage IL-10 Blocks CD8(+) T Cell-Dependent Responses to Chemotherapy by Suppressing IL-12 Expression in Intratumoral Dendritic Cells*. *Cancer Cell*, 2014. **26**(5): p. 623-637.
100. Zhu, Y., et al., *CSF1/CSF1R Blockade Reprograms Tumor-Infiltrating Macrophages and Improves Response to T-cell Checkpoint Immunotherapy in Pancreatic Cancer Models*. *Cancer Research*, 2014. **74**(18): p. 5057-5069.
101. Lin, E.Y., et al., *Colony-Stimulating Factor 1 Promotes Progression of Mammary Tumors to Malignancy*. *Journal of Experimental Medicine*, 2001. **193**(6): p. 727-740.
102. Wyckoff, J.B., et al., *Direct visualization of macrophage-assisted tumor cell intravasation in mammary tumors*. *Cancer Res*, 2007. **67**(6): p. 2649-56.
103. Harney, A.S., et al., *Real-Time Imaging Reveals Local, Transient Vascular Permeability, and Tumor Cell Intravasation Stimulated by TIE2(hi) Macrophage-Derived VEGFA*. *Cancer Discovery*, 2015. **5**(9): p. 932-943.
104. Rohan, T.E., et al., *Tumor Microenvironment of Metastasis and Risk of Distant Metastasis of Breast Cancer*. *Jnci-Journal of the National Cancer Institute*, 2014. **106**(8).
105. Yang, M., et al., *Diverse Functions of Macrophages in Different Tumor Microenvironments*. *Cancer Research*, 2018. **78**(19): p. 5492-5503.
106. Gwak, J.M., et al., *Prognostic Value of Tumor-Associated Macrophages According to Histologic Locations and Hormone Receptor Status in Breast Cancer*. *PLOS ONE*, 2015. **10**(4): p. e0125728.

107. Willingham, S.B., et al., *The CD47-signal regulatory protein alpha (SIRPa) interaction is a therapeutic target for human solid tumors*. Proceedings of the National Academy of Sciences, 2012. **109**(17): p. 6662-6667.
108. Varol, C. and I. Sagi, *Phagocyte—extracellular matrix crosstalk empowers tumor development and dissemination*. The FEBS Journal, 2018. **285**(4): p. 734-751.
109. Acerbi, I., et al., *Human breast cancer invasion and aggression correlates with ECM stiffening and immune cell infiltration*. Integrative Biology, 2015. **7**(10): p. 1120-1134.
110. Medrek, C., et al., *The presence of tumor associated macrophages in tumor stroma as a prognostic marker for breast cancer patients*. BMC Cancer, 2012. **12**.
111. Mwafy, S.E. and D.M. El-Guindy, *Pathologic assessment of tumor-associated macrophages and their histologic localization in invasive breast carcinoma*. Journal of the Egyptian National Cancer Institute, 2020. **32**(1).
112. Opzoomer, J.W., et al., *Macrophages orchestrate the expansion of a proangiogenic perivascular niche during cancer progression*. Science Advances, 2021. **7**(45).
113. Hughes, R., et al., *Perivascular M2 Macrophages Stimulate Tumor Relapse after Chemotherapy*. Cancer Res, 2015. **75**(17): p. 3479-91.
114. Lapenna, A., M. De Palma, and C.E. Lewis, *Perivascular macrophages in health and disease*. Nature Reviews Immunology, 2018. **18**(11): p. 689-702.
115. Linde, N., et al., *Macrophages orchestrate breast cancer early dissemination and metastasis*. Nature Communications, 2018. **9**(1).
116. Coffelt, S.B., et al., *Angiopoietin-2 regulates gene expression in TIE2-expressing monocytes and augments their inherent proangiogenic functions*. Cancer Res, 2010. **70**(13): p. 5270-80.
117. Coffelt, S.B., et al., *Angiopoietin 2 Stimulates TIE2-Expressing Monocytes To Suppress T Cell Activation and To Promote Regulatory T Cell Expansion*. Journal of Immunology, 2011. **186**(7): p. 4183-4190.
118. Eisinger, S., et al., *Targeting a scavenger receptor on tumor-associated macrophages activates tumor cell killing by natural killer cells*. Proceedings of the National Academy of Sciences, 2020. **117**(50): p. 32005-32016.
119. Schwertfeger, K.L., et al., *A critical role for the inflammatory response in a mouse model of preneoplastic progression*. Cancer Research, 2006. **66**(11): p. 5676-5685.

120. Goswami, S., et al., *Macrophages promote the invasion of breast carcinoma cells via a colony-stimulating factor-1/epidermal growth factor paracrine loop*. *Cancer Research*, 2005. **65**(12): p. 5278-5283.
121. Laoui, D., et al., *Tumor Hypoxia Does Not Drive Differentiation of Tumor-Associated Macrophages but Rather Fine-Tunes the M2-like Macrophage Population*. *Cancer research.*, 2014. **74**(1): p. 24-30.
122. Cassetta, L., et al., *Isolation of Mouse and Human Tumor-Associated Macrophages*, in *Advances in Experimental Medicine and Biology*. 2016, Springer International Publishing. p. 211-229.
123. Cassetta, L., et al., *Human Tumor-Associated Macrophage and Monocyte Transcriptional Landscapes Reveal Cancer-Specific Reprogramming, Biomarkers, and Therapeutic Targets*. *Cancer Cell*, 2019. **35**(4): p. 588-602.e10.
124. Glass, G., J.A. Papin, and J.W. Mandell, *Simple: A Sequential Immunoperoxidase Labeling and Erasing Method*. *Journal of Histochemistry & Cytochemistry*, 2009. **57**(10): p. 899-905.
125. Tsujikawa, T., et al., *Quantitative Multiplex Immunohistochemistry Reveals Myeloid-Inflamed Tumor-Immune Complexity Associated with Poor Prognosis*. *Cell Reports*, 2017. **19**(1): p. 203-217.
126. Cheng, S., et al., *A pan-cancer single-cell transcriptional atlas of tumor infiltrating myeloid cells*. *Cell*, 2021. **184**(3): p. 792-809.e23.
127. Matusiak, M., et al., *A spatial map of human macrophage niches reveals context-dependent macrophage functions in colon and breast cancer*. 2023, Research Square Platform LLC.
128. Ma, R.-Y., A. Black, and B.-Z. Qian, *Macrophage diversity in cancer revisited in the era of single-cell omics*. *Trends in Immunology*, 2022. **43**(7): p. 546-563.
129. Mantovani, A., et al., *ROLE OF HOST DEFENSE-MECHANISMS IN THE ANTI-TUMOR ACTIVITY OF ADRIAMYCIN AND DAUNOMYCIN IN MICE*. *Journal of the National Cancer Institute*, 1979. **63**(1): p. 61-66.
130. Kodumudi, K.N., et al., *A Novel Chemoimmunomodulating Property of Docetaxel: Suppression of Myeloid-Derived Suppressor Cells in Tumor Bearers*. *Clinical Cancer Research*, 2010. **16**(18): p. 4583-4594.
131. Nakasone, E.S., et al., *Imaging tumor-stroma interactions during chemotherapy reveals contributions of the microenvironment to resistance*. *Cancer Cell*, 2012. **21**(4): p. 488-503.
132. Shree, T., et al., *Macrophages and cathepsin proteases blunt chemotherapeutic response in breast cancer*. *Genes Dev*, 2011. **25**(23): p. 2465-79.

133. Lin, H.-H., et al., *Heme oxygenase-1 promotes neovascularization in ischemic heart by coinduction of VEGF and SDF-1*. Journal of Molecular and Cellular Cardiology, 2008. **45**(1): p. 44-55.
134. Welford, A.F., et al., *TIE2-expressing macrophages limit the therapeutic efficacy of the vascular-disrupting agent combretastatin A4 phosphate in mice*. Journal of Clinical Investigation, 2011. **121**(5): p. 1969-1973.
135. Ahn, G.O., et al., *Inhibition of Mac-1 (CD11b/CD18) enhances tumor response to radiation by reducing myeloid cell recruitment*. Proceedings of the National Academy of Sciences of the United States of America, 2010. **107**(18): p. 8363-8368.
136. Lin, C.-C., et al., *Abstract CT171: Phase I study of BLZ945 alone and with spartalizumab (PDR001) in patients (pts) with advanced solid tumors*. Cancer Research, 2020. **80**(16_Supplement): p. CT171-CT171.
137. Weiss, S.A., et al., *A Phase I Study of APX005M and Cabiralizumab with or without Nivolumab in Patients with Melanoma, Kidney Cancer, or Non-Small Cell Lung Cancer Resistant to Anti-PD-1/PD-L1*. Clinical Cancer Research, 2021. **27**(17): p. 4757-4767.
138. Gomez-Roca, C.A., et al., *Phase I study of emactuzumab single agent or in combination with paclitaxel in patients with advanced/metastatic solid tumors reveals depletion of immunosuppressive M2-like macrophages*. Annals of Oncology, 2019. **30**(8): p. 1381-1392.
139. Machiels, J.-P., et al., *Phase Ib study of anti-CSF-1R antibody emactuzumab in combination with CD40 agonist selicrelumab in advanced solid tumor patients*. Journal for ImmunoTherapy of Cancer, 2020. **8**(2): p. e001153.
140. Rosenbaum, E., et al., *A Phase I Study of Binimetinib (MEK162) Combined with Pexidartinib (PLX3397) in Patients with Advanced Gastrointestinal Stromal Tumor*. The Oncologist, 2019. **24**(10): p. 1309-e983.
141. Wesolowski, R., et al., *Phase Ib study of the combination of pexidartinib (PLX3397), a CSF-1R inhibitor, and paclitaxel in patients with advanced solid tumors*. Therapeutic Advances in Medical Oncology, 2019. **11**: p. 175883591985423.
142. Razak, A.R., et al., *Safety and efficacy of AMG 820, an anti-colony-stimulating factor 1 receptor antibody, in combination with pembrolizumab in adults with advanced solid tumors*. Journal for ImmunoTherapy of Cancer, 2020. **8**(2): p. e001006.
143. Barreto, C.M.N., et al., *Abstract CT204: High cytotoxic T-cell or polymorphonuclear cell infiltrates in the tumor microenvironment correlate with responses to BL8040 plus pembrolizumab combination therapy in metastatic pancreatic tumors: Scientific correlates of a phase II clinical trial*. Cancer Research, 2020. **80**(16_Supplement): p. CT204-CT204.

144. Bockorny, B., et al., *BL-8040, a CXCR4 antagonist, in combination with pembrolizumab and chemotherapy for pancreatic cancer: the COMBAT trial*. Nature Medicine, 2020. **26**(6): p. 878-885.
145. Boddu, P., et al., *Initial report of a phase I study of LY2510924 with idarubicin and cytarabine (IA) in relapsed/refractory (R/R) AML*. Journal of Clinical Oncology, 2018. **36**(15_suppl): p. 7026-7026.
146. Hidalgo, M., et al., *A multi-center phase 2a trial of the CXCR4 inhibitor motixafortide (BL-8040) (M) in combination with pembrolizumab (P) and chemotherapy (C), in patients with metastatic pancreatic adenocarcinoma (mPDAC)*. Cancer Research, 2021. **81**(13): p. 2.
147. Andtbacka, R.H.I., et al., *Mavorixafor, an Orally Bioavailable CXCR4 Antagonist, Increases Immune Cell Infiltration and Inflammatory Status of Tumor Microenvironment in Patients with Melanoma*. Cancer Research Communications, 2022. **2**(8): p. 904-913.
148. Sandhu, S.K., et al., *A first-in-human, first-in-class, phase I study of carlumab (CNTO 888), a human monoclonal antibody against CC-chemokine ligand 2 in patients with solid tumors*. Cancer Chemotherapy and Pharmacology, 2013. **71**(4): p. 1041-1050.
149. Nywening, T.M., et al., *Targeting tumour-associated macrophages with CCR2 inhibition in combination with FOLFIRINOX in patients with borderline resectable and locally advanced pancreatic cancer: a single-centre, open-label, dose-finding, non-randomised, phase 1b trial*. The Lancet Oncology, 2016. **17**(5): p. 651-662.
150. Adams, D.L., et al., *Safety, efficacy, and clinical outcomes of the anti-CCR5 inhibitor (Leronlimab): A pooled analysis of three clinical trials in patients with mTNBC*. Journal of Clinical Oncology, 2022. **40**(16_suppl): p. e13062-e13062.
151. Cristofanilli, M., et al., *Abstract P5-17-08: A phase Ib/II study of leronlimab combined with carboplatin in patients with CCR5+ metastatic triple-negative breast cancer (mTNBC)*. Cancer Research, 2022. **82**(4_Supplement): p. P5-17-08-P5-17-08.
152. Haag, G.M., et al., *Pembrolizumab and maraviroc in refractory mismatch repair proficient/microsatellite-stable metastatic colorectal cancer – The PICCASSO phase I trial*. European journal of cancer., 2022. **167**: p. 112-122.
153. Halama, N., et al., *Tumoral Immune Cell Exploitation in Colorectal Cancer Metastases Can Be Targeted Effectively by Anti-CCR5 Therapy in Cancer Patients*. Cancer Cell, 2016. **29**(4): p. 587-601.
154. Burris Iii, H.A., et al., *A first-in-human study of AO-176, a highly differentiated anti-CD47 antibody, in patients with advanced solid tumors*. Journal of clinical oncology : official journal of the American Society of Clinical Oncology., 2021. **39**(15_suppl): p. 2516-2516.

155. Zeidan, A.M., et al., *Phase 1 study of anti-CD47 monoclonal antibody CC-90002 in patients with relapsed/refractory acute myeloid leukemia and high-risk myelodysplastic syndromes*. *Annals of Hematology*, 2022. **101**(3): p. 557-569.
156. Lakhani, N.J., et al., *Evorpaccept alone and in combination with pembrolizumab or trastuzumab in patients with advanced solid tumours (ASPEN-01): a first-in-human, open-label, multicentre, phase 1 dose-escalation and dose-expansion study*. *The Lancet oncology.*, 2021. **22**(12): p. 1740-1751.
157. Lakhani, N.J., et al., *A phase Ib study of the anti-CD47 antibody magrolimab with the PD-L1 inhibitor avelumab (A) in solid tumor (ST) and ovarian cancer (OC) patients*. *Journal of clinical oncology : official journal of the American Society of Clinical Oncology.*, 2020. **38**(5_suppl): p. 18-18.
158. Sallman, D.A., et al., *Magrolimab in Combination With Azacitidine in Patients With Higher-Risk Myelodysplastic Syndromes: Final Results of a Phase Ib Study*. *Journal of Clinical Oncology*, 2023. **41**(15): p. 2815-2826.
159. Advani, R., et al., *CD47 Blockade by Hu5F9-G4 and Rituximab in Non-Hodgkin's Lymphoma*. *New England Journal of Medicine*, 2018. **379**(18): p. 1711-1721.
160. Fisher, G.A., et al., *A phase Ib/II study of the anti-CD47 antibody magrolimab with cetuximab in solid tumor and colorectal cancer patients*. *Journal of clinical oncology : official journal of the American Society of Clinical Oncology.*, 2020. **38**(4_suppl): p. 114-114.
161. Ansell, S.M., et al., *Phase I Study of the CD47 Blocker TTI-621 in Patients with Relapsed or Refractory Hematologic Malignancies*. *Clinical cancer research.*, 2021. **27**(8): p. 2190-2199.
162. Patel, K., et al., *TTI-622-01: A phase 1a/1b dose-escalation and expansion trial of TTI-622 in patients with advanced hematologic malignancies, including multiple myeloma*. *Journal of Clinical Oncology*, 2022. **40**(16_suppl): p. TPS8071-TPS8071.
163. Chawla, S.P., et al., *TTI-621-03: A phase I/II study of TTI-621 in combination with doxorubicin in patients with unresectable or metastatic high-grade leiomyosarcoma (LMS)*. *Journal of Clinical Oncology*, 2022. **40**(16_suppl): p. TPS11593-TPS115.
164. Padrón, L.J., et al., *Sotigalimab and/or nivolumab with chemotherapy in first-line metastatic pancreatic cancer: clinical and immunologic analyses from the randomized phase 2 PRINCE trial*. *Nature Medicine*, 2022. **28**(6): p. 1167-1177.
165. Beatty, G.L., et al., *A Phase I Study of an Agonist CD40 Monoclonal Antibody (CP-870,893) in Combination with Gemcitabine in Patients with Advanced*

- Pancreatic Ductal Adenocarcinoma*. *Clinical cancer research.*, 2013. **19**(22): p. 6286-6295.
166. Vonderheide, R.H., et al., *Phase I study of the CD40 agonist antibody CP-870,893 combined with carboplatin and paclitaxel in patients with advanced solid tumors*. *Oncolimmunology*, 2013. **2**(1): p. e23033.
167. Nowak, A.K., et al., *A phase 1b clinical trial of the CD40-activating antibody CP-870,893 in combination with cisplatin and pemetrexed in malignant pleural mesothelioma*. *Annals of oncology.*, 2015. **26**(12): p. 2483-2490.
168. Byrne, K.T., et al., *Neoadjuvant Selicrelumab, an Agonist CD40 Antibody, Induces Changes in the Tumor Microenvironment in Patients with Resectable Pancreatic Cancer*. *Clinical cancer research.*, 2021. **27**(16): p. 4574-4586.
169. Barlesi, F., et al., *291 Phase Ib study of selicrelumab (CD40 agonist) in combination with atezolizumab (anti-PD-L1) in patients with advanced solid tumors*. *Journal for ImmunoTherapy of Cancer*, 2020. **8**(Suppl 3): p. A178-A178.
170. Bonapace, L., et al., *Cessation of CCL2 inhibition accelerates breast cancer metastasis by promoting angiogenesis*. *Nature*, 2014. **515**(7525): p. 130-133.
171. Quail, D.F., et al., *The tumor microenvironment underlies acquired resistance to CSF-1R inhibition in gliomas*. *Science*, 2016. **352**(6288): p. 12.
172. Velasco-Velázquez, M., et al., *CCR5 Antagonist Blocks Metastasis of Basal Breast Cancer Cells*. *Cancer Research*, 2012. **72**(15): p. 3839-3850.
173. Pourmaleki, M., et al., *Moving Spatially Resolved Multiplexed Protein Profiling toward Clinical Oncology*. *Cancer Discovery*, 2023. **13**(4): p. 824-828.
174. Parra, E.R., et al., *Immuno-profiling and cellular spatial analysis using five immune oncology multiplex immunofluorescence panels for paraffin tumor tissue*. *Scientific Reports*, 2021. **11**(1).
175. Harms, P.W., et al., *Multiplex Immunohistochemistry and Immunofluorescence: A Practical Update for Pathologists*. *Modern pathology.*, 2023. **36**(7): p. 100197.
176. Piehowski, P.D., et al., *Automated mass spectrometry imaging of over 2000 proteins from tissue sections at 100- μ m spatial resolution*. *Nature Communications*, 2020. **11**(1).
177. Zhang, H., et al., *Mass spectrometry imaging for spatially resolved multi-omics molecular mapping*. *npj Imaging*, 2024. **2**(1).
178. Han, W., et al., *Cell segmentation for immunofluorescence multiplexed images using two-stage domain adaptation and weakly labeled data for pre-training*. *Scientific Reports*, 2022. **12**(1).

179. Kwan, A., et al., *An Overview of the Bench to Bedside Models of Breast Cancer in the Era of Cancer Immunotherapy*. Medical Research Archives, 2024. **12**(6).
180. Williams, S.T., et al., *Precision oncology using ex vivo technology: a step towards individualised cancer care?* Expert Reviews in Molecular Medicine, 2022: p. 1-48.
181. Muraro, M.G., et al., *Ex-vivo assessment of drug response on breast cancer primary tissue with preserved microenvironments*. OncoImmunology, 2017: p. e1331798.
182. Urbaniak, A., et al., *Limitations of an ex vivo breast cancer model for studying the mechanism of action of the anticancer drug paclitaxel*. European Journal of Pharmacology, 2021. **891**: p. 10.
183. Karekla, E., et al., *Ex Vivo Explant Cultures of Non–Small Cell Lung Carcinoma Enable Evaluation of Primary Tumor Responses to Anticancer Therapy*. Cancer Research, 2017. **77**(8): p. 2029-2039.
184. Sachs, N., et al., *A Living Biobank of Breast Cancer Organoids Captures Disease Heterogeneity*. Cell, 2018. **172**(1-2): p. 373-386.e10.
185. Campaner, E., et al., *Breast Cancer Organoids Model Patient-Specific Response to Drug Treatment*. Cancers, 2020. **12**(12): p. 3869.
186. Nolan, J., et al., *Organ-on-a-Chip and Microfluidic Platforms for Oncology in the UK*. Cancers, 2023. **15**(3): p. 635.
187. Sontheimer-Phelps, A., B.A. Hassell, and D.E. Ingber, *Modelling cancer in microfluidic human organs-on-chips*. Nature Reviews Cancer, 2019. **19**(2): p. 65-81.
188. Whisler, J.A., M.B. Chen, and R.D. Kamm, *Control of Perfusable Microvascular Network Morphology Using a Multiculture Microfluidic System*. Tissue Engineering Part C-Methods, 2014. **20**(7): p. 543-552.
189. Jeon, J.S., et al., *Human 3D vascularized organotypic microfluidic assays to study breast cancer cell extravasation*. Proceedings of the National Academy of Sciences of the United States of America, 2015. **112**(1): p. 214-219.
190. Boussommier-Calleja, A., et al., *The effects of monocytes on tumor cell extravasation in a 3D vascularized microfluidic model*. Biomaterials, 2018.
191. Bingle, L., N.J. Brown, and C.E. Lewis, *The role of tumour-associated macrophages in tumour progression: implications for new anticancer therapies*. Journal of Pathology, 2002. **196**(3): p. 254-265.
192. Schindelin, J., et al., *Fiji: an open-source platform for biological-image analysis*. Nature Methods, 2012. **9**(7): p. 676-682.

193. Lewis, C.E. and J.W. Pollard, *Distinct role of macrophages in different tumor microenvironments*. *Cancer Res*, 2006. **66**(2): p. 605-12.
194. Kramer, C.J.H., et al., *The prognostic value of tumour–stroma ratio in primary breast cancer with special attention to triple-negative tumours: a review*. *Breast Cancer Research and Treatment*, 2019. **173**(1): p. 55-64.
195. Baschong, W., R. Suetterlin, and R.H. Laeng, *Control of autofluorescence of archival formaldehyde-fixed, paraffin-embedded tissue in confocal laser scanning microscopy (CLSM)*. *Journal of Histochemistry & Cytochemistry*, 2001. **49**(12): p. 1565-1571.
196. Falini, B., et al., *PG-M1 - A NEW MONOCLONAL-ANTIBODY DIRECTED AGAINST A FIXATIVE-RESISTANT EPITOPE ON THE MACROPHAGE-RESTRICTED FORM OF THE CD68 MOLECULE*. *American Journal of Pathology*, 1993. **142**(5): p. 1359-1372.
197. Engering, A.J., et al., *The mannose receptor functions as a high capacity and broad specificity antigen receptor in human dendritic cells*. *European Journal of Immunology*, 1997. **27**(9): p. 2417-2425.
198. Martinez-Pomares, L., *The mannose receptor*. *Journal of Leukocyte Biology*, 2012. **92**(6): p. 1177-1186.
199. Pilling, D., et al., *Identification of Markers that Distinguish Monocyte-Derived Fibrocytes from Monocytes, Macrophages, and Fibroblasts*. *Plos One*, 2009. **4**(10).
200. Pulford, K.A.F., et al., *KP1 - A NEW MONOCLONAL-ANTIBODY THAT DETECTS A MONOCYTE MACROPHAGE ASSOCIATED ANTIGEN IN ROUTINELY PROCESSED TISSUE-SECTIONS*. *Journal of Clinical Pathology*, 1989. **42**(4): p. 414-421.
201. Zhang, J., et al., *Role of CD68 in tumor immunity and prognosis prediction in pan-cancer*. *Scientific Reports*, 2022. **12**(1).
202. Cimino-Mathews, A., *Novel uses of immunohistochemistry in breast pathology: interpretation and pitfalls*. *Modern Pathology*, 2021. **34**(S1): p. 62-77.
203. Lertkiatmongkol, P., et al., *Endothelial functions of platelet/endothelial cell adhesion molecule-1 (CD31)*. *Current Opinion in Hematology*, 2016. **23**(3): p. 253-259.
204. Elliott, L.A., et al., *Human Tumor-Infiltrating Myeloid Cells: Phenotypic and Functional Diversity*. *Frontiers in Immunology*, 2017. **8**.
205. Gantzel, R.H., et al., *Macrophage Activation Markers, Soluble CD163 and Mannose Receptor, in Liver Fibrosis*. *Frontiers in Medicine*, 2021. **7**.

206. Pulford, K.A.F., et al., *DISTRIBUTION OF THE CD68 MACROPHAGE MYELOID ASSOCIATED ANTIGEN*. International Immunology, 1990. **2**(10): p. 973-980.
207. Natarajan, V., et al., *Acquired α SMA Expression in Pericytes Coincides with Aberrant Vascular Structure and Function in Pancreatic Ductal Adenocarcinoma*. Cancers, 2022. **14**(10): p. 2448.
208. Valkenburg, K.C., A.E. De Groot, and K.J. Pienta, *Targeting the tumour stroma to improve cancer therapy*. Nature Reviews Clinical Oncology, 2018. **15**(6): p. 366-381.
209. Dixon, K.O., Lahore, G. F. and Kuchroo, V. K., *Beyond T cell exhaustion: TIM-3 regulation of myeloid cells*. Science Immunology, 2024. **9**(93).
210. Aggarwal, V., C.J. Workman, and D.A.A. Vignali, *LAG-3 as the third checkpoint inhibitor*. Nature Immunology, 2023. **24**(9): p. 1415-1422.
211. Doroshov, D.B., et al., *PD-L1 as a biomarker of response to immune-checkpoint inhibitors*. Nature Reviews Clinical Oncology, 2021. **18**(6): p. 345-362.
212. Xie, X.X., et al., *The Expression Pattern and Clinical Significance of the Immune Checkpoint Regulator VISTA in Human Breast Cancer*. Frontiers in Immunology, 2020. **11**: p. 12.
213. Byun, K.D., et al., *T-Cell Immunoglobulin Mucin 3 Expression on Tumor Infiltrating Lymphocytes as a Positive Prognosticator in Triple-Negative Breast Cancer*. Journal of Breast Cancer, 2018. **21**(4): p. 406.
214. Cheng, S.Q., et al., *Expression of Tim-3 in breast cancer tissue promotes tumor progression*. International Journal of Clinical and Experimental Pathology, 2018. **11**(3): p. 1157-1166.
215. Smith, M.C.P., et al., *CXCR4 regulates growth of both primary and metastatic breast cancer*. Cancer Research, 2004. **64**(23): p. 8604-8612.
216. Müller, A., et al., *Involvement of chemokine receptors in breast cancer metastasis*. Nature, 2001. **410**(6824): p. 50-56.
217. Györfy, B., *Survival analysis across the entire transcriptome identifies biomarkers with the highest prognostic power in breast cancer*. Computational and Structural Biotechnology Journal, 2021. **19**: p. 4101-4109.
218. Lefort, S., et al., *CXCR4 inhibitors could benefit to HER2 but not to triple-negative breast cancer patients*. Oncogene, 2017. **36**(9): p. 1211-1222.
219. Zhang, Z., et al., *Expression of CXCR4 and breast cancer prognosis: a systematic review and meta-analysis*. BMC Cancer, 2014. **14**(1): p. 49.
220. Bruni, S., et al., *Cancer immune exclusion: breaking the barricade for a successful immunotherapy*. Frontiers in Oncology, 2023. **13**.

221. Pollard, J.W., *Tumour-educated macrophages promote tumour progression and metastasis*. Nature Reviews Cancer, 2004. **4**(1): p. 71-78.
222. Moamin, M.R., et al., *Changes in the immune landscape of TNBC after neoadjuvant chemotherapy: correlation with relapse*. Frontiers in Immunology, 2023. **14**: p. 13.
223. Wang, L., et al., *PD-L1-expressing tumor-associated macrophages are immunostimulatory and associate with good clinical outcome in human breast cancer*. Cell reports., 2024. **5**(2): p. 101420.
224. Hood, S.P., et al., *Phenotype and Function of Activated Natural Killer Cells From Patients With Prostate Cancer: Patient-Dependent Responses to Priming and IL-2 Activation*. Frontiers in Immunology, 2019. **9**.
225. Dean, I., et al., *Rapid functional impairment of natural killer cells following tumor entry limits anti-tumor immunity*. Nature Communications, 2024. **15**(1).
226. Gaggero, S., et al., *Cytokines Orchestrating the Natural Killer-Myeloid Cell Crosstalk in the Tumor Microenvironment: Implications for Natural Killer Cell-Based Cancer Immunotherapy*. Frontiers in Immunology, 2021. **11**.
227. Bozward, A.G., et al., *Natural Killer Cells and Regulatory T Cells Cross Talk in Hepatocellular Carcinoma: Exploring Therapeutic Options for the Next Decade*. Frontiers in Immunology, 2021. **12**.
228. Chatterjee, S., B. Behnam Azad, and S. Nimmagadda, *The Intricate Role of CXCR4 in Cancer*, in *Advances in Cancer Research*. 2014, Elsevier. p. 31-82.
229. Schioppa, T., et al., *Regulation of the Chemokine Receptor CXCR4 by Hypoxia*. The Journal of Experimental Medicine, 2003. **198**(9): p. 1391-1402.
230. Blaye, C., et al., *An immunological signature to predict outcome in patients with triple-negative breast cancer with residual disease after neoadjuvant chemotherapy*. ESMO Open, 2022. **7**(4): p. 100502.
231. Chuan, T., T. Li, and C. Yi, *Identification of CXCR4 and CXCL10 as Potential Predictive Biomarkers in Triple Negative Breast Cancer (TNBC)*. Medical Science Monitor, 2020. **26**.
232. Wang, Y., et al., *Saikosaponin A Inhibits Triple-Negative Breast Cancer Growth and Metastasis Through Downregulation of CXCR4*. Frontiers in Oncology, 2020. **9**: p. 11.
233. Gupta, N., et al., *CXCR4 expression is elevated in TNBC patient derived samples and Z-guggulsterone abrogates tumor progression by targeting CXCL12/CXCR4 signaling axis in preclinical breast cancer model*. Environmental research., 2023. **232**: p. 116335.

234. Chu, Q.Y.D., et al., *High Chemokine Receptor CXCR4 Level in Triple Negative Breast Cancer Specimens Predicts Poor Clinical Outcome*. Journal of Surgical Research, 2010. **159**(2): p. 689-695.
235. Guembarovski, A.L., et al., *CXCL12 chemokine and CXCR4 receptor: association with susceptibility and prognostic markers in triple negative breast cancer*. Molecular Biology Reports, 2018. **45**(5): p. 741-750.
236. Anastasiadou, D.P., et al., *Abstract 60: An emerging paradigm of Cxcl12 & Cxcr4 involvement in breast cancer metastasis*. Cancer Research, 2023. **83**(7_Supplement): p. 60-60.
237. Del Prete, A., et al., *Functional Role of Dendritic Cell Subsets in Cancer Progression and Clinical Implications*. International Journal of Molecular Sciences, 2020. **21**(11): p. 3930.
238. Tan, R., M. Nie, and W. Long, *The role of B cells in cancer development*. Frontiers in Oncology, 2022. **12**.
239. Jaillon, S., et al., *Neutrophil diversity and plasticity in tumour progression and therapy*. Nature Reviews Cancer, 2020. **20**(9): p. 485-503.
240. Sarradin, V., et al., *Immune microenvironment changes induced by neoadjuvant chemotherapy in triple-negative breast cancers: the MIMOSA-1 study*. Breast Cancer Research, 2021. **23**(1).
241. Chen, M.B., et al., *On-chip human microvasculature assay for visualization and quantification of tumor cell extravasation dynamics*. Nature Protocols, 2017. **12**(5): p. 865-880.
242. Ingber, D.E., *Human organs-on-chips for disease modelling, drug development and personalized medicine*. Nature Reviews Genetics, 2022. **23**(8): p. 467-491.
243. Riley, A., et al., *A novel microfluidic device capable of maintaining functional thyroid carcinoma specimens ex vivo provides a new drug screening platform*. BMC Cancer, 2019. **19**(1).
244. Schuster, B., et al., *Automated microfluidic platform for dynamic and combinatorial drug screening of tumor organoids*. Nature Communications, 2020. **11**(1).
245. Nakatsu, M.N., et al., *Angiogenic sprouting and capillary lumen formation modeled by human umbilical vein endothelial cells (HUVEC) in fibrin gels: the role of fibroblasts and Angiopoietin-1*. Microvascular Research, 2003. **66**(2): p. 102-112.
246. Sackmann, E.K., A.L. Fulton, and D.J. Beebe, *The present and future role of microfluidics in biomedical research*. Nature, 2014. **507**(7491): p. 181-189.

247. Popova, N.V. and M. Jücker, *The Functional Role of Extracellular Matrix Proteins in Cancer*. *Cancers*, 2022. **14**(1): p. 238.
248. Anstee, J.E., et al., *LYVE-1+ macrophages form a collaborative CCR5-dependent perivascular niche that influences chemotherapy responses in murine breast cancer*. *Developmental cell.*, 2023. **58**(17): p. 1548-1561.e10.
249. Ash, S.L., et al., *Targeting the activated microenvironment with endosialin (CD248)-directed CAR-T cells ablates perivascular cells to impair tumor growth and metastasis*. *Journal for ImmunoTherapy of Cancer*, 2024. **12**(2): p. e008608.
250. Carter, J.M., et al., *Distinct spatial immune microlandscapes are independently associated with outcomes in triple-negative breast cancer*. *Nature Communications*, 2023. **14**(1).